Studies on Mode Propagation and Dispersion Engineering Related Phenomena in Photonic Crystal Waveguides

Thesis submitted to

National Institute of Technology, Warangal

in partial fulfilment

of the requirements for the award of the degree of

Doctor of Philosophy

By

Vadapalli Durga Rama Pavan

(Roll No: 701640)

Under the Supervision of

Dr. Sourabh Roy

Associate Professor

Department of Physics

National Institute of Technology

Warangal, T.S., INDIA

June - 2022

राष्ट्रीय प्रौद्योगिकी संस्थान, वारंगल

National Institute of Technology

Warangal – 506 004, T.S. (India)

DEPARTMENT OF PHYSICS

Date:

APPROVAL OF THE VIVA-VOCE BOARD

Certified that the thesis entitled "***Studies on Mode Propagation and Dispersion Engineering Related Phenomena in Photonic Crystal Waveguides***" submitted by **Vadapalli Durga Rama Pavan (Roll No: 701640)** to the National Institute of Technology, Warangal, for the award of the degree ***Doctor of Philosophy*** has been accepted by the external examiners and that the student has successfully defended the thesis in the viva-voce examination held today, i.e., _____

(Prof. R. L. N. Sai Prasad)	(Prof. K. Venugopal Reddy)	(Prof. J. V. Ramana Murthy)
(Internal Member)	(Internal Member)	(Allied Dept. Member)

Dr. Sourabh Roy

(External Examiner) (Supervisor)

Prof. D. Dinakar

(Head of the Department & Chairman of DSC)

राष्ट्रीय प्रौद्योगिकी संस्थान, वारंगल
National Institute of Technology
Warangal – 506 004, T.S. (India)

DEPARTMENT OF PHYSICS

Certificate

This is to certify that the thesis entitled "***Studies on Mode Propagation and Dispersion Engineering Related Phenomena in Photonic Crystal Waveguides***" submitted by **Mr. Vadapalli Durga Rama Pavan (Roll No: 701640)** to National Institute of Technology, Warangal, is a record of bonafide research work under my supervision and I consider it worthy of consideration for the award of the degree of Doctor of Philosophy of the Institute.

(Dr. Sourabh Roy)
Associate Professor
Thesis Supervisor

DECLARATION

This is to certify that the work presented in the thesis entitled "***Studies on Mode Propagation and Dispersion Engineering Related Phenomena in Photonic Crystal Waveguides***" is a Bonafide work done by me under the supervision of Dr. Sourabh Roy, Associate Professor, Department of Physics, National Institute of Technology, Warangal, and was not submitted elsewhere for the award of any degree.

I declare that this written submission represents my ideas in my own words and where others' ideas or words have been included, I have adequately cited and referenced the original sources. I also declare that I have adhered to all principles of academic honesty and integrity and have not miss represented or fabricated or falsified any idea/ data/ fact/ source in my submission. I understand that any violation of the above will be a cause for disciplinary action by the institute and can also evoke penal action from the sources which have thus not been properly cited or from whom proper permission has not been taken when needed.

(**Vadapalli Durga Rama Pavan**)

ACKNOWLEDGEMENTS

I take this opportunity to thank the people who have been involved in my efforts directly or indirectly to complete this dissertation. The words mentioned here may not be sufficient to express my gratitude towards them.

Foremost, I sincerely thank my supervisor, **Dr. Sourabh Roy**, for his valuable guidance, motivation, and encouragement throughout my work. It has been a great pleasure for me to work under his guidance. I am thankful to my supervisor for believing in me, giving me the freedom to pursue my ideas, and patiently bearing me. This thesis wouldn't have been possible without his immense support, academically and personally.

I am thankful to the head of the department **Prof. D. Dinakar**, for his time to time suggestions in moulding the thesis. I am indebted for his administrative support in due course.

I am thankful to my Doctoral Scrutiny Committee members, **Prof. S.V.S. Ramana Reddy (Rtd.), Prof. M. Sai Shankar (Rtd.), Prof. R.L.N. Sai Prasad (Rtd.), Prof. K. Venugopal Reddy,** and **Prof. J. V. Ramana Murthy** (Department of Mathematics) for constantly reviewing my progress and providing valuable suggestions in a constructive way which helped me to carry forward my work successfully.

I want to extend my sincere thanks to **all the faculty members of the department**, who encouraged me all the time during my stay and supported me in all possible ways. I am thankful to the office staff and the students of the Department of Physics for their support whenever necessary.

I respect my teachers, who encouraged me to pursue a doctoral degree. I thank my teachers, **Mr. P. V. S. B. Chalapathi Rao** and **Mr. M. Santhi Sagar**, who inspired me to take up this career in my graduation days.

I am thankful to all the research scholars of the department. Especially, I am grateful to my senior scholars, **Dr. Nanda Kishore**, **Dr. Harikrishna**, **Dr. Sravanthi** and **Dr. Gnaneshwar,** for their kindness towards me. They helped me in learning many scientific methods in doing research.

During my stay at NIT Warangal, I had a great time with my lab mates and juniors, **Mr. Koustav, Mr. Nikhil,** and **Mr. Anirvan**. The time spent with these people was full of joy and invigorated me to work with more determination. I am also thankful to **Mr. Sampath** and **Mr. Rajesh** for their support in all needy times. I thank **Mrs. Ramani** who treated me like a son and motivated me in tough times.

I thank **SPIE, OSA, JJAP** and **MOC** societies for offering me travel grants to attend international conferences across the globe.

No words can adequately express my gratitude towards the love, support, and patience that I received from my family. The constant motivation from my parents has guided me through the odds and helped me to complete the work. I thank my sisters for their support in all aspects. Finally, I would like to thank my life partner for the love and affection showered on me all the time.

- Vadapalli Durga Rama Pavan

To my parents and teachers who supported me all the way

Contents

NOTATIONS

E	- Electric field
$\vec{r}$	- Position vector
$\vec{H}\left(\vec{r},t\right)$	- Time dependent magnetic field
$\vec{E}\left(\vec{r},t\right)$	- Time dependent electric field
$\nabla\times$	- Curl operator
$\vec{u}\left(\vec{r}\right)$	- Periodic function
$\vec{R}$	- Lattice vector
n	- Refractive index of a medium
c	- Velocity of light in vacuum
v_g	- Group velocity
n_g	- Group index
a	- Lattice constant
r	- Radius of air cylinder
r'	- Radius of inner air cylinder
s	- Shift introduced in lattice
t	- Twist introduced in lattice
w	- Width of waveguide
r/a	- Fraction filling ratio
$2r$	- Air cylinder diameter
β_2	- Second order dispersion
β_4	- Fourth order dispersion
k	- Wave-number
ω	- Angular frequency
Δt	- Time-delay
Δf	- Flat band
$\left(\Delta\omega/\omega_o\right)$	- Normalized bandwidth.
$n\left(E\right)$	- Electric field dependent refractive index
$n(T)$	- Temperature dependent refractive index
$n(T_{ref})$	- Refractive index at reference temperature T_{ref}

ABBREVIATIONS

ANN	-	Artificial neural network
BBG	-	Broadband generation
BBS	-	Broadband source
C-band	-	Conventional (“erbium window”) band
DBP	-	Delay-bandwidth product
DL	-	Deep learning
E-band	-	Extended band
FBG	-	Fibre Bragg grating
FDTD	-	Finite differences time-domain method
FEM	-	Finite element method
FOS	-	Fibre optic sensors
FWM	-	Four-wave mixing
GVD	-	Group velocity dispersion
L-band	-	Long wavelengths band
LC	-	Liquid crystal
LPG	-	Long-period grating
ML	-	Machine learning
MLP	-	Multilayer perceptron
MMF	-	Multimode fibre
MPB	-	MIT photonic-bands
MSE	-	Mean squared error
NBG	-	Narrowband generation
NDBP	-	Normalized delay-bandwidth product
O-band	-	Original band
OSA	-	Optical spectrum analyser
PA	-	Parametric amplification
PBG	-	Photonic bandgap
PC	-	Photonic crystal
PCF	-	Photonic crystal fibres
PCW	-	Photonic crystal waveguide
PMPCF	-	Polarization-maintaining PCF
PSO	-	Particle swarm optimization

PWE	-	Plane wave expansion
ReLU	-	Rectified linear activation unit
RI	-	Refractive index
S-band	-	Short wavelengths band
SCG	-	Supercontinuum generation
SHG	-	Second harmonic generation
SL	-	Slow light
SOI	-	Silicon-on-insulator
SPM	-	Self-phase modulation
TE	-	Transverse electric
THG	-	Third harmonic generation
TM	-	Transverse magnetic
WDD	-	Wavelength division de-multiplexing
WDM	-	Wavelength division multiplexing

List of Figures

List of Tables

ABSTRACT

Photonic crystals and photonic crystal waveguides are the periodic structures formed in dielectric media. The numerous light controlling capabilities of these structures attracted many researchers to develop various linear and nonlinear application-specific photonic structures. Tunable photonic bandgap, controllable eigen wavelengths and dispersion features help to develop wavelength filters, wavelength routers, optical switches, slow light devices, and all-optical integrated circuits.

The present dissertation focused on tunable features and dispersion features of 2-dimensional photonic crystal waveguides. The tunable features of the waveguide are achieved by active tuning of the refractive index, while the dispersion tailoring is used for developing waveguide structures for slow light applications. MIT Photonic-Bands software is used for performing the simulations. We propose tunable bandgap and dispersion engineering based applications, including a temperature sensor, reconfigurable waveguide, and broadband generation. Machine learning is adopted for simulating the waveguide structures to overcome computational challenges.

A comprehensive and systematic study is performed to achieve increased control over the dispersion curve of the waveguide by geometry tailoring. The radius of air cylinders and their lattice positions are perturbed to enhance the performance of the waveguide. Rings are introduced in the innermost rows for further improvement in the characteristics. Active tuning of the waveguide is achieved in GaAs based 2-dimensional waveguides using electro-optic effect and thermo-optic effect. With the effect of external electric field and slab temperature, PCW features are studied in detail. The work is extended in all the communication bands, including O-band, E-band, S-band, C-band, and L-band. These results can realize tunable optical filters, wavelength routers, and optical interconnectors.

A temperature sensor is modelled to measure a broad range of temperatures using an actively tunable GaAs-based waveguide to study the device applications of photonic waveguides. The structure is designed to get the eigen wavelengths in the near-infrared region. The sensor has a better sensitivity than currently available sensors.

The air cylinders of a lattice shifted waveguide are filled with a refractive index of 1.3. Due to the shift in the innermost row and the microfluidic infiltration, the dispersive properties are enhanced, and the group index is maintained constant over a wider band. The structures are readily reconfigurable by using liquids of different refractive indices. For post-fabrication tuning, this method provides an effective solution.

Broadband generation in a waveguide is studied using a large photonic bandgap waveguide. A photonic bandgap of 108 nm is used for this purpose. A pump at the zero-crossing point of 1515 nm with a peak power of 1 kW is used to study the broadband generation in a waveguide of length 3 mm. The study confirms the possible generation of broadband inside the waveguide structures with a spectral broadening of nearly 89 nm.

Conventional study of PCW using numerical methods is time-consuming. Throughout our studies, we used MIT Photonics Bands software to calculate the structures' eigen frequencies and group velocities. However, with this, the computational times are extensive. We modelled an artificial neural network and trained it using the data generated from conventional sources to overcome this issue. We predicted the dispersion values and group indices within the trained data range. The predicted values are close enough to the conventionally calculated data, with less computational time.

Further, these studies can be extended to design slow light devices based on dispersion tailoring, wideband structures for various linear and nonlinear applications, reconfigurable structures using machine learning, and studying the nonlinear behaviour of the waveguides using machine learning.

Chapter – 1
Introduction

1.1 A brief overview of photonic crystals and photonic crystal waveguides:

Today, high-speed data rates are achieved using optical networks that take information from one point to another. However, these high-speed signals are challenging to control at the network nodes, and hence, various methods are being investigated for achieving control over the optical signals in the time domain [1-3]. The photonic circuits are composed of micro-structured light controlling elements like optical fibres and waveguides. Engineering these waveguides offer potential applications in optical networks, signal routing, switching, and optical buffering [4-7]. In optical networks, Photonic crystals (PCs), photonic crystal waveguides (PCWs), and photonic crystal fibres (PCFs) are attractive with their light controlling capabilities.

PCs are the structures formed by periodic arrangement of refractive index, for achieving specific applications like transmission or reflection of a band of frequencies, slowdown of light due to dispersion mechanism, parametric amplification, optical switching, and even nonlinear effects such as second harmonic generation, four-wave mixing [8-12]. The structures are realized by various methods, including creating air holes and placing parallel cylindrical rods in semiconductor material slabs [13-14]. These structures possess a photonic bandgap, which determines the frequency of operation. The most common method of altering a PC's bandgap and dispersion features is altering its geometry [15-18]. PCWs are generated by eliminating one row of air holes/cylinders from the geometry.

In the past two decades, the scientific community has shown greater interest in tailoring PCW for nonlinear applications. To design application-specific waveguides, the geometrical parameters and the effective refractive index of the waveguide are tailored. The dispersion engineering by geometrical parameters offers many exciting applications. Tailoring the geometry by employing variation in air cylinders' radius by varying their lattice positions and waveguide width controls the dispersion features [18-21]. Such methods report various waveguides for applications like slow light, second harmonic generation, four-wave mixing, optical switching, and supercontinuum generation [10, 22-25]. However, geometrical tailoring has certain limitations. Once the design process is completed, and the fabrication is done, the waveguide features cannot be altered. Hence this method leads to the passive tuning

of the photonic bandgap. On the other side, the waveguide features can be tuned post-fabrication by applying an external electric field, magnetic field, heat, and optofluidic infiltration. In these methods, the material's refractive index from which the waveguide is fabricated is tuned by refractive index dependence on the external electric field, magnetic field, or heat [4, 26-29]. With the dependence of the refractive index on external parameters, the features of the waveguide can be controlled precisely, and such methods can also be used for sensing applications.

1.1.1 Classification of PC structures:

PCs can be classified based on their refractive index periodicity. One-dimensional PCs are often alternating layers with different dielectric constants, such as Bragg mirrors. Two-dimensional PCs usually consist of periodic holes or rods in a dielectric medium. The variation in the refractive index is in two directions, while in the other direction, it is fixed. Three dimensional PCs are structures with refractive index variation in three directions and are the most difficult to fabricate. Proposed constructions of such periodic nanostructures include spheres in a diamond lattice, Yablonovite, the woodpile crystal, inverse opals and stacks of two-dimensional crystals. Figure 1.1 shows the schematic arrangement of one-, two-, and three-dimensional PC structures.

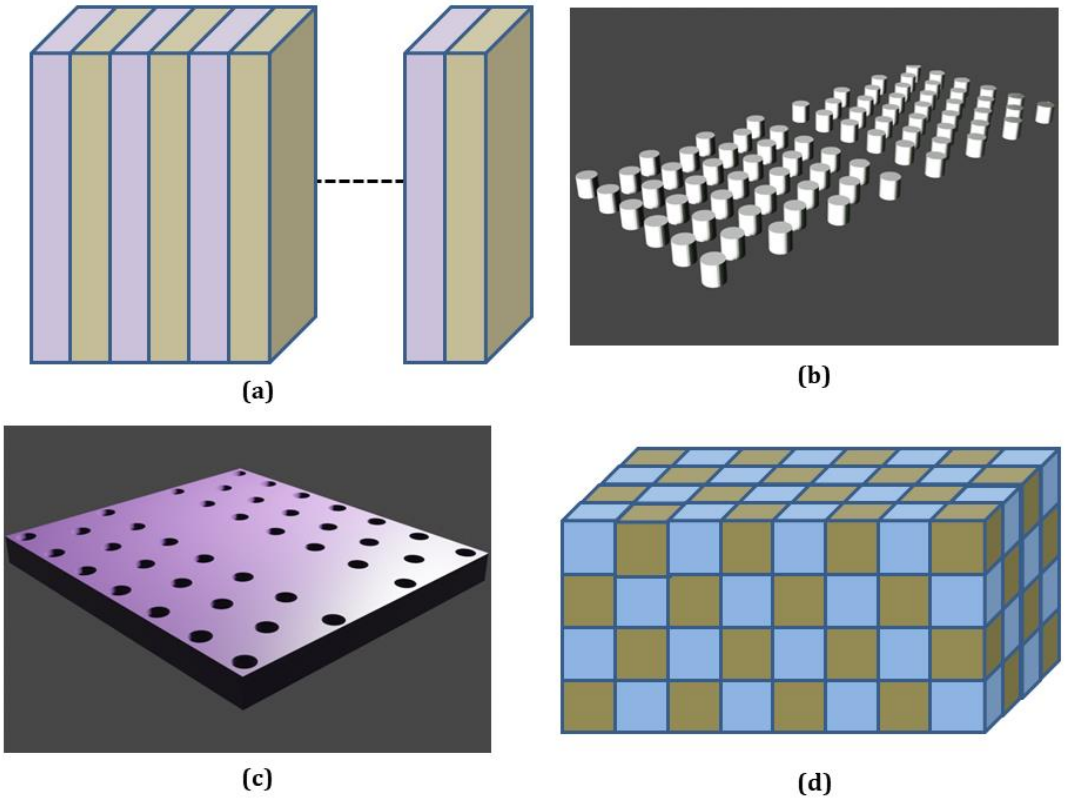

Figure 1.1: (a) one-dimensional PC (b) two-dimensional PC with dielectric cylinders (c) two-dimensional PCW with air cylinders in dielectric slab and (d) three-dimensional PC.

1.1.2 Photonic crystal waveguides:

PCWs can support small bending radius waveguide bends with the almost total transmission. This feature makes PCWs a candidate for waveguides in densely integrated photonic circuits. PCW can be formed by creating a line defect in a one- or two-dimensional PC. Figure 1.1 (c) is a PCW formed by eliminating one row from the lattice of the two-dimensional PC.

Conventional dielectric waveguides confine propagating beams by an index of refraction difference between the waveguide core and the waveguide cladding. PCWs are most often formed by a linear defect, consisting of a row of modified lattice, patterned into a high index dielectric membrane. The guiding is due to a mixture of total internal reflection at the high index membrane/low index cladding interfaces and distributed reflections from the PC in-plane. Because this confinement does not exclusively dependent on the total internal reflection, the transmission loss through small bending radius waveguide branches and bends can be made very small. Optical couplers, wavelength division multiplexing (WDM), and beam splitters can be realized using these structures.

1.1.3 Modes in PCW:

Even though PCW structures are mixed dielectric media, the light propagation obeys the well-known macroscopic Maxwell's equations. A position vector can map different regions of a PCW with a homogeneous dielectric material. One can consider the following assumptions for solving these equations for PCW structures.

i) No free charge carriers or currents are present inside the structure.

ii) Time invariant structure.

iii) The field strengths are small, and the medium is lossless.

By the above assumptions, Maxwell's equations can be modified, and by doing this, one can find the electric and magnetic fields associated with the structure.

The electric and magnetic fields are space and time dependent. However, as Maxwell's equations are linear, the time and space dependences can be separated, resulting in the equations for light propagation in PCW. These equations are known as harmonic modes or states of the system. One can obtain the spatial dependent field by writing the harmonic modes as the complex-valued fields and picking up the real part. By writing the harmonic mode as a product of spatial pattern and a complex exponential, it is given by [30]

$$\vec{H}\left(\vec{r},t\right)=\vec{H}\left(\vec{r}\right)e^{-i\omega t} \qquad (1.1)$$

$$\vec{E}\left(\vec{r},t\right)=\vec{E}\left(\vec{r}\right)e^{-i\omega t} \tag{1.2}$$

Substituting the equations (1.1) and (1.2) in Maxwell's equations and solving them for the spatial field, it is given by [30]

$$\nabla\times\vec{E}\left(\vec{r}\right)-i\omega\mu_0\vec{H}\left(\vec{r}\right)=0 \tag{1.3}$$

$$\nabla\times\vec{H}\left(\vec{r}\right)+i\omega\varepsilon_0\varepsilon\left(\vec{r}\right)\vec{E}\left(\vec{r}\right)=0 \tag{1.4}$$

By coupling the equations (1.3) and (1.4) and by eliminating $\vec{E}$, one can get an equation containing only $\vec{H}$ which is given by [30]

$$\nabla\times\left(\frac{1}{\varepsilon(r)}\nabla\times\vec{H}\left(\vec{r}\right)\right)=\left(\frac{\omega}{c}\right)^2\vec{H}\left(\vec{r}\right) \tag{1.5}$$

Similarly, the equation for $\vec{E}$ is given by

$$\nabla\times\nabla\times\vec{E}(r)=\left(\frac{\omega^2}{c^2}\right)\varepsilon(r)\vec{E}(r) \tag{1.6}$$

Due to the symmetry in PCWs, the electromagnetic modes can be written as Bloch states. To adopt Bloch's theorem, a periodic function $\vec{u}\left(\vec{r}\right)$ must be defined, and it is considered here as

$$\vec{u}\left(\vec{r}\right)=\vec{u}\left(\vec{r}+\vec{R}\right) \tag{1.7}$$

for all lattice vectors $\vec{R}$. And then the existing Bloch state in the structure can be re-written as

$$\vec{H}\left(\vec{r}\right)=\exp\left[i\vec{k}\cdot\vec{r}\right]\vec{u}\left(\vec{r}\right) \tag{1.8}$$

By substituting this expression in the equations (1.5) & (1.6) and solving, one can calculate the eigen states in the PCW. In the present case, MPB is used on the Ubuntu platform for performing the simulations.

1.1.4 Numerical methods and computational techniques:

Numerical methods such as finite differences time-domain method (FDTD) [23], finite element method (FEM) [31], and plane wave expansion (PWE) [32] are used frequently for solving the coupled equations (1.5 and 1.6) stated in the previous section. The designed eigen problem can also be solved using various computer programs and software packages. Our studies used MIT Photonic-Bands (MPB) software [33] on the Ubuntu platform to obtain the eigen frequencies, group velocities, and field distributions in the waveguide. Apart from MPB, MEEP and MATLAB can also be used for solving these coupled equations.

1.2 Research gaps and scope of the work:

Application-specific waveguides can be achieved by dispersion engineering. Some of the dispersion engineering works in the recent past include investigation of the group velocity dispersion in a PCW with a triangular lattice [34], structural tuning [35], adopting circular and elliptical air holes in the lattice [36], using graded refractive index profiles [37], longitudinal lattice shift of innermost rows [38], designing optical buffer using PC coupled-cavity waveguide [39] subjected to an external electric field, tunable photonic bandgap by external heat [40], by liquid crystal infiltration [26, 41] and microfluidic infiltration [28,42]. Slow light of the order of c/100, four-wave mixing, electric field sensing, optical buffers, and wavelength filters are realized using such waveguide designs.

The designing of optical elements before fabrication is an essential process. This process helps reduce the fabrication time and costs during optical milling. Various numerical methods can do the designing and analysis of PCWs. The geometrical parameters, the introduced perturbations, refractive indices, and their variation with external electric field and heat are programmed and executed to obtain the features of the waveguides. The output parameters are analyzed to choose the best design. By understanding the importance of dispersion engineering, we majorly focused on tailoring the geometry and refractive index modulation to improve the waveguide's features.

We identified the following research gaps which have considerable scope for working.

- Dispersion engineered structures for slow light applications
- Sensing by engineered photonic crystal waveguides
- Conventional methods of computing the bandgap
- Active and reconfigurable structures for on-chip application

1.3 Objectives of the thesis:

The present research work is carried out based on the following objectives:

- Studying the dispersion tailoring features of 2-dimensional PCWs.
- Exploring the new designs of PCWs for slow-light device applications and to improve their efficiency.
- Designing tunable structures for wavelength filters and light modulating applications.
- Developing the algorithms for training the machine for optical data prediction.

1.4 Organization of the thesis:

Our work majorly focused on the dispersion engineering of the PCWs. Initially, we focused on dispersion engineering by geometry. Variation in the radius of holes, lattice shift, lattice twist, and ring-like structures are introduced in the waveguide to improve its features. Later we studied the features of the waveguide by modulating the refractive index using an external electric field and applied heat. The photonic bandgap is tuned, and applications based on the tunable bandgap are proposed. An algorithm is modelled to train the machine using conventionally generated data to predict the waveguide's dispersion values and group index at random physical perturbations. Figure 1.2 illustrates the organization of the thesis work.

Brief literature on the dispersion engineering of the PCW structures is presented in Chapter 2. Dispersion engineering by tailoring the geometry (passive tuning) and refractive index modulation (active tuning) are systematically presented. Further, application-specific structures are also presented.

In Chapter 3, we present a comprehensive and systematic study to achieve increased control over the dispersion curve of the waveguide operating at telecom wavelengths. The effect of the air cylinder's radius and lattice positions on the dispersion features is studied chiefly in a line-defect PCW. For this purpose, perturbations are introduced in the radius and positions of the air cylinders. The combined effect of lattice shift, lattice twist, and introduction of rings in the innermost rows on the slow light features is also studied. The rings are introduced in the first and second innermost rows of the waveguide. Slow light is characterized by calculating the group index, second and fourth-order dispersions, and delay-bandwidth products. The calculations are performed using the MPB software, and the waveguide is characterized. This systematic study can tune the waveguide with the desired range of group index and bandwidth with controlled dispersion properties. Structures with a flat band of 30 nm and above are achieved with very low dispersion. The developed structures may find applications in optical delays and optical buffers.

In Chapter 4, the effect of external electric field and slab temperature on PCW features is studied in detail. A two-dimensional PCW is used for studying the effects of external electric field and slab temperature. The active tuning of the PBG is achieved by the temperature and electric field dependence of the refractive index of the slab. Electro-optic and thermo-optic effects are employed to calculate the refractive index of the slab material.

Organization of the thesis

Chapters	Key structures/Properties	Aim and studied cases
3	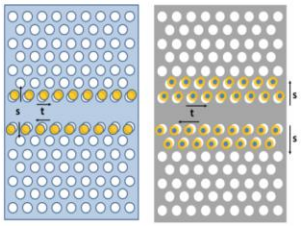 Lattice perturbed ring introduced photonic crystal waveguides	• Geometrical perturbations such as radius, lattice shift and twist • Introducing ring like structures • Slow light features
4	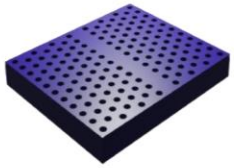 Photonic crystal waveguide with external electric filed and heat	• Active tuning and wavelength filtering by controlling temperature • Active tuning by external electric field • Temperature effect on slow light bands
5	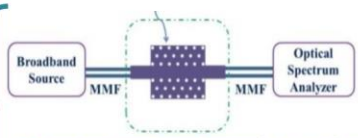 Temperature sensor using active photonic crystal waveguide	• Temperature sensing by photonic crystal waveguide • Large range of sensing with higher sensitivity
6	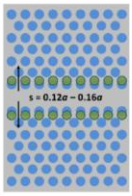 Liquid infiltrated active photonic crystal waveguide	• Reconfigurable photonic crystal waveguide and refractive index sensing • Higher flat-band with microfluidic infiltration
7	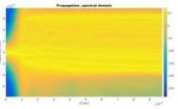 Broadband generation in photonic crystal waveguide	• Broadband generation in dispersion engineered photonic crystal waveguides
8	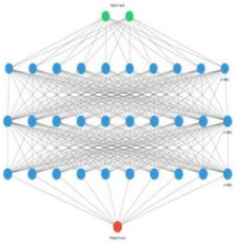 Artificial neural network for studying photonic crystal waveguide	• Studying photonic crystal waveguides using Artificial Neural Networks (ANNs) • Analysing the eigen wavelengths • Prediction within selected range

Figure 1.2: Organization of the thesis

The refractive index variations are considered in the temperature range of 100 K to 400 K and the electric field in the range of 0 – 500 kV/cm. The bandgap values ranging from 24 nm to 58 nm are achieved by external control. The work is extended in all the communication bands, including O-band, E-band, S-band, C-band, and L-band. The group indices are also calculated with changes in temperature and electric field. These results can be realized by tunable optical filters, wavelength routers, and optical interconnectors.

In Chapter 5, a temperature sensor is modelled to measure a broad range of temperatures using an actively tunable GaAs-based PCW. A hexagonal lattice structure with seven rows of air cylinders is used to form the waveguide. The thermo-optic effect is employed to consider the variations in the refractive index of the slab material with temperature, and these refractive indices are used to calculate the variations in the photonic bandgap, band edges, and the eigen wavelengths. Temperatures ranging from 10 K to 400 K are considered for this purpose. Simulations are performed in MPB software to calculate the eigen frequencies of the structure. The structure is designed to get the eigen wavelengths in the near-infrared region. In these studies, sensitivity in the range of $375.16 \pm 0.791 \times 10^{-3}$ to $378.55 \pm 0.794 \times 10^{-3}$ pm/K is observed. The proposed structure may be used as a temperature sensor in high and low-temperature regions with higher sensitivity.

Reconfigurable PCW structures are presented in Chapter 6. Group index and dispersive properties of the PCW can be varied by microfluidic infiltration in the waveguide lattice to achieve a reconfigurable waveguide. Initially, we studied the dispersive properties of a GaAs-based PCW. In this waveguide, a shift is introduced in the first innermost row, and the air cylinders are filled with liquid of refractive index 1.3. Due to the shift in the innermost row and the microfluidic infiltration, the dispersive properties are enhanced, and the group index is maintained constant over a wider band. The structures are readily reconfigurable by using liquids of different refractive indices. However, in our study, all the PCWs are designed to obtain the eigen wavelengths near around 1550 nm wavelength. Electrically active liquids can also be introduced inside the lattice, and methods such as the electro-optic effect can be accompanied to enhance the features of the PCW. Reconfigurable optical devices can be realized from these studies.

In Chapter 7, broadband generation in a PCW is studied with developed large photonic bandgap waveguides. A PCW with a photonic bandgap of 108 nm is used for this purpose. A pump at the zero-crossing point of 1515 nm with a peak power of 1 kW is used to study the broadband generation in a PCW of length 3 mm. The study confirms the possible generation of broadband in the PCW structure.

Conventional study of PCW using numerical methods is time-consuming. Throughout our studies, we used MPB programming for calculating the eigen frequencies and group velocities of the structures. However, with MPB, the computational times are extensive. We modelled a neural network and trained it using the data generated from the MPB programming to overcome this issue. We predicted the dispersion values and group indices within the trained range by training the model. These results are presented in Chapter 8. The predicted values are close enough to the conventionally calculated data, with less computational time. Chapter 9 presents brief conclusions on our work and a road map for future studies.

References:

[1] T. F. Krauss, "Slow light in photonic crystal waveguides," *J. Phys. D. Appl. Phys.*, vol. 40, no. 9, pp. 2666–2670, May 2007, https://doi.org/10.1088/0022-3727/40/9/S07

[2] T. Baba, H. C. Nguyen, N. Yazawa, Y. Terada, S. Hashimoto, and T. Watanabe, "Slow-light Mach-Zehnder modulators based on Si photonic crystals," *Sci. Technol. Adv. Mater.*, vol. 15, no. 024602, pp. 1-11, Apr. 2014, https://doi.org/10.1088/1468-6996/15/2/024602

[3] Y. A. Vlasov, M. O'Boyle, H. F. Hamann, and S. J. McNab, "Active control of slow light on a chip with photonic crystal waveguides," *Nature*, vol. 438, no. 7064, pp. 65–69, Nov. 2005, https://doi.org/10.1038/nature04210

[4] M. Haurylau, S. P. Anderson, K. L. Marshall, and P. M. Fauchet, "Electrical modulation of silicon-based two-dimensional photonic bandgap structures," *Appl. Phys. Lett.*, vol. 88, no. 061103, pp. 1–3, Feb. 2006, https://doi.org/10.1063/1.2172070.

[5] L. O'Faolain, D. M. Beggs, T. P. White, T. Kampfrath, K. Kuipers, and T. F. Krauss, "Compact optical switches and modulators based on dispersion engineered photonic crystals," *IEEE Photonics J.*, vol. 2, no. 3, pp. 404–414, Jun. 2010, https://doi.org/10.1109/JPHOT.2010.2047918

[6] T. Baba, "Slow light in photonic crystals," *Nat. Photonics*, vol. 2, no. 8, pp. 465-473, Aug. 2008, https://doi.org/10.1038/nphoton.2008.146

[7] M. R. Sprague et al., "Broadband single-photon-level memory in a hollow-core photonic crystal fibre," *Nat. Photonics*, vol. 8, no. 4, pp. 287–291, Mar. 2014, https://doi.org/10.1038/nphoton.2014.45

[8] A. Willinger, S. Roy, M. Santagiustina, S. Combrié, A. De Rossi, and G. Eisenstein, "Narrowband optical parametric amplification measurements in $Ga_{0.5}In_{0.5}P$ photonic crystal waveguides," *Opt. Express*, vol. 23, no. 14, pp. 17751-17757, Jun. 2015, https://doi.org/10.1364/oe.23.017751

[9] T. Tanabe, M. Notomi, S. Mitsugi, A. Shinya, and E. Kuramochi, "All-optical switches on a silicon chip realized using photonic crystal nanocavities," *Appl. Phys. Lett.*, vol. 87, no. 151112, pp. 1–3, Oct. 2005, https://doi.org/10.1063/1.2089185

[10] T. V. Murzina, F. Y. Sychev, I. A. Kolmychek, and O. A. Aktsipetrov, "Tunable ferroelectric photonic crystals based on porous silicon templates infiltrated by sodium nitrite," *Appl. Phys. Lett.*, vol. 90, no. 16, Apr. 2007, https://doi.org/10.1063/1.2724928

[11] H. Saghaei and A. Ghanbari, "White light generation using photonic crystal fiber with sub-micron circular lattice," *J. Electr. Eng.*, vol. 68, no. 4, pp. 282–289, Sep. 2017, https://doi.org/10.1515/jee-2017-0040

[12] L. Velazquez-Ibarra, A. Diez, E. Silvestre, and M. V. Andres, "Tunable Four-Wave Mixing Light Source Based on Photonic Crystal Fibers with Variable Chromatic Dispersion," *J. Light. Technol.*, vol. 37, no. 22, pp. 5722–5726, Nov. 2019, https://doi.org/10.1109/JLT.2019.2944215

[13] S. I. Takayama, H. Kitagawa, Y. Tanaka, T. Asano, and S. Noda, "Experimental demonstration of complete photonic band gap in two-dimensional photonic crystal slabs," *Appl. Phys. Lett.*, vol. 87, no. 061107, pp. 1–3, Aug. 2005, https://doi.org/10.1063/1.2009060

[14] D. M. Pustai, A. Sharkawy, S. Shi, and D. W. Prather, "Tunable photonic crystal microcavities," *Appl. Opt.*, vol. 41, no. 26, pp. 5574-5579, Sep. 2002, https://doi.org/10.1364/AO.41.005574

[15] N. L. Janrao, R. Zafar, and V. Janyani "Improved design of photonic crystal waveguides with elliptical holes for enhanced slow light performance," *Opt. Eng.*, vol. 51, no. 6, pp. 064001(1-7), Jun. 2012, https://doi.org/10.1117/1.OE.51.6.064001

[16] A. Saynatjoki, M. Mulot, J. Ahopelto, and H. Lipsanen, "Dispersion engineering of photonic crystal waveguides with ring-shaped holes," *Opt. Express*, vol. 15, no. 13, pp. 8323-8328, Jun. 2007, https://doi.org/10.1364/OE.15.008323

[17] J. Li, T. P. White, L. O'Faolain, A. Gomez-Iglesias, and T. F. Krauss, "Systematic design of flat band slow light in photonic crystal waveguides," *Opt. Express*, vol. 16, no. 9, pp. 6227-6232, Apr. 2008, https://doi.org/10.1364/oe.16.006227

[18] D. Wang et al., "Slow light engineering in polyatomic photonic crystal waveguides based on square lattice," *Opt. Commun.*, vol. 284, no. 24, pp. 5829–5832, Dec. 2011, https://doi.org/10.1016/j.optcom.2011.07.080

[19] M. Pourmand, A. Karimkhani, and F. Nazari, "Wideband and low-dispersion engineered slow light using liquid infiltration of a modified photonic crystal waveguide," *Appl. Opt.*, vol. 55, no. 35, pp. 10060-10066, Dec. 2016, https://doi.org/10.1364/ao.55.010060

[20] L. H. Frandsen, A. V. Lavrinenko, J. Fage-Pedersen, and P. I. Borel "Photonic crystal waveguides with semi-slow light and tailored dispersion properties," *Opt. Express*, vol. 14, no. 20, pp. 9444-9450, Sep. 2006, https://doi.org/10.1364/OE.14.009444

[21] P. Colman, S. Combrié, G. Lehoucq, and A. De Rossi, "Control of dispersion in photonic crystal waveguides using group symmetry theory," *Opt. Express*, vol. 20, no. 12, pp. 13108-13114, May 2012, https://doi.org/10.1364/OE.20.013108.

[22] S. M. Mirjalili, "Ellipse-ring-shaped-hole photonic crystal waveguide," *Optik (Stuttg).*, vol. 126, no. 1, pp. 56–60, Jan. 2015, https://doi.org/10.1016/j.ijleo.2014.07.123

[23] J. Ma and C. Jiang, "Demonstration of ultraslow modes in asymmetric line-defect photonic crystal waveguides," *IEEE Photonics Technol. Lett.*, vol. 20, no. 14, pp. 1237–1239, Jun. 2008, https://doi.org/10.1109/LPT.2008.926018

[24] C. Monat et al., "Four-wave mixing in slow light engineered silicon photonic crystal waveguides," *Opt. Express*, vol. 18, no. 22, pp. 22915-22927, Oct. 2010, https://doi.org/10.1364/oe.18.022915.

[25] L. C. Van, A. Anuszkiewicz, and A. Ramaniuk, "Supercontinuum generation in photonic crystal fibres with core filled with toluene." *J. Opt.*, vol. 19, no. 125604, pp. 1-9, Nov. 2017, https://doi.org/10.1088/2040-8986/aa96bc

[26] S. M. Weiss, M. Haurylau, and P. M. Fauchet, "Tunable photonic bandgap structures for optical interconnects," *Opt. Mater. (Amst).*, vol. 27, no. 5, pp. 740–744, Feb. 2005, https://doi.org/10.1016/j.optmat.2004.08.007

[27] B. K. Singh and P. C. Pandey, "Tunable temperature-dependent THz photonic bandgaps and localization mode engineering in 1D periodic and quasi-periodic structures with graded-index materials and InSb," *Appl. Opt.*, vol. 57, no. 28, pp. 8171-8181, Oct. 2018, https://doi.org/10.1364/ao.57.008171.

[28] Y. Zhao, Y. N. Zhang, and Q. Wang, "Optimization of slow light in slotted photonic crystal waveguide with liquid infiltration," *J. Light. Technol.*, vol. 31, no. 14, pp. 2448–2454, Jun. 2013, https://doi.org/10.1109/JLT.2013.2267272.

[29] F. Ghasemi, S. R. Entezar, and S. Razi, "Terahertz tunable photonic crystal optical filter containing graphene and nonlinear electro-optic polymer," *Laser Phys.*, vol. 29, no. 056201, pp. 1-8, Mar. 2019, https://doi.org/10.1088/1555-6611/ab05c2

[30] J. D. Joannopoulos, S. G. Johnson, J. N. Winn, and R. D. Meade, "*Photonic Crystals: Molding the Flow of Light*," 2nd Edn., Princeton University Press, Oct. 2011, http://ab-initio.mit.edu/book/photonic-crystals-book.pdf

[31] M. F. O. Hameed, M. Y. Azab, A. M. Heikal, S. M. El-Hefnawy, and S. S. A. Obayya, "Highly sensitive plasmonic photonic crystal temperature sensor filled with liquid crystal," *IEEE Photonics Technol. Lett.*, vol. 28, no. 1, pp. 59–62, Jan. 2016, https://doi.org/10.1109/LPT.2015.2480339

[32] J. Cos, J. Ferré-Borrull, J. Pallarès, and L. F. Marsal, "Analysis of tunable bandgaps in liquid crystal-infiltrated 2D silicon photonic crystals," *Appl. Phys. B Lasers Opt.*, vol. 100, no. 4, pp. 833–839, Aug. 2010, https://doi.org/10.1007/s00340-010-4172-x

[33] S. G. Johnson and J. D. Joannopoulos, "Block-iterative frequency-domain methods for Maxwell's equations in a planewave basis," *Opt. Express*, vol. 8, no. 3, pp: 173-190, Jan. 2001, https://doi.org/10.1364/OE.8.000173 and software available at http://ab-initio.mit.edu/mpb/doc/mpb.pdf

[34] A. Y. Petrov and M. Eich, "Zero dispersion at small group velocities in photonic crystal waveguides," *Appl. Phys. Lett.*, vol. 85, no. 21, pp. 4866–4868, Nov. 2004, https://doi.org/10.1063/1.1815066

[35] M. Notomi, A. Shinya, K. Yamada, J. Takahashi, C. Takahashi and I. Yokohama, "Structural tuning of guiding modes of line-defect waveguides of silicon-on-insulator photonic crystal slabs," *IEEE J. Quantum Electron.*, vol. 38, no. 7, pp. 736-742, Jul. 2002, https://doi.org/10.1109/JQE.2002.1017583

[36] N. L. Janrao, R. Zafar, and V. Janyani "Improved design of photonic crystal waveguides with elliptical holes for enhanced slow light performance," *Opt. Eng.*, vol. 51, no. 6, pp. 064001(1-7), Jun. 2012, https://doi.org/10.1117/1.OE.51.6.064001

[37] B. K. Singh, P. Kumar, and P. C. Pandey, "Tunable photonic band-gaps in one-dimensional photonic crystals containing linear graded index material," *Appl. Phys. B Lasers Opt.*, vol. 117, no. 3, pp. 947–956, Aug. 2014, https://doi.org/10.1007/s00340-014-5913-z

[38] A. Hocini, M. Maache, and D. Khedrouche, “Wideband and low dispersion slow light by altering the geometry of a photonic crystal waveguide,” *Opt. Commun*., vol. 427, no. 15, pp. 396–404, Jul. 2018, https://doi.org/10.1016/j.optcom.2018.06.077

[39] H. Tian, F. Long, W. Liu, and Y. Ji, “Tunable slow light and buffer capability in photonic crystal coupled-cavity waveguides based on electro-optic effect,” *Opt. Commun.,* vol. 285, no. 10–11, pp. 2760–2764, May 2012, https://doi.org/10.1016/j.optcom.2012.01.086

[40] P. Halevi and F. Ramos-Mendieta, “Tunable photonic crystals with semiconducting constituents,” *Phys. Rev. Lett*., vol. 85, no. 9, pp. 1875–1878, Aug. 2000, https://doi.org/10.1103/PhysRevLett.85.1875

[41] G. Mertens, R. B. Wehrspohn, H. S. Kitzerow, S. Matthias, C. Jamois, and U. Gösele, “Tunable defect mode in a three-dimensional photonic crystal,” *Appl. Phys. Lett.*, vol. 87, no. 241108, pp. 1–3, Dec. 2005, https://doi.org/10.1063/1.2139846

[42] Y. Peng, J. Hou, Y. Zhang, Z. Huang, R. Xiao, and Q. Lu, “Temperature sensing using the bandgap-like effect in a selectively liquid-filled photonic crystal fiber,” *Opt. Lett.*, vol. 38, no. 3, pp. 263-265, Feb. 2013, https://doi.org/10.1364/ol.38.000263

Chapter – 2
Dispersion Engineering in Photonic Crystal Waveguides

This chapter presents the brief literature on the tuning of photonic bandgap, active tuning, dispersion engineering, and slow light generation in photonic crystal waveguides. Various methods to achieve tunable bandgap, their implementation, advantages, and disadvantages are discussed. Factors affecting dispersion engineering, slow light generation and maintenance are analysed. The recent developments in computation techniques in machine learning and deep learning associated with photonic crystals and photonic crystal waveguides are also presented. In addition, various selective applications and devices based on photonic crystal waveguides and the research gaps have discoursed.

2.1 Dispersion engineering:

Dispersion engineering is the designing and modifying the waveguides for light controlling applications. It is an effective tool for a wide range of photonic applications. The optimization process includes geometrical engineering, fabrication techniques and material processing methods to design low dispersion structures. In figure 2.1 most used dispersion engineering methods are presented. The dispersion engineering in PC was discussed by Petrov and Eich [1] in detail. The group velocity dispersion of a PC with a triangular lattice was studied meticulously. The authors explained the engineering of dispersion relations in a PCW for achieving slow light. The effect of the radii of the holes on the group velocity was demonstrated. With altered waveguide width of W0.7, it was found that PCW offers enough degrees of freedom to achieve a 1 THz bandwidth with a constant group velocity of 0.02c. The second and third-order dispersions were reduced entirely in the proposed PCW.

In the subsequent sections, we discussed dispersion engineering by tuning the PBG with passive and active methods, slow light generation and maintenance, device applications and machine learning techniques. In the passive tuning, fabrication methods, geometrical perturbations such as lattice shift, lattice twist, variation in radius of air holes and introduction of ring-like structures are discussed. In the active tuning of the PBG, the effect of mechanical stress, electro-optic effect, thermo-optic effect, magneto-optic effect, microfluidic infiltration, and liquid crystal infiltration are discussed. Device and sensor

applications of the dispersion engineered structures and nonlinear applications of slow light such as supercontinuum generation, broadband and narrowband generation are discussed. The research gaps are mentioned wherever found.

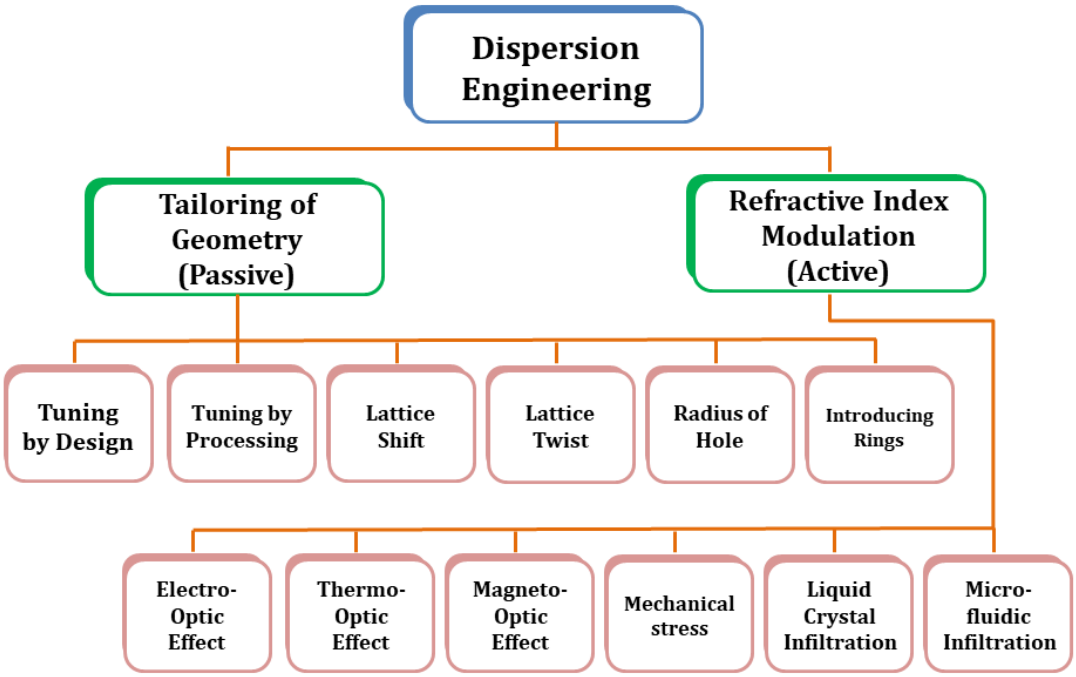

Figure 2.1: Methods of dispersion engineering in PC and PCW.

2.2 Tuning of photonic bandgap:

The fundamental feature of the PC structures is PBG, which arises from the periodic arrangement of dielectric materials. The periodic dielectric modulation of electromagnetic waves results in the manipulation of light. Since the first PBG structure was discovered, the capability to tune the PBG across a wide wavelength range has been highly desirable [2]. Therefore, obtaining PC structures having a large on-demand PBG has been an ever-attractive study but has remained a challenge.

The PBG of a PC or PCW is readily tunable. As discussed earlier, the eigen wavelengths can be tuned either by changing the geometry or the effective refractive index. If the tuning is achieved by changing geometry or the base material, such tuning is referred to as passive tuning. Once the PC or PCW is fabricated, its PBG is fixed in this method. In the other methods, the material's refractive index is tuned post-fabrication. This change in refractive index can be implemented by electro-optic effect, thermo-optic effect, magneto-optic effect, liquid infiltration and introduction of liquid crystals to the crystal lattice. As the tuning is done post-fabrication, this method is called active tuning and can be implemented to achieve desired eigen wavelengths with high precision.

2.3 Passive tuning of photonic bandgap:

2.3.1 Geometry:

Geometrical tailoring is one of the chief tools in dispersion engineering. For designing application-specific PC and PCW, one can alter the geometry in various ways. Figure 2.2 shows the geometrical alterations like point defect PC, line defect PC, PC with bend and bend waveguide. These methods majorly depend on the fabrication methods for achieving dispersion engineering. John and Busch [3] described the fabrication of three dimensional PBG materials based on self-organizing templates. FCC lattice of closely packed weakly sintered spheres were organized to form the band structure. HCP and hexagonal self-organizing lattice-based PCs were also fabricated in this method. The PBG materials were formed by infiltrating the base structure with semiconductor materials, such as Si, Ge or GaP and removing the template. This method forms the inverse opals structures by filling them with high refractive index materials. The structures exhibit a pseudo-PBG and full PBG in the near-visible spectrum. Large scale 3-dimensional PBG structures can be realized from this method. Also, by this semiconductor infiltration method, perfect periodicity over a few hundred lattice constants was reported. However, fine-tuning of the PBG can be achieved by the material synthesis process.

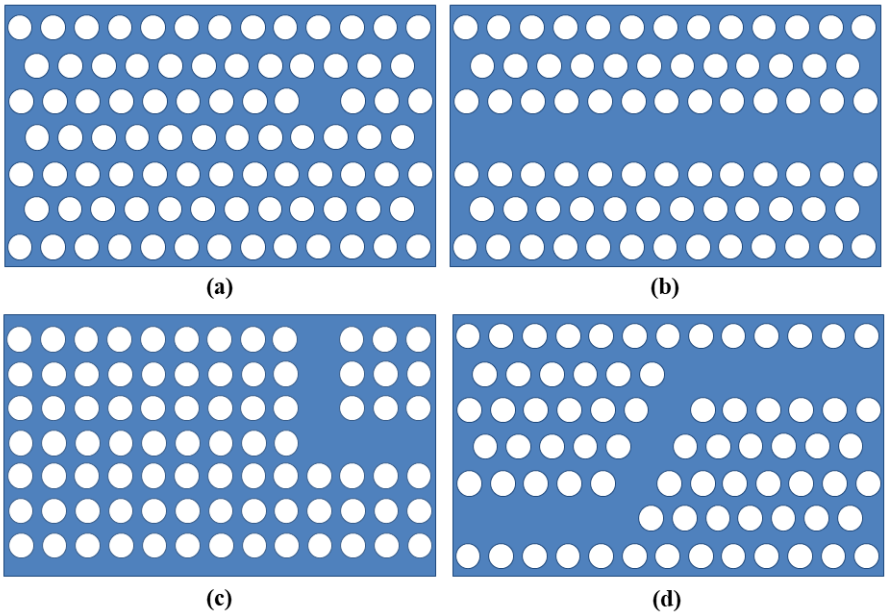

Figure 2.2: (a) Point defect in PC (b) line defect in PC (PCW) (c) PC with bend (d) Waveguide with bend

Robust localization of photons or trapping can be observed in structures with single point defects, while multiple defects can control the propagation. Noda et al. [4] introduced artificial defects into the lattice of the PC slabs and manipulated the light. The photon trapping was demonstrated in the 2-dimensional PBG structure by introducing a single defect

in the structure. In the proposed structure, the defect is of the order of one wavelength. In this work, the photons propagating through the linear waveguide were localized and trapped by the artificial defect. Later these photons were emitted to free space. The structure can be used as an optical add or drop filter in optical communication. Such add or drop filters are helpful in ultra-small optical devices. The other advantage of this structure is that the structure's geometry can control the defect's Q-value, and hence the working frequency can be directly controlled.

In 2002, Notomi et al. [5] demonstrated the structural tuning of the PCW. Efficient single-mode waveguides were realized by tuning the width of the waveguide. Silicon-on-insulator PC slabs are used for this purpose. Also, these experimental results were well agreed with the 3-dimensional FDTD calculations. In this method, a propagation loss of 6 dB/mm was measured. It was observed that the modes of the PCW can be tuned by controlling the geometrical width of the waveguide. The propagation loss was sufficiently small for optical circuits. Generally, the line defect PC slab modes are not helpful for integrated circuits. However, by tuning the width of the waveguide, the modes were within the PBG and are helpful in PCW based integrated circuits. For a rectilinear motion of the light, the width of the waveguide can be reduced, while for a bend, modification in the geometry is required. Hence, controlling the width of the waveguide was one of the structural tuning methods for tuning the PBG. Compared to conventional total internal reflection-based waveguiding, the line defect PCW offers much freedom in designing. With line-defect waveguides, one can combine the Bragg reflection and total internal reflection and achieve various guiding and confining techniques. Maybe this is the first work that demonstrated the possibility of designing a line defect waveguide and its structural tuning.

Takayama et al. [6] investigated the complete bandgap in 2-dimensional PC slabs. In these structures, both TE and TM modes exhibit the complete bandgap. Theoretically, a full band PBG was observed. However, a complete PBG was not observed in a fabricated 2-dimensional slab. Air holes arranged in triangular lattice were used to achieve the PBG. The overlapping of TE and TM polarization modes in PBG was also reported in this method.

In 2012, Janrao et al. [7] proposed a new design for SL generation in PCW. In this method, circular and elliptical air holes were used in a hexagonal lattice of the PCW. As a part of the geometrical engineering, the width of the PCW was varied, and the two innermost rows were replaced with elliptical holes. A background material with a refractive index of 2.84 was used to form the PCW. A large, normalized delay-bandwidth product (NDBP) was obtained by introducing the elliptical air cylinders. A nearly zero-dispersion was achieved

with a larger bandwidth. Ultra-low group velocity dispersion (GVD) was observed in the above bandwidth. It was also observed that the orientation of the elliptical holes affects the NDBP of the waveguide. The NDBP of the waveguide was controlled using radius R1 of the elliptical hole, and a maximum NDBP was observed at R1 = 0.395*a* and R2 = 0.206*a*, where '*a*' is the lattice constant of the waveguide. The increase in R1 increased the bandwidth of the waveguide.

In 2014, Singh et al. [8] had demonstrated a method to control the PBG in 1-dimensional PC using graded-index materials. Fibonacci sequence was used to form the unit cell of the PC structure. Ten periods of the second, third and fourth generation of the sequence were used in the design. During the design of 1-dimensional PC, linear graded-index material was used to form one layer while a standard dielectric material formed another layer. The analysis of the PBG was done in the THz region using a theoretical model based on the transfer matrix method. PBG was controlled by changing the grading profiles and thickness of the layers. Also, the number of PBGs increased with an increase in the thickness of the layers. Here, the bandwidth of the PBG could be controlled by changing the contrast of the refractive indices of the graded layers. Therefore, using this method, one can introduce graded index layers in the 1-dimensional PC structures and tune the band region and bandwidths.

Hocini et al. [9] proposed a novel method to generate almost a constant group index over a large bandwidth. The holes of the PC were enlarged, and innermost rows were shifted in a longitudinal direction to tune the features of the PCW. In this work, relatively larger group indices in the range of 18 to 40 were achieved with a bandwidth of 11-24 nm. The NDBP ranging from 0.282 – 0.465 has been reported.

In 2018, Li et al. [2] proposed an analytical method for achieving higher-order 2-dimensional PC with tunable PBG. In this work, the authors presented a general mechanism based on the Bloch mode analysis for the design of a PC. Using the Bloch mode analysis for periodic structures, the PC's unit cell was designed, providing full PBG on demand. For all polarizations, this bandgap was observed.

In 2019, Trabelsi et al. [10] proposed narrowband transmission optical filters which are entirely tunable. The transfer matrix method was used to generate the structures. The layers of the structure were arranged in a generalized Thue-Morse sequence. Yttrium Barium Copper Oxide (YBCO) and SiO2 material were used to fabricate the structure. In this method, the thickness of the material and the operating temperatures were changed to tune

the PBG. As the temperature was used to control the PBG, this structure can also be used as a temperature sensor.

Therefore, the PBG of a PC or PCW can be controlled by the thickness of the layers, operating temperature, and the refractive index profile. The tuning methods discussed so far are static. Once the PC structure is formed, the PBG is fixed. The eigen frequencies can be moved to any part of the spectrum by changing the geometry and refractive index profile. Also, the PBG can be either increased or decreased by these techniques.

As the PBG and dispersion features of the PCW depend on the geometry, the fabrication significantly impacts its performance. A variation of one wavelength can result in the completely diversified performance of the PCW. In this section, we briefly discussed a few fabrication techniques to tune the PBG and achieve specific applications.

Campbell et al. [11] described a method for producing 3-dimensional PCW with micrometre periodicity. The method was based on 3-dimensional holographic lithography. Initially, with this technique, micro-periodic polymeric structures were fabricated, and these were used as templates to create PC structures with higher refractive index contrast. The method has a high spatial resolution, an essential parameter for fabricating PC structures for the visible spectrum. Compared to other methods, this method is economical, rapid and scalable for the production.

In 2001, Vlasov et al. [12] proposed a method for naturally assembling colloidal microspheres to create 3-dimensional periodic structures. However, this method results in irregular and polycrystalline PC and PCWs which are difficult to incorporate into a device. Also, this method can cause structural defects in the PC and can destroy the PBG. The colloidal spheres were assembled on a thin silicon substrate layer to overcome these disadvantages. Planar, regular, and single crystalline silicon PC were achieved with sufficiently low defects with this mechanism. The fabricated silicon PC has a PBG with an operating wavelength of around 1.3 μm. In this method, intentional doping and patterning can be performed for changing the operating wavelengths.

O'Faolain et al. [13] examined the effect of disorder on propagation loss in W1 PCW. For this purpose, the disorder was introduced into the PCW by randomly displacing the holes. The controlled disorder allowed distinguishing two types of losses in PCW. Near the band-edge, reflection loss occurs, while away from the band-edge, the slow light loss scales with the group velocity. The study helped to understand the losses in PCW due to fabrication errors and discussed possible methods to control the losses.

Awan et al. [14] proposed a helpful method in the post-processing of the PCW. With this method, the operating wavelength can be tuned, offsetting the effects of fraction filling ratio (*r/a*) and slab thickness variations. This method used wet chemical surface oxidation followed by oxide stripping. The theoretical model shows that the change in optical behaviour can be predictable, and hence controlled PBG tuning can be achieved by changing the number of processing cycles. It was calculated that one processing cycle removes nearly 0.25 nm material from the surface, and a blue shift of 1.6 nm can be achieved. The wet chemical process with controlled oxidation followed by oxide removal is used in stepwise tuning of the operating wavelength. This method can be used after the fabrication of PC structure and hence any errors that occur during the fabrication can be corrected. Hence this method can precisely control the operating wavelength and fine-tuning. Experimentally, this is observed in the silicon etching process by the chemical etching method. This model can also determine the number of processing cycles required to tune the operating wavelength to a new wavelength. The method is helpful in fabricating slow light based PCW, and optical devices for routing and switching.

2.3.2 Linear lattice shift:

Another potential geometrical perturbation that produces PBG on demand is lattice shift. In this method, air cylinders in the adjacent rows of the waveguide are shifted away to tune the PBG. Potential applications can be realized by this method. The shift can create a waveguide with a fixed width or variable width, as shown in figure 2.3.

Li et al. [15] presented a systematic procedure based on lattice shift for designing flat bands in PCW for slow light applications. In this method, the first two innermost rows of the W1 waveguide were shifted to produce the maximum group index-bandwidth product. Nearly constant DBP was achieved in this method, with group indices in the range of 30-90. By shifting the innermost rows of holes, the authors experimentally demonstrated the flat band slow light with constant group index in the range of 32 - 49 over bandwidth in the range of 9 - 14 nm near 1550 nm wavelength.

In 2009, Hamachi et al. [16] discovered that wideband and low dispersion slow light could be achieved in silicon-on-insulator PCW, whose lattice was shifted along the waveguide. This was considered the first experimental demonstration of nonlinear enhancement by slow light in PCW. At the PCW, the delayed transmission of picosecond optical pulses was observed during the experiment. Also, two-photon absorption and self-phase modulation enhanced by the high internal light intensity in the slow light regime were

noticed. The PCW has low group velocity and low dispersion with group indices in the range of 25 - 60 with a flat band of 3 - 12 nm was observed.

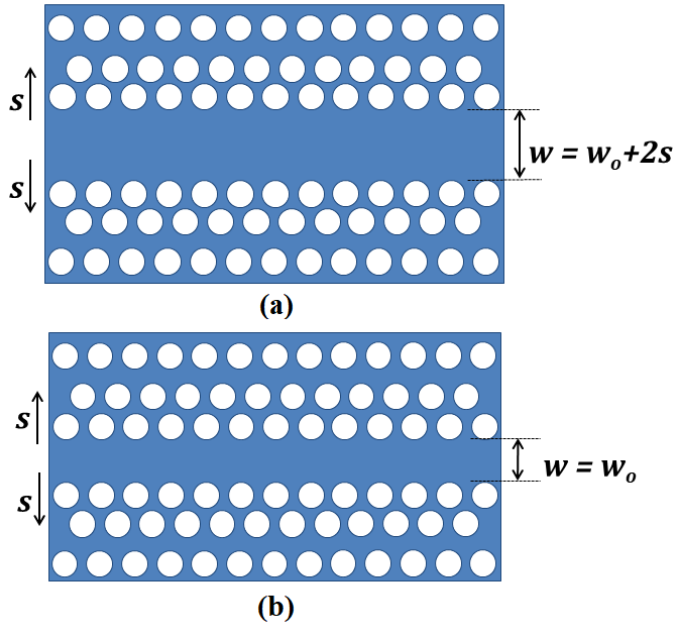

Figure 2.3: (a) waveguide with variable width (b) waveguide with fixed width.

Hao et al. [17] improved the DBP in PCWs by introducing the variations in the radius of holes in innermost rows and their position. Although larger DBP was achieved, the group indices were relatively small when the lattice shift was applied. In this regard, the authors changed the lattice positions of the holes and their radius simultaneously to achieve higher group indices with larger DBP. A group index of 90 was achieved while the DBP improved from 0.15 to 0.35.

Bagci and Akaoglu [18] examined the impact of the number of rows shifted to improve the slow light features. In this method, the width of the waveguide was maintained constant. The authors found that PCW with lattice shift in two rows has better slow light features than PCW with a shift in one row. The authors also introduced the ring-like structures in the innermost rows. The shift in one innermost row of rings in the PCW was preferable to shifting second and third innermost rows of rings. Shifting the third row has no considerable impact on the slow light features of the PCW.

In 2015 Tamura et al. [19] calculated the number of photonic bands of the waveguide modes in a lattice shifted PCW. The shift in the lattice was introduced in various models and found that the shift of two rows produces low dispersion slow light. Also, the mixed shift of the first and the third rows generate low dispersion. The group indices in the range of 34 - 36, with a bandwidth of 10 nm at telecom wavelengths, were achieved.

2.3.3 Transverse lattice shift or twist:

The lattice is said to be twisted if the rows adjacent to the waveguide are asymmetrically moved in the opposite directions. Similar to lattice shift, lattice twist also improves the linear and nonlinear features of the PCW. Figure 2.4 shows a general schematic of the twist in the innermost rows of a waveguide.

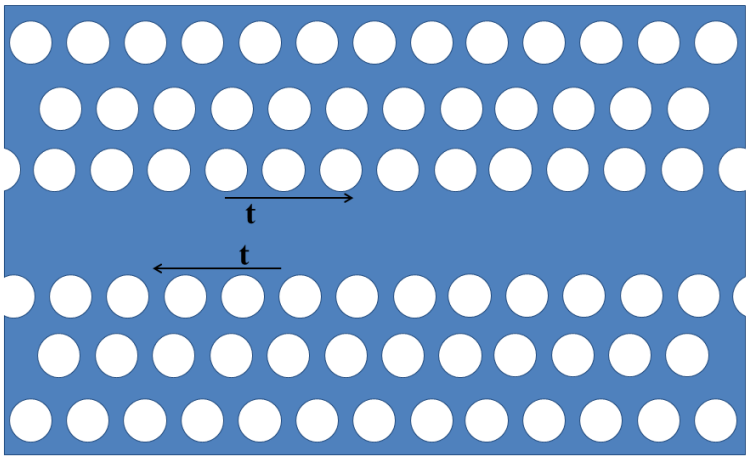

Figure 2.4: Twist induced waveguide

Ma and Jiang [20] proposed an asymmetric PCW formed by moving the first innermost rows in the opposite direction along with the waveguide core. The slow mode dispersion curve was made flat by adjusting the structural parameters of the PCW. The authors reported an ultra-flat band reduced distortion. FDTD method was used to verify the results obtained.

In 2012, Roy et al. [21] introduced a twist in the lattice, enabling the engineering of nonlinear dispersion. Generally, the nano-structures are explored for linear dispersion engineering. However, in this work, the authors explored the nonlinear dispersion in PCW by asymmetrical translation of air holes. A PCW with a twist was proposed to consider the nonlinear dispersion. Large group index and low group velocity were reported by introducing a twist in the lattice. The holes adjacent to the core were subjected to asymmetric translation to produce the shift in the lattice. The twist parameter directly controlled the self-phase modulation in the PCW. Cross phase modulation and four-wave mixing coefficients were also derived from self-phase modulation.

Colman et al. [22] demonstrated the dispersion tailoring in PCW by coupling the even and the odd modes using a twist of the lattice. The theoretical analysis of the PCW found new ways of controlling the dispersion. Group symmetry theory was used to find the suitable perturbation that only couples even and odd modes in the waveguide.

2.3.4 Variation of radius of hole:

The radius of the holes (figure 2.5) is one of the design parameters that can control the dispersion features of the waveguide structures for slow light and nonlinear applications. In 2006, Frandsen et al. [23] tailored the dispersion features of the PCW by introducing variations in the radii of the first and second innermost rows of holes. In general, this concept can be applied to PCWs made of any material. Waveguides having low loss, high bandwidths and low group velocity dispersion can be designed by this method. In this work, a W1 waveguide fabricated in silicon-on-insulator material with a bandwidth of 11 nm was reported, with a nearly constant group velocity of $c_0/34$.

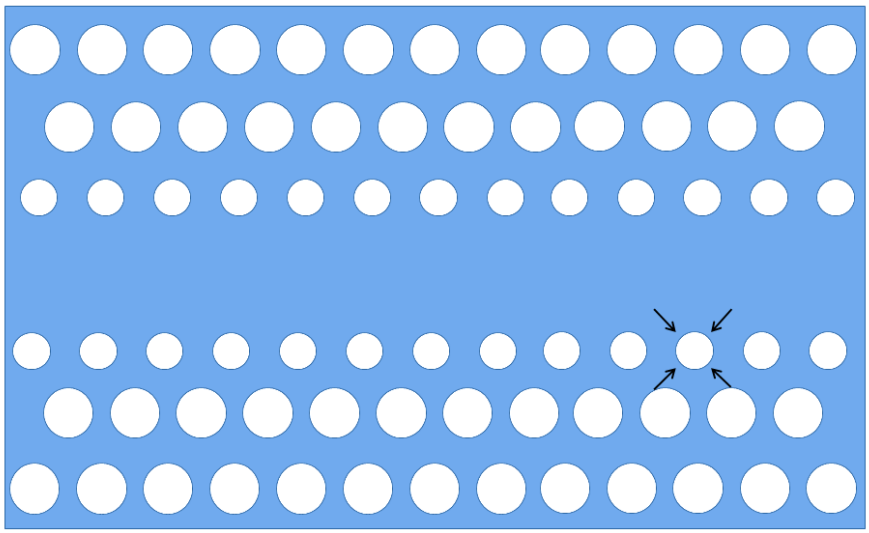

Figure 2.5: varying the radius of holes in the innermost row(s)

Niemi et al. [24] developed a wavelength division de-multiplexing (WDD) device based on planar PCW. The filtering of the wavelengths was realized by shifting the cut off frequency of the PBG. This shift was realized by modifying the size of the innermost holes. The diameter of the holes was increased from one end of the waveguide to the other end for filtering the wavelengths.

Theoretically, it is expected that PC slab structures with line defect and with slightly small innermost holes will have low group velocity and low dispersion. Kubo et al. [25] experimentally verified these low group velocity and low dispersion features in a PCW made of a silicon-on-insulator substrate. In this work, the group index, PBG, bandwidth and nonlinear properties were controlled by choosing the proper ratio between outer hole diameter (2r) and innermost hole diameter (2r'). When the ratio was slightly smaller than unity, the group index was observed constant. Constant group indices in the range of 30 - 37 were observed with a central wavelength of 1.53 μm.

Hao et al. [17] improved the DBP of the PCW structures by changing the radius of the innermost holes and by shifting their lattice positions. The normalized DBP was increased from 0.15 to 0.35, while the group index remains unchanged at a higher value of 90 with a step-by-step optimization mechanism. The width of the waveguide and the diameter of the innermost row of holes were used to generate a larger NDBP.

In 2011, Wang et al. [26] investigated the slow light properties of polyatomic PC. A U-type group index-frequency curve with a nearly constant group index was achieved with a square lattice. The radius and the position of the innermost rows were varied under the study. The study confirmed that the holes with smaller radii control the dispersion. The authors also found that the decrease in group velocity while maintaining the larger NDBP can be achieved by modifying the radius of the innermost holes.

Wan et al. [27] introduced eye-shaped scatterers in the first & second rows of the waveguide, and group index in the range of 14 – 32 was achieved. Also, a group index in the range of 36-287 was achieved by replacing all air holes with eye-shaped scatterers. By replacing all the holes, low dispersion at a large group index was achieved. The dispersion of the structure was controlled by adjusting the lattice constant '*a*' and parameter '*e*', which is inversely related to the ratio of the radius of the minor axis to that of the major axis. This method achieved slow light with a bandwidth of 23 – 70 nm with a group index in the range of 14-32. Also, a large group index of 287 was achieved with a bandwidth of 3-30 nm. A near-zero dispersion PCW was designed by adjusting the lattice parameter.

Bagci and Akaoglu [18] proposed new structures with larger control on the dispersion features. The innermost rows were filled with dielectric cylinders to form ring-like structures. The diameter of the holes and rings was varied to control the dispersion features of the waveguide. The width of the waveguide remains constant while the diameters of the holes and rings in the innermost rows are varied. The PCW with the variation of radius of holes in two rows has produced improved features than variations in one row. In the case of rings, the inner and outer diameters of the rings were varied to achieve control over dispersion curves.

In 2019, Abood et al. [28] investigated the PC coupled-cavity for slow light with low dispersion. Periodically arranged cavities of air holes with specific defect were used for the study. The radius and the position of the cavities were modified to achieve the desired slow light modes. This method achieved a group index of 70.75 over an operating bandwidth of 12 nm. The NDBP was calculated to be 0.5873. This NDBP is higher than that in other structures with low dispersion.

2.3.5 Introducing ring like structures:

The PBG of the PCW originates from the effective refractive index of the slab. The PBG is controlled by the first and second innermost rows geometry and their effective refractive index. By introducing the dielectric cylinders in the lattice, many authors tuned the PBG of the PCW. The ring-like structures contributed to tunable PBG, flat band generation, larger group indices, and low dispersion. Figure 2.6 shows the introduction of the ring-like structures in the first innermost row to tailor the dispersion properties.

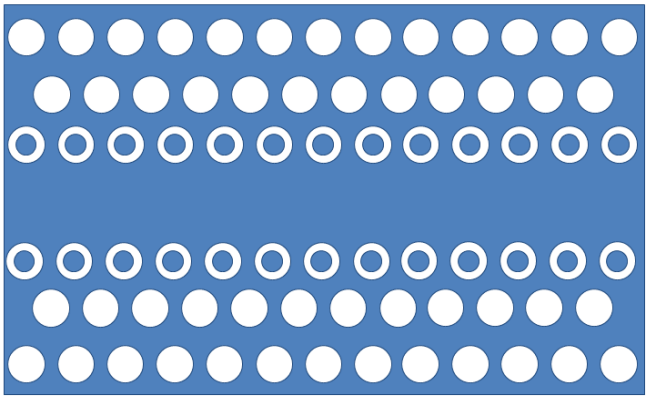

Figure 2.6: Introduction of ring like structures in the first innermost row of the waveguide.

In 2007, Saynatjoki et al. [29] had introduced the ring-like structures in PCW and optimized the structure to minimize the dispersion losses. By introducing rings in the lattice, the group index made nearly constant was achieved with values above 20 with bandwidths of more than 8 nm. Low dispersion was observed due to the widening of the propagation mode close to the lower band PBG edge. The ring PCW was reported with a constant group index of 25 - 37 in the slow light region.

A single defect PCW with rings was proposed by Mulot et al. [30] to achieve low group velocity with relatively low dispersion. This work achieved a group index of 20 with low group velocity over a bandwidth of 5 nm. The waveguide was manufactured with ring-shaped holes on a silicon-on-insulator substrate. The group index values of the fabricated waveguide were measured and found to be as large as 22. A nearly constant group velocity dispersion of 4.2 ps/nm/mm was achieved.

Hou et al. [31] investigated the flat band properties of a line defect PCW with dielectric cylinders in the air holes of the innermost row. The radius of the dielectric cylinders inside the air holes was manipulated to tune the flat band. A linear band in band structure was observed with this manipulation, which is an evidence for the slow light. FDTD simulations were used to calculate the band structure. A relatively higher group index in the range of 74 - 90 was observed with a bandwidth of 2 - 3 nm.

Zhai et al. [32] improved the slow light features of a PCW by introducing ring-shaped holes. Numerically the band features of the ring PCW were investigated. The results illustrate that both the inner and outer radii of the rings in the first and second rows adjacent to the waveguide effect the slow light features. Therefore authors proposed that by optimizing the inner and outer radii of the rings, the slow light features can be controlled. The orientation of the dielectric cylinders and their effect on slow light bands was also studied. A high group index in the range of 28-115 with a bandwidth of 3.57 – 24.67 nm was reported. The study also found that oblique cylinders are helpful for slow light applications. However, the fabrication of such oblique cylinders in the PCW is challenging.

Due to this reason, it attracted many to design PCWs with ring shape holes. The radius of rings has control over the dispersion features, and hence to slow down the light, one can optimize the radius of the rings in the innermost rows. Mirjalili et al. [33] optimized the radius of the rings to achieve flat band structures. Particle Swarm Optimization (PSO) algorithm is one of the best optimization algorithms in Artificial Intelligence and was used to optimize the rings. The optimization was performed to achieve maximum NDBP of ring PCW. Nearly 34% improvement in NDBP and 41% improvement in the bandwidth were observed compared to previous works.

The number of rows filled to achieve the slow light features is limited. Bagci and Akaoglu [18] found this. The authors investigated the effect of the number of rows filled to achieve slow light and found that the filling of second and third rows will confine the improvement. The line width of the waveguide was kept constant during the simulation. The innermost rows were filled with dielectric cylinders, and the outer and inner radii of the rings were varied to study the slow light features. The introduction of the rings also increased the available parameters to tune the PBG for slow light applications.

In the ring-shaped holes, new geometries were introduced to enhance the features of the PCW. Ellipse-shaped rings are one of such geometries [34]. The authors replaced the conventional circular rings with elliptical rings in this work. Fifteen structural parameters were identified with the elliptical rings to design the PCWs. FDTD method was employed to calculate the band structure. Constant and larger group index with improved NDBP was observed in these elliptical ring PCWs.

The ring PCWs were also used for gas sensing applications. Goyal and Pal [35] used the 3-dimensional FDTD method to analyse the sensing application of ring PCW. The proposed structure was fabricated by etching ring-shaped holes in the silicon PCW. The spectral transmission characteristics and the sensitivity were analysed by varying the radius

of the rings and etching depths. For a change in the refractive index of the order of 10^{-4}, a shift of 0.05 nm in the transmission spectrum confirms highly sensitive performance.

For developing a high refractive index measurement sensor, PCW with ring-shaped holes was analysed by Kassa-Baghdouche and Cassan [36]. The edge of the transmission spectrum of the PCW shifts with ring-shaped holes. The 3-dimensional simulation results were applied to a silicon waveguide on a membrane. The observation shows that the performance of the waveguide was susceptible to the variations in the ambient environment's refractive index. The sensor was sensitive to both opto-geometric factors and the environment's index. For this reason, the ring PCW can be used as a micro-strain sensor in addition to refractive index sensing. The device insertion loss was estimated as very low with magnitudes of – 3 dB.

2.4 Active tuning of photonic bandgap:

2.4.1 Electro-optic effect:

Geometrical modifications of the PCW provide limited applications of tunable PBG. Once the PCW is fabricated, its PBG, dispersion, group index and working wavelength are fixed. However, one can tune the effective refractive index of the PCW and alter its dispersion features. In electrical tuning of the PBG, one can apply an external electric field and change the effective refractive index of the PC or PCW. This change in refractive index tunes the PBG and provides instant control over the features of the PCW.

Ozaki et al. [37] studied the electrical tuning of the PCW. The wavelength of the lasing mode in a 1-dimensional PC was electrically tuned. The studies were performed on a 1-dimensional PC infiltrated with dye-doped nematic liquid crystal. The lasing wavelength was widely tuned by applying an external electric field. The tunable PBG emits a lasing wavelength that can be tuned widely with electric field.

Using polystyrene colloidal templates, Kuai et al. [38] fabricated electrochromic tungsten trioxide (WO3) inverse opals. The WO3 structure was achieved through a dip infiltration sol-gel process. The calcination process in subsequent steps removed polymer microspheres. The scanning electron micrographs (SEM) confirm the hexagonal macroporous structures. The PBG of the structure was then tuned by inserting the lithium into the lattice. The first reflection peak of the reflection spectra shifts about 36 nm, while the second reflection peak shifts by 28 nm. In the applied electric field, these shifts are useful for tunable PBG.

Electrical tuning of the 2-dimensional PBG structures was reported by Haurylau et al. [39]. The silicon-based PC structures were infiltrated with liquid crystals to achieve tuning. The electrode configurations were modified to avoid the electric field screening by the conductive silicon. The tuning was demonstrated using the field below 1 V/m. These results can be adapted to PBG structures with any electro-optic materials. The tunable PBG controlled by the electric field leads to fast and efficient light modulators.

The effective refractive index of the composite materials has electric field dependence. Wang et al. [40] theoretically designed the electrically tunable 1-dimensional PCs. Nonlinear composite materials with dielectric layers were used to design the PC. The PBG of the composite based PC can be readily tuned by choosing appropriate ac or dc electric fields. The tuning was extensive and precise.

Optically or electrically controlled PC structures were proposed by Park et al. [41]. Active semiconductor nanowires were used to design such PC structures. The PC under the electric field can either transmit or filter different wavelengths. Under the application of the external electric field, the PBG can be tuned up to several wavelengths.

Y. Fu et al. [42] reported an electro-optic multi-channel tunable filter. A 2-dimensional ferroelectric PC made of barium titanate was used to design the filter. The properties of the PC filter can be tunable under an external electric field. A shift of about 30 nm was observed when a voltage of 54.8 V was applied. In addition to the electric field, structural perturbations were also introduced in the PC to tune the filtering properties

An enhanced PC coupled-cavity waveguide was proposed by Tian et al. [43] in 2012. The waveguide was designed to achieve a compact, ultrafast and high-performance optical buffer. The cavity spacing and the hole size around the cavity were adjusted to achieve slow light and buffer performance. In the optimized structure, the group velocity was below 2.713×10^{-4} c. Then the dynamic modulation of the waveguide was studied systematically. As the applied voltage increases, the buffer capacity and the physical size of bits are unchanged. The eigen wavelength was shifting linearly with applied voltage.

Skoromets et al. [44] demonstrated a 1-dimensional PC possessing electric tunability. The PC structure consists of two Bragg mirrors made of alternate quarter wave layers of SiO_2 and CeO_2. The layers of the PC were separated by ferroelectric $SrTiO_3$ layers. Electrodes were used on both sides of this defect layer to apply the electric field. The in-plane dielectric function was modified by the applied electric field. A relative tunability of 6.5% was achieved under an electric field of 60 kV/cm and at a temperature of 105 K. The observed

tunable behaviour of the PC was in agreement with soft mode behaviour in $SrTiO_3$ single crystal.

Looking at the applications of electrical tuning, recently, electrically tunable liquid PC was proposed by Q. Fu et al. [45] in 2018. The liquid PCs have tunable PBG and hence tunable structural colours with the applied electric field. This is due to the change of crystal lattice under the electric field. The liquid PC has wide PBG due to the large dielectric contrast between CeO_2@SiO_2 particles and propylene carbonate. With large PBG, the structural colour stands long tuning range. Due to CeO_2, the response time of the liquid PC is relatively short. High performance electrically tunable PCs were helpful in developing the display devices.

2.4.2 Thermo-optic effect:

Thermal tuning produces relatively larger tuning and, therefore, applications involving temperature. However, the response times are relatively larger compared to electro-optic effect based PC or PCW.

In 2000, Halevi et al. [46] proposed that the PBG of a semiconductor-based PC can be tunable if free carrier density is relatively high. The dielectric constant of a semiconductor material depends on the temperature and its impurity concentration 'N'. The authors showed that the PBG could be altered and even can be closed through applied temperature. Doping and temperature played an important role in controlling the PBG. The absorption can be controlled by choosing proper materials, changing the geometry and by the spectral range.

Nemec et al. [47] demonstrated a high-quality filter for terahertz range with a tunability of 20%. A single crystal of $KTaO_3$ was inserted in the lattice of a 1-dimensional PC, resulting in a narrow transmission band. The refractive index of the defect mode controlled the frequencies of the structure. The strong temperature-dependent properties of the $KTaO_3$ contributed to the high tunability of the structure.

1-dimensional PBG structures made of ferroelectric materials were tuned by Murzina et al. [48]. Sodium nitrite was infiltrated to the nanostructure's porous silicon template to form the temperature tunable PC. In the temperature range of 50-165 ^oC, a tuning of 15 nm was reported. The tuning of the structure was originated from the strong temperature dependence of the refractive index of the ferroelectric sodium nitrite.

Omnidirectional terahertz PBG structures were proposed by Dai et al. [49]. Tunability of 1-dimensional PC made of alternating layers of InSb and SiO_2 was theoretically studied. The PBG of the PC strongly depends on the lattice constants and the thickness ratio of the

constituent layers. The omnidirectional PBG can be controlled by the external temperature. As the temperature increases, the upper and lower frequency limits of the PBG shifts to higher frequencies and the bandwidth of the structure becomes narrow.

Graded index materials were also investigated for temperature-dependent tunability. Singh et al. [50] designed InSb based PC structures for terahertz frequencies. Various periodic and quasi-periodic structures were designed under the study. Graded index profiles were introduced to the layers of the 1-dimensional PC structures. It was found that the temperature of the structure determines the operational frequency. The layer thickness controls the number of bands in the PB structure. In case of the quasi-periodic structures, the temperature-controlled the localization of the modes. The authors also studied the electric field distributions inside the structure when subjected to the external temperature. Tunable PBG and localization of the modes can be controlled by the temperature and can draw potential applications in the terahertz region.

A compact temperature sensor was developed by Peng et al. [51] using a temperature tunable PC fibre (PCF). Liquid of high refractive index was filled in the first ring around the core for tuning the PBG while the outer rings of the PCF were filled with air. The PBG of the liquid filled rings was analysed further to design the temperature sensor. It was found that the absorption spectrum of the PCF was highly controlled by the refractive index of the liquid and hence for temperature measurements. The temperature dependence of the refractive index of the liquid was used for sensing. A mixture of dimethyl sulfoxide and aqueous gold colloids was injected to the PCF lattice. It was experimentally verified that the sensor has a sensitivity of – 5.5 nm/^{o}C.

Thermally tunable filter by cascading two 1-dimensional superconductor dielectric PCs was designed by Upadhyay et al. [52]. The filter is capable of separating 12 equally distributed wavelength channels. The filtering capability was originated from the superconductor layers, whose characteristics were controlled by the temperature. Wavelength division multiplexing and routing of the signals can be achieved by these tunable filters, without distorting the signal.

2.4.3 Micro-fluidic infiltration:

Microfluidic infiltration is one of the easiest methods to tune the PBG. An optical fluid can be injected into the lattice of the PC or PCW, and the effective refractive index can be modified. The method can be used for tuning the PBG, improving PCW features and as a refractive index sensor. The infiltration can be done partially or fully as shown in figure 2.7.

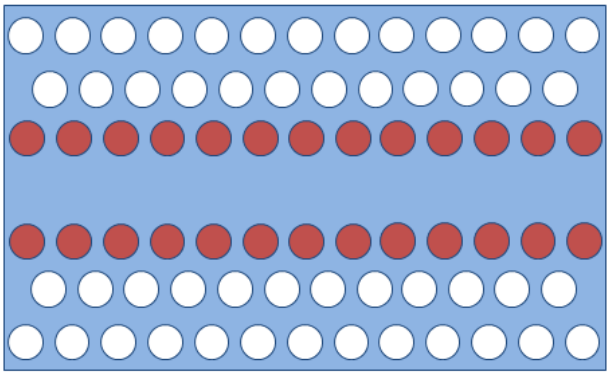

(a)

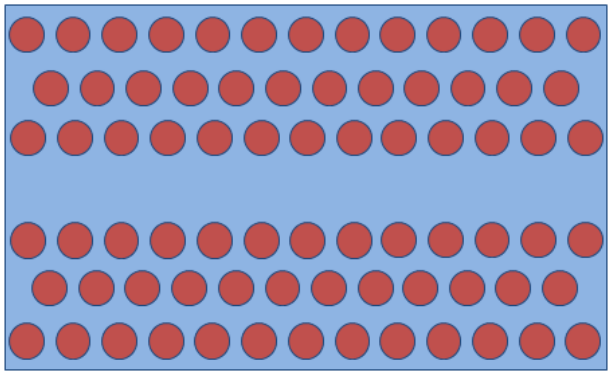

(b)

Figure 2.7: Microfluidic infiltration in PCW (a) partial infiltration (b) completely liquid filled PCW

Mansouri- Birjandi et al. [53] studied the liquid infiltration of opto-fluids in the second row of the waveguide. The holes in the first row of the waveguide remained filled with air and shifted away from the waveguide. A group index of 10 - 32 was achieved with a flat band of 10 - 21.5 nm. A low GVD of the order of 10^{-24} s^2/m was reported. The highest flat band in the study was observed in the PCW with a shift of 0.11a in the first row of air cylinders and with the second row of holes filled with opto-fluid.

Zhao et al. [54] theoretically optimized the slotted PCW for slow light applications. Slow light with a high group index and low dispersion was achieved by infiltrating the first and second rows of air holes with selective fluids. The simulation results showed that nearly constant group indices of 50, 82.5, 150, and 176 were achieved over bandwidths of 6.9 nm, 3.1 nm, 1.65 nm, and 1.15 nm, respectively. The method can be used for reconfigurable slotted PCW. Tunable slow light was achieved in these reconfigurable slotted PCW. Also, this method can be used for correcting the fabrication errors.

Yang et al. [55] developed a temperature sensor based on liquid-filled PCF. A fibre ring laser embedded with PCF was used to demonstrate the sensor experimentally. The sensing head was developed by filling high refractive index liquid into the PCF. This liquid-

filled PCF was used as the laser filter. With the increase in temperature, a shift in the output wavelength of the fibre laser was observed. With the shift in wavelength, the output intensity increased due to change in PBG. Temperature sensitivity of – 1.747 nm/^{0}C was obtained with wavelength modulation. Also, a high signal-to-noise ratio was observed in the experiment (~ 55 dB).

Selective filling of PCF lattice with various linear and nonlinear media such as gasses, liquids, and liquid crystals reconfigures its features. In 2010, Vieweg et al. [56] reported that selective infiltration provides the possibility of achieving various linear and nonlinear applications. Supercontinuum generation over 600 nm bandwidth was experimentally demonstrated using a femtosecond oscillator as a pump source. Even spatial-temporal solitons can be generated by achieving control over temporal and spatial dispersions.

A high sensitive temperature sensor was developed by Peng et al. [51] by selective liquid-filled PCF. A mixture of dimethyl sulfoxide and aqueous gold colloids with a high thermo-optic coefficient was injected into the first ring around the core while the outer rings of holes were filled with air. Using the bandgap like effect, a temperature sensitivity up to −5.5 nm/^{o}C was experimentally calculated.

Monfared et al. [57] theoretically investigated a polarization-maintaining PCF (PMPCF), filled with toluene, for temperature sensing application via Sagnac interferometer. The dependence of the performance of the proposed PMPCF on the hole dimensions and fabrication imperfections was studied. It was identified that the PMPCF has a good tolerance to any geometrically induced imperfections in the fabrication process. Furthermore, the authors show that the spectral range can be increased to values larger than 137 nm by decreasing the infiltration length of the PMPCF.

Bougriou et al. [58] reported a new design of infiltrated opto-fluidic sensors based on a 2-dimensional PC slab with a triangular lattice pattern of ring-shaped holes. The properties of the sensor were simulated using the FDTD method. By changing the refractive index of holes, the transmission spectrum was measured and it was found that the wavelength position of the transmission spectrum shifts with increasing the refractive index. To realize large measurement range, high sensitivity and improved transmission, the radius and the shape of the air holes localized at each side of the line defect were optimized. A sensitivity of more than 636 nm/RIU was observed in this method.

A wideband and low dispersion slow light PCW with large NDBP was demonstrated by Pourmand et al. [59]. The PCW can be used as an optical switch and modulator. The microfluid was infiltrated into the first and second rows of the holes, adjacent to the

waveguide. The simulation results show that NDBP can be enhanced to a larger value of 0.469 with a wide bandwidth of 36.8 nm.

In 2019, Luo et al. [60] proposed a refractive index sensor based on alcohol-filled optical fibre. The sensor consists of a single-mode fibre-PCF-single-mode fibre (SMF-PCF-SMF) structure. The proposed structure was experimentally verified for the sensing of refractive index. A Mach–Zehnder interferometer, which was fabricated by splicing a section of uncoated PCF between two short sections of SMF with a fibre fusion splicer, was used in the experiment. The air holes of the PCF were filled with alcohol to fabricate a refractive sensing probe that can detect changes in the external refractive index. The results show that the position of the wavelength was shifting with changes in the external refractive index. The sensitivity of the proposed structure was measured to be 386.6 nm/RIU.

2.5 Applications of slow light:

The slow light generated in PCW has various linear and nonlinear applications. The structures can be used as optical switches, light modulators, nonlinear enhancers and sensors. In this section, we briefly discussed the applications based on slow light in PCW.

Recently, Guo et al. [61] proposed a graphene-based PCW by creating periodical air holes in a silicon layer. The structure was optimized around 30THz with a large group index of 166 and with very low dispersion loss – 2.1 dB/μm. A high NDBP of 4.00 was achieved in this graphene-based PCW. The slow light performance can be dynamically tuned by changing the bias voltage. The tuning was achieved between 19.1 and 27.4 THz. The studies show that graphene-based PCW structures are promising for slow light devices.

Ebnali-Heidari et al. [62] investigated four-wave mixing (FWM) in short dispersion engineered slow light PCW. The authors demonstrated larger FWM conversion efficiency and increased the FWM bandwidth (~ 10 nm). The improvement in FWM efficiency is due to net slow light enhancement.

A nonlinear optical process with slow light enhancement in 2-dimensional silicon PCW was reported by Corcoran et al. [63]. Third harmonic generation (THG) at a wavelength of 520 nm was observed in the waveguide. The nonlinear enhancement was due to the reduced group velocity of the near infrared pump signal with only a few watts of peak power. The observations confirm the possible tunable THG with tunable slow light.

Vlasov et al. [64] experimentally demonstrated a 300-fold reduction of the group velocity in a silicon chip via ultra-compact silicon PCW. The waveguide can support optical modes with sub-micrometre cross-section and low loss. Using a micro heater, the authors

demonstrated a fast and efficient active control of the group velocity by localised heating of PCW.

FWM was experimentally investigated by Monat et al. [65] in a short dispersion engineered slow light silicon PCW. Nearly constant group velocities of the order of *c*/30 were reported. The conversion efficiency is found to be – 9 dB between the idler and the continuous wave probe with pump power of 1 W and 6 nm pump probe detuning. The conversion efficiency is larger than that of silicon nanowires.

2.6 Broadband, narrowband and supercontinuum generation:

Another interesting nonlinear application based on PC and PCF structures is supercontinua generation. In this, many nonlinear processes act together on the pump beam and broaden the output spectrum.

Ebnali-Heidari et al. [66] achieved control over the chromatic dispersion in an opto-fluidic infiltrated PCF for supercontinuum generation. Low confinement loss and ultra-flattened band with near-zero dispersion were achieved by selective infiltration of PCF. Simulations show that femtosecond laser pulses can generate supercontinuum spectrum when the pulses pass through a PCF of length 250 mm or more, whose dispersion profile was engineered via selective infiltration.

Willinger et al. [67] reported the first demonstration of narrowband parametric amplification in a PC structure. A dispersion engineered $Ga_{0.5}In_{0.5}P$ PCW was used to demonstrate the phenomenon. The PCW with dispersion function that exhibits two zero crossings was used with a pulsed pump source. A tunable probe beam was used to scan on either side of the pump. Conversion efficiency of – 10 dB was observed with a peak pump power of 650 mW.

The first demonstration of an optical memory in a hollow-core PCF was demonstrated by Sprague et al. [68]. Using far-detuned Raman interactions, a gigahertz bandwidth light was stored in the hyperfine coherence of caesium atoms at room temperature. A memory efficiency of 27+/-1% was demonstrated. The result shows that a fibre integrated optical memory can be used for implementing local nodes of quantum information.

Saghaei and Ghanbari [69] achieved a high range supercontinuum in a PCF with circular lattice. Various linear and nonlinear parameters were engineered by varying the diameter of the air holes. Operational wavelengths were obtained in the visible and near-infrared regions with zero dispersion. One hundred femtosecond input pulses of 532 nm from a Ti:Sapphire laser was launched into a 100 mm long PCF to study the effect. The authors

numerically demonstrated that supercontinua as wide as 290, 440 and 830 nm could be achieved using a pump with peak power of 1, 2 and 5 kW, respectively.

A coherent supercontinuum was observed in a toluene filled PCF by Van et al. [70]. The hollow core of a PCW was filled with toluene, and the dispersion characteristics were studied. Two structures with lattice constant 2 μm each with filling fractions 0.3 and 0.35 and toluene core of diameters of 3.34 and 3.23 μm have flat dispersion in the near-infrared region. The structure with a fraction filling ratio of 0.3 has all-normal dispersion characteristics in whole near-infrared wavelength range, while the second structure has anomalous dispersion for wavelengths longer than 1.5 μm. Although confinement losses in the considered structures were as high as 0.4 dB/cm, authors show that generation of coherent supercontinuum in the range of 1.0 – 1.7 μm with the pulse energy conversion of 16% was feasible in 4 cm long PCF with standard femtosecond lasers.

Octave-spanning supercontinuum was demonstrated and reported by Stepniewski et al. [71] with an all-solid, all-normal dispersion PCF, pumped with a source of 1360 nm and 120 femtosecond pulses. The fibre was drawn from thermally matched oxide soft glasses with a hexagonal lattice 35 μm in diameter and 2.5 μm solid core. The fibre was designed for normal-dispersion broadly flattened in the range of 1200-2800 nm. The supercontinuum was observed in the range of 900-1900 nm bandwidth and found a good agreement with numerical modeling.

Saini et al. [72] proposed a new design with a triangular core PCF in As_2Se_3-based chalcogenide glasses. The structure has nearly zero dispersion. The numerical results show that ultra-broadband supercontinuum spanning 1.9 – 10 μm can be obtained using 6 mm long PCF pumped with 50 femtosecond laser pulses at 4.5 μm wavelength. Compared to previously reported works, ultra-broadband supercontinuum spectra achieved using relatively low peak power.

2.7 Device applications based on dispersion engineering and tunable photonic bandgap:

The PC structures are attractive due to their ability to control optical device characteristics by lithographically varying the geometry. The tunable PBG has potential applications in light controlling and sensing.

In 2000, Painter et al. [73] demonstrated a 10x10 array of optically pumped 2-dimensional PC defect lasers with varying lattice parameters. By adjusting the lattice constant and hole diameter, authors reported a tunable laser with varying wavelengths from 1500 to 1625 nm on a monolithic InP–InGaAsP wafer. A wavelength resolution of 10 nm from

device to device was obtainable, limited by the lithography and etching tolerances. A 125 nm laser wavelength tuning range was obtainable through lithographic control of the lattice parameters of the 2-dimensional PC. FDTD simulations of the laser cavities were also used to accurately model the tuning of the laser mode.

Tanabe et al. [74] demonstrated all-optical switching in the telecommunication bands using a silicon PC at high speeds as ~ 50 ps, with extremely low switching energy as a few 100 fJ, and high switching contrast ~ 10 dB. The proposed devices consist of ultra-small high-quality factor nano-cavities connected to input and output waveguides. Switching was induced by a nonlinear refractive-index change caused by the plasma effect of carriers generated by two-photon absorption in silicon.

The optical switches play an important role in optical circuits and are a major research topic in photonics. Various techniques were adopted to realize these optical switches. Optical switches function by imposing a phase shift between two sections of the device and directing the light from one part to another. However, the change in refractive index is used for this shifting, and the typical changes are trivial. Conventional methods address this issue by using long devices, thus increasing the size, or using resonant enhancement, thus reducing the bandwidth. Beggs et al. [75] proposed an optical switch based on slow light enhancement. The device is 36 times shorter than a conventional optical switch for the same refractive index change and has a switching length of 5.2 μm. The design is flexible and allows different operating points to suit individual requirements.

A refractive index sensor with improved sensitivity was developed by Dutta et al. [76]. The ring-shaped holes in the silicon-on-insulator substrate were used to develop the sensor. The proposed design was analysed by a 3-dimensional FDTD tool. The shift in the upper band edge of the transmission spectrum was measured to estimate the sensitivity. For improving the sensitivity, the holes in the first innermost row were filled with a ring-like structure. The analysis shows that the PCW with ring like structures has more sensitivity than PCW with only holes. Further, the output signal was also strong in the ring PCW. The optimized design shows a wavelength shift of 210 nm for a change in refractive index from air (refractive index = 1.0) to Xylene (refractive index = 1.5). The average sensitivity was found to be 420 nm/RIU.

The PC or PCW lattice can be readily filled by gasses and liquids and used for sensing applications. Pergande et al. [77] presented an optical gas sensor based on an ultra-compact PC gas cell. The device is conceptually based on low group velocities inside a PC gas cell. Experimentally, an enhancement of the CO_2 infrared absorption by a factor of 2.6 to 3.5

compared to an empty cell due to slow light inside a 2-dimensional silicon PC gas cell was observed. The experimental results coincided with the numerical simulations. However, the overall transmission and thus the performance of the device, is limited by fluctuations of the pore diameter.

Temperature sensing can be performed by liquid-filled PCF structures. Peng et al. [51] proposed a temperature sensor based on selectively liquid-filled PCF using controlled hole collapse in PCF post-processing. The first ring around the core was filled with liquid of higher refractive index, while the outer rings of holes were remains filled with air. The PBG of the high refractive index ring was analysed for temperature sensing. A mixture of dimethyl sulfoxide and aqueous gold colloids with a high thermo-optic coefficient were injected into the lattice of PCF. Temperature sensitivity up to -5.5 nm / ^{o} C was experimentally confirmed.

Slow light interferometric optical modulators in PC can have not only high bandwidth but also highly compact size. PC structures, with their light controlling abilities, can be used for light switching and modulation requirements. A PC structure to enhance optical switching and modulation in silicon was proposed by O'Faolain et al. [78]. Using dispersion-engineered designs, a switch as short as 5 μm was achieved, in which the authors have demonstrated rerouting of optical pulses on a 3 ps time scale through the absorption of a femtosecond pulse. The authors also demonstrated a modulator with a Mach–Zehnder interferometer (MZI) configuration with flat-band slow-light PC phase shifters.

First sub-100 μm silicon Mach-Zehnder modulators (MZMs) were proposed by Nguyen et al. [79] that operate at more than 10 Gb/s. The modulator was designed by exploiting low-dispersion slow-light in lattice-shifted PCW. The authors demonstrated 10 Gb/s and 40 Gb/s modulators operation with phase shifter lengths of 50 μm and 90 μm, respectively.

Using slow light effect, a microtube PC based gas spectrometer was proposed by Kraeh et al. [80]. Conventional gas spectrometers are bulk in size and unsuitable for on-chip applications. Due to slow light, the absorption path length was achieved. Slow light enhanced gas absorption by a factor of 5.8 was experimentally confirmed at 5400 nm.

2.8 State of art computational methods in optical waveguide studies:

Numerical methods such as FDTD, PWE, and FEM can be implemented using various software packages for studying the features of an optical waveguide. However, conventional approaches of numerical and analytical methods are time-consuming, especially

when several parameters have to be simultaneously optimized. Machine learning (ML) and deep learning (DL) are the advanced methods to study a large amount of data and is envisioned to play a decisive role in addressing many applications, ranging from light modulation to nonlinear optical signal processing to high power fibre amplifiers to sensing applications. In ML based approach, the user trains the machine (*the model*) with various datasets containing input and output data obtained from conventional sources. Artificial neural network (ANN) is one of the important algorithms in ML. These algorithms predict the output parameters for an untrained input dataset. The accuracy of the prediction depends on the range of data used for training, the resolution of the data, and the successful creation of relations between input and output data. Figure 2.8 shows a general model used in ML for predicting the data. Here we review various methods in ML approaches, advantages and challenges in adopting ML techniques for PC and PCW studies.

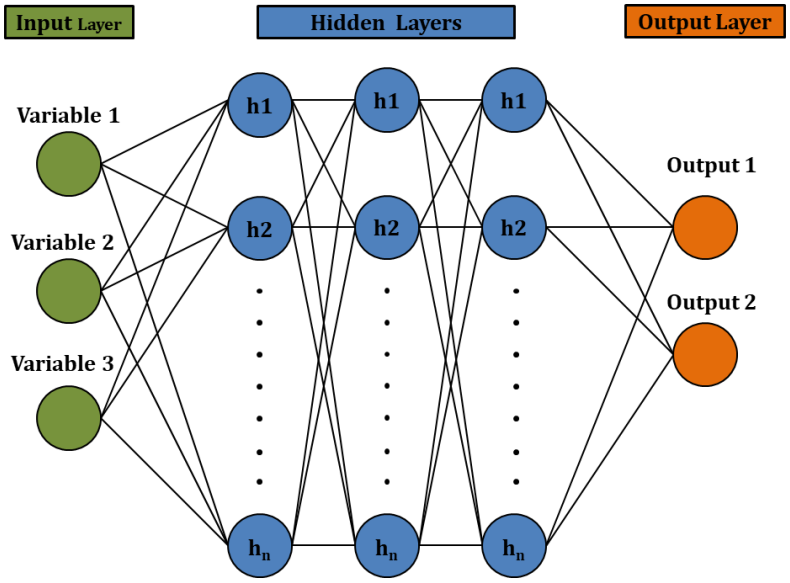

Figure 2.8: A general ANN model. The model consists of three input parameters, and two output parameters. The predictions are made by 3 hidden layers composed of 'n' nodes

Mescia et al. [81] have proposed a method based on ANNs to perform refinement and design of erbium-doped PCF amplifiers. Using conventional numerical methods is time-consuming, especially when several parameters need to be optimized. Using ANN, the nonlinear functional link among the physical and geometrical characteristics of the fibre amplifier was captured by a neural network and is exploited. The PCF amplifier gain and noise were thoroughly analyzed using ANN. The method was employed to determine the optimal values of the parameters that maximize the gain. Numerical results show that the proposed approach finds the design parameters in good accordance with respect to the conventional method.

A multilayer perceptron (MLP) is a class of feed-forward ANN. Malheiros-Silveira and Hernández-Figueroa [82] presented the prediction of dispersion relations and PBG in a 2-dimensional PC using MLP. Two case studies were conducted to evaluate the approach in conjunction with numerical methods. The ANN results were very close to those obtained by conventional numerical solvers with very short processing time. In some situations, the results provided by MLP were more accurate than the interpolated ones.

Ferreira et al. [83] computed the dispersion relations of PC using MLP. 2-dimensional and 3-dimensional structures presenting distinct dispersion relations and PBG were optimised. The optical properties of a set of PC structures with similar geometries and different dimensions were calculated by an electromagnetic solver to provide input data to ANN training. These ANN models could provide accurate dispersion relations curves in a concise time.

Asano and Noda [84] presented an approach to optimize the Q factors of two-dimensional PC nano-cavities based on DL. A data set generated from 1000 nano-cavities was used to train the model. For this purpose, randomly displaced air holes in the base nano-cavity were used. Using the prepared data set, a four-layer ANN consisting of a convolutional layer was trained to identify the relationship between the displacement of the air holes and the Q-factors. After the training, the ANN model could estimate the Q-factor of the PC cavity with an error of 13% in standard deviation. Using the back propagation method, the trained ANN model estimated the Q-factor with respect to the displacement of air holes with short processing time.

Khan et al. [85] presented a novel approach to design PC based optical filters using ML based mathematical model. The design and spectral response of the filter can be predicted using the proposed mathematical model, which can considerably reduce simulation time and effort. However, the mathematical modelling of the highly nonlinear behaviour in transmission spectra can be further improved by considering an excessive amount of training data and going to higher-order polynomial regressions.

Recently, ML techniques were used to calculate numerous optical properties of the PCF, including effective refractive index, effective mode area, dispersion properties and confinement loss [86]. These ML algorithms based on ANNs were able to make accurate predictions of the optical properties for usual parameter space of wavelength ranging from 0.5 -1.8 µm, pitch from 0.8-2.0 µm, and diameter by pitch from 0.6-0.9 and number of rings as 4 or 5 in a silica solid-core PCF. The authors demonstrated the use of simple and fast-

trained feed-forward ANNs that can predict the output for unknown device parameters faster than traditional numerical methods.

ANNs based on ML can interpolate well within the trained dataset. However, their ability to extrapolate is highly limited by several fundamental issues. Wu et al. [87] introduced an operator parameter space to improve the network's capability. Physical entities encoded with Maxwell's equations are used for this process. PCs were studied using this model, which was trained with operator parameter. Improved results were observed both within and beyond the trained space. Hence, by choosing appropriate operator parameter, the ANN models can be trained to predict the features of higher dimensional PC structures. This physics adopted network model with the operator parameter provides an alternative solution to conventional methods to design PC structures.

ML assisted PC design and analysis offers a great potential for transforming the field of quantum optics [88]. Different ML and DL techniques have been tested to design and analyse the PC structures. While the initial design and analysis results are encouraging, the fundamental limits of ML in artificial intelligence and the analysis techniques, in general, are yet to be explored.

References:

[1] A. Y. Petrov and M. Eich, "Zero dispersion at small group velocities in photonic crystal waveguides," *Appl. Phys. Lett.*, vol. 85, no. 21, pp. 4866–4868, Nov. 2004, https://doi.org/10.1063/1.1815066.

[2] S. Li, H. Lin, F. Meng, D. Moss, X. Huang, and B. Jia, "On-Demand Design of Tunable Complete Photonic Band Gaps based on Bloch Mode Analysis," *Sci. Rep.*, vol. 8, no. 14283, pp. 1–8, Sep. 2018, https://doi.org/10.1038/s41598-018-32422-1.

[3] S. John and K. Busch, "Photonic bandgap formation and tunability in certain self-organizing systems," *J. Light. Technol.*, vol. 17, no. 11, pp. 1931–1943, Nov. 1999, https://doi.org/10.1109/50.802976.

[4] S. Noda, A. Chutinan, and M. Imada, "Trapping and emission of photons by a single defect in a photonic bandgap structure," *Nature*, vol. 407, no. 6804, pp. 608–610, Oct. 2000, https://doi.org/10.1038/35036532.

[5] M. Notomi, A. Shinya, K. Yamada, J. -. Takahashi, C. Takahashi and I. Yokohama, "Structural tuning of guiding modes of line-defect waveguides of silicon-on-insulator photonic crystal slabs," *IEEE J. Quantum Electron.*, vol. 38, no. 7, pp. 736-742, Jul. 2002, https://doi.org/10.1109/JQE.2002.1017583.

[6] S. I. Takayama, H. Kitagawa, Y. Tanaka, T. Asano, and S. Noda, "Experimental demonstration of complete photonic band gap in two-dimensional photonic crystal slabs," *Appl. Phys. Lett.*, vol. 87, no. 061107, pp. 1–3, Aug. 2005, https://doi.org/10.1063/1.2009060.

[7] N. L. Janrao, R. Zafar, and V. Janyani "Improved design of photonic crystal waveguides with elliptical holes for enhanced slow light performance," *Opt. Eng*., vol. 51, no. 6, pp. 064001(1-7), Jun. 2012, https://doi.org/10.1117/1.OE.51.6.064001.

[8] B. K. Singh, P. Kumar, and P. C. Pandey, "Tunable photonic band-gaps in one-dimensional photonic crystals containing linear graded index material," *Appl. Phys. B Lasers Opt.*, vol. 117, no. 3, pp. 947–956, Aug. 2014, https://doi.org/10.1007/s00340-014-5913-z.

[9] A. Hocini, M. Maache, and D. Khedrouche, "Wideband and low dispersion slow light by altering the geometry of a photonic crystal waveguide," *Opt. Commun*., vol. 427, no. 15, pp. 396–404, Jul. 2018, https://doi.org/10.1016/j.optcom.2018.06.077.

[10] Y. Trabelsi, N. Ben Ali, and M. Kanzari, "Tunable narrowband optical filters using superconductor/dielectric generalized Thue-Morse photonic crystals," *Microelectron. Eng.*, vol. 213, no. 15, pp. 41–46, Apr. 2019, https://doi.org/10.1016/j.mee.2019.04.016.

[11] M. Campbell, D. N. Sharp, M. T. Harrison, R. G. Denning, and A. J. Turberfield, "Fabrication of photonic crystals for the visible spectrum by holographic lithography," *Nature*, vol. 404, no. 6773, pp. 53–56, Mar. 2000, https://doi.org/10.1038/35003523.

[12] Y. A. Vlasov, X. Z. Bo, J. C. Sturm, and D. J. Norris, "On-chip natural assembly of silicon photonic bandgap crystals," *Nature*, vol. 414, no. 6861, pp. 289–293, Nov. 2001, https://doi.org/10.1038/35104529.

[13] L. O'Faolain, T. P. White, D. O'Brien, X. Yuan, M. D. Settle, and T. F. Krauss, "Dependence of extrinsic loss on group velocity in photonic crystal waveguides," *Opt. Express*, vol. 15, no. 20, pp. 13129-13138, Sep. 2007, https://doi.org/10.1364/oe.15.013129.

[14] K. M. Awan, S. A. Schulz, D. X. Liu, K. Dolgaleva, J. Upham, and R. W. Boyd, "Post-process wavelength tuning of silicon photonic crystal slow-light waveguides," *Opt. Lett*., vol. 40, no. 9, pp. 1952-1955, May 2015, https://doi.org/10.1364/ol.40.001952.

[15] J. Li, T. P. White, L. O'Faolain, A. Gomez-Iglesias, and T. F. Krauss, "Systematic design of flat band slow light in photonic crystal waveguides," *Opt. Express*, vol. 16, no. 9, pp. 6227-6232, Apr. 2008, https://doi.org/10.1364/oe.16.006227.

[16] Y. Hamachi, S. Kubo, and T. Baba, "Slow light with low dispersion and nonlinear enhancement in a lattice-shifted photonic crystal waveguide." *Opt. Lett.*, vol. 34, no. 7, pp. 1072-1074, Apr. 2009, https://doi.org/10.1364/OL.34.001072.

[17] R. Hao, E. Cassan, X. L. Roux, D. Gao, V. D. Khanh, L. Vivien, D. Marris-Morini, and X. Zhang, "Improvement of delay-bandwidth product in photonic crystal slow-light waveguides," *Opt. Express*, vol. 18, no. 16, pp. 16309-16319, Jul. 2010, https://doi.org/10.1364/oe.18.016309.

[18] F. Bagci and B. Akaoglu, "A systematic analysis of hole size, hole-type and rows shifting on slow light characteristics of photonic crystal waveguides with ring-shaped holes," *Optik (Stuttg).*, vol. 125, no. 11, pp. 2702–2707, Feb. 2014, https://doi.org/10.1016/j.ijleo.2013.11.032.

[19] T. Tamura, K. Kondo, Y. Terada, Y. Hinakura, N. Ishikura, and T. Baba, "Silica-Clad Silicon Photonic Crystal Waveguides for Wideband Dispersion-Free Slow Light," J. *Light. Technol.*, vol. 33, no. 14, pp. 3034–3040, Apr. 2015, https://doi.org/10.1109/JLT.2015.2420685.

[20] J. Ma and C. Jiang, "Demonstration of ultraslow modes in asymmetric line-defect photonic crystal waveguides," *IEEE Photonics Technol. Lett.*, vol. 20, no. 14, pp. 1237–1239, Jun. 2008, https://doi.org/10.1109/LPT.2008.926018.

[21] S. Roy, M. Santagiustina, P. Colman, S. Combrié, and A. De Rossi, "Modeling the dispersion of the nonlinearity in slow mode photonic crystal waveguides," *IEEE Photonics J.*, vol. 4, no. 1, pp. 224–233, Feb. 2012, https://doi.org/10.1109/JPHOT.2011.2181942.

[22] P. Colman, S. Combrié, G. Lehoucq, and A. De Rossi, "Control of dispersion in photonic crystal waveguides using group symmetry theory," *Opt. Express*, vol. 20, no. 12, pp. 13108-13114, May 2012, https://doi.org/10.1364/OE.20.013108.

[23] L. H. Frandsen, A. V. Lavrinenko, J. Fage-Pedersen, and P. I. Borel "Photonic crystal waveguides with semi-slow light and tailored dispersion properties," *Opt. Express*, vol. 14, no. 20, pp. 9444-9450, Sep. 2006, https://doi.org/10.1364/OE.14.009444.

[24] M. Kristensen, L. H. Frandsen, K. K. Hede, A. Harpøth, and P. I. Borel, "Wavelength-Division Demultiplexing Using Photonic Crystal Waveguides," *IEEE*

Photonics Technol. Lett., vol. 18, no. 1, pp. 226–228, Jan. 2006, https://doi.org/10.1109/LPT.2005.860001.

[25] S. Kubo, D. Mori, and T. Baba, "Low-group-velocity and low-dispersion slow light in photonic crystal waveguides," *Opt. Lett.*, vol. 32, no. 20, pp. 2981-2983, Oct. 2007, https://doi.org/10.1364/ol.32.002981.

[26] D. Wang et al., "Slow light engineering in polyatomic photonic crystal waveguides based on square lattice," *Opt. Commun.*, vol. 284, no. 24, pp. 5829–5832, Dec. 2011, https://doi.org/10.1016/j.optcom.2011.07.080.

[27] Y. Wan, K. Fu, C. Li, and M. Yun, "Improving slow light effect in photonic crystal line defect waveguide by using eye-shaped scatterers," *Opt. Commun.*, vol. 286, no. 1, pp. 192–196, Jan. 2013, https://doi.org/10.1016/j.optcom.2012.09.025.

[28] I. Abood, S. Elshahat, K. Khan, L. Bibbò, A. Yadav, and Z. Ouyang, "Slow light with high normalized delay-bandwidth product in low-dispersion photonic-crystal coupled-cavity waveguide," *Opt. Commun.*, vol. 439, no. 1, pp. 181–186, Jan. 2019, https://doi.org/10.1016/j.optcom.2019.01.063.

[29] A. Saynatjoki, M. Mulot, J. Ahopelto, and H. Lipsanen, "Dispersion engineering of photonic crystal waveguides with ring-shaped holes," *Opt. Express*, vol. 15, no. 13, pp. 8323-8328, Jun. 2007, https://doi.org/10.1364/OE.15.008323.

[30] M. Mulot, A. Säynätjoki, S. Arpiainen, H. Lipsanen, and J. Ahopelto, "Slow light propagation in photonic crystal waveguides with ring-shaped holes," *J. Opt. A Pure Appl. Opt.*, vol. 9, no. 9, pp.415-418, Aug. 2007, https://doi.org/10.1088/1464-4258/9/9/S22.

[31] J. Hou, D. Gao, H. Wu, R. Hao, and Z. Zhou, "Flat band slow light in symmetric line defect photonic crystal waveguides," *IEEE Photonics Technol. Lett.*, vol. 21, no. 20, pp. 1571–1573, Sep. 2009, https://doi.org/10.1109/LPT.2009.2030160.

[32] Y. Zhai, H. Tian, and Y. Ji, "Slow light property improvement and optical buffer capability in ring-shape-hole photonic crystal waveguide," *J. Light. Technol.*, vol. 29, no. 20, pp. 3083–3090, Aug. 2011, https://doi.org/10.1109/JLT.2011.2165334.

[33] S. M. Mirjalili, K. Abedi, and S. Mirjalili, "Optical buffer performance enhancement using Particle SwarmOptimization in Ring-Shape-Hole Photonic Crystal Waveguide," *Optik (Stuttg).*, vol. 124, no. 23, pp. 5989–5993, Dec. 2013, https://doi.org/10.1016/j.ijleo.2013.04.114.

[34] S. M. Mirjalili, "Ellipse-ring-shaped-hole photonic crystal waveguide," *Optik (Stuttg).*, vol. 126, no. 1, pp. 56–60, Jan. 2015, https://doi.org/10.1016/j.ijleo.2014.07.123.

[35] A. K. Goyal and S. Pal, "Design and simulation of high-sensitive gas sensor using a ring-shaped photonic crystal waveguide," *Phys. Scr.*, vol. 90, no. 25503, pp. 1-5, Jan. 2015, https://doi.org/10.1088/0031-8949/90/2/025503.

[36] L. Kassa-Baghdouche and E. Cassan, "Sensitivity analysis of ring-shaped slotted photonic crystal waveguides for mid-infrared refractive index sensing," *Opt. Quantum Electron.*, vol. 51, no. 328, pp. 1-11, Sep. 2019, https://doi.org/10.1007/s11082-019-2040-4.

[37] R. Ozaki, T. Matsui, M. Ozaki, and K. Yoshino, "Electrically color-tunable defect mode lasing in one-dimensional photonic-band-gap system containing liquid crystal," *Appl. Phys. Lett.*, vol. 82, no. 21, pp. 3593–3595, May 2003, https://doi.org/10.1063/1.1577829.

[38] S. L. Kuai, G. Bader, and P. V. Ashrit, "Tunable electrochromic photonic crystals," *Appl. Phys. Lett.*, vol. 86, no. 221110, pp. 1–3, May 2005, https://doi.org/10.1063/1.1929079.

[39] M. Haurylau, S. P. Anderson, K. L. Marshall, and P. M. Fauchet, "Electrical modulation of silicon-based two-dimensional photonic bandgap structures," *Appl. Phys. Lett.*, vol. 88, no. 061103, pp. 1–3, Feb. 2006, https://doi.org/10.1063/1.2172070.

[40] G. Wang, J. P. Huang, and K. W. Yu, "Electrically tunable photonic crystals with nonlinear composite materials," *Appl. Phys. Lett.*, vol. 91, no. 191117, pp. 1–3, Nov. 2007, https://doi.org/10.1063/1.2809389.

[41] H. G. Park, C. J. Barrelet, Y. Wu, B. Tian, F. Qian, and C. M. Lieber, "A wavelength-selective photonic-crystal waveguide coupled to a nanowire light source," *Nat. Photonics*, vol. 2, no. 10, pp. 622–626, Sep. 2008, https://doi.org/10.1038/nphoton.2008.180.

[42] Y. Fu, J. Zhang, X. Hu, and Q. Gong, "Electro-optic tunable multi-channel filter in two-dimensional ferroelectric photonic crystals," *J. Opt.*, vol. 12, no. 7, pp. 1-7, Jul. 2010, https://doi.org/10.1088/2040-8978/12/7/075202.

[43] H. Tian, F. Long, W. Liu, and Y. Ji, "Tunable slow light and buffer capability in photonic crystal coupled-cavity waveguides based on electro-optic effect," *Opt.*

Commun., vol. 285, no. 10–11, pp. 2760–2764, May 2012, https://doi.org/10.1016/j.optcom.2012.01.086.

[44] V. Skoromets, H. Němec, C. Kadlec, D. Fattakhova-Rohlfing, and P. Kužel, "Electric-field-tunable defect mode in one-dimensional photonic crystal operating in the terahertz range," *Appl. Phys. Lett.*, vol. 102, no. 24, pp. 1–5, Jun. 2013, https://doi.org/10.1063/1.4809821.

[45] Q. Fu, H. Zhu, and J. Ge, "Electrically Tunable Liquid Photonic Crystals with Large Dielectric Contrast and Highly Saturated Structural Colors," *Adv. Funct. Mater.*, vol. 28, no. 43, pp. 1–9, Sep. 2018, https://doi.org/10.1002/adfm.201804628.

[46] P. Halevi and F. Ramos-Mendieta, "Tunable photonic crystals with semiconducting constituents," *Phys. Rev. Lett.*, vol. 85, no. 9, pp. 1875–1878, Aug. 2000, https://doi.org/10.1103/PhysRevLett.85.1875.

[47] H. Němec et al., "Thermally tunable filter for terahertz range based on a one-dimensional photonic crystal with a defect," *J. Appl. Phys.*, vol. 96, no. 8, pp. 4072–4075, Oct. 2004, https://doi.org/10.1063/1.1787623.

[48] T. V. Murzina, F. Y. Sychev, I. A. Kolmychek, and O. A. Aktsipetrov, "Tunable ferroelectric photonic crystals based on porous silicon templates infiltrated by sodium nitrite," *Appl. Phys. Lett.*, vol. 90, no. 161120, pp. 1-3, Apr. 2007, https://doi.org/10.1063/1.2724928.

[49] X. Dai, Y. Xiang, S. Wen, and H. He, "Thermally tunable and omnidirectional terahertz photonic bandgap in the one-dimensional photonic crystals containing semiconductor InSb," *J. Appl. Phys.*, vol. 109, no. 053104, pp. 1-6, Mar. 2011, https://doi.org/10.1063/1.3549834.

[50] B. K. Singh and P. C. Pandey, "Tunable temperature-dependent THz photonic bandgaps and localization mode engineering in 1D periodic and quasi-periodic structures with graded-index materials and InSb," *Appl. Opt.*, vol. 57, no. 28, pp. 8171-8181, Oct. 2018, https://doi.org/10.1364/ao.57.008171.

[51] Y. Peng, J. Hou, Y. Zhang, Z. Huang, R. Xiao, and Q. Lu, "Temperature sensing using the bandgap-like effect in a selectively liquid-filled photonic crystal fiber," *Opt. Lett.*, vol. 38, no. 3, pp. 263-265, Feb. 2013, https://doi.org/10.1364/ol.38.000263.

[52] M. Upadhyay, S. K. Awasthi, L. Shiveshwari, P. K. Srivastava, and S. P. jha, "Thermally Tunable Photonic Filter for WDM Networks Using 1D Superconductor Dielectric Photonic Crystals," *J. Supercond. Nov. Magn.*, vol. 28, pp. 2275–2280, Mar. 2015, https://doi.org/10.1007/s10948-015-3031-8.

[53] M. A. Mansouri-Birjandi, M. Janfaza, and A. Tavousi, “Flat-Band Slow Light in a Photonic Crystal Slab Waveguide by Vertical Geometry Adjustment and Selective Infiltration of Optofluidics,” *J. Electron. Mater.*, vol. 46, no. 11, pp. 6528–6534, Jul. 2017, https://doi.org/10.1007/s11664-017-5695-2.

[54] Y. Zhao, Y. N. Zhang, and Q. Wang, “Optimization of slow light in slotted photonic crystal waveguide with liquid infiltration,” *J. Light. Technol.*, vol. 31, no. 14, pp. 2448–2454, Jun. 2013, https://doi.org/10.1109/JLT.2013.2267272.

[55] X. Yang, Y. Lu, B. Liu, and J. Yao, “Fiber Ring Laser Temperature Sensor Based on Liquid-Filled Photonic Crystal Fiber,” *IEEE Sens. J.*, vol. 17, no. 21, pp. 6948–6952, Nov. 2017, https://doi.org/10.1109/JSEN.2017.2754640.

[56] M. Vieweg et al., “Ultrafast nonlinear optofluidics in selectively liquid-filled photonic crystal fibers,” *Opt. Express*, vol. 18, no. 24, pp. 25232-25240, Nov. 2010, https://doi.org/10.1364/oe.18.025232.

[57] Y. E. Monfared, C. Liang, R. Khosravi, B. Kacerovska, and S. Yang, “Selectively toluene-filled photonic crystal fiber Sagnac interferometer with high sensitivity for temperature sensing applications,” *Results Phys.*, vol. 13, no. 102297, pp. 1-6, May 2019, https://doi.org/10.1016/j.rinp.2019.102297.

[58] F. Bougriou, T. Bouchemat, M. Bouchemat, and N. Paraire, “Optofluidic sensor using two-dimensional photonic crystal waveguides,” *EPJ Appl. Phys.*, vol. 62, no. 11201, pp. 1–5, Apr. 2013, https://doi.org/10.1051/epjap/2013110442.

[59] M. Pourmand, A. Karimkhani, and F. Nazari, “Wideband and low-dispersion engineered slow light using liquid infiltration of a modified photonic crystal waveguide,” *Appl. Opt.*, vol. 55, no. 35, pp. 10060-10066, Dec. 2016, https://doi.org/10.1364/ao.55.010060.

[60] Y. Luo, R. Fan, Y. Zhang, Q. Wu, Z. Ren, and B. Peng, “Novel optical fiber refractive sensor fabricated with an alcohol-filled photonic crystal fiber based on a Mach–Zehnder interferometer,” Opt. Fiber Technol., vol. 48, no. August 2018, pp. 278–282, 2019, https://doi.org/10.1016/j.yofte.2019.01.003

[61] X. Guo, X. Wu, H. Cui, F. Yang, and J. Zhou, “Slow light performance enhancement of graphene-based photonic crystal waveguide,” *Phys. Lett. Sect. A*, vol. 383, no. 16, pp. 1983–1987, Jun. 2019, https://doi.org/10.1016/j.physleta.2019.03.032.

[62] M. Ebnali-Heidari, C. Monat, C. Grillet, and M. K. Moravvej-Farshi, “A proposal for enhancing four-wave mixing in slow light engineered photonic crystal waveguides

and its application to optical regeneration," *Opt. Express*, vol. 17, no. 20, pp. 18340-18353, Sep. 2009, https://doi.org/10.1364/oe.17.018340.

[63] B. Corcoran et al., "Green light emission in silicon through slow-light enhanced third-harmonic generation in photonic-crystal waveguides," *Nat. Photonics*, vol. 3, no. 4, pp. 206–210, Mar. 2009, https://doi.org/10.1038/nphoton.2009.28.

[64] Y. A. Vlasov, M. O'Boyle, H. F. Hamann, and S. J. McNab, "Active control of slow light on a chip with photonic crystal waveguides," *Nature*, vol. 438, no. 7064, pp. 65–69, Nov. 2005, https://doi.org/10.1038/nature04210.

[65] C. Monat et al., "Four-wave mixing in slow light engineered silicon photonic crystal waveguides," *Opt. Express*, vol. 18, no. 22, pp. 22915-22927, Oct. 2010, https://doi.org/10.1364/oe.18.022915.

[66] M. Ebnali-Heidari, H. Saghaei, F. Koohi-Kamali, M. Naser Moghadasi and M. K. Moravvej-Farshi, "Proposal for Supercontinuum Generation by Optofluidic Infiltrated Photonic Crystal Fibers," *IEEE J. Sel. Top. Quantum Electron.*, vol. 20, no. 5, pp. 582-589, Sept.-Oct. 2014, https://doi.org/10.1109/JSTQE.2014.2307313.

[67] A. Willinger, S. Roy, M. Santagiustina, S. Combrié, A. De Rossi, and G. Eisenstein, "Narrowband optical parametric amplification measurements in $Ga_{0.5}In_{0.5}P$ photonic crystal waveguides," *Opt. Express*, vol. 23, no. 14, pp. 17751-17757, Jun. 2015, https://doi.org/10.1364/oe.23.017751.

[68] M. R. Sprague et al., "Broadband single-photon-level memory in a hollow-core photonic crystal fibre," *Nat. Photonics*, vol. 8, no. 4, pp. 287–291, Mar. 2014, https://doi.org/10.1038/nphoton.2014.45.

[69] H. Saghaei and A. Ghanbari, "White light generation using photonic crystal fiber with sub-micron circular lattice," *J. Electr. Eng.*, vol. 68, no. 4, pp. 282–289, Aug. 2017, https://doi.org/10.1515/jee-2017-0040.

[70] L. C. Van, A. Anuszkiewicz, and A. Ramaniuk, "Supercontinuum generation in photonic crystal fibres with core filled with toluene." *J. Opt.*, vol. 19, no. 125604, pp. 1-9, Nov. 2017, https://doi.org/10.1088/2040-8986/aa96bc.

[71] G. Stepniewski et al., "Broadband supercontinuum generation in normal dispersion all-solid photonic crystal fiber pumped near 1300 nm," *Laser Phys. Lett.*, vol. 11, no. 055103, pp. 1-5, Mar. 2014, https://doi.org/10.1088/1612-2011/11/5/055103.

[72] T. S. Saini, A. Kumar, and R. Kumar Sinha, "Broadband mid-IR supercontinuum generation in As_2Se_3 based chalcogenide photonic crystal fiber: A new design and

analysis," *Opt. Commun.*, vol. 347, pp. 13–19, Jul. 2015, https://doi.org/10.1016/j.optcom.2015.02.049.

[73] O. Painter et al., "Lithographic tuning of a two-dimensional photonic crystal laser array," *IEEE Photonics Technol. Lett.*, vol. 12, no. 9, pp. 1126–1128, Sep. 2000, https://doi.org/10.1109/68.874210.

[74] T. Tanabe, M. Notomi, S. Mitsugi, A. Shinya, and E. Kuramochi, "All-optical switches on a silicon chip realized using photonic crystal nanocavities," *Appl. Phys. Lett.*, vol. 87, no. 151112, pp. 1–3, Oct. 2005, https://doi.org/10.1063/1.2089185.

[75] D. M. Beggs, T. P. White, L. O'Faolain, and T. F. Krauss, "Ultracompact and low-power optical switch based on silicon photonic crystals," *Opt. Lett.*, vol. 33, no. 2, pp. 147-149, Jan. 2008, https://doi.org/10.1364/ol.33.000147.

[76] H. S. Dutta, A. K. Goyal, and S. Pal, "Sensitivity enhancement in photonic crystal waveguide platform for refractive index sensing applications," *J. Nanophotonics*, vol. 8, no. 083088, pp.1-6, Jun. 2014, https://doi.org/10.1117/1.jnp.8.083088.

[77] D. Pergande et al., "Miniature infrared gas sensors using photonic crystals," *J. Appl. Phys.*, vol. 109, no. 083117, pp. 1-7, Apr. 2011, https://doi.org/10.1063/1.3575176.

[78] L. O'Faolain, D. M. Beggs, T. P. White, T. Kampfrath, K. Kuipers, and T. F. Krauss, "Compact optical switches and modulators based on dispersion engineered photonic crystals," *IEEE Photonics J.*, vol. 2, no. 3, pp. 404–414, Jun. 2010, https://doi.org/10.1109/JPHOT.2010.2047918.

[79] H. C. Nguyen, S. Hashimoto, M. Shinkawa, and T. Baba, "Compact and fast photonic crystal silicon optical modulators," *Opt. Express*, vol. 20, no. 20, pp. 22465-22474, Sep. 2012, https://doi.org/10.1364/oe.20.022465.

[80] C. Kraeh, J. L. Martinez-Hurtado, A. Popescu, H. Hedler, and J. J. Finley, "Slow light enhanced gas sensing in photonic crystals," *Opt. Mater.*, vol. 76, pp. 106–110, Feb. 2018, https://doi.org/10.1016/j.optmat.2017.12.024.

[81] L. Mescia, G. Fornarelli, D. Magarielli, F. Prudenzano, M. De Sario, and F. Vacca, "Refinement and design of rare earth doped photonic crystal fibre amplifier using an ANN approach," *Opt. Laser Technol.*, vol. 43, no. 7, pp. 1096–1103, Oct. 2011, https://doi.org/10.1016/j.optlastec.2011.02.005.

[82] G. N. Malheiros-Silveira and H. E. Hernandez-Figueroa, "Prediction of dispersion relation and PBGs in 2-D PCs by using artificial neural networks," *IEEE Photonics Technol. Lett.*, vol. 24, no. 20, pp. 1799–1801, Oct. 2012, https://doi.org/10.1109/LPT.2012.2215846.

[83] A. Da Silva Ferreira, G. N. Malheiros-Silveira, and H. E. Hernandez-Figueroa, "Computing Optical Properties of Photonic Crystals by Using Multilayer Perceptron and Extreme Learning Machine," *J. Light. Technol.*, vol. 36, no. 18, pp. 4066–4073, Sep. 2018, https://doi.org/10.1109/JLT.2018.2856364.

[84] T. Asano and S. Noda, "Optimization of photonic crystal nanocavities based on deep learning," *Opt. Express*, vol. 26, no. 25, pp. 32704-32717, Nov. 2018, https://doi.org/10.1364/oe.26.032704.

[85] Y. Khan et al., "Mathematical modeling of photonic crystal based optical filters using machine learning," *2018 Int. Conf. Comput. Electron. Electr. Eng. ICE Cube 2018*, pp. 1–5, Jan. 2019, https://doi.org/10.1109/ICECUBE.2018.8610986.

[86] S. Chugh, A. Gulistan, S. Ghosh, and B. M. A. Rahman, "Machine learning approach for computing optical properties of a photonic crystal fiber," *Opt. Express*, vol. 27, no. 25, pp. 36414-36425, Dec. 2019, https://doi.org/10.1364/oe.27.036414.

[87] B. Wu, K. Ding, C. T. Chan, and Y. Chen, "Machine Prediction of Topological Transitions in Photonic Crystals," *Phys. Rev. Appl.*, vol. 14, no. 044032, pp. 1-7, Oct. 2020, https://doi.org/10.1103/PhysRevApplied.14.044032.

[88] Z. A. Kudyshev, V. M. Shalaev, and A. Boltasseva, "Machine Learning for Integrated Quantum Photonics," *ACS Photonics*, vol. 8, no. 1, pp. 34–46, Jan. 2021, https://doi.org/10.1021/acsphotonics.0c00960.

Chapter – 3
Effect of Geometrical Parameters on Dispersion Features and Slow Light

Dispersion engineering of photonic crystal waveguides is attractive due to their potential applications in linear and nonlinear phenomena. Here, in this chapter, we present a comprehensive and systematic study to achieve increased control over the dispersion curve of the waveguide operating at telecom wavelengths. The effect of the radius of air cylinders, and their lattice position on the dispersion features are studied chiefly in a line-defect photonic crystal waveguide. For this purpose, perturbations are introduced in the radius and positions of the air cylinders. The combined effect of lattice shift, lattice twist and introduction of ring-like structures (rings) in the innermost rows on the slow light features is also studied. The rings are introduced in the first and second innermost rows of the waveguide. Slow light is characterized by calculating the group index, second and fourth-order dispersions, and delay-bandwidth products. Using the MIT Photonic-Bands software, the calculations are performed, and the waveguide is characterized. With this systematic study, one can tune the waveguide with the desired range of group index and bandwidth with controlled dispersion properties. With very low dispersion, structures with a flat band of the order of 30 nm and above are achieved. The developed structures may find applications in optical delays, optical buffers and nonlinear applications.

3.1 Introduction:

Dispersion engineering of PCW is interesting because of its capability in SL generation, nonlinear effects, optical buffers and optical delays [1-3]. In specific, the light modes in PCW exhibit smaller group velocities near the Brillouin zone edge [4-5]. At these lower group velocities, exploring the PCW can provide enhanced light-matter interactions and nonlinear effects [5-9]. In the past two decades, the scientific community has shown greater interest in the tailoring of PCW for nonlinear applications. Tailoring the structure's geometry is one of the easiest ways in dispersion engineering. Lithographic and laser-based machinery are available for fabricating such nano-scale structures. For designing next-generation optical devices such as optical buffers, photonic routers, optical storage, all-optical circuits, and all-optical switches, PCW is a promising technology [10-14].

For dispersion engineering, usually, the geometrical parameters and the effective refractive index of the PCW are modified to achieve various applications. By changing the diameter of the air cylinders [15] in PCW, controlled group velocity and semi-slow light were reported. This change in diameter has achieved various features such as group velocity in the range of ~ $c_o/100$, low propagation loss, and controlled GVD. Varying the waveguide width has produced control over the group velocity, and these methods resulted in constant group velocity and even zero third-order dispersion [16]. The position of the air cylinder is shifted systematically to design PCW with flat band slow light and reported nonlinear enhancement [17-18]. High and nearly constant group indices were presented in these cases. Introducing the shift in the innermost rows in the engineered waveguides resulted in parametric amplification (PA) [19-20].

Changing the radius of rings directly affects the width of the flat band window. Hence, researchers have introduced a ring-like structure (rings) in the PCW [11, 21-22] to minimize the dispersion in some studies. A flat band line defect PCW is developed by introducing these rings in the lattice, and very low GVD is achieved. Dispersion engineering was also reported by filling selective micro-fluids in PCW lattice [10, 23]. By introducing the micro-fluids in the lattice, group velocities of the range of ~ $c_o/110$ were attained. Also, this mechanism helped to design reconfigurable PCW. All these studies aim to control the dispersion, achieve high and constant group indices, and enhance nonlinear properties in the PCW to find the applications in optical delays, nonlinear effects, all-optical circuits and on-chip devices.

Compared to other methods of generation of SL such as electromagnetically induced transparency in a vapour [24], micro-ring resonators [25], stimulated Brillouin scattering [26], stimulated Raman scattering [27], photonic crystals have wider bandwidths. Besides, it has the potential to miniaturize the size of the optical devices, on-chip compatibility, and can offer dispersion-free propagation by engineering the structure [28-30].

These studies conclude that the constructive perturbation of PCW and filling of air cylinders with micro-fluids or solid cylinders may result in controlled dispersion features and slow light generation. However, to the best of our knowledge, the combined effect of variation of radius of ring and geometrical perturbations on the slow light features is not studied.

Hence, in this chapter, we systematically revisit dispersion engineering by studying the effect of the radius of air cylinders and their lattice position on the linear and nonlinear properties of the line-defect waveguide. The study aims to present the combined effect of the

geometrical perturbations on the dispersion features and SL properties of line-defect PCW. The impact of change in radius and lattice position is studied independently. The radius of the air cylinders is optimized between 0.21*a* and 0.30*a*, and lattice perturbations in the range of 0.00*a* to 0.20*a* are used for this study where '*a'* is the lattice constant of the structure. At the latter stage, the combined effect of all these geometrical variations is incorporated. Group index (n_g), second-order dispersion (β_2) and fourth-order dispersion (β_4) are studied principally for the description of the nonlinear parameters. Ring-like structures are introduced in the waveguide's first and second innermost rows to produce further impact. This rigorous study showed that the combined shift and twist effects with an optimized radius of air cylinders resulted in a higher and flat group index with a considerably larger bandwidth. The structure with shift, twist and rings in the two innermost rows (S2) has resulted in improved features of SL than the structure with shift, twist and rings in one innermost row (S1). By this method, we propose an organized way to develop the PCWs with desired delay and wide ranges of bandwidth. These PCWs can be used as optical buffers and switches to produce nonlinear effects such as parametric amplification.

3.2 Geometrical Design:

Figure 3.1 (a) shows the geometrical design of the proposed PCW structure. A two dimensional periodic hexagonal air-cylinder pattern with a lattice constant (*a*) 465 nm is used as the base structure. Air cylinders with a radius of 0.25*a* (116.25 nm) in GaAs substrate are used for this purpose. One row of air cylinders (row-8) is eliminated to form the waveguide (W15) structure with a width of 1.72*a* (800 nm). Figure 3.1 (b) shows the partial filling of air holes with the same material to form a ring-like structure (rings). The holes, just adjacent to the waveguide, up to the second row are filled to form the rings. The inner cylinder's radius (r′) is optimized between 0.08*a* to 0.16*a* and is found to be 0.12*a* (55.8 nm). At this r′, the PCW results with maximum slow light features.

Figure 3.1 (c) shows the proposed study in a nutshell. To investigate the properties of PCW, at the commencement of the work, we studied the effect of the radius of holes adjacent to the waveguide. Later studies involved the lattice shift and twist of the holes. Also, in the ring-like structure, the upshot of change in radius, shift and twist are examined. Besides, we studied the integrated effect of radius, shift and twist on the dispersion features of the PCW. SL features are characterized by calculating the NDBP, β_2 and β_4 of the structure. Improvement is observed in the waveguide features with applied shift, twist and change in hole radius. Structures with rings resulted in flat band structures.

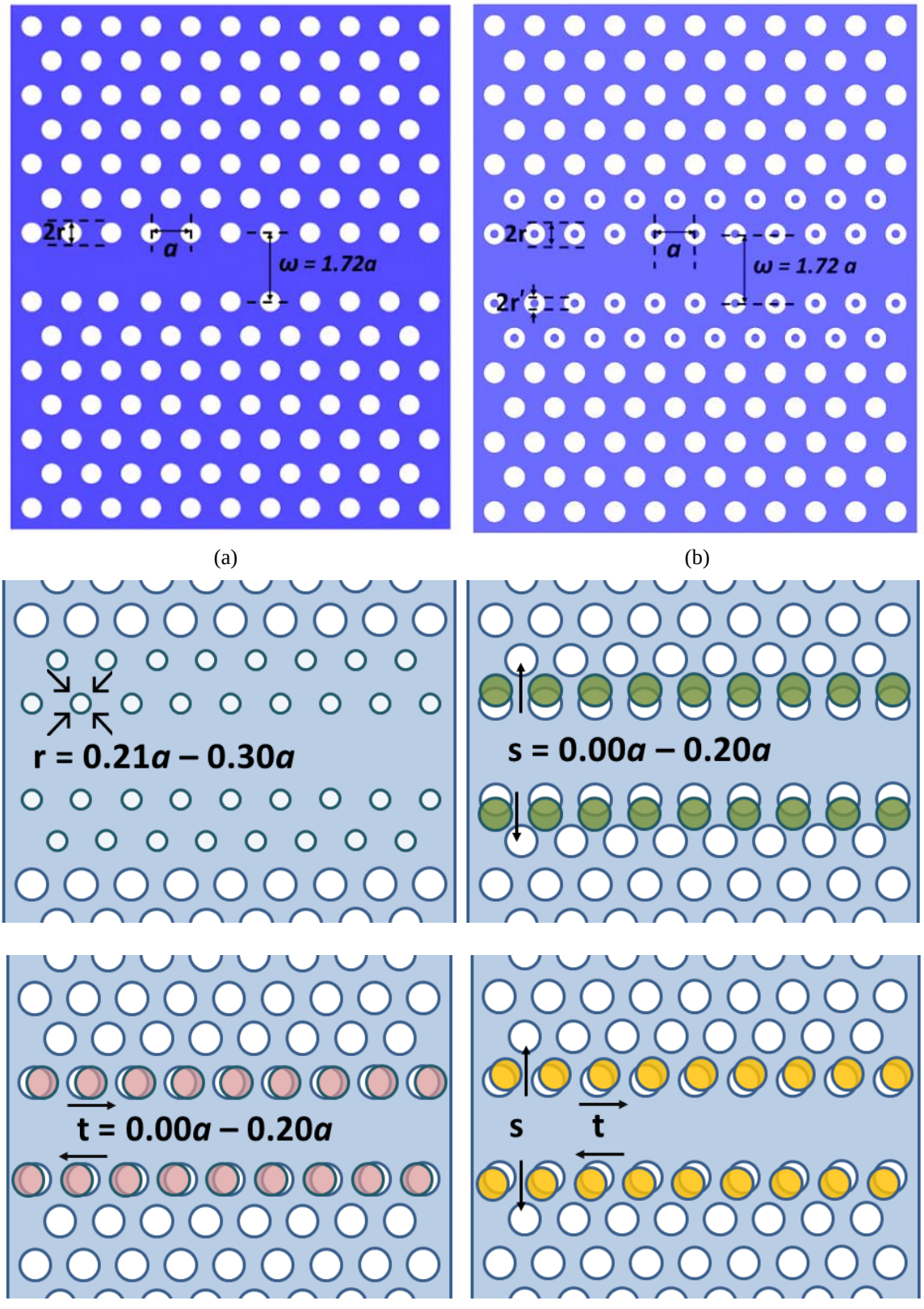

Figure 3.1: Schematic of the proposed structure. (a) 2-D hexagonal lattice with air cylinders to form the waveguide. (b) waveguide with rings (c) illustration of change in radius, introducing shift and twist effects.

3. 3 Theory of analyzing parameters:

In this study, MIT Photonic-Bands (MPB) [31] on the Ubuntu platform is used to simulate the structure and to calculate the group velocity and group index values at a given frequency. The group index, which is considered as the slow-down factor or the delay, is defined as $n_g = (c/v_g)$. A critical parameter in dispersion engineered PCW is the group velocity v_g, defined as the inverse of the first-order dispersion [2]

$$v_g = \left(\frac{dk}{d\omega} \right)^{-1} \tag{3.1}$$

where k is the wavenumber and ω is the angular frequency. The other parameter which determines the nonlinear behaviour of the light in PCW is the β_2 or GVD, which is defined as [2]

$$\beta_2 = \left(\frac{d^2k}{d\omega^2} \right) \tag{3.2}$$

The PCW is best described with n_g, GVD or β_2 and the normalized bandwidth. However, for a given structure, the n_g and the bandwidth over which n_g is maintained constant are inversely proportional. The delay (Δt) is one of the chief factors that confirm the capability of the PCW as an optical buffer. To quantify the performance of the PCW, a delay-bandwidth product (DBP) is used. The bandwidth over which the group index maintained approximately constant is referred as the flat band (Δf). The product of delay and bandwidth (DBP) is an essential parameter for SL devices (DBP = $\Delta t.\Delta f$) [2]. To compare the performance of PCWs of different lengths, normalized delay-bandwidth product (NDBP) is defined [2], which is the product of average group index n_g and normalized bandwidth $\left(\Delta\omega / \omega_o \right)$.

$$NDBP = n_g \cdot \left(\Delta\omega / \omega_o \right) \tag{3.3}$$

Hence, for applications like SL, one requires the PCW with a large DBP to provide a larger buffering time. In this study, for every structure, the average n_g, bandwidth, β_2 and β_4 parameters are calculated, and their changes with geometrical perturbations are plotted.

3.4 Results and Discussion:

Figure 3.2 shows the photonic band diagram of the base structure. The substrate band exists between bands 14 and 15. The first PBG exists between bands 15 and 16. Theoretically, it is found to be 0.006215 *c/a*. Using the lattice constant's value, it is 28.51 nm.

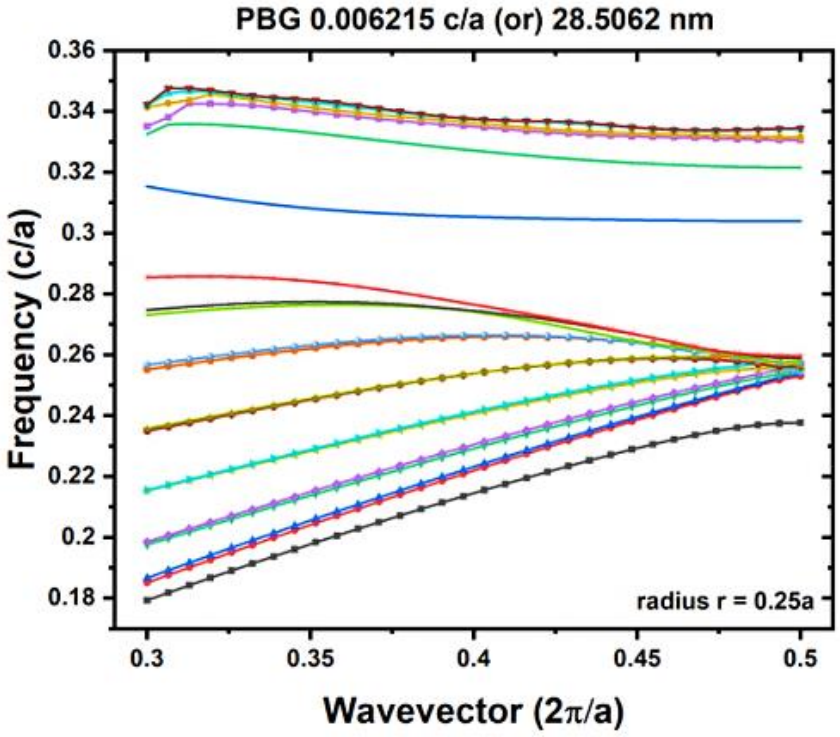

Figure 3.2: Photonic band diagram of the structure. The PCW structure with hole radius r = 0.25*a* is taken as a reference in the study.

In the coming sections, we studied the effect of radius of holes, lattice shift, lattice twist, the introduction of rings and the combined effect on the dispersion features and slow light properties of the PCW.

3.4.1 Effect of radius:

In this step, the radius of the air cylinders and the rings is optimized to achieve control over the dispersion curve. Further, these achieved results are used in the next steps to increase the dispersion features. As discussed by [15-16], the change in radius of the air cylinder provides great control over the group velocity. To follow up this study, at first, the effect of hole's radius on the PBG and the dispersion properties is studied. The line defect in PCW supports the modes categorized as index guided and gap guided [32]. The interactions between these modes determine the realization of nonlinear effects in the PCW. To study the effect of radius of hole on the PBG of the structure, band 15 is considered for further analysis. In the simulation, the radius of the air hole, just adjacent to the waveguide is changed and the corresponding bands are plotted with wave vector. In figure 3.3 (a), band 15 is plotted with a wave vector for PCW with air cylinders. Different curves in the plot represent the band 15 (band edge) of the structure with different hole radii. Figure 3.3 (b) represents the same of the PCW with rings.

In the ring's structure, only the radius of the outer cylinder is changed from 0.21*a* to 0.30*a*, while the inner cylinder's radius remains constant as 0.12*a*. The slope of these dispersion curves gives the group velocity of the mode. The increase in the slope of these dispersion curves with a decrease in the radius of hole indicates the possibility of the flat band region. This flat band indicates the possibility of achieving nonlinear effects such as four-wave mixing (FWM), supercontinuum generation (SCG), PA, and SL. Therefore, nonlinear effects could be generated in this region by decreasing the radius of the holes adjacent to the waveguide and introducing the rings in the structure.

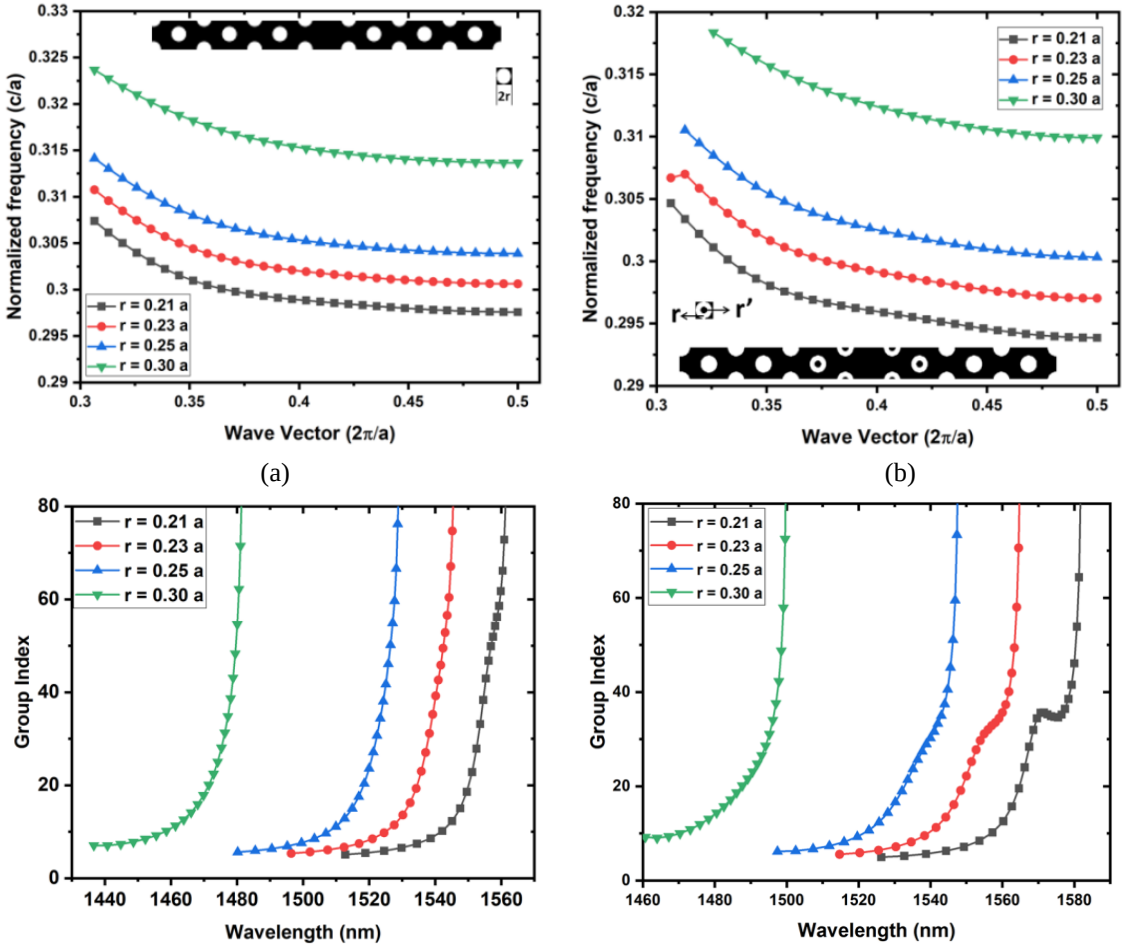

Figure 3.3: Band 15 from the band diagram of the PCW (a) with holes and (b) with rings. Group index plot of the PCW (c) with holes and (d) with rings.

For studying the features of the PCW, the calculated n_g is plotted against the calculated wavelengths (figure 3.3 (c-d)). As discussed by others, [33] wavelength and n_g plot changes from shoulder to step-like shape in case of PCW with holes and U-shape in case of PCW with rings. In both cases, r/*a* = 0.21 resulted in the possibility of nonlinear effects. Variation of β_2 and β_4 (fourth-order dispersion) with wavelength are shown in figure 3.4 (a-d)

for the structures with holes and rings, respectively. At r/a = 0.21, the smallest among our considered fraction filling values, β_2 and β_4 have a clear change from positive to the negative range and vice versa. This reveals the possibility of dispersion compensation in the structure. In contrast, the increase in the radius of the hole and ring has lowered the changes in these values which confirm the possible distortion of optical pulse in the PCW.

The waveguide with rings and air cylinders of radius 0.21a (figure 3.4 (c-d)) has the highest dispersion compensation. The β_2 and β_4 values spread across positive and negative regions and confirm the ultra-low dispersion.

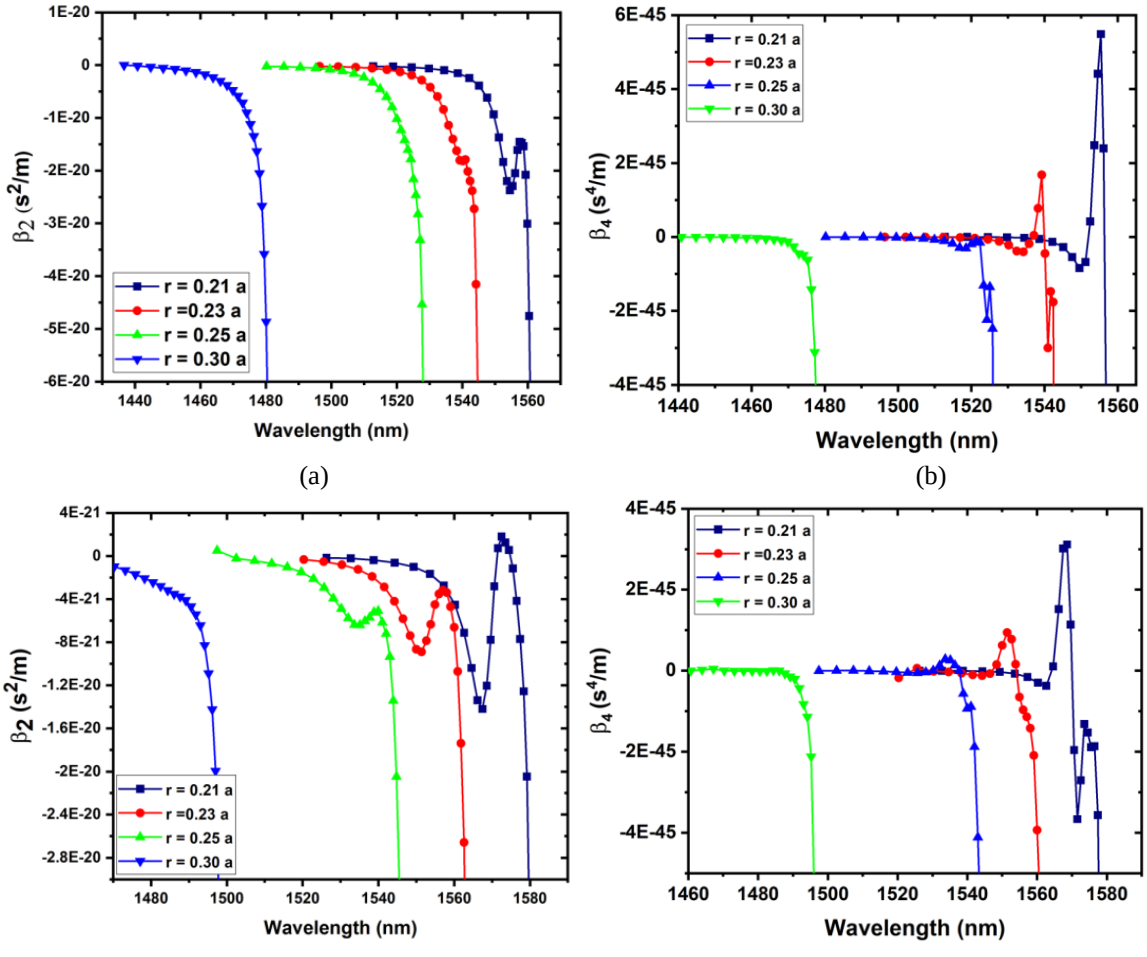

Figure 3.4: Dispersion characteristics corresponding to figure 3.3 (c-d). (a) β_2 of PCW with holes (b) β_4 of PCW with holes (c) β_2 of PCW with rings (d) β_4 of PCW with rings.

Here, in the initial structure with r = 0.25a, no nonlinear effects are observed. However, the change in hole radius affects the profiles of β_2 and β_4. At r = 0.21a, considerable changes in n_g, β_2 and β_4 are observed. Though technologically alteration of the hole size is challenging, yet it is interesting due to the nonlinear applications. In a further study, this optimized radius value r = 0.21a is used to improve the features of the structure.

3.4.2 Effect of lattice shift:

By changing the position of the holes in the PCW, one can produce a nearly constant group index over a large bandwidth [17]. The shift in the lattice produces different linear and nonlinear effects, which have potential applications [18]. The shift introduced in the lattice directly impacts the dispersive curve and produces a flat band. Considering the previously published results, the shift (s) in the lattice is introduced in the range of $0.00a$ – $0.20a$ with $0.04a$ step. From our first result, the radius of the holes and rings remains taken as $0.21a$. So far, either the position or the radius of the holes and rings is changed to enhance the dispersion and SL features of the PCW.

In this study, we combined both the effects and calculated the resultant performance of the PCW. With the applied shift, the innermost rows move away from each other and the waveguide width increases. This widening of the width contributes to dispersion engineering. The position of band 15 is plotted against the wave vector (figure 3.5), and the first and second-order derivatives are calculated. Figure 3.6 shows the variation of the group index with wavelength. Table 3.1 summarizes n_g and bandwidth with the shift in the lattice in holes and rings structure.

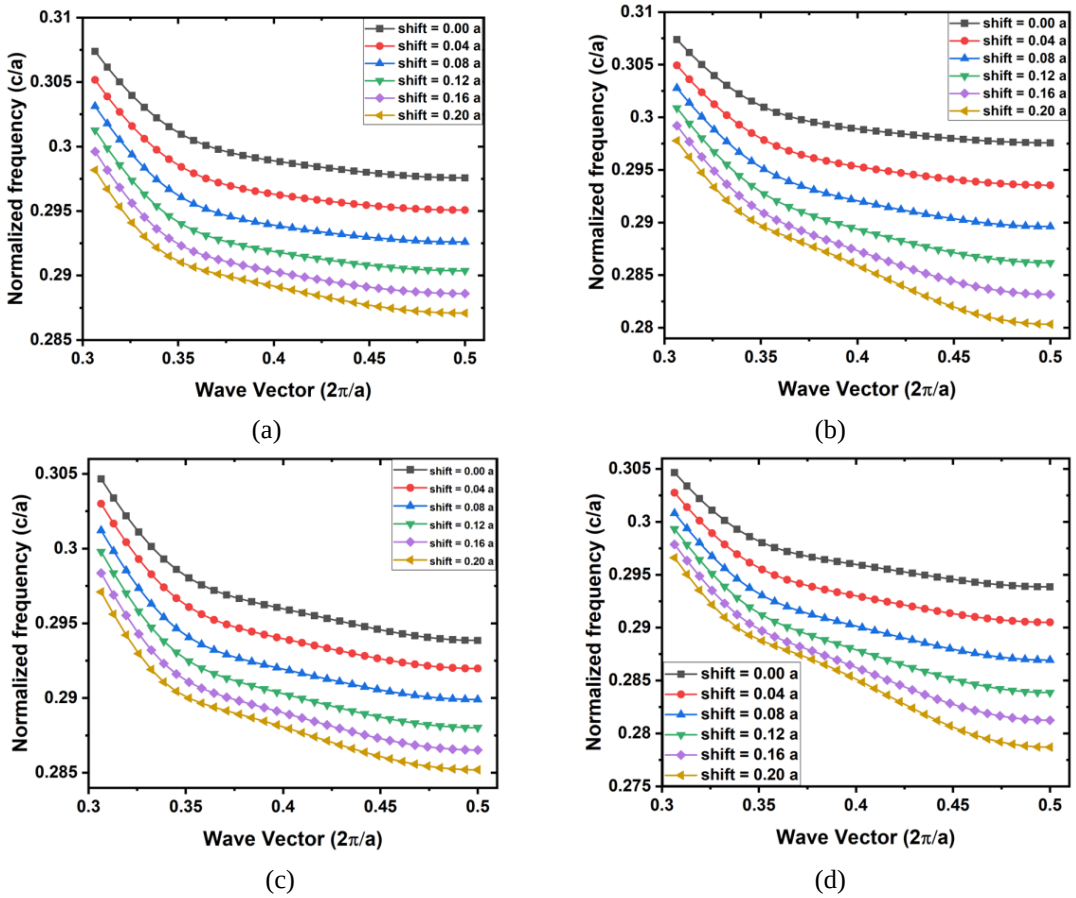

Figure 3.5: Band 15 from the band diagram of PCW with holes and (a) shift in one row (b) shift in two rows. Band 15 from the band diagram of PCW with rings and (c) shift in one row (d) shift in two rows.

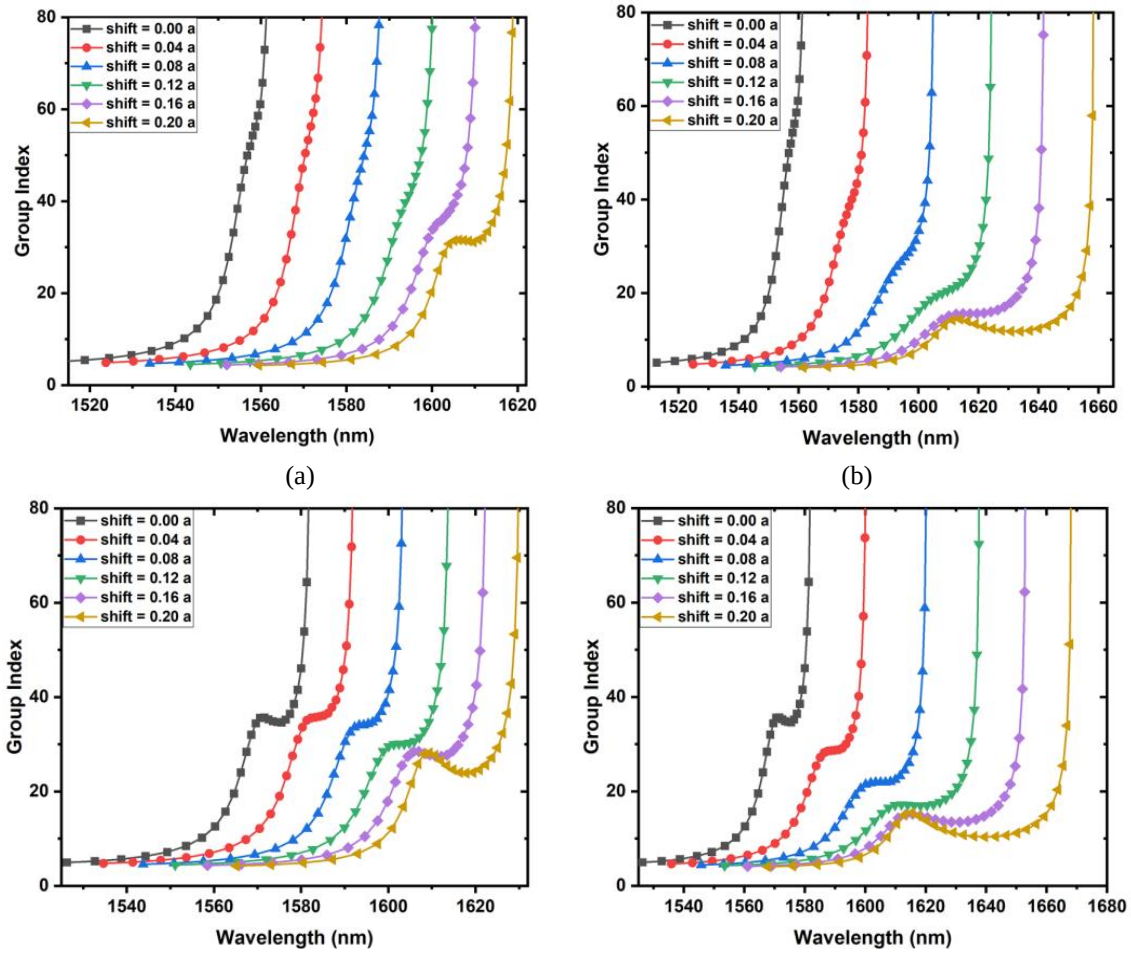

Figure 3.6: Group index - wavelength plot of the PCW with holes and (a) shift in one row (b) shift in two rows. Group index - wavelength plot of the PCW with rings and (c) shift in one row (d) shift in two rows.

Table 3.1: Calculated group index and bandwidth of the waveguide at different shift values in first and second rows

Holes			**Rings**		
shift (s)	n_g	**bandwidth (nm)**	**shift (s)**	n_g	**bandwidth (nm)**
Shift in one row					
0.00*a**	-	-	0.00*a*	34.72	1.98
0.04*a**	-	-	0.04*a*	35.55	2.92
0.08*a**	-	-	0.08*a*	34.27	3.09
0.12*a**	-	-	**0.12*a***	**30.41**	**5.87**
0.16*a**	-	-	0.16*a*	27.58	3.92
0.20*a*	**31.42**	**7.97**	0.20*a*	24.22	6.01
Shift in two rows					
0.00*a**	-	-	0.00*a*	34.72	1.98
0.04*a**	-	-	0.04*a*	28.66	6.1
0.08*a**	-	-	0.08*a*	21.82	8.16
0.12*a*	20.70	1.74	**0.12*a***	**17.17**	**14.8**
0.16*a*	**15.56**	**13.95**	0.16*a*	13.73	13.49
0.20*a*	11.88	9.36	0.20*a*	10.54	14.22

*No flat band is observed with constant group index.

Like in the previous case, β_2 and β_4 are calculated and plotted against the wavelength. Here the shift is applied in the first and second rows of the holes and rings of the structure to enhance the dispersion and SL features of the PCW. As the shift in the lattice is increased, a gradual increase in the 'band' of β_2 and β_4 curves is observed. In figures 3.7 & 3.8, we have shown the plots of β_2 and β_4 against wavelength, respectively. Table 3.2 gives the introduced shift, corresponding maximum and minimum values of β_2 and β_4 for both holes and rings structures.

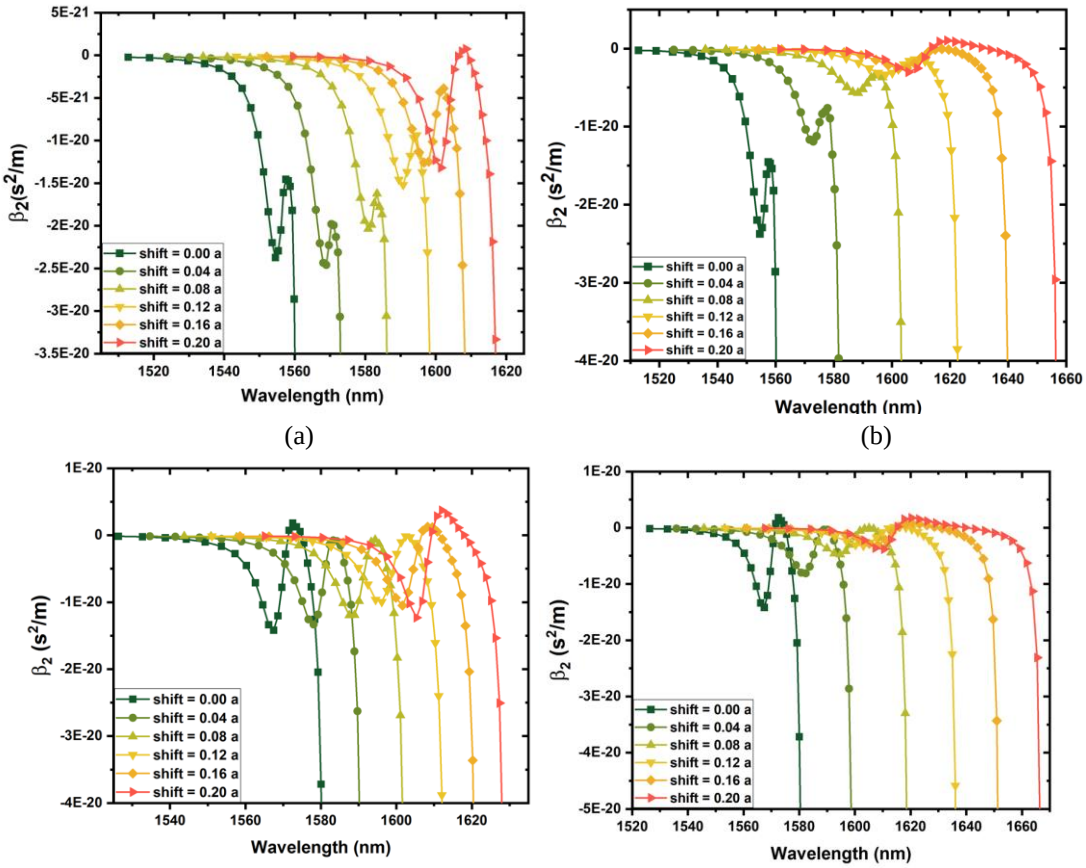

Figure 3.7: Dispersion characteristics corresponding to figure 3.6 (a-d).
(a) β_2 of PCW with holes and shift in one row (b) β_2 of PCW with holes and shift in two rows
(c) β_2 of PCW with rings and shift in one row (d) β_2 of PCW with rings and shift in two rows.

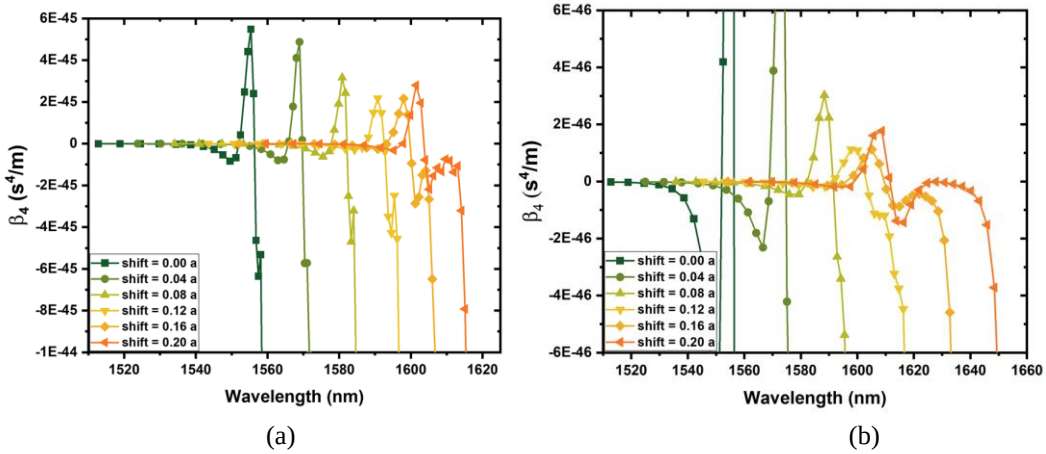

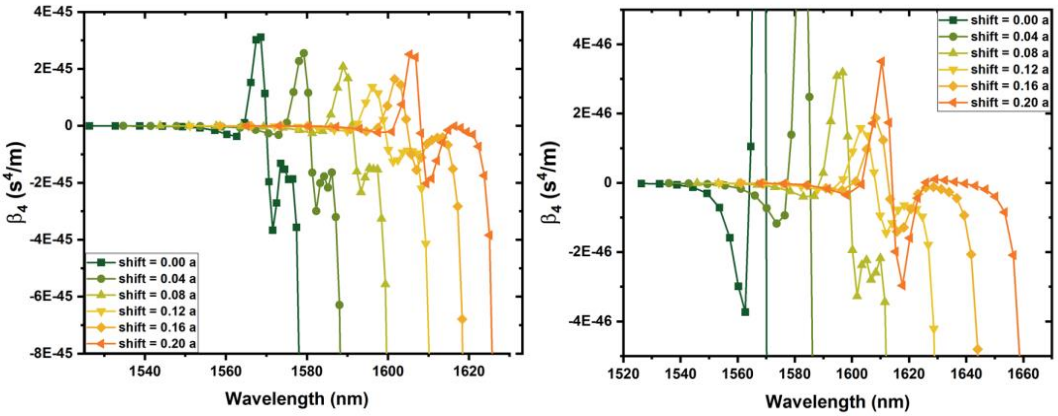

(c) (d)

Figure 3.8: Dispersion characteristics corresponding to figure 3.6 (a-d).
(a) β_4 of PCW with holes and shift in one row (b) β_4 of PCW with holes and shift in two rows
(c) β_4 of PCW with rings and shift in one row (d) β_4 of PCW with rings and shift in two rows.

Table 3.2: Calculated β_2 and β_4 values of the waveguide with applied shift.

Holes					Rings				
shift (s)	**β_2(max.) x 10^{-20} s^2/m**	**β_2(min.) x 10^{-20} s^2/m**	**β_4(max.) x 10^{-45} s^4/m**	**β_4(min.) x 10^{-45} s^4/m**	**shift (s)**	**β_2(max.) x 10^{-20} s^2/m**	**β_2(min.) x 10^{-20} s^2/m**	**β_4(max.) x 10^{-45} s^4/m**	**β_4(min.) x 10^{-45} s^4/m**
Shift in one row									
0.00*a*	-1.454	-2.373	5.486	-6.352	0.00*a*	0.1807	-1.418	3.116	-3.666
0.04*a*	-1.979	-2.458	4.874	-5.731	0.04*a*	-0.0885	-1.332	2.553	-2.990
0.08*a*	-1.622	-2.036	3.159	-4.705	0.08*a*	-0.0677	-1.196	2.082	-2.330
0.12*a*	-0.9657	-1.519	2.177	-4.273	0.12*a*	-0.0132	-0.9954	1.363	-1.255
0.16*a*	-0.3879	-1.259	2.159	-2.871	0.16*a*	0.1263	-1.050	1.641	-1.547
0.20*a*	0.0749	-1.318	2.799	-2.188	0.20*a*	0.3713	-1.231	2.511	-2.027
Shift in two rows									
0.00*a*	-1.454	-2.373	5.486	-6.352	0.00*a*	0.1807	-1.418	3.116	-3.666
0.04*a*	-0.7649	-1.190	1.282	-5.444	0.04*a*	-0.0338	-0.8104	0.9339	-1.0378
0.08*a*	-0.3413	-0.5681	0.3025	-0.3404	0.08*a*	-0.0044	-0.4778	0.3189	-0.3273
0.12*a*	-0.1405	-0.3322	0.1125	-0.1196	0.12*a*	-0.0096	-0.3184	0.1580	-0.1445
0.16*a*	-0.0037	-0.2586	0.1123	-0.0876	0.16*a*	0.0803	-0.3010	0.1872	-0.1410
0.20*a*	0.1024	-0.3007	0.1776	-0.1436	0.20*a*	0.1766	-0.3797	0.3506	-0.2964

The above β_2 and β_4 values confirm the low dispersion in the proposed PCW. These dispersion values are well suitable for typical applications of PC and PCW at the central wavelength 1550 nm and lattice constant about 400 nm [11]. Thus it can be treated as ultralow dispersion for practical applications. In a few structures, the β_2 and β_4 curves present both a negative and positive range. This reveals the possibility of dispersion-compensating applications.

The shift effect produces more impact when two rows are shifted. At lattice shifts of 0.12*a* and 0.16*a*, the impact is the highest in our observation. Even the rows can be shifted further, but this shift causes the generation of the original hexagonal lattice of the base structure.

3.4.3 Effect of twist:

Previously, dispersion tailoring is demonstrated by introducing a twist effect in the lattice structure [9, 13]. In the twist induced PCW, the dispersion profile is controlled by achieving anti-crossing between even and odd modes. Like the lattice shift, the twist introduced in the lattice directly impacts the dispersive curve and produces the flat band. Considering the previous results of different structures [16], the twist (t) in the lattice is introduced in the range of 0.00a – 0.20a with 0.04a step. From our prior result, the radius of the holes and rings remains taken as 0.21a. Figure 3.9 shows the dispersion curves of the waveguide for both holes and rings structures. We introduced the twist in the first and second rows of the structure and studied the dispersion profile. The instituted twist has widened the group index-wavelength plot, which is shown in figure 3.10. For instance, in the case of ring-like structure, almost a constant n_g of 11.67 is observed over a bandwidth of 27.87 nm when the structure is affected by a twist parameter of 0.16a, compared to the base structure with n_g 34.72 over a bandwidth of 1.98 nm. Table 3.3 gives the summary of applied twist, corresponding n_g and the wavelength range for the PCWs with holes and rings.

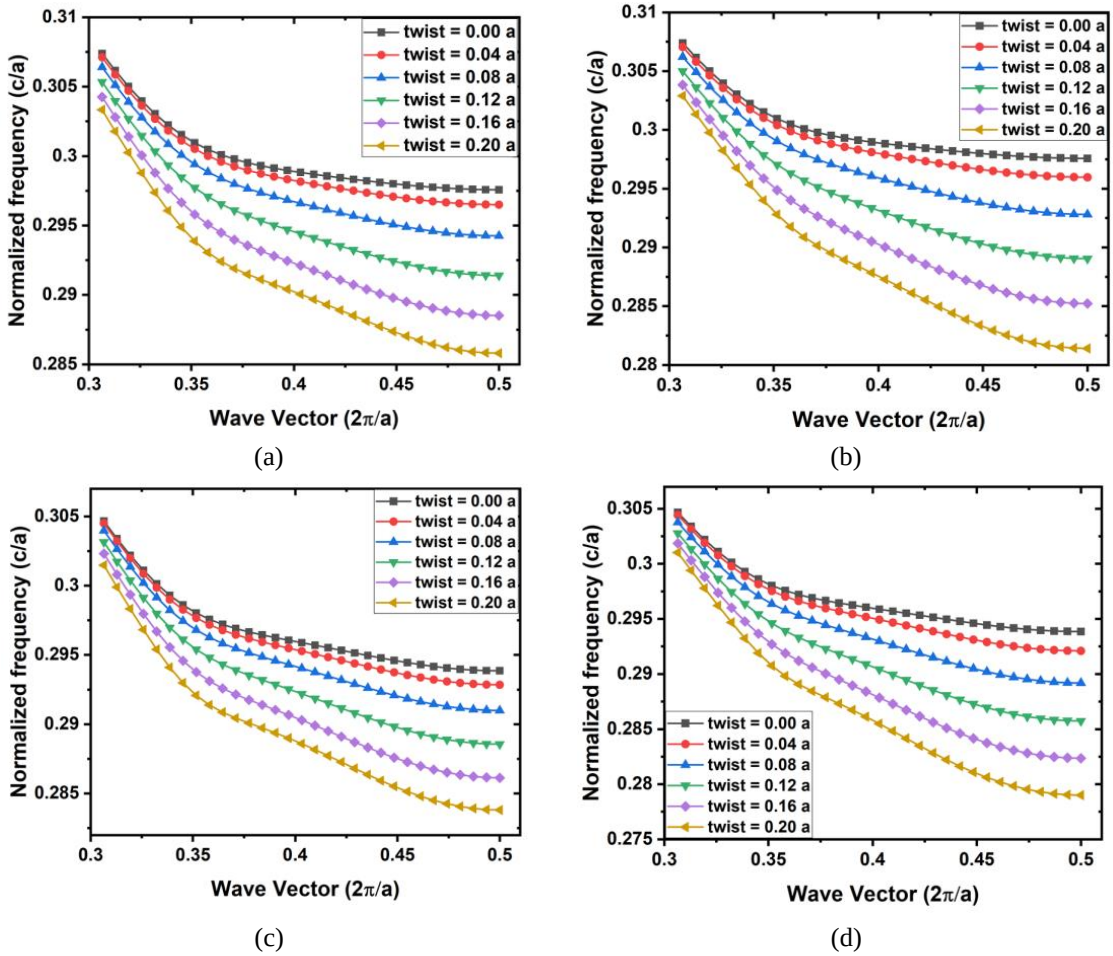

Figure 3.9: Band 15 from the band diagram of PCW with holes and (a) twist in one row (b) twist in two rows. Band 15 from the band diagram of PCW with rings and (c) twist in one row (d) twist in two rows.

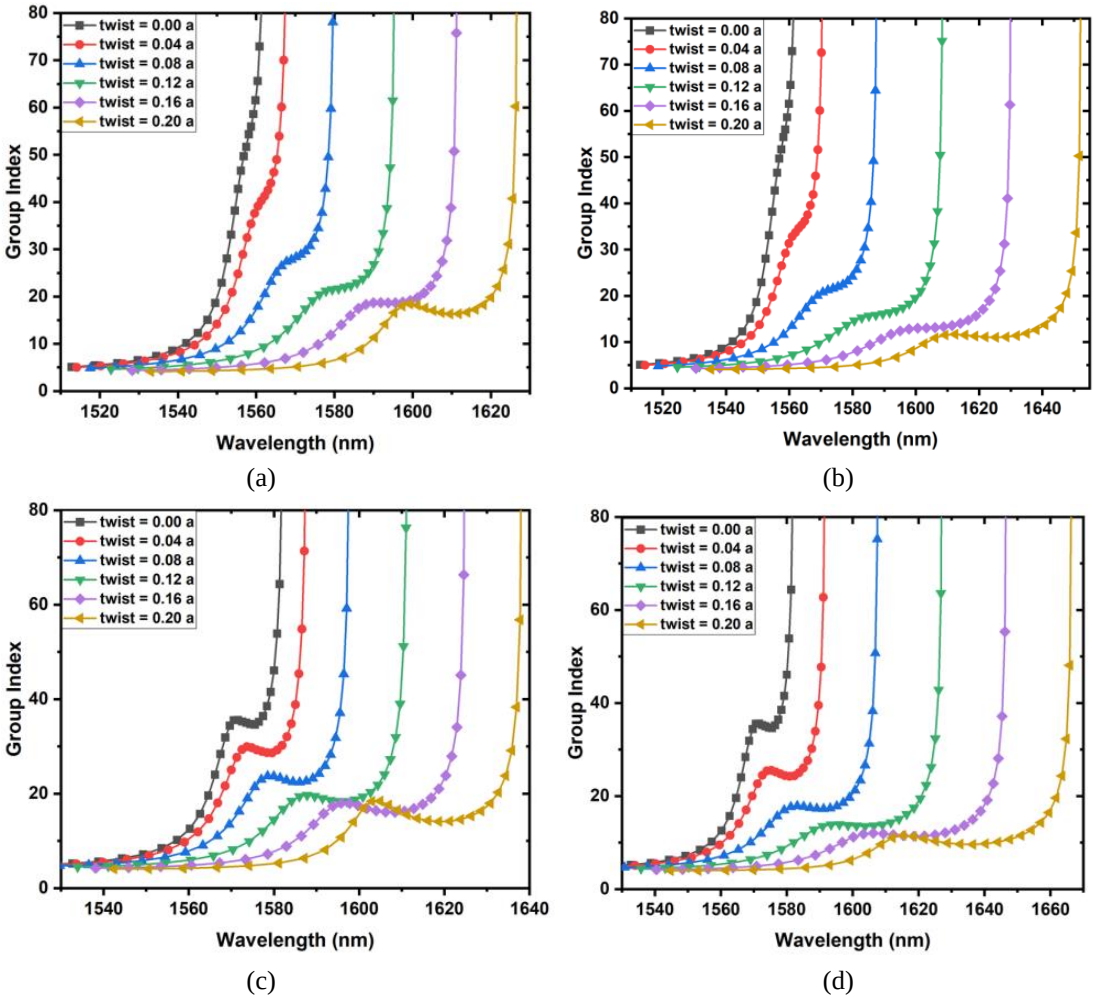

Figure 3.10: Group index - wavelength plot of the PCW with holes and (a) twist in one row (b) twist in two rows. Group index - wavelength plot of the PCW with rings and (c) twist in one row (d) twist in two rows.

Table 3.3: Calculated group index and bandwidth of the waveguide at different twist values in first and second rows

Holes			Rings		
twist (t)	**n_g**	**bandwidth (nm)**	**twist (t)**	**n_g**	**bandwidth (nm)**
Twist in one row					
0.00*a**	-	-	0.00*a*	34.72	1.98
0.04*a**	-	-	0.04*a*	29.56	3.47
0.08*a*	28.61	1.20	0.08*a*	22.60	4.64
0.12*a*	22.40	3.11	0.12*a*	18.61	7.61
0.16*a*	**18.72**	**11.29**	**0.16*a***	**16.43**	**10.97**
0.20*a*	16.59	8.7	0.20*a*	14.38	10.18
Twist in two rows					
0.00*a**	-	-	0.00*a*	34.72	1.98
0.04*a**	-	-	0.04*a*	24.67	7.04
0.08*a*	21.61	3.18	0.08*a*	17.51	15.96
0.12*a*	15.58	4.46	0.12*a*	13.70	18.14
0.16*a*	13.20	10.86	**0.16*a***	**11.67**	**27.87**
0.20*a*	**11.34**	**28.91**	0.20*a*	9.73	11.48

*No flat band is observed with constant group index.

Like the shift parameter, the twist in the lattice has directly controlled β_2 and β_4. Figure 3.11 & 3.12 shows the β_2 and β_4 variations with wavelength, respectively. Here, one can choose to select the structure for different applications. One can select a high n_g PCW with narrow bandwidth or a low n_g PCW with broad bandwidth. In these plots, the negative β_2 & β_4 values and positive β_2 & β_4 values are observed for different wavelengths. Hence, the dispersion compensation can be achieved within the waveguide. With the increase in the twist from 0.00*a* to 0.20*a*, the curve becomes flatter and the broad band is noticed with positive and negative peaks. Table 3.4 summarizes the applied twist, corresponding maximum and minimum β_2 and β_4 values for holes and rings structures. We also noticed that the structures with rings have the dispersion curves near the zero-dispersion line even if the twist values are small in magnitude.

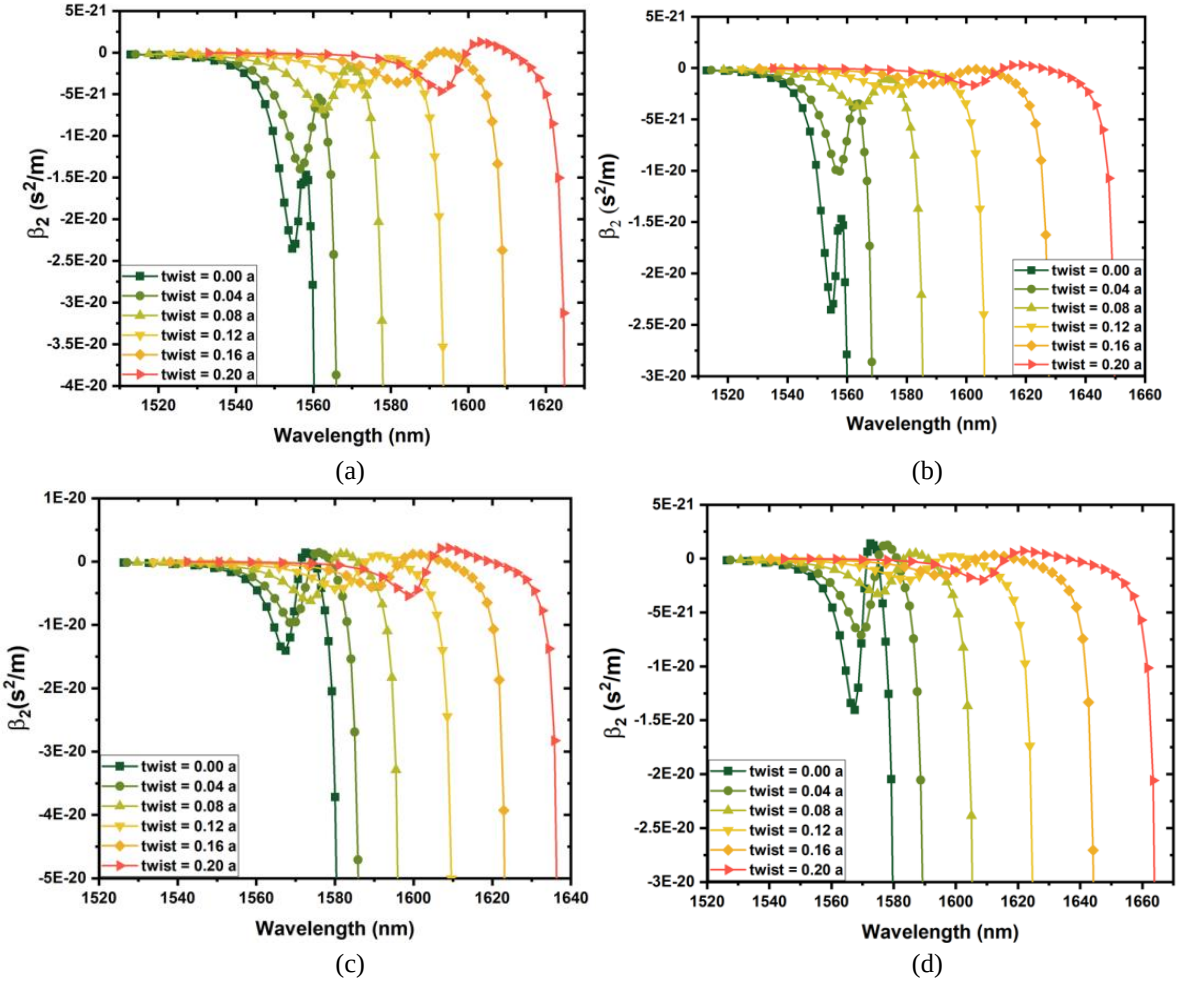

Figure 3.11: Dispersion characteristics corresponding to figure 3.10 (a-d).
(a) β_2 of PCW with holes and twist in one row (b) β_2 of PCW with holes and twist in two rows
(c) β_2 of PCW with rings and twist in one row (d) β_2 of PCW with rings and twist in two rows.

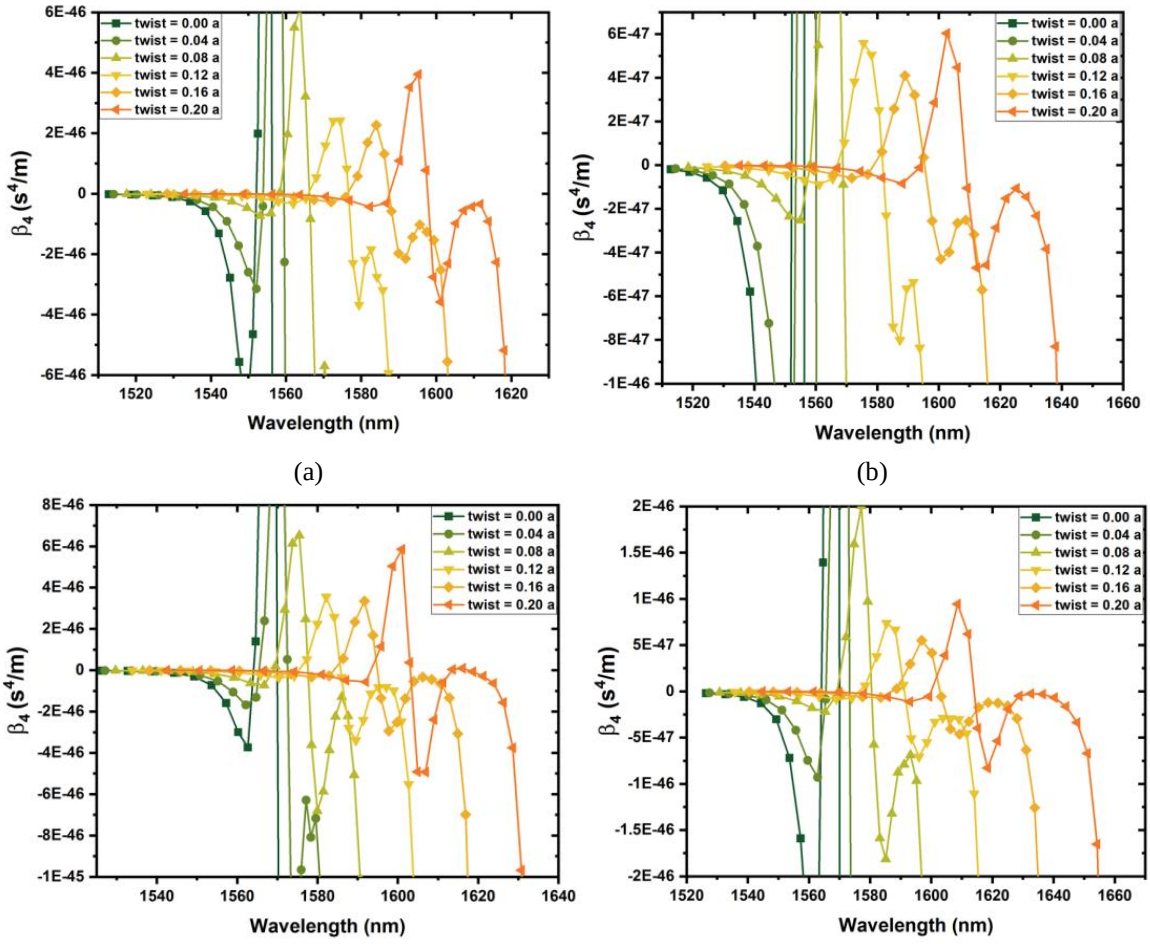

Figure 3.12: Dispersion characteristics corresponding to figure 3.10 (a-d).
(a) β_4 of PCW with holes and twist in one row (b) β_4 of PCW with holes and twist in two rows
(c) β_4 of PCW with rings and twist in one row (d) β_4 of PCW with rings and twist in two rows.

Table 3.4: Calculated β_2 and β_4 values of the waveguide with applied twist

Holes					Rings				
twist (t)	**β_2(max.) x 10^{-20} s^2/m**	**β_2(min.) x 10^{-20} s^2/m**	**β_4(max.) x 10^{-45} s^4/m**	**β_4(min.) x 10^{-45} s^4/m**	**twist (t)**	**β_2(max.) x 10^{-20} s^2/m**	**β_2(min.) x 10^{-20} s^2/m**	**β_4(max.) x 10^{-45} s^4/m**	**β_4(min.) x 10^{-45} s^4/m**
Twist in one row									
0.00*a*	-1.466	-2.353	6.051	-4.929	0.00*a*	0.1405	-1.403	3.107	-3.634
0.04*a*	-0.5429	-1.396	1.910	-3.594	0.04*a*	0.1432	-0.9607	1.647	-1.740
0.08*a*	-0.1703	-0.6881	0.6186	-0.7869	0.08*a*	0.1248	-0.6192	0.6526	-0.6805
0.12*a*	-0.0649	-0.4145	0.2414	-0.3680	0.12*a*	0.1025	-0.4269	0.3555	-0.3395
0.16*a*	0.0056	-0.3641	0.2270	-0.2148	0.16*a*	0.1172	-0.4029	0.3347	-0.2935
0.20*a*	0.1284	-0.4644	0.3953	-0.3582	0.20*a*	0.2176	-0.5393	0.5856	-0.4924
Twist in two rows									
0.00*a*	-1.466	-2.353	6.051	-4.929	0.00*a*	0.1405	-1.403	3.10759	-3.634
0.04*a*	-0.3467	-1.005	1.172	-2.364	0.04*a*	0.1249	-0.7096	0.904635	-0.8689
0.08*a*	-0.1038	-0.3732	0.1993	-0.2038	0.08*a*	0.0488	-0.3278	0.200412	-0.1813
0.12*a*	-0.0443	-0.2053	0.0557	-0.0801	0.12*a*	0.0249	-0.1959	0.0737149	-0.0707
0.16*a*	-0.0113	-0.1543	0.0410	-0.0429	0.16*a*	0.0312	-0.1604	0.0551592	-0.0462
0.20*a*	0.0298	-0.1683	0.0603	-0.0469	0.20*a*	0.0708	-0.1995	0.0944128	-0.0828

From the above table 3.4, β_2 and β_4 values confirm the low dispersion in the proposed PCW with lattice twist. Structures with 0.16*a* and 0.20*a* twists, the β_2 and β_4 curves represent positive and negative peaks. Also, in the PCW with rings, in all the structures, the β_2 and β_4 spread across positive and negative regions. This confirms the dispersion compensation in the waveguide.

3.4.4 Combined effect of change in radius, lattice shift and twist:

To combine the impact of all the geometrical parameters on the features of PCW, the change in radius, lattice shift and twist are introduced in the structure. For this purpose, in the input program, the shift ranging from 0.00*a* to 0.20*a*, twists ranging from 0.00*a* to 0.20*a* and a radius of 0.21*a* are introduced. With these geometrical changes, the dispersion curves got modified and at s = 0.16*a*, t = 0.16*a*, and r = 0.21*a*, the structure has resulted in dispersive curves of the highest slope. Figure 3.13 shows band 15 from the photonic band diagram of the PCW with holes and rings structures.

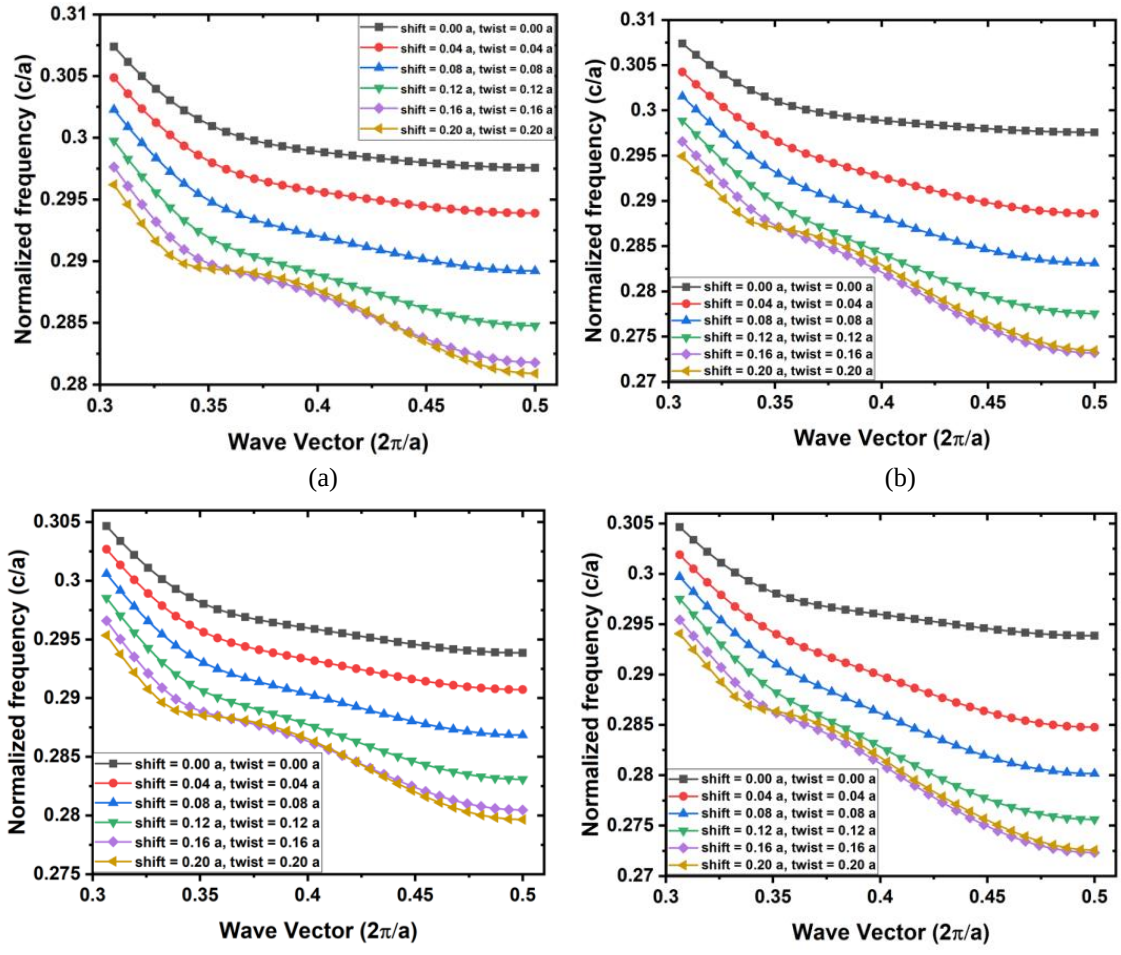

Figure 3.13: Band 15 from the band diagram of PCW with holes and applied (a) shift and twist in one row (b) shift and twist in two rows. Band 15 from the band diagram of PCW with rings and applied (c) shift and twist in one row (d) shift and twist in two rows.

Figure 3.14 shows the change in group index with wavelength for all the structures. A nearly constant group index is observed over a wide range with s = t = 0.16*a* and r = 0.21*a* when only the first row is spatially changed. This flatness increases when the shift and twist are introduced in the second row of holes/rings. However, the group index dropped to a lower value. Here, the sudden kink in the group index plots is due to the closeness of the bands in the band structure. Table 3.5 summarizes n_g values and the bandwidth that the n_g is maintained almost constant due to the lattice shift and twist.

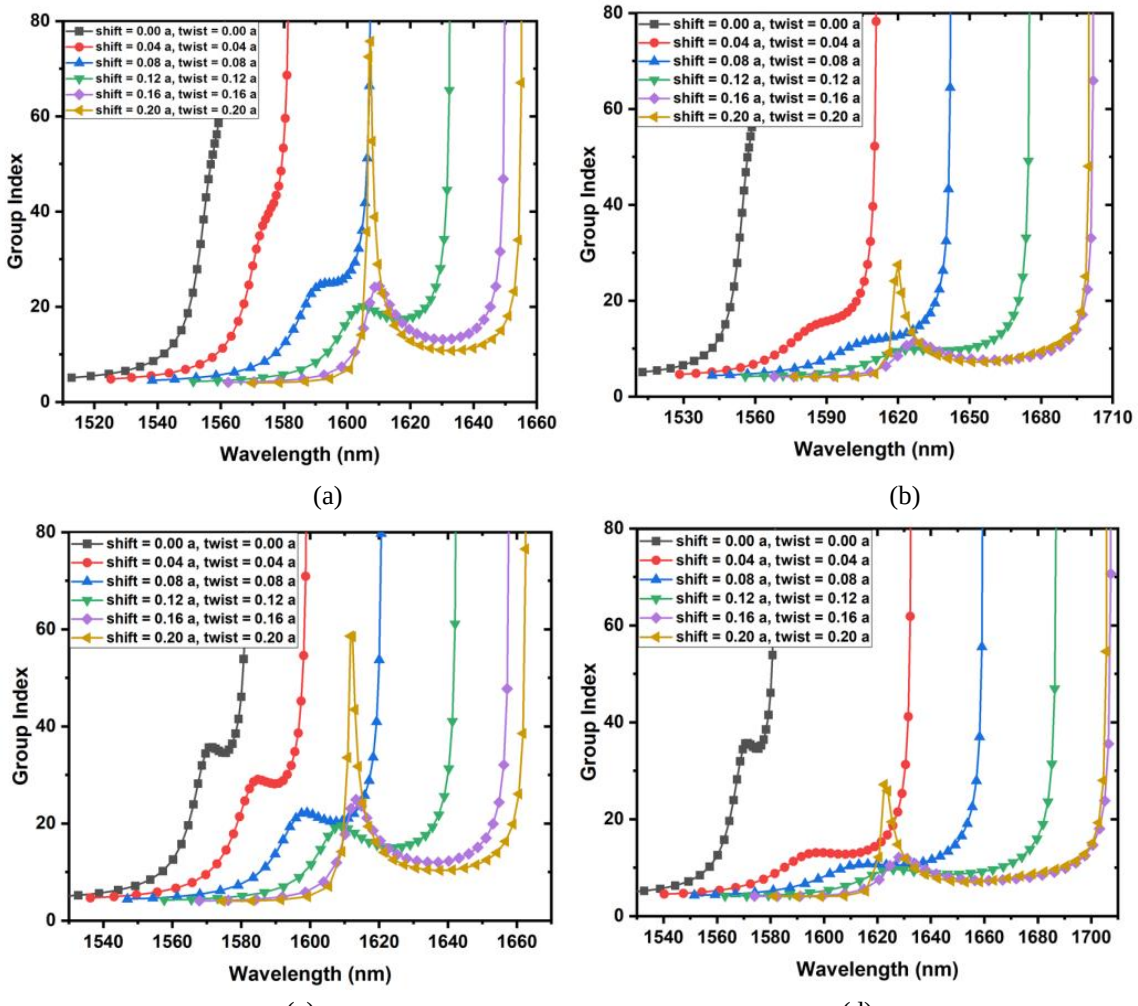

Figure 3.14: Group index - wavelength plot of the PCW with holes and applied (a) shift and twist in one row (b) shift and twist in two rows. Group index - wavelength plot of the PCW with rings and applied (c) shift and twist in one row (d) shift and twist in two rows.

Figures 3.15 & 3.16 show the β_2 and β_4 profile of the PCW with holes and rings structures with the induced shift and twist. In these plots, the β_2 and β_4 are changing sharply between positive and negative values. This change in β_2 and β_4 between positive and negative values confirms the dispersion compensation in PCW.

Table 3.5: Calculated group index and bandwidth of the waveguide at different shift and twist values (combined) in first and second rows

Holes			Rings		
shift (s) and twist (t)	**n_g**	**bandwidth (nm)**	**shift (s) and twist (t)**	**n_g**	**bandwidth (nm)**
Shift and twist in one row					
0.00*a**	-	-	0.00*a*	34.71	1.98
0.04*a**	-	-	0.04*a*	28.51	6.16
0.08*a*	24.61	4.27	0.08*a*	20.61	6.98
0.12*a*	17.61	8.26	0.12*a*	15.33	9.61
0.16*a*	**13.37**	**11.11**	**0.16*a***	**12.37**	**15.14**
0.20*a*	10.86	6.84	0.20*a*	10.57	14.18
Shift and twist in two rows					
0.00*a**	-	-	0.00*a*	34.72	1.98
0.04*a*	15.37	4.55	0.04*a*	12.89	11.11
0.08*a*	12.25	11.81	0.08*a*	10.61	24.04
0.12*a*	9.68	26.70	0.12*a*	8.86	21.39
0.16*a*	**7.88**	**29.42**	**0.16*a***	**7.64**	**30.41**
0.20*a*	7.49	25.64	0.20*a*	7.39	26.08

*No flat band is observed with constant group index.

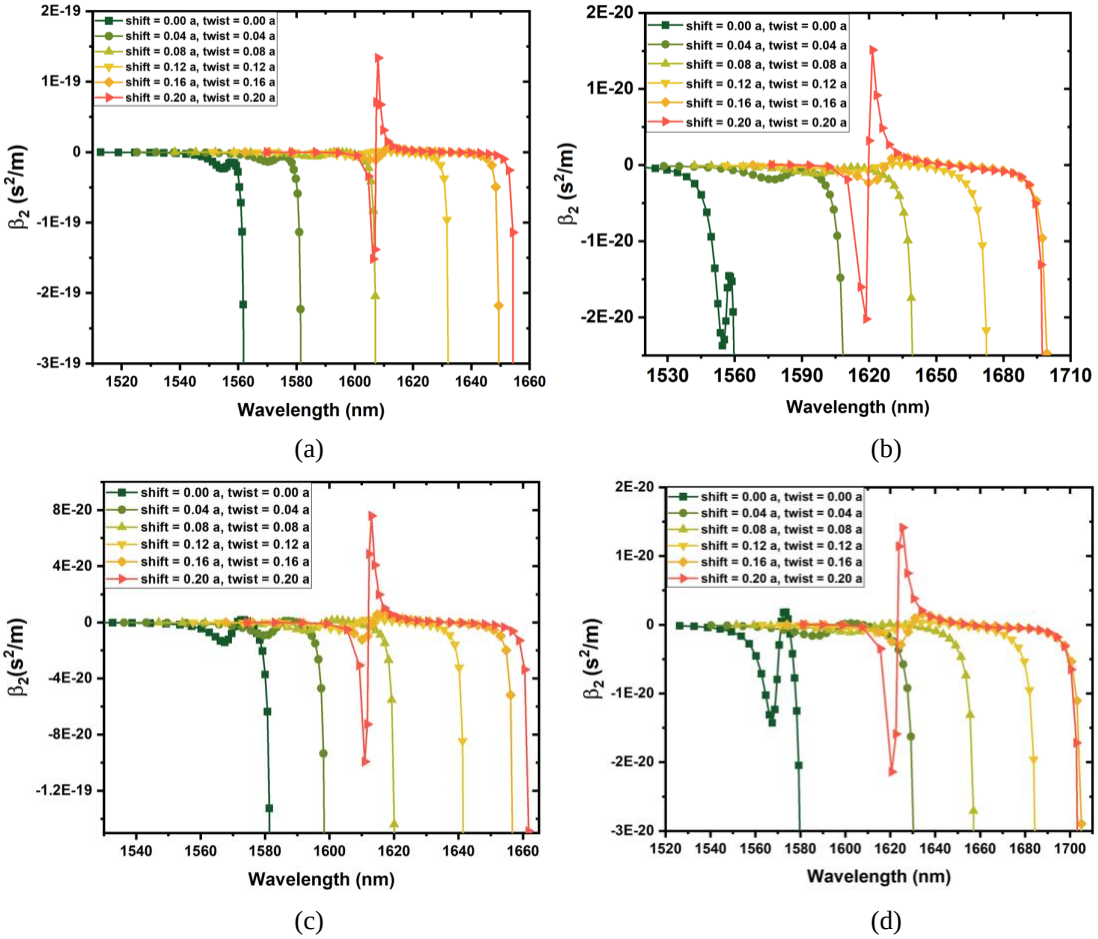

Figure 3.15: Dispersion characteristics corresponding to figure 3.14 (a-d). β_2 of PCW with holes and applied (a) shift and twist in one row (b) shift and twist in two rows. β_2 of PCW with rings and applied (c) shift and twist in one row (d) shift and twist in two rows.

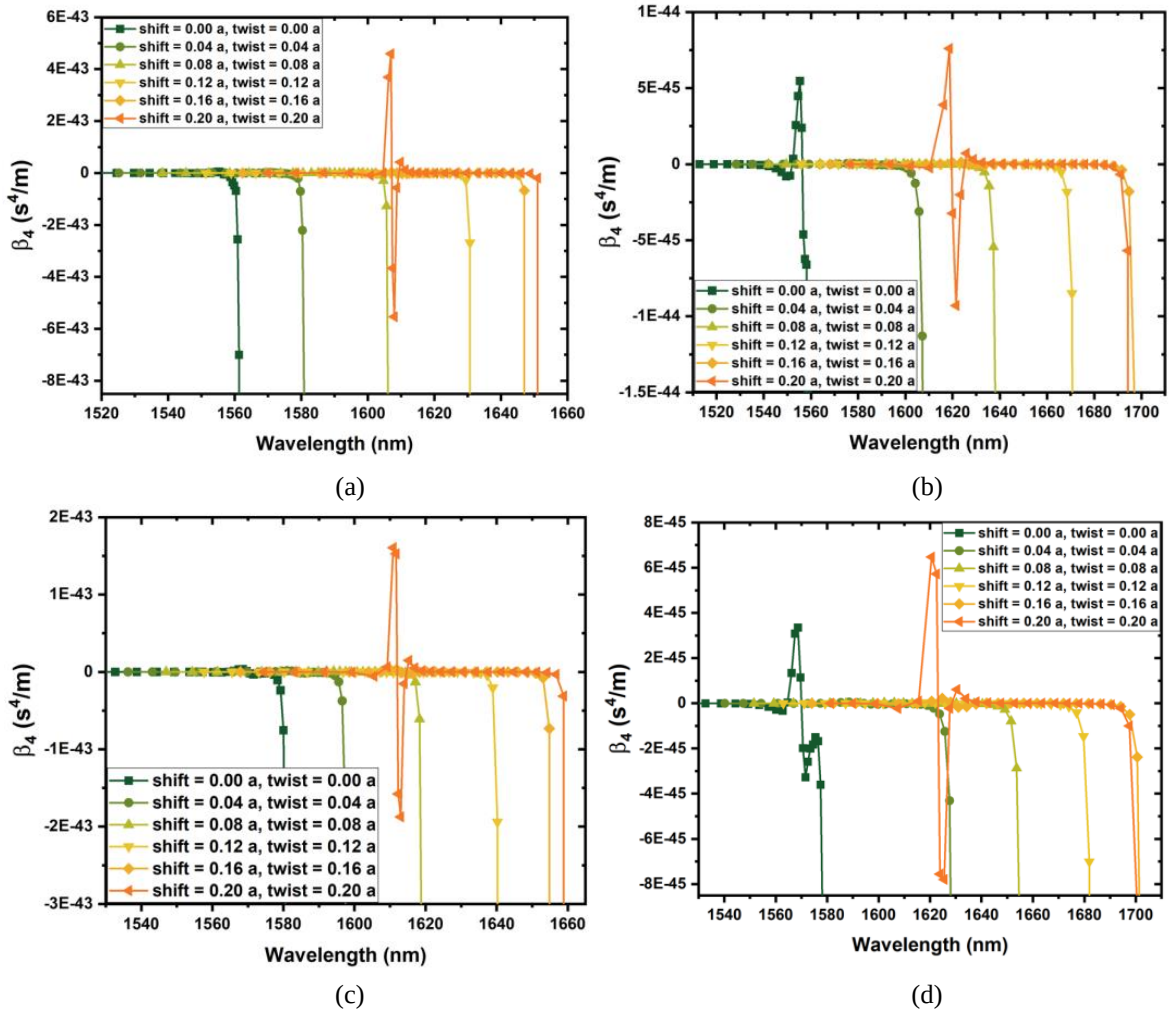

Figure 3.16: Dispersion characteristics corresponding to figure 3.14 (a-d). β_4 of PCW with holes and applied (a) shift and twist in one row (b) shift and twist in two rows. β_4 of PCW with rings and applied (c) shift and twist in one row (d) shift and twist in two rows.

In these figures, the negative and positive β_2 & β_4 values are observed at different wavelengths. Therefore, the dispersion compensation can be achieved by cascading two sections of such waveguides with opposite β_2 & β_4 values, as discussed by Hou et al. [11].

The SL features such as group index, second and fourth-order dispersions can also be influenced by temperature besides the effect of lattice shift, lattice twist and radius of the hole/ring [34-35]. We studied the effect of temperature, and found that the flat band and hence the SL region are shifting linearly with a change in temperature [36]. However, the magnitude of the shift in the SL bands depends on the material used for the fabrication of PCW. Table 3.6 summarizes applied shift, twist and corresponding β_2 and β_4 values for holes and rings structures.

Table 3.6: Calculated β_2 and β_4 values of the waveguide with combined shift and twist

Holes					Rings				
shift(s) and twist(t)	**β_2 (max.) x 10^{-20} s^2/m**	**β_2 (min.) x 10^{-20} s^2/m**	**β_4(max.) x 10^{-45} s^4/m**	**β_4 (min.) x 10^{-45} s^4/m**	**shift(s) and twist(t)**	**β_2 (max.) x 10^{-20} s^2/m**	**β_2 (min.) x 10^{-20} s^2/m**	**β_4 (max.) x 10^{-45} s^4/m**	**β_4(min.) x 10^{-45} s^4/m**
Shift and twist in one row									
0.00*a*	-1.455	-2.374	5.463	-6.242	0.00*a*	0.1817	-1.427	3.350	-3.278
0.04*a*	-0.5733	-1.362	1.904	-2.051	0.04*a*	0.1042	-0.9210	1.493	-1.434
0.08*a*	-0.0124	-0.6058	0.6210	-0.5677	0.08*a*	0.1438	-0.5893	0.5994	-0.5480
0.12*a*	0.1568	-0.5144	0.4670	-0.4057	0.12*a*	0.2153	-0.5400	0.5973	-0.5207
0.16*a*	0.5627	-1.091	2.818	-2.323	0.16*a*	0.6742	-1.233	3.026	-3.156
0.20*a*	13.36	-15.51	459.5	-553.3	0.20*a*	7.584	-9.919	160.4	-187.5
Shift and twist in two rows									
0.00*a*	-1.455	-2.374	5.463	-6.242	0.00*a*	0.1817	-1.427	3.350	-3.278
0.04*a*	-0.0608	-0.1876	0.0480	-0.0556	0.04*a*	0.0222	-0.1616	0.0527	-0.0487
0.08*a*	-0.0312	-0.1136	0.0176	-0.0222	0.08*a*	0.0117	-0.1118	0.0249	-0.0222
0.12*a*	0.0118	-0.0970	0.0217	-0.0191	0.12*a*	0.0332	-0.1068	0.0317	-0.0270
0.16*a*	0.1114	-0.2317	0.1245	-0.1206	0.16*a*	0.1557	-0.2888	0.2158	-0.1781
0.20*a*	1.513	-2.021	7.605	-9.298	0.20*a*	1.414	-2.139	6.472	-7.795

Referring to the above table, it is possible to achieve dispersion compensation in the PCW with a higher lattice shift and twist. Moreover, this is possible even at the lower lattice shift and twist parameters in the PCW structure with rings. However, the PCW can be selected for an application by considering the other parameters like group index, NDBP and flat band. In the present study, the structures with shift = twist = 0.16*a* and with hole radius 0.21*a* has shown higher performance than the other structures.

In a further study, we analyzed all the above structures and then identified one structure to enhance the SL features. A trade-off between group index and flat band region is used to finalize the structure for SL studies.

3.5 Slow light features of the structure:

As an attempt to make the PCW with higher delay over a larger flat band and with enhanced SL features, the combined effect of shift, twist and rings is precisely examined. The corresponding eigen frequencies, group index, group velocity, and bandwidth are calculated. Figure 3.17 (a) and (b) shows the group index corresponding to the applied shift and twist in the PCW in the first and second innermost rows, respectively.

Out of these structures, at s = t = 0.16*a*, a larger flat band is observed with a relatively higher group index and bandwidth. Though the group index is high at the other shift and twist values, the bandwidth is observed moderately low. Hence, in further study, these shift and twist parameters are used to enhance the SL features.

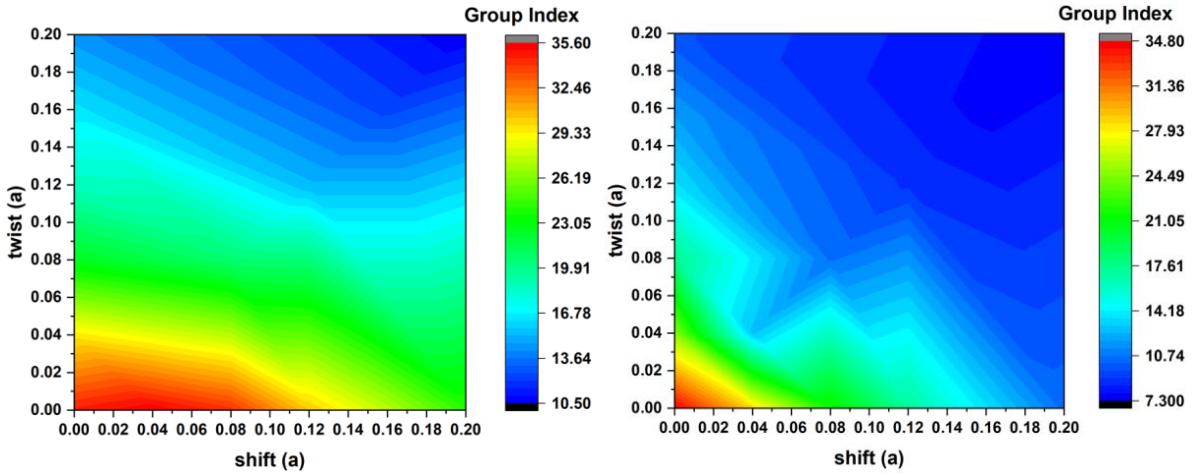

(a) (b)

Figure 3.17: Counter map representing the variation of group index with introduced shift and twist in (a) S1 structure (b) S2 structure.

At s = t = 0.16*a*, the radius of the rings is optimized to enhance the SL features. This is again varied between 0.08*a* and 0.16*a* in steps of 0.02*a*. The corresponding eigen frequency, group index, group velocity and bandwidth are calculated. Rings with a radius of 0.14*a* have resulted in a larger slope in the dispersion curves, which are evident for the enhancement of the SL features.

At the ring radius r = 0.14*a*, the group index of the structures S1 and S2 is calculated. At this radius, relatively a larger flat band is observed with a nearly constant group index. Figure 3.18 (a) and (b) shows the variation of the group index of these structures with wavelength. In the S1 structure, a flat band of 17.71 nm is observed with a group index value of 12.72. And the group index is decreased to 7.77 with a flat band over 40.15 nm in the S2 structure. Though the group index is decreased, the flat band is observed relatively over a larger region.

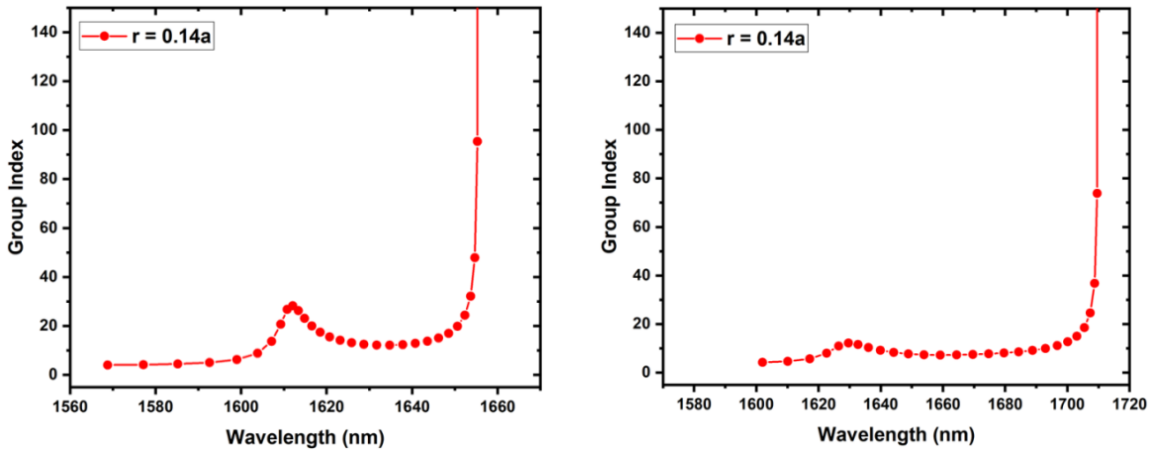

(a) (b)

Figure 3.18: Variation of group index with the wavelength in (a) S1 structure and (b) S2 structure

The GVD or β_2 determines the signal distortion in the SL regime. Figure 3.19 (a) and (b) shows the variation of β_2 with wavelength. In these figures, it can be seen that the value of β_2 can exist in both positive and negative ranges for different wavelengths in the same PCW. Therefore the dispersion compensation would be easily performed in these waveguides by serial cascading of waveguides with opposite β_2 values. By using the technique, broadband can also be achieved [11].

Moreover, the variation of β_2 is almost negligible in the flat band regions between 1625.84 nm and 1643.55 nm in the S1 structure and between 1644.15 nm and 1684.31 nm in the S2 structure (figure 3.19). This also indicates the associated third-order dispersion as very low. Also, in these two plots, it can be observed that the β_2 is in the range of 10 ps^2/mm or less, which is an acceptable range for the SL applications [11, 37].

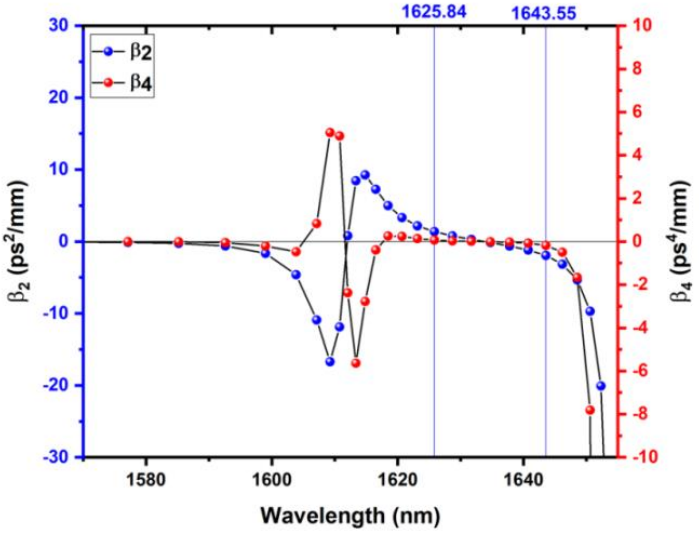

(a)

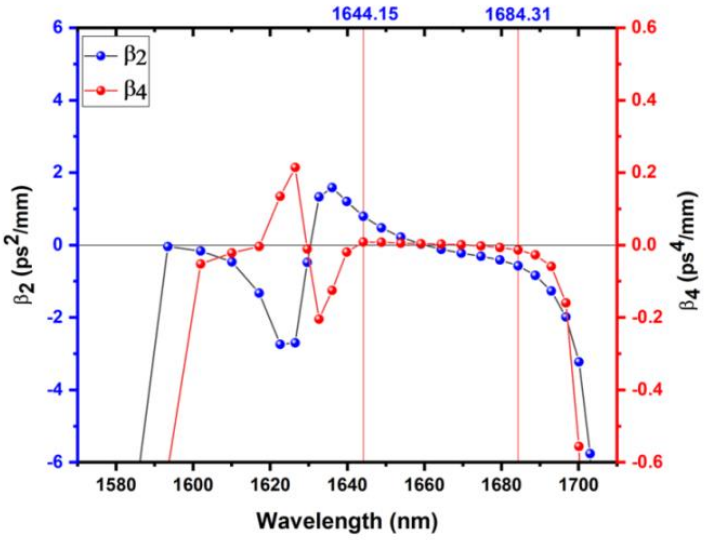

(b)

Figure 3.19: The variation of β_2 and β_4 with the wavelength in (a) S1 structure and (b) S2 structure.

The fourth-order dispersion (β_4) in the proposed structures S1 and S2 is also observed constant (flat band region). For the structure S2, this constant β_4 is observed between 1644.15 nm and 1684.31 nm with a group index of 7.77 which is better than the structure S1 with a group index of 12.72 over the band 1625.84 nm and 1643.55 nm. The NDBP of the structures is calculated at every step, and in table 3.7, group index, flat band and NDBP of S1 and S2 structures are summarized.

Table 3.7: Group Index, flat band and NDBP of the structures S1 and S2.

Structure with applied perturbation	Group index	Flatband (nm)	NDBP
Base Structure	34.72	1.978	0.0436
S1 (shift)	21.41	5.05	0.0672
S2 (shift)	12.88	9.36	0.0738
S1 (twist)	16.78	6.57	0.0684
S2 (twist)	13.21	10.86	0.0893
S1 (shift+twist)	17.61	8.26	0.0899
S2 (shift+twist)	7.73	19.89	0.0927
S1 (shift+twist+rings)	12.71	17.71	0.1378
S2 (shift+twist+rings)	7.77	40.16	0.1874

Table 3.7 shows the SL properties of S1 and S2 structures by introducing shift, twist and rings in the lattice. For S1 with shift, twist and rings, the group index is 12.71 over 17.71 nm, and the corresponding NDBP is 0.1378. Moreover, for S2 with shift, twist and the rings, the group index is 7.77 over 40.16 nm, and the corresponding NDBP is 0.1874. The introduction of rings in the second row in perturbed PCW lattice has increased the DBP. This rise in DBP supports the increase in the SL features.

3.6 Conclusions:

In this chapter, the effect of change in radius of holes and rings, the effect of lattice shift and twist, and the combined effect of all three are studied. The perturbation is introduced in the structure of PCW in such a way that the dispersion curve can be controlled over the desired bandwidth with desired group index. This has increased the degrees of freedom to control the dispersive curve. This dispersion engineering has also enhanced the group index – bandwidth product. Based on this study, one can design a waveguide with a nearly constant and low n_g over a broad wavelength range or a waveguide with a nearly constant and high n_g with a narrow band. The second and fourth-order dispersion curves are also under control with the introduced perturbation.

Introducing the twist and shift in the second row of the PCW further elevated the studying parameters. With applied shift and twist in the lattice, a constant group index of 31.42 over a bandwidth of 7.97 nm and 7.64 over 30.41 nm with very low dispersion is achieved. β_2 and β_4 values in the range of 10^{-20} s^2/m and 10^{-45} s^4/m, respectively, clearly indicate the controlled dispersion. Even these results apply to PCW made from other materials. However, the magnitude of change in a physical parameter may depend on the material properties.

For enhancing the SL features, GaAs waveguide with air cylinders is used. SL with improved features is observed at shift (s) = 0.16*a* and twist (t) = 0.16*a* and r = 0.14*a*. At these shift and twist values, the rings are introduced in the first and second rows of the waveguide. Group index, bandwidth, DBP, second and fourth-order dispersions are calculated to characterize the SL. In the S1 structure, a flat band of 17.71 nm is observed with a group index value of 12.72. The NDBP is observed as 0.1378. In the S2 structure, the group index is decreased to 7.77 with an increase in the flat band over 40.15 nm.

The NDBP is observed as 0.18740. This value is nearly 4.3 times higher in comparison with the NDBP value of the base structure (0.0436) and approximately two times higher than the engineered structure (0.0927). Also, the second and fourth-order dispersions are observed within the acceptable range. This study can help to design application-specific devices like optical buffer memories, optical switches, to generate efficient nonlinear effects such as supercontinuum generation, and devices with desired slow light features.

References:

1. S. A. Schulz, L. O'Faolain, D. M. Beggs, T. P. White, A. Melloni, and T. F. Krauss, "Dispersion engineered slow light in photonic crystals: A comparison," *J. Opt.*, vol. 12, Art. no. 104004, pp. 1-10, Sep. 2010, https://doi.org/10.1088/2040-8978/12/10/104004
2. T. Baba, "Slow light in photonic crystals," *Nat. Photonics*, vol. 2, no. 8, pp. 465–473, Aug. 2008, https://doi.org/10.1038/nphoton.2008.146
3. T. F. Krauss, "Slow light in photonic crystal waveguides," *J. Phys. D. Appl. Phys.*, vol. 40, pp. 2666–2670, May 2007, https://doi.org/10.1088/0022-3727/40/9/S07
4. X. Letartre, C. Seassal, C. Grillet, P. Rojo-Romeo, P. Viktorovitch, L V D'Yerville, D. Cassagne, and C. Jouanin, "Group velocity and propagation losses measurement in a single-line photonic-crystal waveguide on InP membranes," *Appl. Phys. Lett.*, vol. 79, no. 15, pp. 2312-2314, Oct. 2001, https://doi.org/10.1063/1.1405146

5. Y. A. Vlasov, M. O'Boyle, H. F. Hamann, and S. J. McNab, "Active control of slow light on a chip with photonic crystal waveguides," *Nature*, vol. 438, pp. 65–69, Nov. 2005, https://doi.org/10.1038/nature04210
6. M. Soljacic, and J. D. Joannopoulos, "Enhancement of nonlinear effects using photonic crystals," *Nat. Mater.*, vol. 3, pp. 211–219, Apr. 2004, https://doi.org/10.1038/nmat1097
7. J. T. Li, and J. Y. Zhou, "Nonlinear optical frequency conversion with stopped short light pulses," *Opt. Express*, vol. 14, no. 7, pp. 2811 – 2816, Apr. 2006, https://doi.org/10.1364/OE.14.002811
8. S. Roy, and P. R. Chaudhuri, "Analysis of nonlinear multilayered waveguides and MQW structures: A field evolution approach using finite-difference formulation," *IEEE J. Quantum Electron.*, vol. 45, no. 4, pp. 345 – 350, Apr. 2009, https://doi.org/10.1109/JQE.2009.2013084
9. P. Colman, S. Combrié, G. Lehoucq, and A. De Rossi, "Control of dispersion in photonic crystal waveguides using group symmetry theory," *Opt. Express*., vol. 20, no. 12, pp. 13108 – 13114, Jun. 2012, https://doi.org/10.1364/oe.20.013108
10. M. Ebnali-Heidari, C. Grillet, C. Monat, and B. J. Eggleton, "Dispersion engineering of slow light photonic crystal waveguides using microfluidic infiltration," *Opt. Express*., vol. 17, no. 3, pp. 1628 – 1635, Feb. 2009, https://doi.org/10.1364/OE.17.001628
11. J. Hou, D. Gao, H. Wu, R. Hao, and Z. Zhou, "Flat band slow light in symmetric line defect photonic crystal waveguides," *IEEE Photonics Technol. Lett.*, vol. 21, no. 20, pp. 1571–1573, Oct. 2009, https://doi.org/10.1109/LPT.2009.2030160
12. S. Roy, A. Willinger, S. Combrie, A. De Rossi, G. Eisenstein, and M. Santagiustina, "Narrowband optical parametric gain in slow mode engineered GaInP photonic crystal waveguides," *Opt. Lett.*, vol. 37, no. 14, pp. 2919 – 2921, Jul. 2012, https://doi.org/10.1364/OL.37.002919
13. S. Roy, M. Santagiustina, P. Colman, S. Combrié, and A. De Rossi, "Modeling the dispersion of the nonlinearity in slow mode photonic crystal waveguides," *IEEE Photonics J.*, vol. 4, no. 1, pp. 224 – 233, Feb. 2012, https://doi.org/10.1109/JPHOT.2011.2181942
14. A. Willinger, S. Roy, M. Santagiustina, S. Combrie, A. De Rossi, I. Cestier, and G. Eisenstein, "Parametric gain in dispersion engineered photonic crystal waveguides,"

Opt. Express., vol. 21, no. 4, pp. 4995 – 5004, Feb. 2013, https://doi.org/10.1364/OE.21.004995

15. L. H. Frandsen, A. V. Lavrinenko, J. Fage-Pedersen, and P. I. Borel, "Photonic crystal waveguides with semi-slow light and tailored dispersion properties," *Opt. Express*., vol. 14, no. 20, pp. 9444 – 9450, Oct. 2006, https://doi.org/10.1364/OE.14.009444
16. A. Y. Petrov, and M. Eich, "Zero dispersion at small group velocities in photonic crystal waveguides," *Appl. Phys. Lett*., vol. 85, no. 21, pp. 4866 – 4868, Nov. 2004, https://doi.org/10.1063/1.1815066
17. J. Li, T. P. White, L. O'Faolain, A. Gomez-Iglesias, and T. F. Krauss, "Systematic design of flat band slow light in photonic crystal waveguides," *Opt. Express.*, vol. 16, no. 9, pp. 6227 – 6232, Apr. 2008, https://doi.org/10.1364/OE.16.006227
18. Y. Hamachi, S. Kubo, and T. Baba, "Slow light with low dispersion and nonlinear enhancement in a lattice-shifted photonic crystal waveguide," *Opt. Lett.*, vol. 34, no. 7, pp. 1072 – 1074, Apr. 2009, https://doi.org/10.1364/OL.34.001072
19. S. Roy, M. Santagiustina, A. Willinger, G. Eisenstein, S. Combrié, and A. De Rossi, "Parametric Gain and Conversion Efficiency in Nanophotonic Waveguides with Dispersive Propagation Coefficients and Loss," *J. Lightwave Technol*., vol. 32, no. 6, pp. 1177 – 1182, Mar. 2014, https://doi.org/10.1109/JLT.2014.2298913
20. A. Willinger, S. Roy, M. Santagiustina, S. Combrié, A. De Rossi, and G. Eisenstein, "Narrowband optical parametric amplification measurements in $Ga_{0.5}In_{0.5}P$ photonic crystal waveguides," *Opt. Express*, vol. 23, no. 14, pp. 17751 - 17757, Jun. 2015, https://doi.org/10.1364/OE.23.017751
21. A. Saynatjoki, M. Mulot, J. Ahopelto, and H. Lipsanen, "Dispersion engineering of photonic crystal waveguides with ring-shaped holes," *Opt. Express*, vol. 15, no. 13, pp. 8323-8328, Jun. 2007, https://doi.org/10.1364/OE.15.008323
22. Y. Zhai, H. Tian, and Y. Ji, "Slow light property improvement and optical buffer capability in ring-shape-hole photonic crystal waveguide," *IEEE J. Light. Technol.*, vol. 29, no. 20, pp. 3083–3090, Oct. 2011, https://doi.org/10.1109/JLT.2011.2165334
23. A. Casas-Bedoya, C. Husko, C. Monat, C. Grillet, N. Gutman, P. Domachuk, and B. J. Eggleton, "Slow-light dispersion engineering of photonic crystal waveguides using selective microfluidic infiltration," *Opt. Lett.*, vol. 37, no. 20, pp. 4215 – 4217, Oct. 2012, https://doi.org/10.1364/OL.37.004215

24. L. V. Hau, S. E. Harris, Z. Dutton, and C. H. Behroozi, “Light speed reduction to 17 metres per second in an ultracold atomic gas,” *Nature*, vol. 397, pp. 594–598, Feb. 1999, https://doi.org/10.1038/17561
25. M. Bahadoran, A. Afroozeh, J. B. Ali, and P. P. Yupapin, “Slow light generation using microring resonators for optical buffer application,” *Opt. Eng.*, vol. 51, no. 4, Art. no. 04460, Apr. 2012, https://doi.org/10.1117/1.OE.51.4.044601
26. Z. Zhu, A. M. C. Dawes, D. J. Gauthier, L. Zhang, and A. E. Willner, “Broadband SBS slow light in an optical fiber,” *IEEE J. Light. Technol.*, vol. 25, no. 1, pp. 201–206, Jan. 2007, https://doi.org/10.1109/JLT.2006.887188
27. G. Qin, R. Jose, and Y. Ohishi, “Stimulated Raman scattering in tellurite glasses as a potential system for slow light generation,” *J. Appl. Phys.*, vol. 101, no. 9, Art. no. 093109, pp. 1–5, May 2007, https://doi.org/10.1063/1.2730566
28. Y. A. Vlasov, X. Z. Bo, J. C. Sturm, and D. J. Norris, “On-chip natural assembly of silicon photonic bandgap crystals,” *Nature*, vol. 414, pp. 289–293, Nov. 2001, https://doi.org/10.1038/35104529
29. Y. Zhang, and B. Li, “Photonic crystal-based bending waveguides for optical inter-connections,” *Opt. Express*, vol. 14, no. 12, pp. 5723 – 5732, Jun. 2006, https://doi.org/10.1364/OE.14.005723
30. C. Wang, C. Z. Zhou, and Z.Y. Li, “On-chip optical diode based on silicon photonic crystal heterojunctions,” *Opt. Express*, vol. 19, no. 27, pp. 26948 – 26955, Dec. 2011, https://doi.org/10.1364/OE.19.026948
31. S. G. Johnson, and J. D. Joannopoulos, “Block-iterative frequency-domain methods for Maxwell’s equations in a planewave basis,” *Opt. Express*, vol. 8, no. 3, pp. 173 – 190, Jan. 2001, https://doi.org/10.1364/OE.8.000173
32. M. Notomi, K. Yamada, A. Shinya, J. Takahashi, C. Takahashi, and I. Yokohama, “Extremely large group-velocity dispersion of line-defect waveguides in photonic crystal slabs,” *Phys. Rev. Lett.*, vol. 87, Art. no. 253902, pp. 1 – 4, Dec. 2001, https://doi.org/10.1103/PhysRevLett.87.253902
33. F. Bagci, and B. Akaoglu, “Effects of innermost rows on slow light properties of photonic crystal waveguides,” *2012 International Conference on Photonics in Switching*, pp. 1-3, Sep. 2012, https://ieeexplore.ieee.org/document/6608281
34. J. V. Malik, K. D. Jindal, V. Kumar, Vipin Kumar, A. Kumar, K. S. Singh, and T. P. Singh, “Effect of temperature on photonic band gaps in semiconductor-based one-

dimensional photonic crystal," *Adv. Opt. Technol*., vol. 2013, Article no. 798087, pp. 1-8, Aug. 2013, https://doi.org/10.1155/2013/798087

35. K. D. Xuan, L. C. Van, V. C. Long, Q. H. Dinh, L. V. Mai, M. Trippenbach, and R. Buczynski, "Influence of temperature on dispersion properties of photonic crystal fibers infiltrated with water" *Opt. Quant. Electron.*, vol. 49, Article no. 87, pp. 1-12, Feb. 2017, https://doi.org/10.1007/s11082-017-0929-3
36. V. D. R. Pavan and S. Roy, "Temperature Effects on Dispersion Tailoring of Slow Light Engineered Photonic Crystal Waveguide," *2019 24th Microoptics Conference (MOC),* pp. 268-269, Nov. 2019, https://doi.org/10.23919/MOC46630.2019.8982894
37. J. Ma and C. Jiang, "Demonstration of ultraslow modes in asymmetric line-defect photonic crystal waveguides," *IEEE Photonics Technol. Lett.*, vol. 20, no. 14, pp. 1237–1239, Jul. 2008, https://doi.org/10.1109/LPT.2008.926018

Chapter – 4
Active Tuning in Lattice Shifted Photonic Crystal Waveguide

In this chapter, the effect of external electric field and slab temperature on the PCW is studied. A two-dimensional lattice shifted PCW is used for studying the effects of external electric field and slab temperature. GaAs is used as substrate material. The active tuning of the PBG is achieved by the dependence of the RI of the slab on external heat and electric field. Electro-optic effect and thermo-optic effect are employed to calculate the RI of the slab material. These refractive indices and, therefore, the dielectric constants are used in the simulations performed in MIT photonic bands software. For this, the RI variations are considered over the temperature range of 100 K to 400 K and external electric field in the range of 0 - 500 kV/cm. The PBG values ranging from 24 nm to 58 nm are achieved by controlling the external parameters. The work is extended in the communication bands, including O-band, E-band, S-band, C-band and L-band.

In the first part of the work, the electro-optic effect is studied, on the unperturbed lattice. In the subsequent studies, a shift is introduced in the lattice of the PCW to achieve higher PBG. The thermo-optic effect is used in the later studies to achieve active tuning of the PBG. It is observed that the range of tuning of the PBG with the electro-optic effect is relatively smaller than that of the thermo-optic effect. However, accompanying other methods like the insertion of liquid crystals and electro-active polymers in the photonic crystal lattice may increase the tuning effect. Also, this method is easy to adopt in practice than the thermo-optic effect. Optically active devices, optical switching, thermally tunable optical filters, wavelength routers, and optical interconnectors are feasible with these structures.

4.1 Introduction:

The PBG of a PC or PCW originates from its geometry and the refractive index of the material from which it is made [1]. Both passive and active tuning of the PBG can be done in a PCW. A structure is said to be passively tuned if the anticipated PBG is achieved through varying the geometry, RI of the material and profile of the RI [2-4]. In this method, once the fabrication is completed, the PBG and dispersion features are immutable. These methods bound the devices as static.

On the other hand, to achieve the active tuning of the PBG, methods such as changing the temperature of the structure, external electric field, and external magnetic field are used. By these phenomena, one can change the RI of the material to some extent and produce variations in the PBG [5-6]. Though the change in refractive index is small, these methods are adaptable along with the techniques such as insertion of magnetic materials, liquid crystals and micro-fluids [7-8]. By the active tuning of the PCW, the PBG and the dispersion features are mutable. This method of tuning has potential applications in real-time light controlling devices.

In the recent past, passive tuning of the PBG was reported by the arrangement of layers of one-dimensional PC in different types of quasi-periodic sequences, which resulted in tunable PBG in the terahertz region [9]. In these structures, grading RI profile and temperature effects are adopted to achieve tunability. Instead of the graded-index profile, by using the linearly graded-index materials, tunability was achieved in a one-dimensional PC [3]. Higher bandwidths are achieved by maximum contrast of the RI. Using lithographic techniques, recently, the geometry of the PC structures has been altered, and the tunability of the PBG has been reported [10]. In this method, using a monolithic semiconductor wafer as the active medium, a laser wavelength is tuned between 1500 and 1625 nm.

The light controlling applications are limited by these structures due to passive tuning. PCWs made of ferroelectric, ferromagnetic and ferrimagnetic materials offer significant active tuning of PBG in the moderate external electric or magnetic field. Roussey et al. [11] designed the electro-optic effect based lithium niobate PC and demonstrated the shift of stop band with an external voltage. Slow light generated in the PC is used to observe this shift. PCs made of magneto-optic materials are used as spatial light modulators [12]. For this purpose, electric and magnetic materials are infiltrated in the PC lattice. An electro-optic tunable multi-channel filter was developed by Fu et al. [13]. In this, a two-dimensional ferroelectric PC made of barium titanate was used. Here, the properties of the filter can be tuned by the applied voltage. Ferroelectric thin film PCW is developed by Lin et al. [14]. In this method, the PCW properties are tunable and controllable by the electro-optic effect. Recently, an optical filter made of stacked SiO_2 isotropic dielectric slabs separated by monolayer graphene sheets was demonstrated [15].

Tunable PBG was achieved by inserting liquid crystals and single-crystal $KTaO_3$ in the PC matrix and applying external heat or electric field [5, 16-17]. Active tuning was accomplished in omnidirectional terahertz range PCs by external temperature effect [18]. The tunability was realized from the temperature dependence of the constituent semiconductor

and dielectric materials. With the impact of temperature on free carrier charge density and by the density of dopants, tunability of PBG was reported [19]. In this method, even the PBG can be closed by external temperature control.

However, tunable PCs based on electro-optic effect provide limited tunability. This is because of possible changes in the refractive index are relatively smaller with the electro-optic effect. Though the attainable tuning is minor, this is one of the most suitable methods to tune the bandgap and to address the applications based on the tuning of the bandgap [20-21]. Also, applying the electric field to a PC device can be done quickly. With current technology, various microcircuits can be designed to use electric fields. Tunable PC configurations based on polymer, electro-active and liquid crystals are more popular [15].

In this chapter, we present the active tuning of the PBG and dispersion features in a 2-dimensional lattice-shifted PCW. The shift in PCW is largely used to tailor the dispersion features. Here, this method is used to enhance the PBG, as well as reposition the flat bands of the PCW. The active tuning is achieved by the dependence of the RI of GaAs on temperature and external electric field. Temperatures ranging from 100 K to 400 K and external electric fields in the range of 0 - 500 kV/cm are considered for this study. In most recent results, thermal methods are used in 1-dimensional PC and PCW [5, 22-23] to achieve the tunable PBG. In our work, thermal tuning was directly implemented in 2-dimensional PCW for tunable PBG. Relatively larger temperature ranges are used than the existing results. Simulations are performed in MPB on the Ubuntu platform. This work attained PBGs ranging from 24 – 58 nm. With active tuning, the PBG varies in the range of 20 – 34 nm in the communication bands. The group indices are calculated, and the repositioning of the flat bands is observed. Besides this, the second-order dispersion (β_2) is estimated to study the dispersion of the propagating mode.

4.2 Electro-optic effect based active tuning:

4.2.1 Tuning of RI by electro-optic effect:

The refractive index of an electro-optic medium is a function of the applied electric field [24], and the effect is referred to as the electro-optic effect. For the quadratic electro-optic effect, the refractive index takes the form of [24],

$$n(E) = n - \frac{1}{2}\beta n^3 E^2 \qquad (4.1)$$

where 'n' is the refractive index at zero electric field. This is 3.3734 at 1.55 μm wavelength. 'β' is the quadratic electro-optic coefficient or Kerr coefficient. Its value depends

on the medium is chosen and ranges between 10^{-18} and 10^{-14}. For GaAs material it is -5.1 x 10^{-17} for TE polarization and -9.30 x 10^{-17} for TM polarization. '*E*' is the applied electric field. In this work, the electric field is taken in the range of 0 – 500 kV/cm.

Using equation (4.1), the refractive indices and the corresponding dielectric constants are calculated at 1.55 µm wavelength. Figure 4.1 (a) shows the calculated refractive indices, and figure 4.1 (b) shows the corresponding calculated dielectric constants.

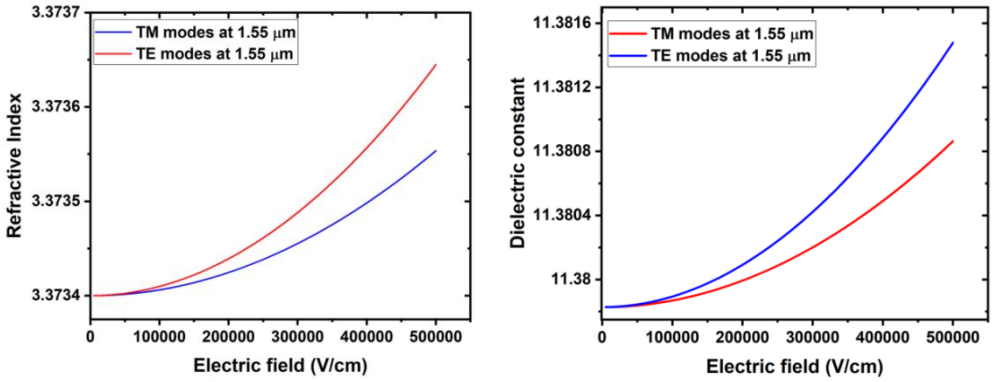

(a) (b)

Figure 4.1: (a) Calculated refractive indices at 1.55 µm and (b) calculated dielectric constants 1.55 µm.

4.2.2 Geometrical design:

For simulating the system, air holes arranged in a hexagonal lattice are considered in the GaAs substrate. Moreover, it is assumed that the structure is placed in an electric field, as shown in figure 4.2. Air cylinders of radius 0.25*a* are used to form the structure where '*a*' is the lattice constant. To form the waveguide, the central row of air cylinders is removed from the structure. The thickness of the slab is assumed to be 180 nm. Refractive indices calculated from equation (4.1) are used in the simulations performed in MPB. In the case of the PCW, the width of the waveguide is taken as 0.8*a*. The photonic band diagrams are plotted to study further the structure and the effect of the electro-optic effect on the PBG. In the second part of the work, a shift in the innermost row is introduced to enhance the waveguide's features.

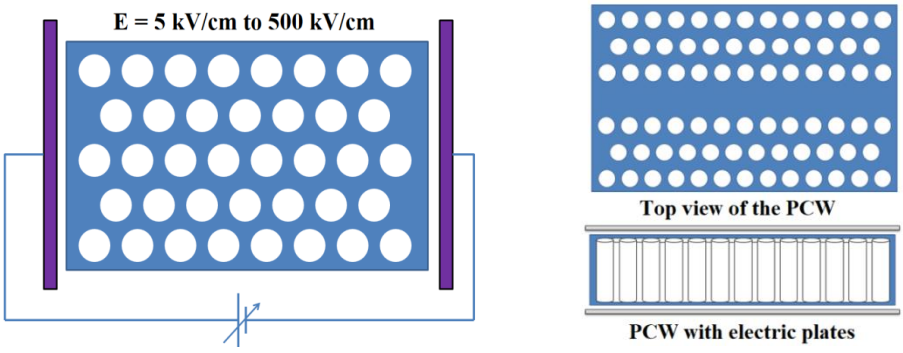

(a) (b)

Figure 4.2: Schematic of the proposed structures (a) PC with applied electric field (b) PCW with applied electric field

4.2.3 The photonic band structure in PC and PCW:

The initial study shows that the bandgap exists between band 1 and band 2 in the case of TM modes in PC. In the PCW structure, the PBG exists between band 6 and band 7 with TM modes. Throughout the study, we focused on the TM modes in the structures. Figure 4.3 shows the band diagrams of PC and PCW structures with zero electric field and the corresponding PBG.

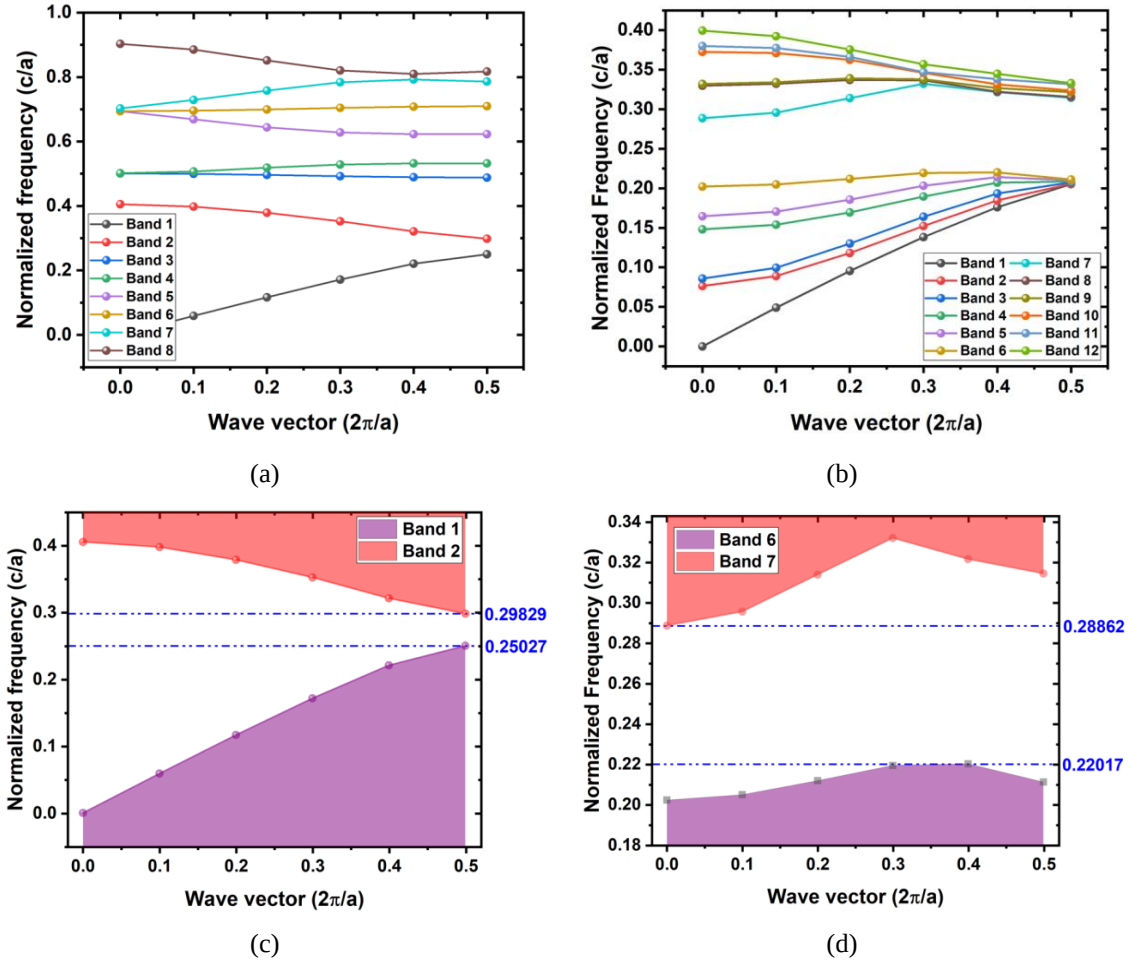

Figure 4.3: Band diagram of (a) PC (b) PCW structures. PBG in (c) PC and (d) PCW

The PBG is calculated and is found to be 0.04802 *c/a* in the case of PC, while it is 0.06852 *c/a* in the case of PCW. In further studies, the PC and PCW are treated with the electric field, and the corresponding eigen frequencies are obtained.

4.2.4 Results based on electro-optic effect:

The PC is simulated for studying the electro-optic effect. Using equation (4.1), the refractive indices and the corresponding dielectric constants are calculated and used in the simulation. Figure 4.4 shows the shift in bands 1 and 2 with the applied electric field.

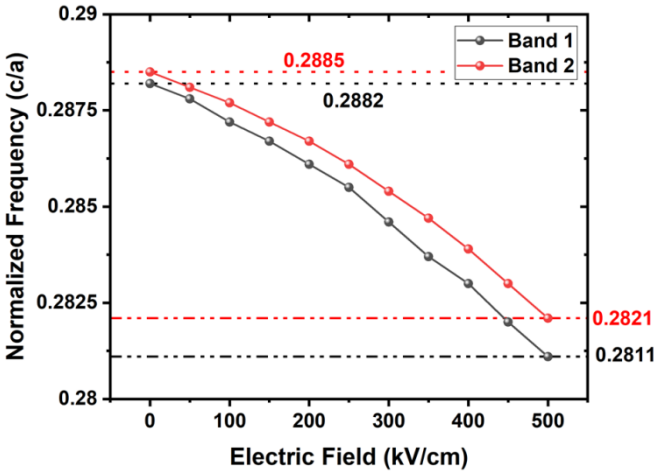

Figure 4.4: Shift in band 1 and band 2 with electric field.

With the applied electric field, the photonic bands are shifted. The band 1, initially at 0.2882 *c/a*, moved to 0.2811 *c/a* by applying an electric field of 500 kV/cm. With the same electric field, band 2 moved from 0.2885 *c/a* to 0.2821 c/a. The overall PBG is shifted from 0.0003 *c/a* to 0.001 *c/a*. To realize the structure of PC and the PBG, the lattice constant value is evaluated and is found to be 447 nm.

The PCW provides a relatively larger PBG than PC and offers additional control over the dispersion curves due to the design parameters. In the present structure, the PBG exists between bands 6 and 7. Simulations are performed to calculate the PBG in PCW, and it is noticed that similar to PC structure, the bands in PCW are also shifting with the applied electric field. At zero electric field, band 6 is located at 0.2201 *c/a* while band 7 is at 0.2886 *c/a*. With applied electric fields, the bands are shifting, and at an electric field of 500 kV/cm, band 6 is observed at 0.2090 *c/a*, and band 7 is observed at 0.2781 *c/a*. Figure 4.5 shows the variation in bands 6 and 7 with the applied electric field. To observe the eigen wavelengths in telecommunication bands, the lattice constant is calculated and is found to be 355 nm.

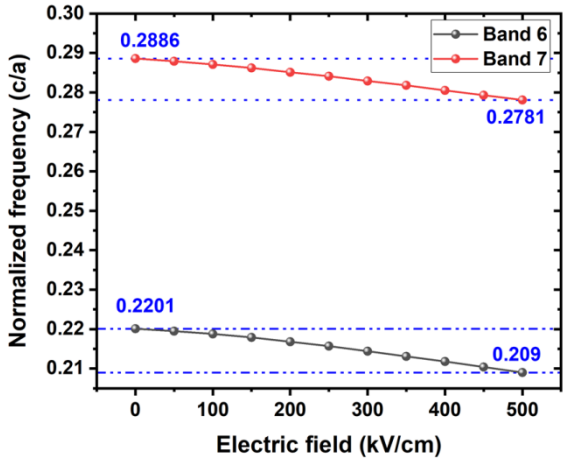

Figure 4.5: Variation of band 6 and band 7 with applied electric field.

4.2.5 Simultaneous effect of lattice shift and external electric field:

To enhance the electro-optic effect in PCW, a shift is introduced in the first innermost row of the waveguide. Shift values in the range of 0.00*a* - 0.15*a* in steps of 0.05*a* are applied to the structure. Due to the shift of the innermost row and the applied electric field, there is an enhancement in the observed results. Figure 4.6 (a-b) shows the shift in band 6 and band 7 with applied electric field in lattice shifted PCW. The observed shift is increased due to the lattice shift in the PCW.

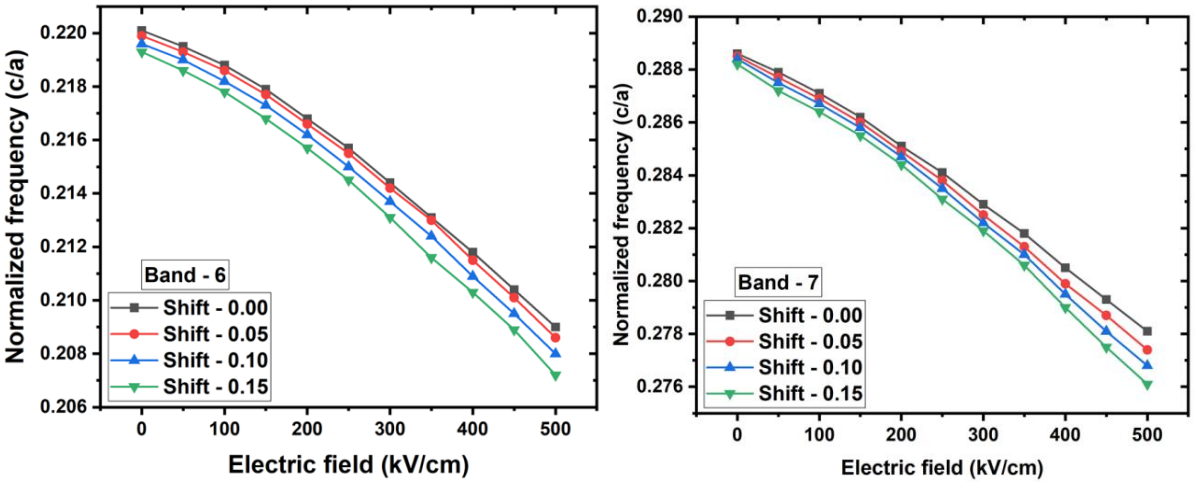

(a) (b)

Figure 4.6: Effect of electric field on band positions in lattice shifted PCW.
(a) position of band 6 (b) position of band 7

4.3 Thermo-optic effect based active tuning:

4.3.1 Tuning of RI by thermo-optic effect:

It is well known that the RI of a material is a function of temperature. According to McCaulley, et al. [25], the temperature dependence of the RI of GaAs in the near-infrared region is given by,

$$n(T) = n(T_{ref}).\exp\left[\left(T - T_{ref}\right)\beta\right] \qquad (4.2)$$

where $\boldsymbol{n(T)}$ is the RI of GaAs at temperature $\boldsymbol{T}$,

$\boldsymbol{n(T_{ref})}$ is the RI of GaAs at a reference temperature $\boldsymbol{T_{ref}}$ and

$\boldsymbol{\beta}$ is the thermo-optic coefficient of GaAs.

Here, for all the wavelengths, $\boldsymbol{T_{ref}}$ is chosen as 300 K, and $\boldsymbol{\beta}$ is taken as 2.25 x 10^{-4} K^{-1}. The RI of GaAs is calculated using the equation (4.2), in the range of 100 K – 400 K temperatures and in the near-infrared regions including O-band, E-band, S-band, C-band and L-band with central wavelengths 1.31 μm, 1.41 μm, 1.50 μm, 1.55 μm, and 1.59 μm

respectively. The colour map in figure 4.7 shows the variations of RI against the wavelengths and temperature.

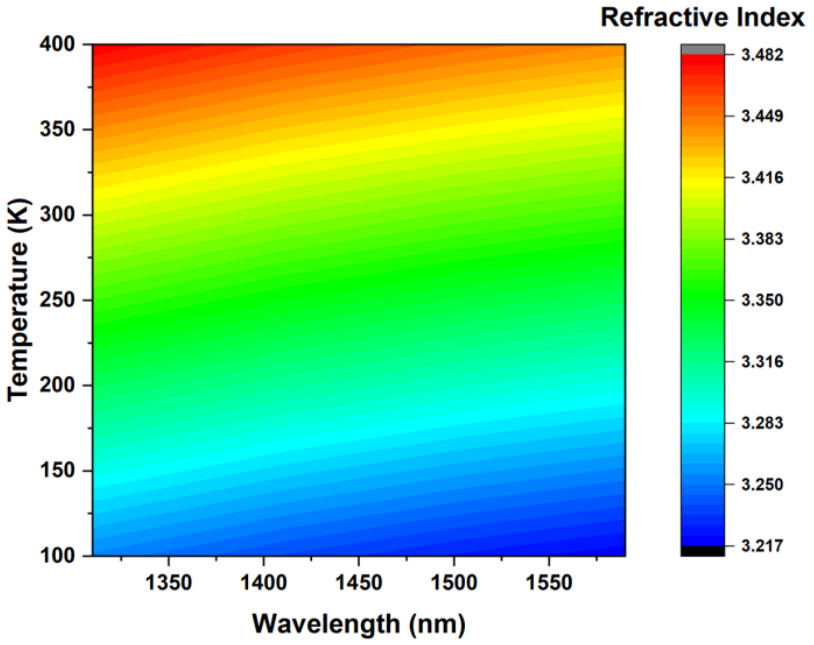

Figure 4.7: Variation of RI of GaAs with the temperature at different communication bands.

These calculated RI values and hence the dielectric constant values are used during the simulations in MPB. During these simulations, normalised frequencies, eigen wavelengths, and group velocities are calculated.

4.3.2 Optimization of geometrical parameters:

The present structure is designed to realize the actively tunable PBG with controlled dispersion. In a waveguide or a fibre, dispersion plays a vital role during the propagation of electromagnetic waves, and this dispersion profile can be controlled by modifying the geometry [26]. Keeping this in view, the geometrical parameters are calculated to control the dispersion in PCW. For achieving the control over the dispersion, the existing literature [27] suggests that the radius of air cylinders (r) in the range of $0.22a$ – $0.28a$ is preferred with a slab thickness (h) of $0.4a$ – $0.5a$ where 'a' is the lattice constant of the structure. Though varying the radius of the air cylinder engineers the dispersion curve, controlling the radius of air cylinders and producing systematic variations during the fabrication is difficult. Dispersion control can also be achieved by displacing the row of air cylinders and can be useful in developing the slow light PCW [28]. Also, the displacement of air cylinders is preferable over the variation of their radius. This shift parameter (s) can be in the range of $0.12a$ – $0.18a$ [28].

As the displacement of the row of air cylinders affects the PBG, now, to select the appropriate displacement factor, simulations are performed by considering the PCW at 300 K temperature at 1310 nm wavelength. Figure 4.8 shows the variations in the PBG of the proposed structure with a lattice shift. This study suggests that the increase in lattice-shift offers larger PBG. However, as the shift continues, the group index gets affected. As a compromise, the shift value needs to be optimized for further study. Hence the shift parameter (*s*) is chosen as 0.18a.

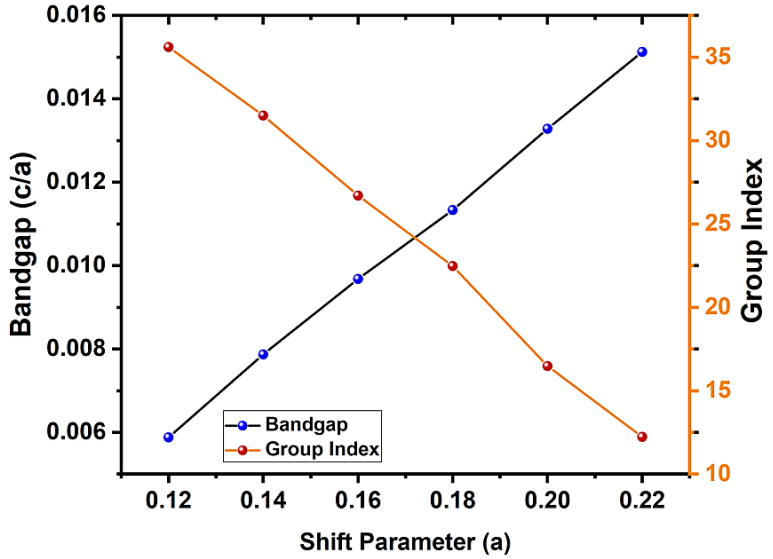

Figure 4.8: Variation of PBG with lattice-shift. This is performed at 1310 nm wavelength and 300 K temperature.

4.3.3 Schematic structure of the PCW:

For studying the tunability of the PBG, a hexagonal lattice structure is considered in a symmetrical PCW. Seven rows of air cylinders in the GaAs slab are considered on both sides of the line defect. The geometrical parameters of the slab, including thickness (*h*), the radius of air cylinders (*r*), and width of the line defect (*w*), are chosen as 0.383*a*, 0.25*a*, and 0.86*a*, respectively. For achieving the larger PBG, the first innermost row of the air cylinders just adjacent to the line defect is moved away from the line defect by a shifting parameter (s) 0.18*a*. The 3-dimensional view of the structure and proposed lattice shifted study with thermo-optic effect are shown in figure 4.9.

A micro-heater, whose plates are connected to an electronic driving circuit, can keep the slab at the desired temperature. This arrangement produces the thermo-optic effect and changes the RI of the slab with temperature. For real-time applications such as sensing, the quick heating and cooling of the slab play a significant role. Also, the thermal expansion of the material should not impact the geometry of the structure.

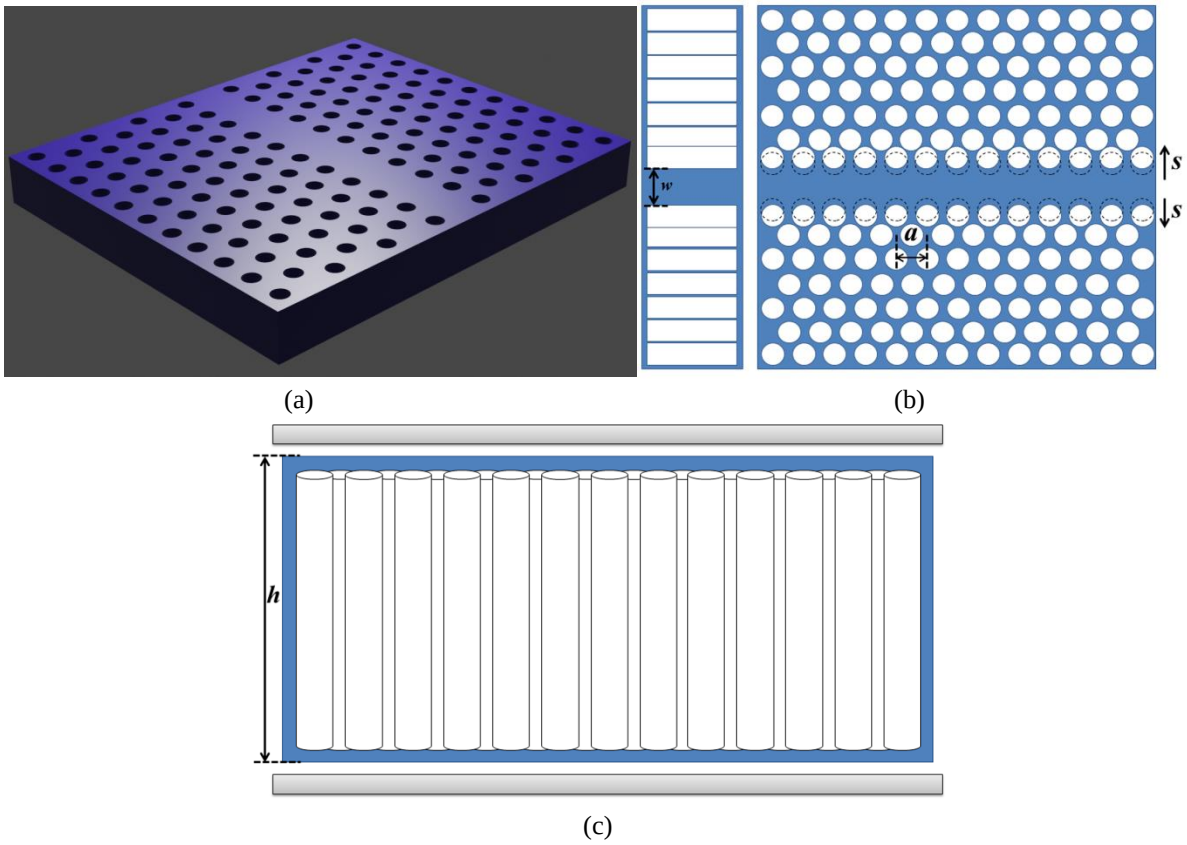

Figure 4.9: The proposed waveguide with hexagonal lattice. (a) 3-dimensional view of the unperturbed structure. (b) Top and side views of the PCW with proposed study of lattice shift and (c) Front view of the PCW with micro-heater plates for temperature control.

In the present study, the thermal expansion of the GaAs is negligible and is not affecting the geometry of the PCW, which we discussed in further sections. The PBG of the structure is calculated at the selected temperature intervals. For this purpose, temperatures in the range of 100 K – 400 K are considered. Using equation (4.2), the RI values and the corresponding dielectric constants of GaAs are calculated at various wavelengths and temperatures (figure 4.7).

4.3.4 Photonic bandgap of the structure:

The simulations resulted in the eigen frequencies and band positions of the structure. The initial studies are performed by considering the PCW at 300 K temperature. The band diagram is obtained at the wavelengths 1310 nm, 1410 nm, 1500 nm, 1550 nm, and 1590 nm, corresponding to the O-band, E-band, S-band, C-band and L-band, respectively. Band diagrams show that the PBG exists between band 16 and band 17. Figure 4.10 (a-e) shows the band diagram of the proposed lattice shifted PCW structures, and figure 4.10 (f-j) shows the bands 16 and 17 and the PBG of the structure.

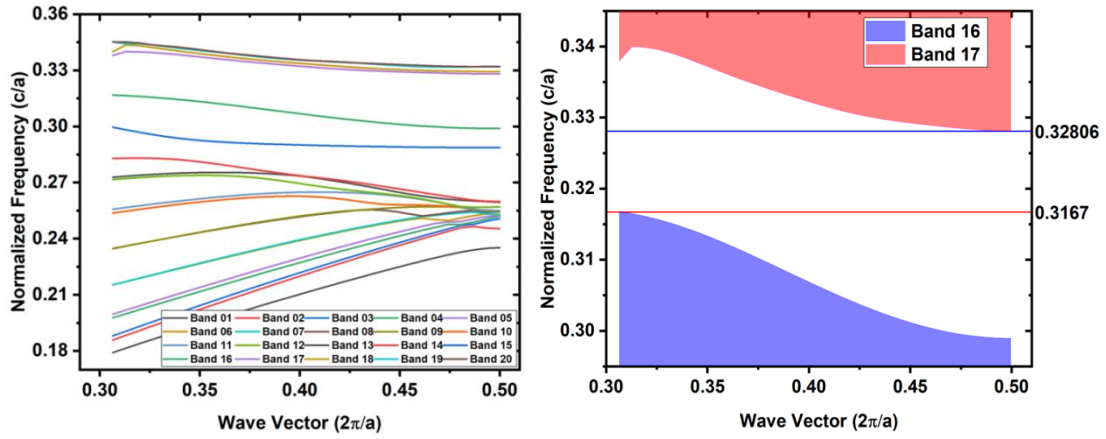
Normalized Frequency (c/a)
Wave Vector (2π/a)
Band 01 Band 02 Band 03 Band 04 Band 05
Band 06 Band 07 Band 08 Band 09 Band 10
Band 11 Band 12 Band 13 Band 14 Band 15
Band 16 Band 17 Band 18 Band 19 Band 20
Band 16
Band 17
0.32806
0.3167

(a) (f)

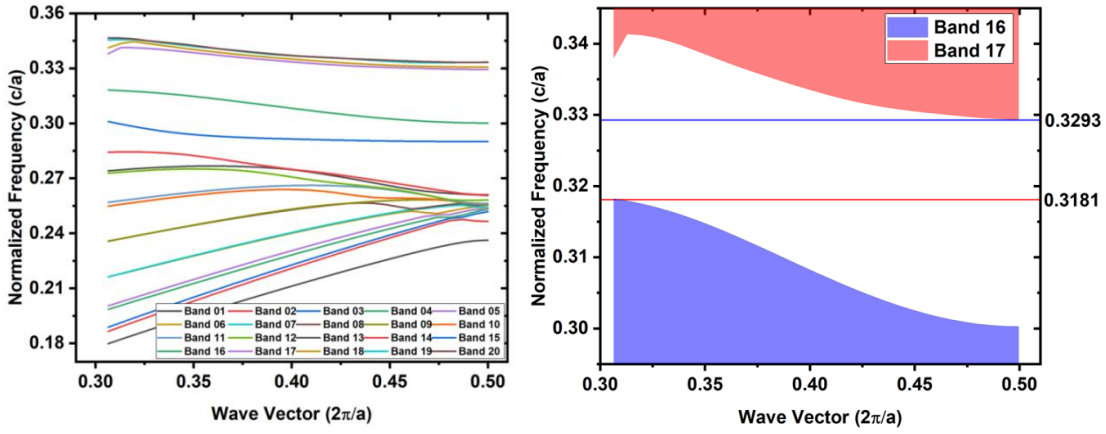
Normalized Frequency (c/a)
Wave Vector (2π/a)
Band 01 Band 02 Band 03 Band 04 Band 05
Band 06 Band 07 Band 08 Band 09 Band 10
Band 11 Band 12 Band 13 Band 14 Band 15
Band 16 Band 17 Band 18 Band 19 Band 20
Band 16
Band 17
0.3293
0.3181

(b) (g)

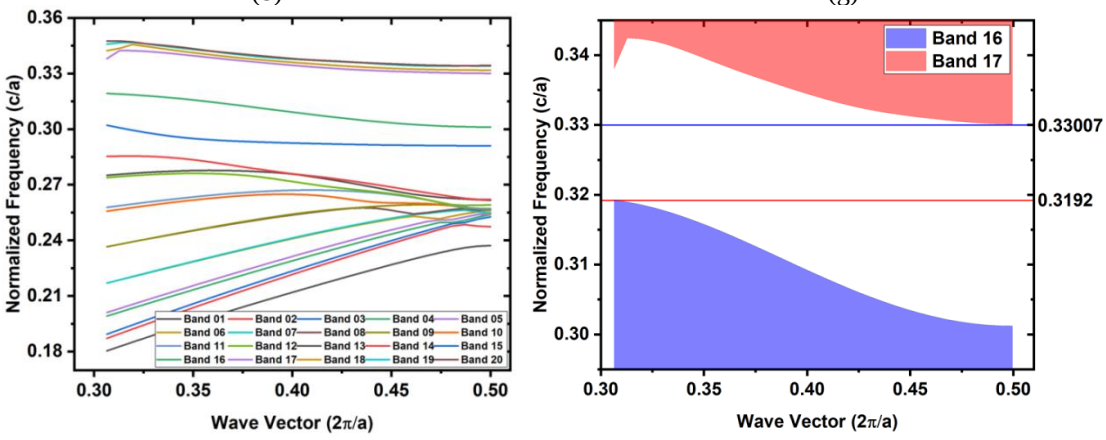
Normalized Frequency (c/a)
Wave Vector (2π/a)
Band 01 Band 02 Band 03 Band 04 Band 05
Band 06 Band 07 Band 08 Band 09 Band 10
Band 11 Band 12 Band 13 Band 14 Band 15
Band 16 Band 17 Band 18 Band 19 Band 20
Band 16
Band 17
0.33007
0.3192

(c) (h)

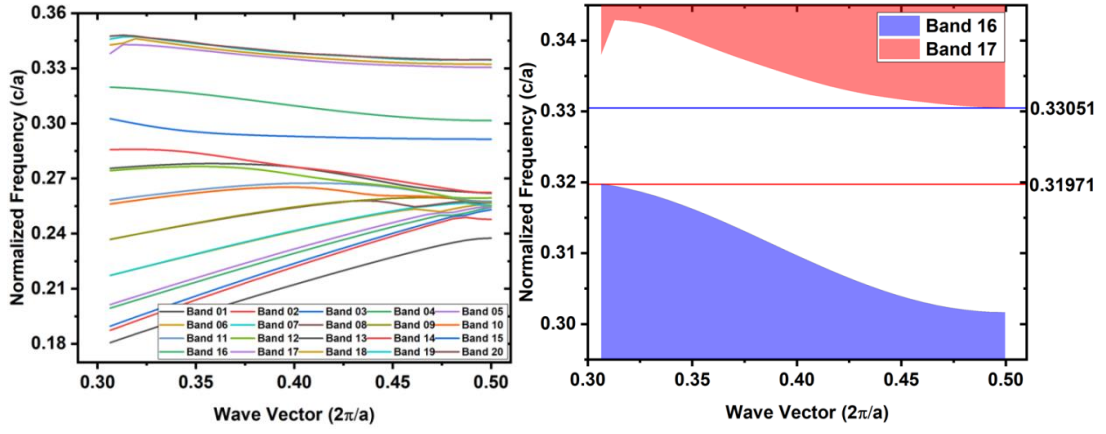
Normalized Frequency (c/a)
Wave Vector (2π/a)
Band 01 Band 02 Band 03 Band 04 Band 05
Band 06 Band 07 Band 08 Band 09 Band 10
Band 11 Band 12 Band 13 Band 14 Band 15
Band 16 Band 17 Band 18 Band 19 Band 20
Band 16
Band 17
0.33051
0.31971

(d) (i)

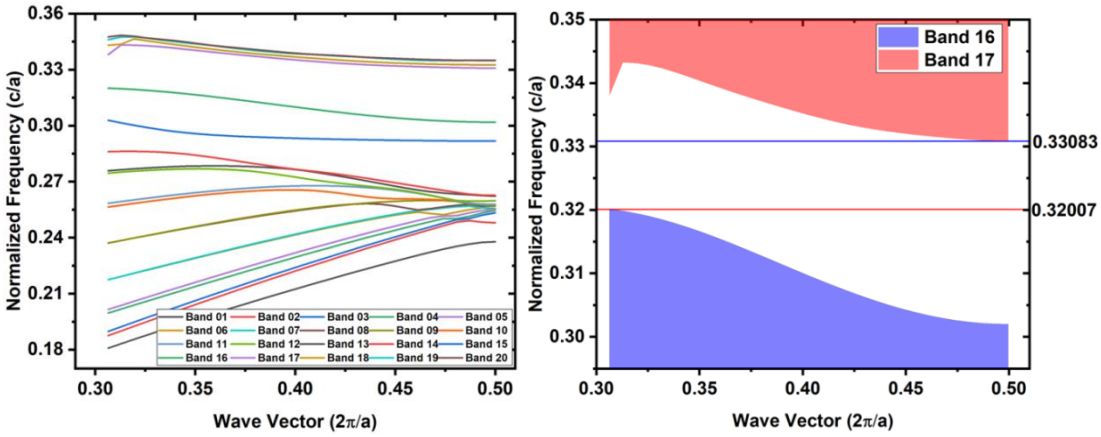

(e) (j)

Figure 4.10: Band diagram of the PCW at (a) 1310 nm (b) 1410 nm (c) 1500 nm (d) 1550 nm and (e) 1590 nm. Band 16, band 17 and PBG of the PCW at (f) 1310 nm (g) 1410 nm (h) 1500 nm (i) 1550 nm and (j) 1590 nm.

In table 4.1, the positions of band 16, band 17 and the calculated PBG of the structure at 300 K across various communication bands are given.

Table 4.1: PBG of the structure at 300 K temperature

Band of wavelengths	Position of band 16 (units c/a)	Position of band 17 (units c/a)	Bandgap (units c/a)
O – band (1.31 μm)	0.316727	0.328060	0.011333
E – band (1.41 μm)	0.318170	0.329353	0.011183
S – band (1.50 μm)	0.319227	0.330070	0.010843
C – band (1.55 μm)	0.319714	0.330506	0.010792
L – band (1.59 μm)	0.320078	0.330831	0.010753

By considering the lattice constant value of the structure, one can get the absolute value of the PBG. To observe the eigen wavelengths and the PBG in the near-infrared region, the lattice constants are calculated and are found to be in the range of 440 - 520 nm. Existing technology supports the production of PCW with these geometrical parameters. In section 4.3.6, these lattice constants of the structure are calculated.

4.3.5 Tuning of the bandgap:

Using equation (4.2), the RI of the GaAs slab is calculated at wavelengths 1310 nm, 1410 nm, 1500 nm, 1550 nm, and 1590 nm, within the slab temperatures of 100 – 400 K. In the present case, as the PBG exists between bands 16 and 17, the positions of these bands are noted at every temperature interval. As expected, the bands are shifting with temperature. The PBG between bands 16 and 17 is calculated and confirmed the shift in PBG with temperature. As we are interested in the PBG between bands 16 and 17, only these two bands are plotted

against the wave vector of the structure. Figure 4.11 (a-j) shows the variation of bands with the temperature at all the simulated wavelengths.

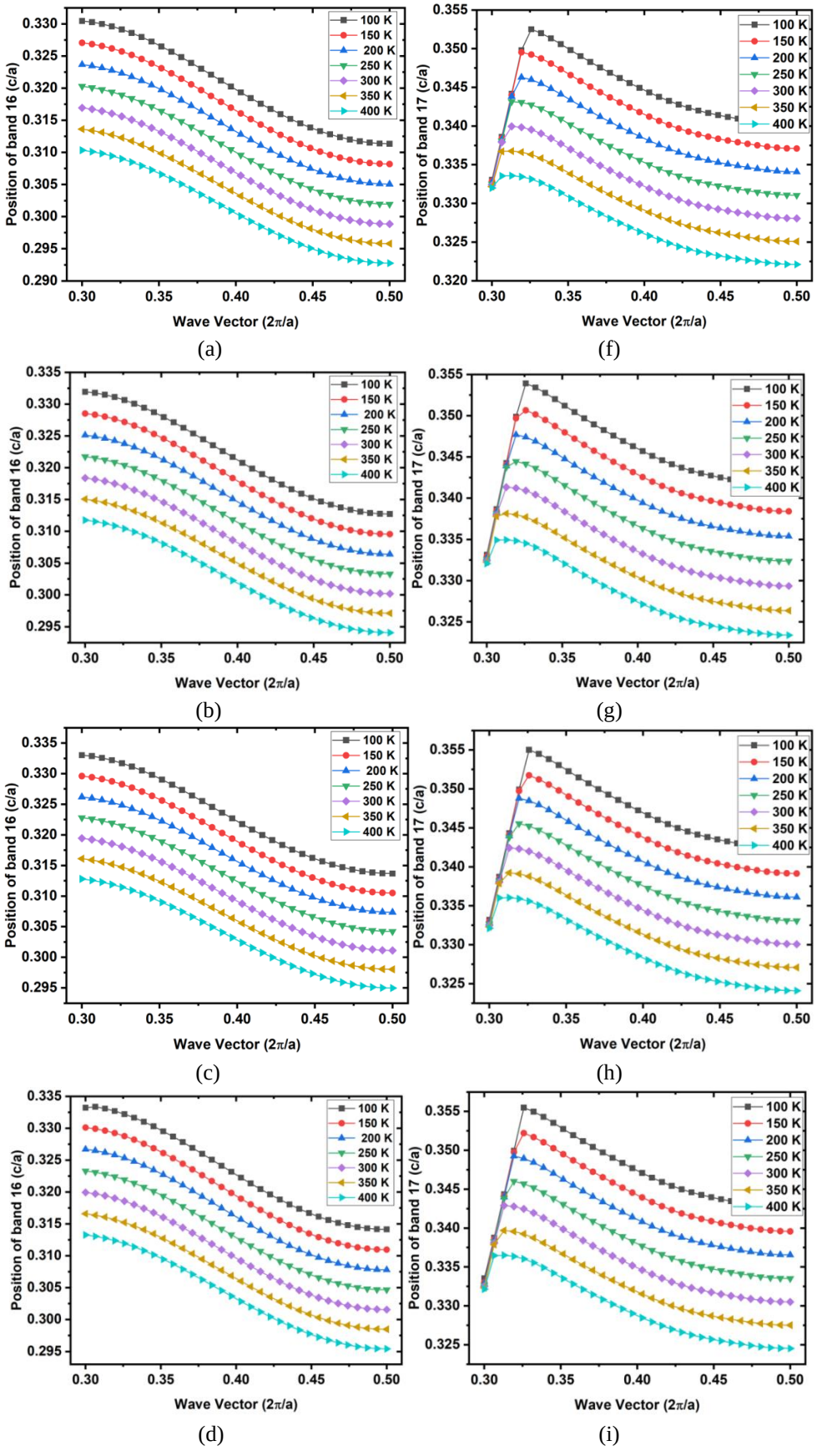

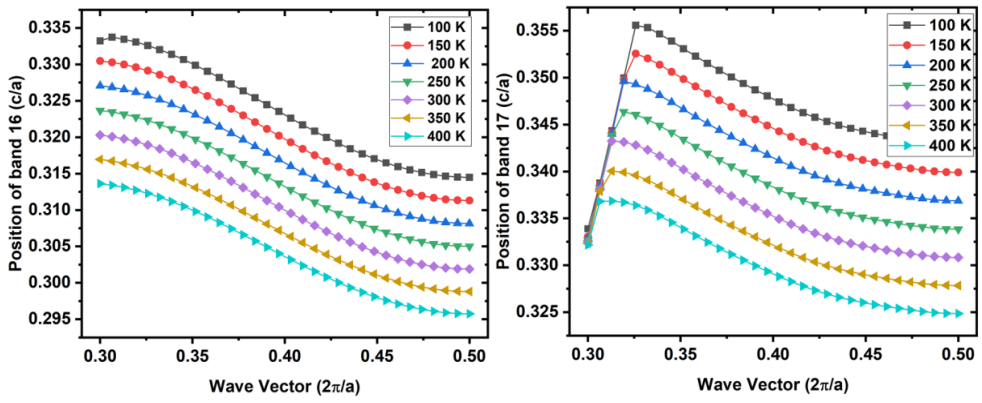

(e) (j)

Figure 4.11: Shift in the position of bands with temperature. (a-e) Shift of band 16 at wavelengths 1310 nm, 1410 nm, 1500 nm, 1550 nm, and 1590 nm. (f-j) Shift of band 17 at wavelengths 1310 nm, 1410 nm, 1500 nm, 1550 nm, and 1590 nm.

From this data, the PBG of the structure is calculated at every temperature interval and selected wavelengths. The changes in PBG are observed with temperature, and figure 4.12 shows these variations.

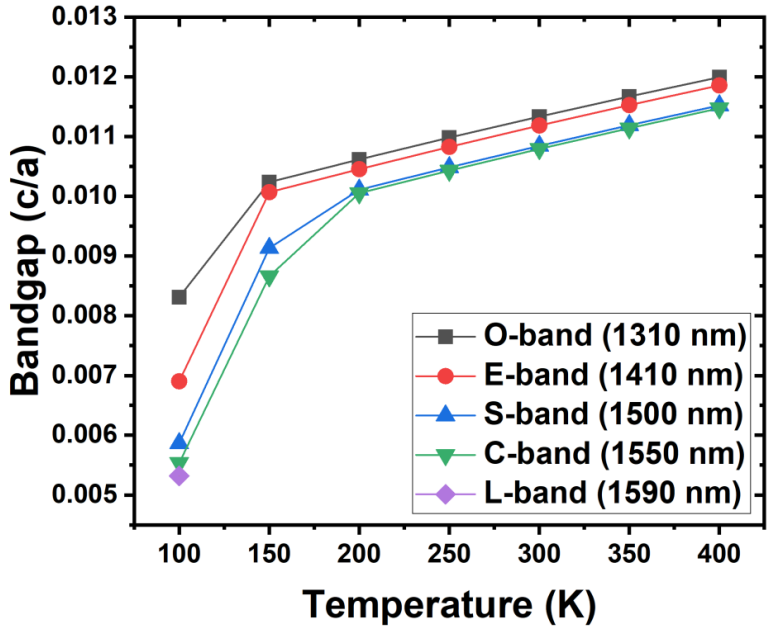

Figure 4.12: Shift in bandgap with change in temperature.

The PBG of a PCW arises from the geometry and the RI of the material of PCW. In the present study, the variations of RI with temperature are considered. To study the effect of thermal expansion on the structure and, therefore on the PBG, the PCW structure is simulated by considering the thermal expansion of GaAs. It is found that the thermal expansion of GaAs does not affect the PBG, as it is negligible in magnitude. Nevertheless, for other materials, thermal expansion may also affect the PBG. Therefore in the present study, the shift is due to the changes in the RI, which is emerging from the thermo-optic effect. Hence, a

plot is drawn to integrate the changes in the bandgap with the RI variations, and it is shown in figure 4.13.

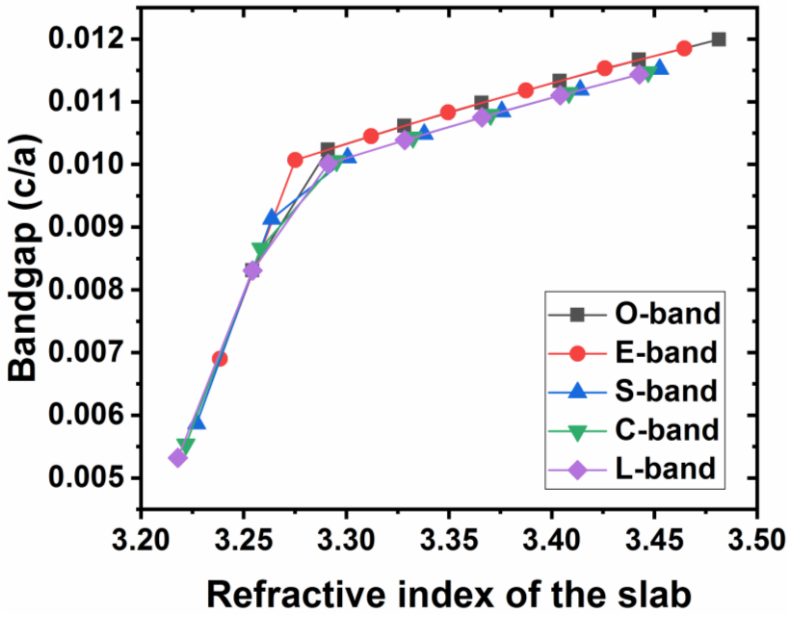

Figure 4.13: Variation of bandgap with RI of the slab.

4.3.6 Calculating the lattice constants:

The output of MPB simulations has units in terms of '*c*' and '*a*'. For realizing the structures, lattice constant values need to be calculated. Table 4.2 shows the PBG of the structures at different temperatures with calculated lattice constants.

Table 4.2: PBG of the structure at different communication bands and at different temperatures.

Temperature (K)	**Calculated PBG (nm)**				
	a = 440 nm and in O – band	*a* = 460 nm and in E –band	*a* = 485 nm and in S – band	*a*=500 nm and in C – band	*a* = 520 nm and in L – band
100	32.71	28.26	25.24	24.52	24.49
150	40.88	41.68	39.71	38.76	38.63
200	43.23	44.13	44.74	45.74	47.28
250	45.60	46.60	47.31	48.39	50.03
300	47.99	49.09	49.91	51.07	52.80
350	50.40	51.60	52.52	53.75	55.60
400	52.82	54.13	55.15	56.47	58.42

Figure 4.14 gives the graphical representation of the data in table 4.2. The variation of the PBG purely depends on the temperature and the calculated lattice constants. At the lower temperatures, the PBG variations are very sharp since the variation in RI is high. Moreover, at higher temperatures, the change in PBG is relatively tiny.

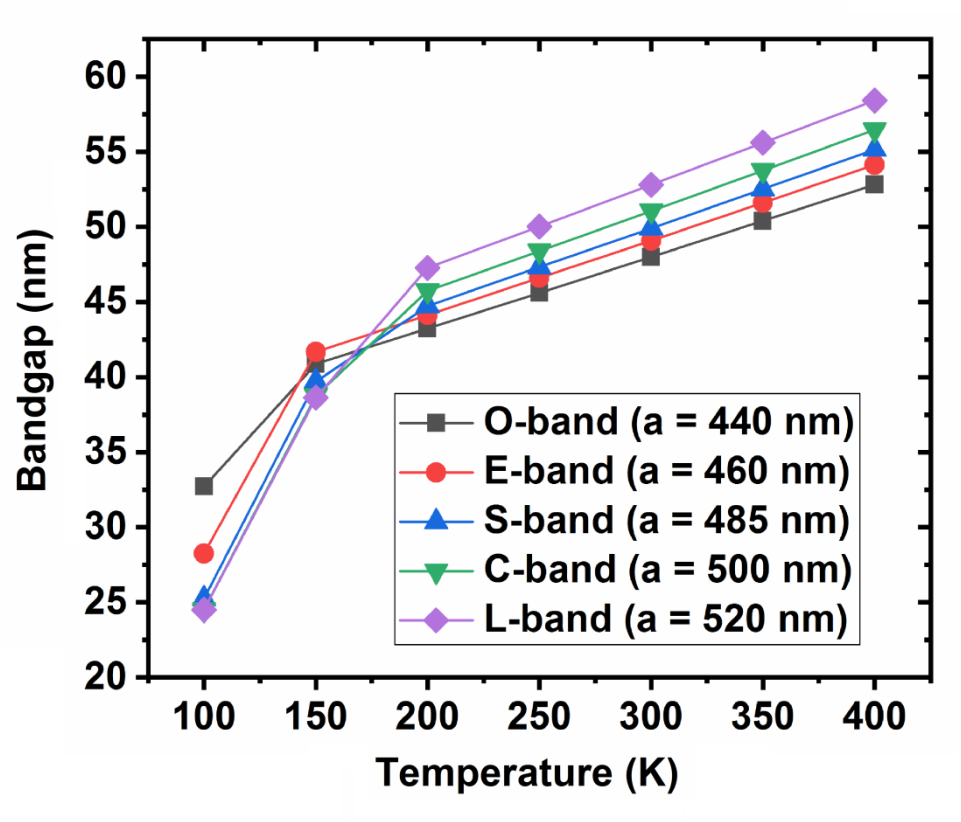

Figure 4.14: Variation of bandgap with change in temperature at different wavelengths and lattice constants.

From the figure, it is clear that the bandgap increases with the temperature rise. To achieve the PBG and eigen wavelengths in the near-infrared region, the lattice constants are selected carefully. However, it is essential to investigate the methods for quick heating and cooling of the structure to use it for the applications like filtering and routing the wavelengths. This PCW can also be used as a temperature sensor with a relatively more significant response time, limiting its applications in real-time temperature monitoring.

4.3.7 Effect of temperature on flat bands:

Group velocity is given by the inverse of the first-order dispersion in the waveguides. Moreover, the group index measures the group velocity in the waveguide. To observe the slow light in the PCW structures, the group index must be constant over a band of wavelengths, referred to as bandwidth. The preliminary simulations show that the lattice-shifted waveguide has a flat band and can generate slow light. In figure 4.15 (a-j), the group index, a measure of slow light is plotted against the normalized frequency in the temperature range of 100 K to 400 K.

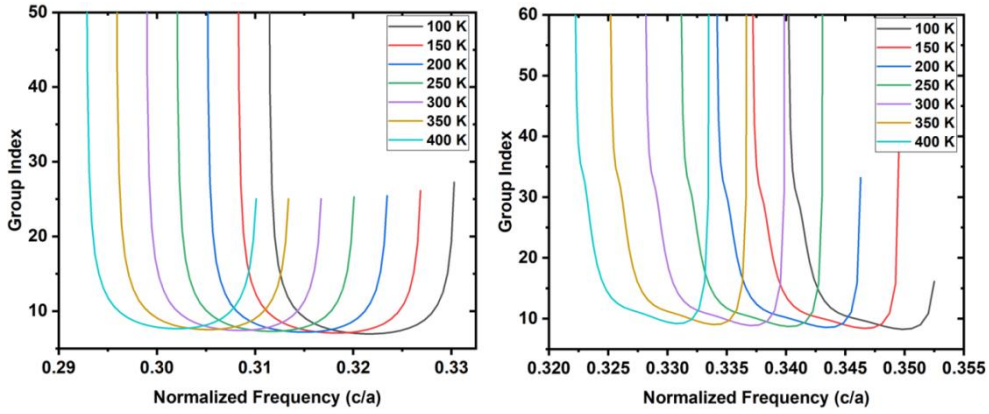
Group Index
Normalized Frequency (c/a)
100 K
150 K
200 K
250 K
300 K
350 K
400 K

(a) (f)

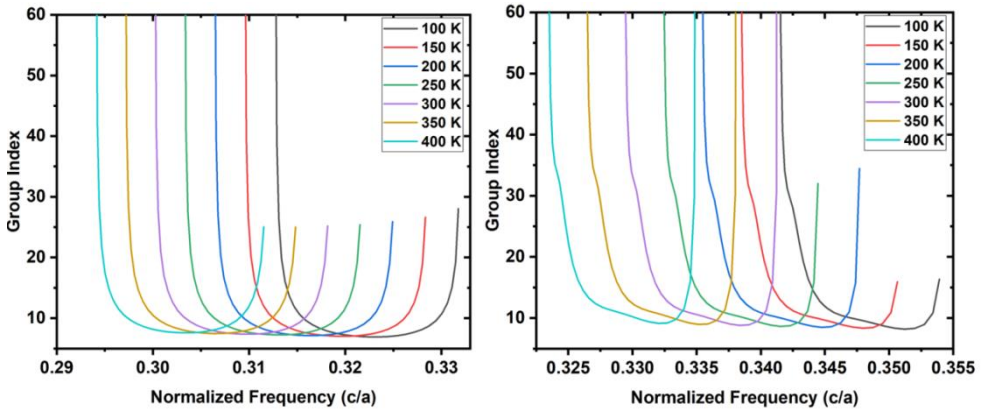
Group Index
Normalized Frequency (c/a)
100 K
150 K
200 K
250 K
300 K
350 K
400 K

(b) (g)

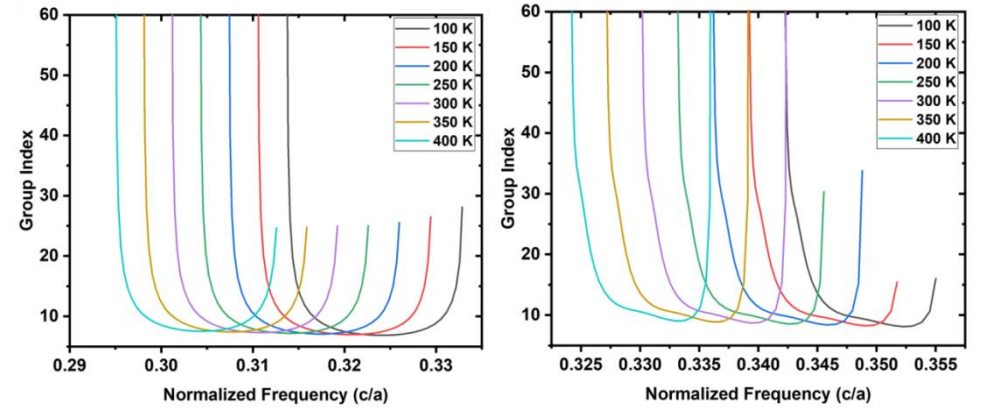
Group Index
Normalized Frequency (c/a)
100 K
150 K
200 K
250 K
300 K
350 K
400 K

(c) (h)

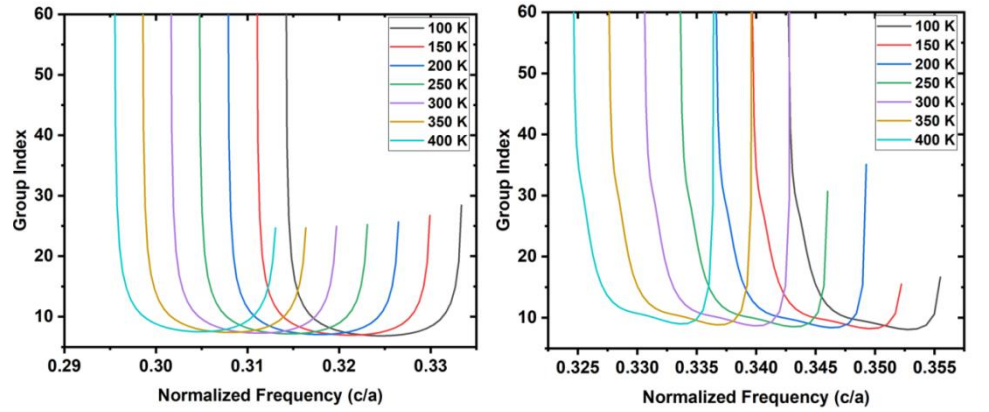
Group Index
Normalized Frequency (c/a)
100 K
150 K
200 K
250 K
300 K
350 K
400 K

(d) (i)

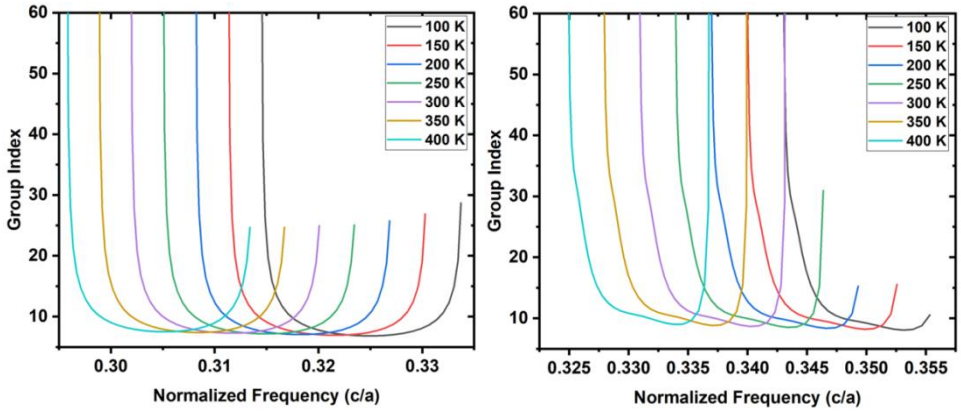

Figure 4.15: Group index as a function of normalized frequency. Group index calculated at band 16 in (a) O – band, (b) E – band (c) S – band (d) C – band (e) L – band. Group index calculated at band 17 in (f) O – band (g) E – band (h) S – band (i) C – band and (j) L – band.

Figure 4.16 (a-j) shows the group index profile of the structure within the temperature range of 100 K to 400 K at all the communication bands. As a necessary condition of the slow light dispersion devices [28], the wideband is observed in these plots. The constant group index is observed about a band of width 30 nm and above. Also, the group indices are determined by the change in temperature. The flat band dispersion region is almost preserved to be constant for a shift of about 40 nm. It is found that the slow light dispersion region is shifting to higher wavelengths as the temperature increases.

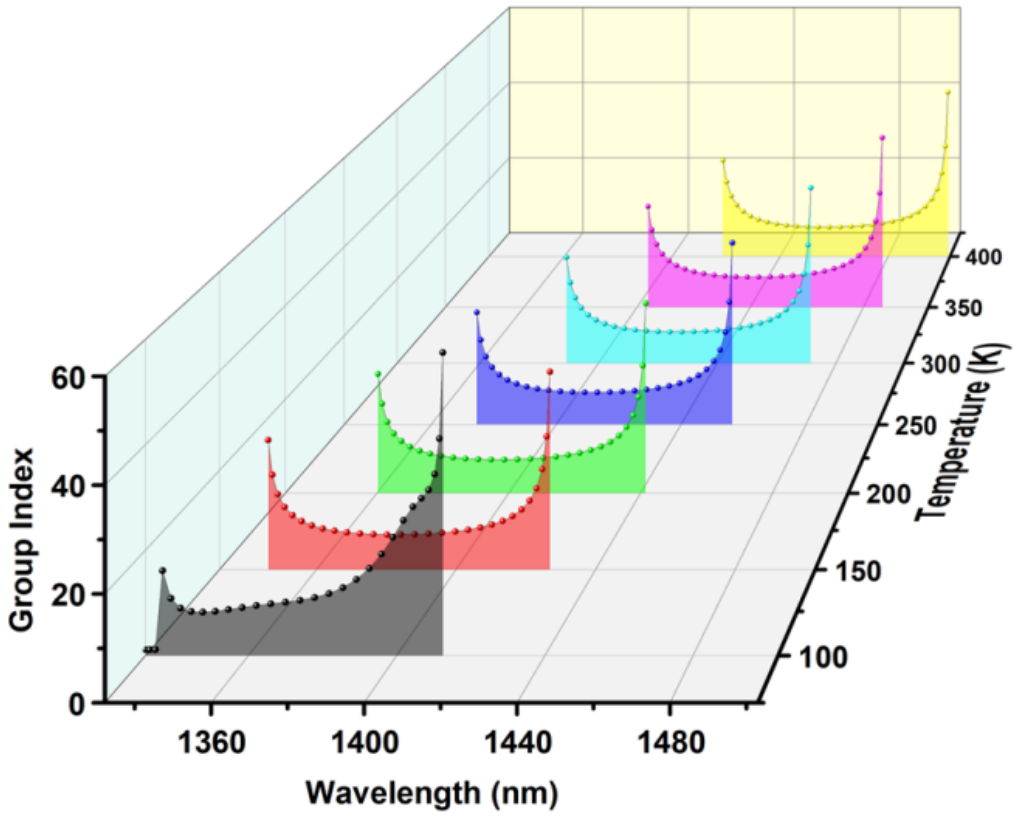

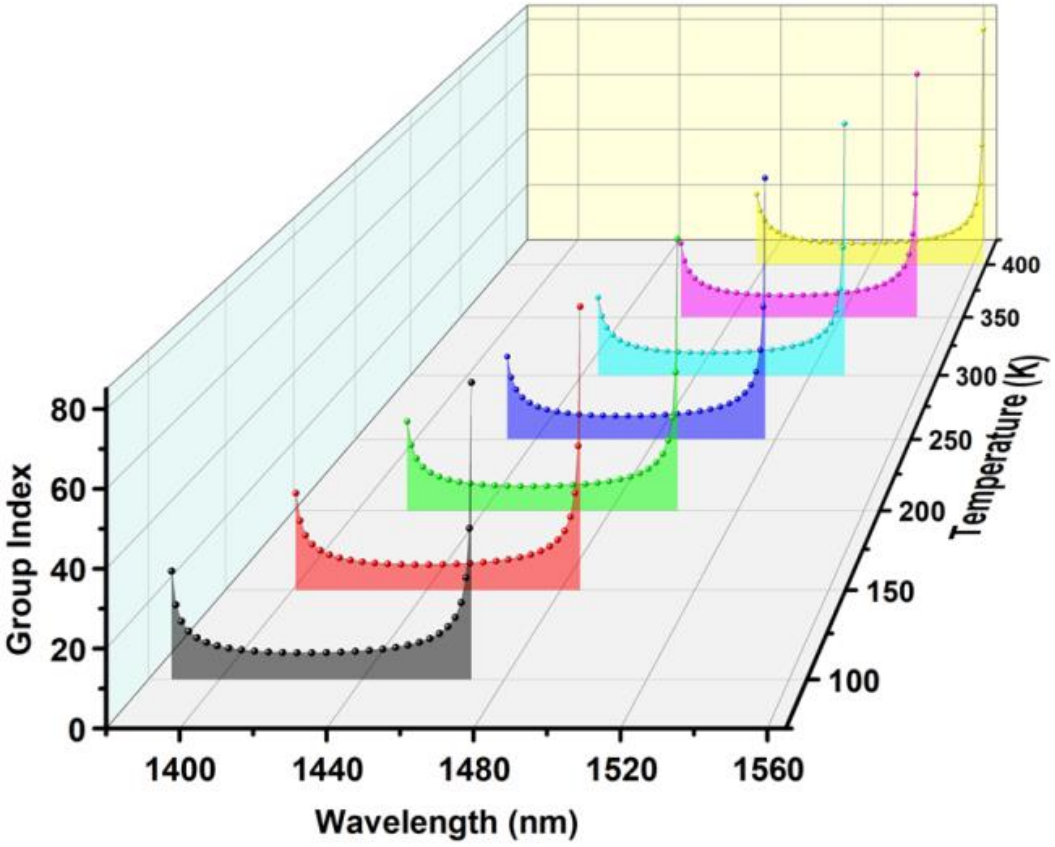
Group Index
0
20
40
60
80
1400
1440
1480
1520
1560
Wavelength (nm)
100
150
200
250
300
350
400
Temperature (K)

(b)

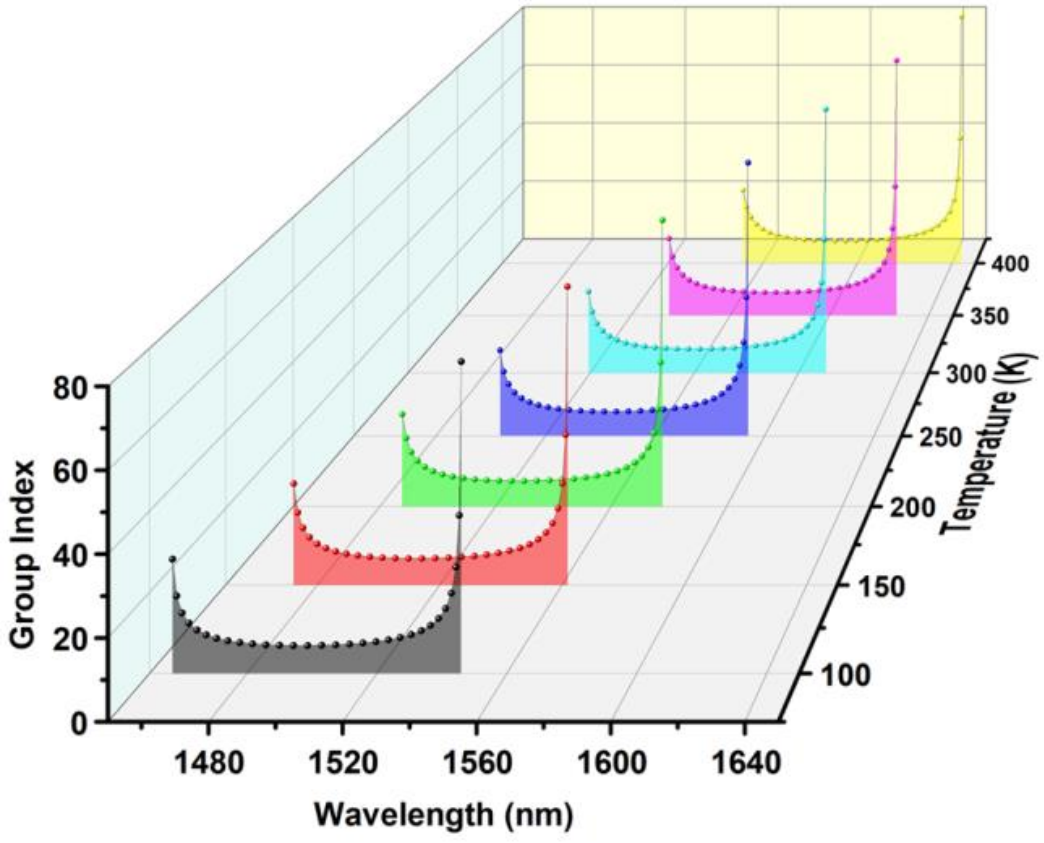
Group Index
0
20
40
60
80
1480
1520
1560
1600
1640
Wavelength (nm)
100
150
200
250
300
350
400
Temperature (K)

(c)

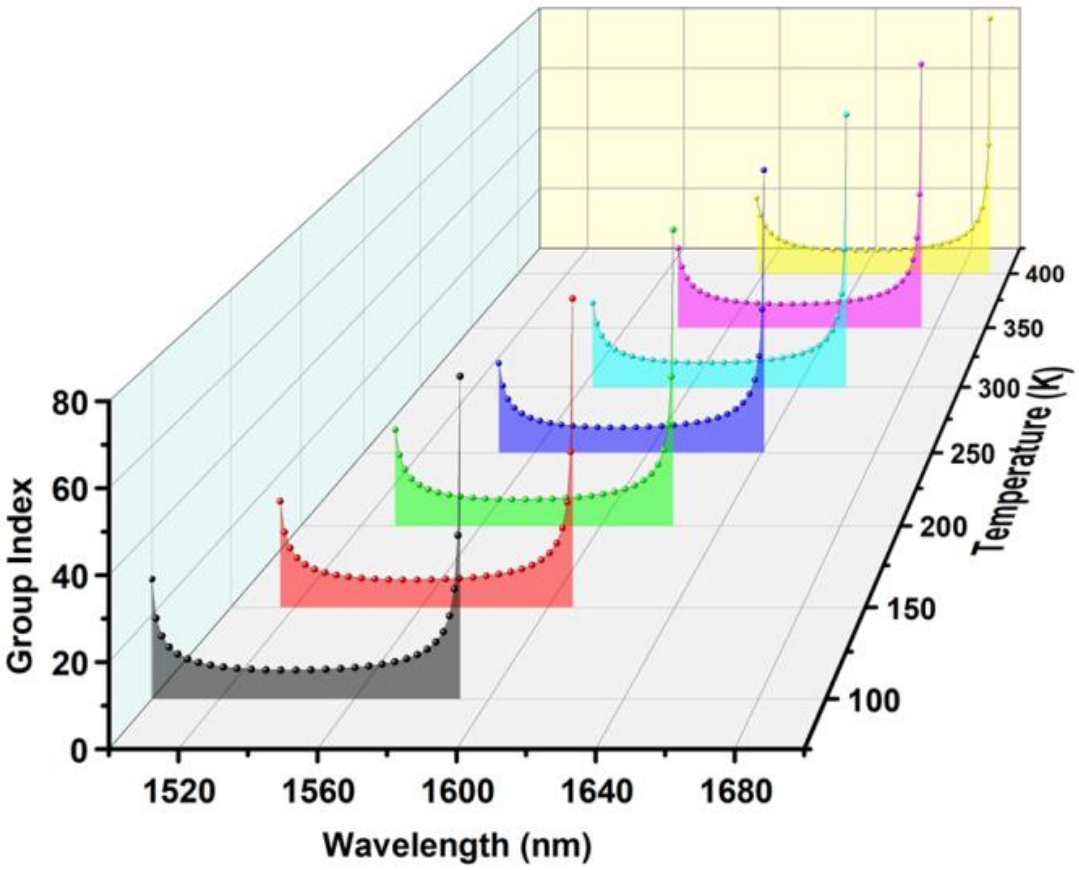
Group Index
0
20
40
60
80
1520
1560
1600
1640
1680
Wavelength (nm)
100
150
200
250
300
350
400
Temperature (K)

(d)

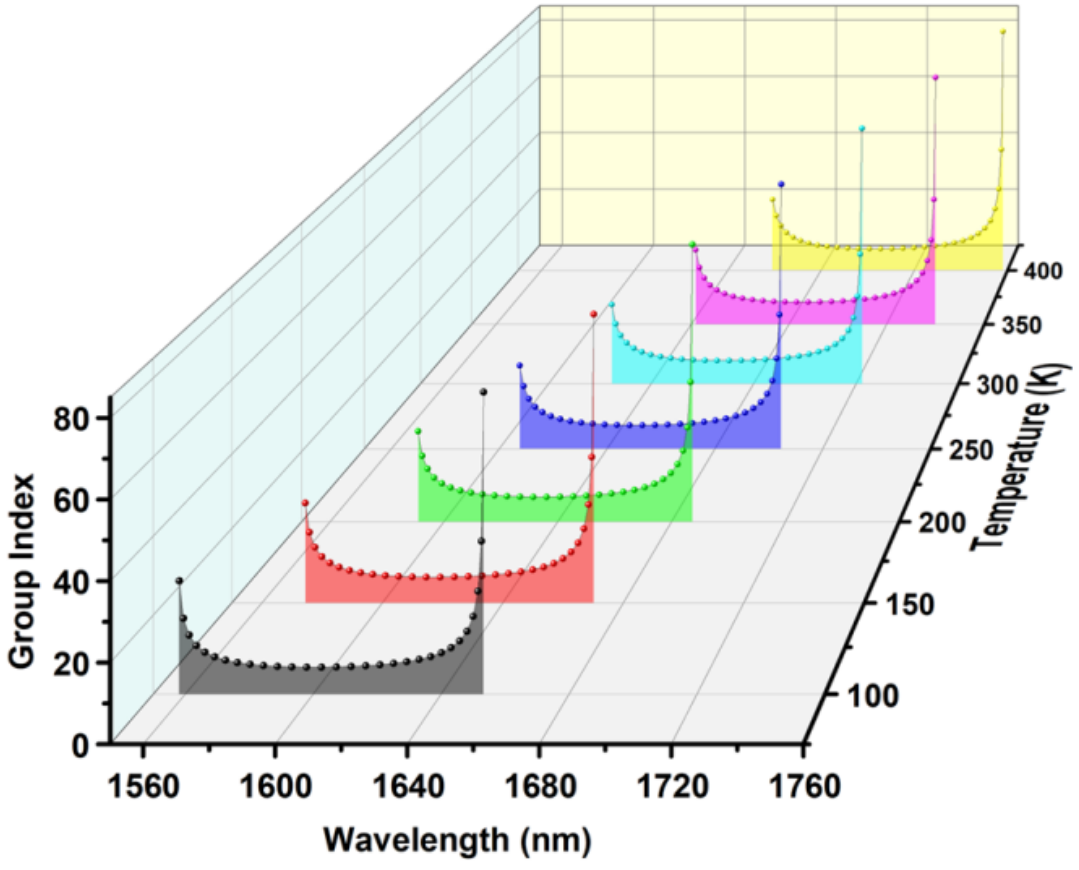
Group Index
0
20
40
60
80
1560
1600
1640
1680
1720
1760
Wavelength (nm)
100
150
200
250
300
350
400
Temperature (K)

(e)

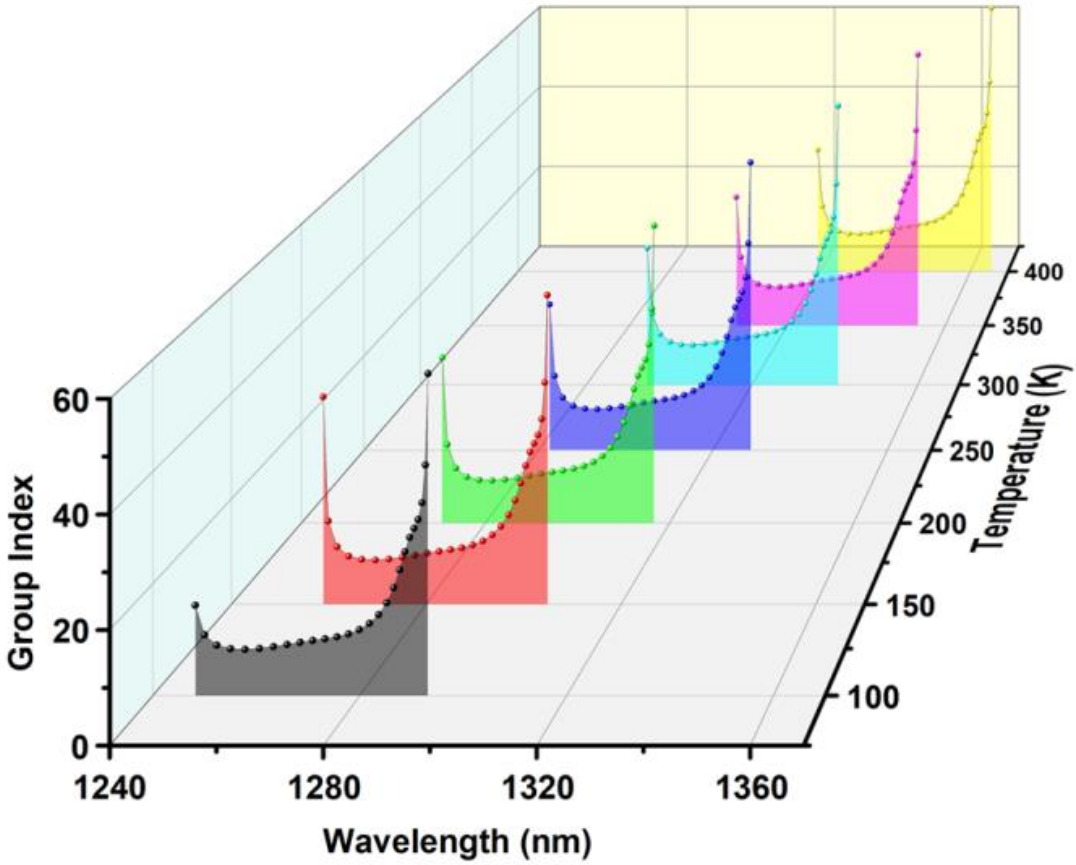
Group Index
0
20
40
60
1240
1280
1320
1360
Wavelength (nm)
100
150
200
250
300
350
400
Temperature (K)

(f)

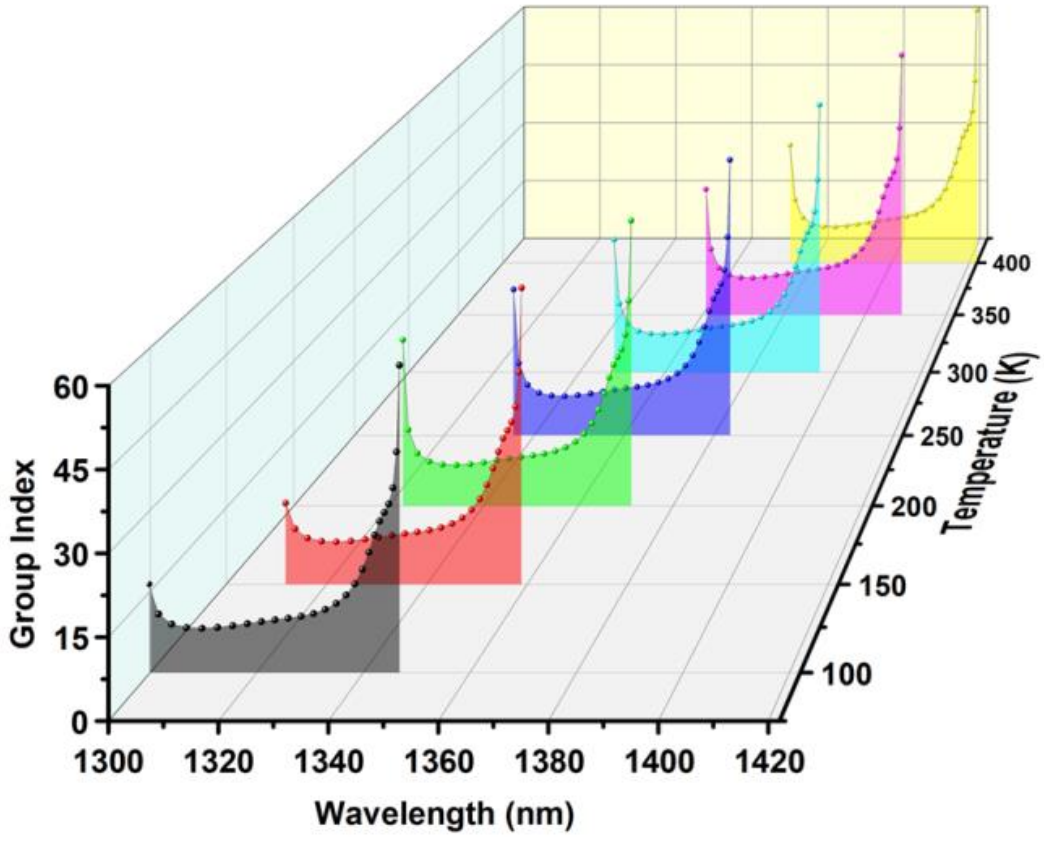
Group Index
0
15
30
45
60
1300
1320
1340
1360
1380
1400
1420
Wavelength (nm)
100
150
200
250
300
350
400
Temperature (K)

(g)

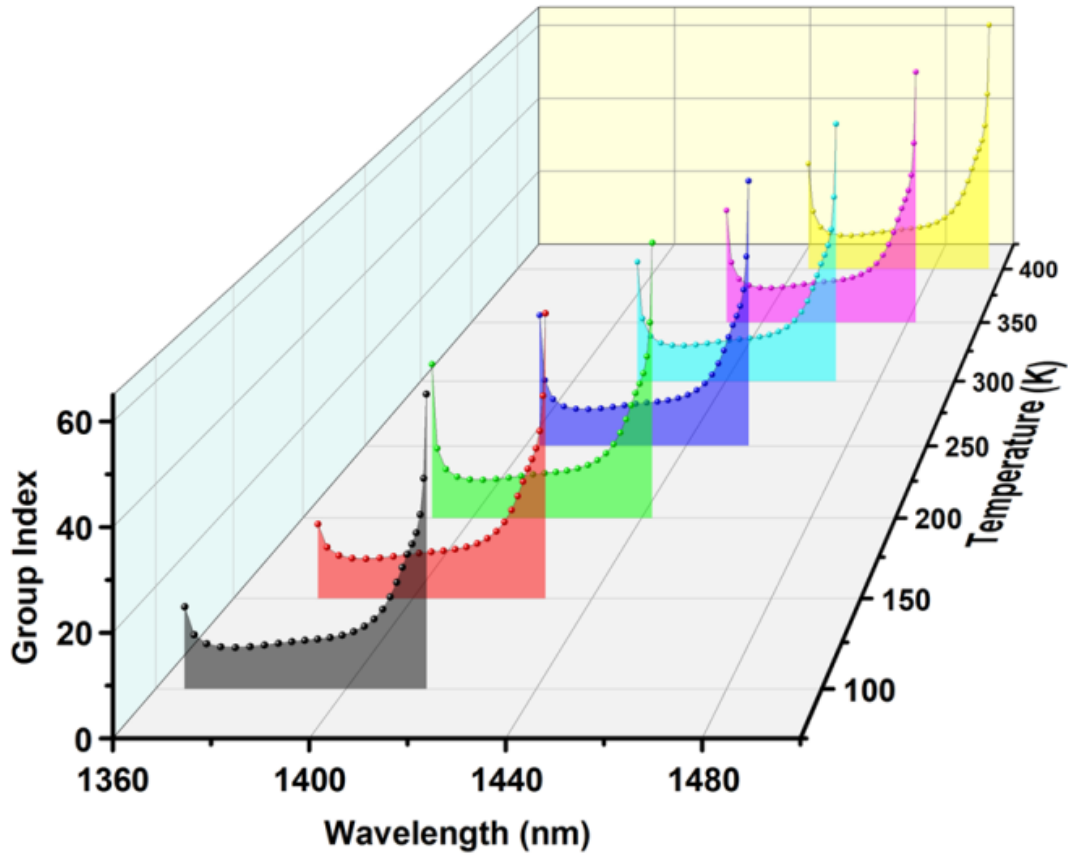
Group Index
0
20
40
60
1360
1400
1440
1480
Wavelength (nm)
100
150
200
250
300
350
400
Temperature (K)

(h)

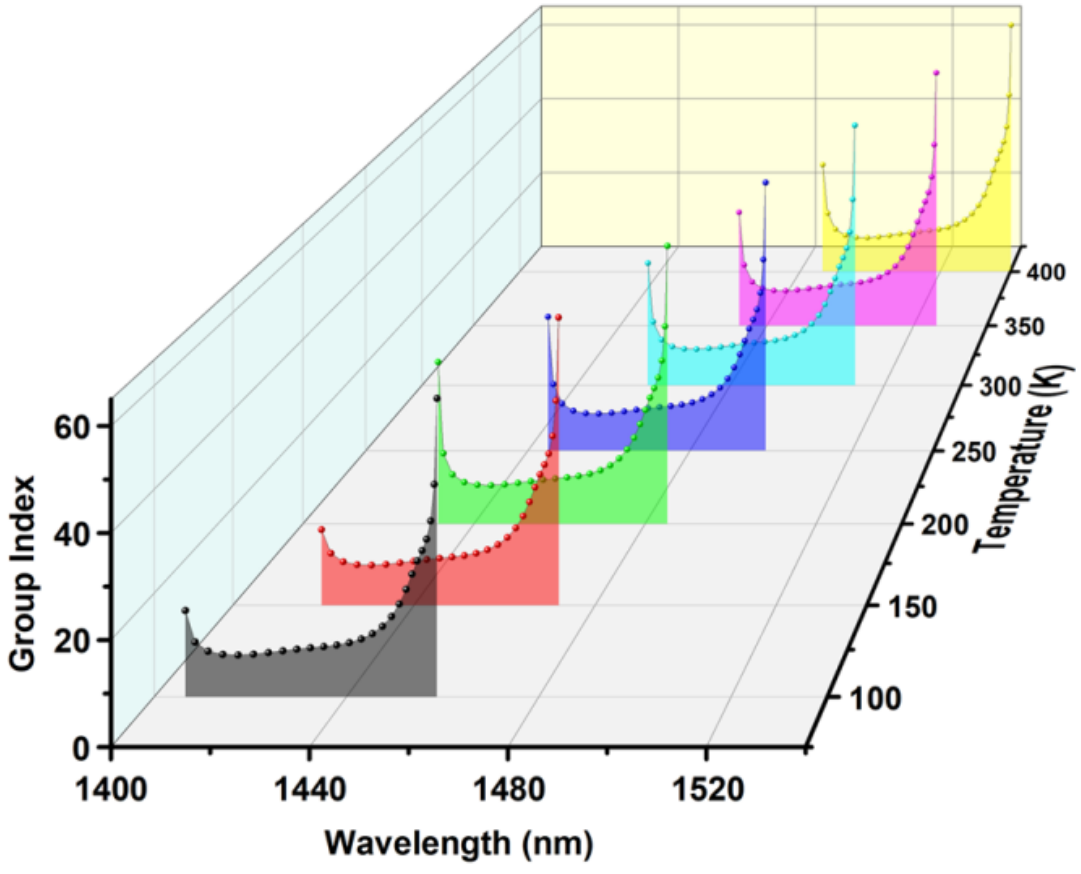
Group Index
0
20
40
60
1400
1440
1480
1520
Wavelength (nm)
100
150
200
250
300
350
400
Temperature (K)

(i)

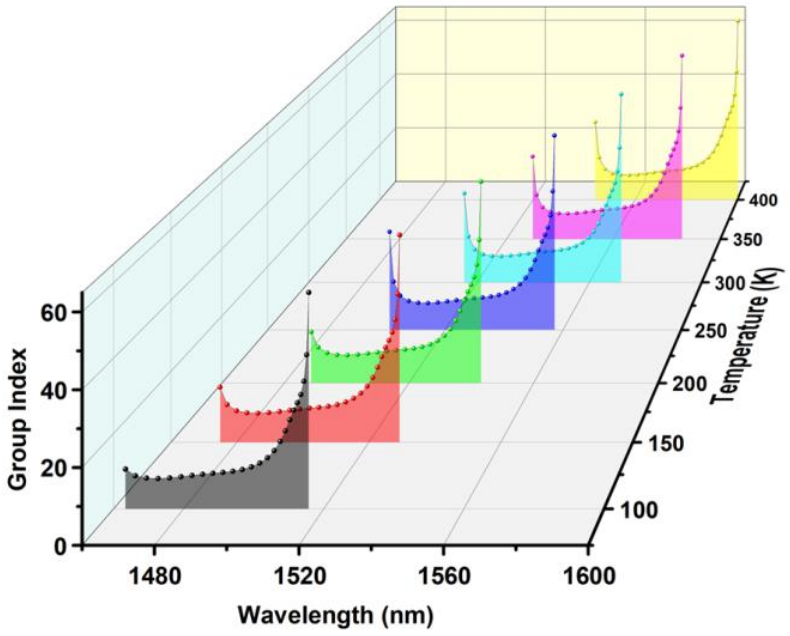

(j)

Figure 4.16: Group index as a function of wavelength at different temperatures. Group index calculated at band 16 in (a) O – band, (b) E – band (c) S – band (d) C – band (e) L – band. Group index calculated at band 17 in (f) O – band (g) E – band (h) S – band (i) C – band and (j) L – band.

The slow light bands are shifting due to the shift in PBG with the temperature. The bands are shifting, and the flat band is preserved with a temperature change. In general, this tunability of PBG is due to the change in temperature, which allows the change in refractive index to approximately 1% and the group index about 20-60 [29]. In table 4.3, we present the bandwidth of the flat band and the corresponding group index with temperature. For any slow light device application, the bandwidth of the device and group index needs to be optimized. Though there exists an inverse relationship between these parameters, the optimal values need to be selected for the device operation. Figure 4.17 shows the variation of these parameters with temperature.

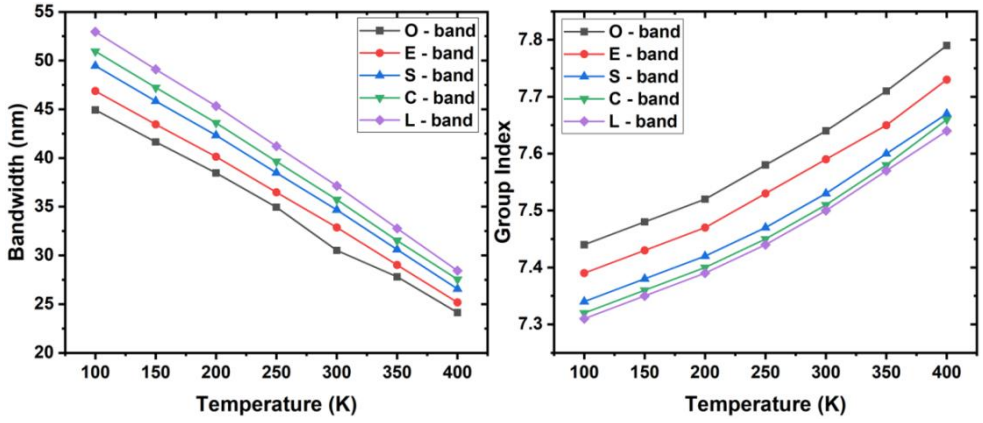

(a) (b)

Figure 4.17: Effect of temperature on the waveguide properties at communication bands. (a) Variation of bandwidth with temperature. (b) Variation of group index with temperature.

Table 4.3: Variation of group index with temperature and the corresponding flat bandwidth.

Communication Band	Temperature (K)	Bandwidth (nm)	Group Index
O – band	100	44.94	7.44
	150	41.65	7.48
	200	38.47	7.52
	250	34.95	7.58
	300	30.52	7.64
	350	27.81	7.71
	400	24.14	7.79
E – band	100	46.88	7.39
	150	43.45	7.43
	200	40.13	7.47
	250	36.48	7.53
	300	32.87	7.59
	350	29.02	7.65
	400	25.18	7.73
S – band	100	49.46	7.34
	150	45.84	7.38
	200	42.33	7.42
	250	38.48	7.47
	300	34.68	7.53
	350	30.61	7.60
	400	26.57	7.67
C – band	100	50.95	7.32
	150	47.24	7.36
	200	43.61	7.40
	250	39.64	7.45
	300	35.73	7.51
	350	31.53	7.58
	400	27.55	7.66
L – band	100	52.96	7.31
	150	49.1	7.35
	200	45.33	7.39
	250	41.21	7.44
	300	37.14	7.50
	350	32.78	7.57
	400	28.44	7.64

4.3.8 Dispersion analysis:

Second-order dispersion (β_2) and the group velocity dispersion (GVD) are the parameters that deal with the distortion of the optical pulse in the waveguide. Second-order dispersion can be calculated by [30]

$$\beta_2 = \left(\frac{d^2 k}{d\omega^2} \right) \tag{4.3}$$

From the dispersion diagram, the β_2 can be calculated. GVD or β_2 parameters are responsible for the dispersion and pulse broadening in the optical waveguides. For device applications, the parameter should be under control in order to have undistorted optical pulses. The calculated β_2 with wavelength at different temperatures are shown in figure 4.18. The nonlinear performance and the dispersion features of the PCW can be predicted from these graphs.

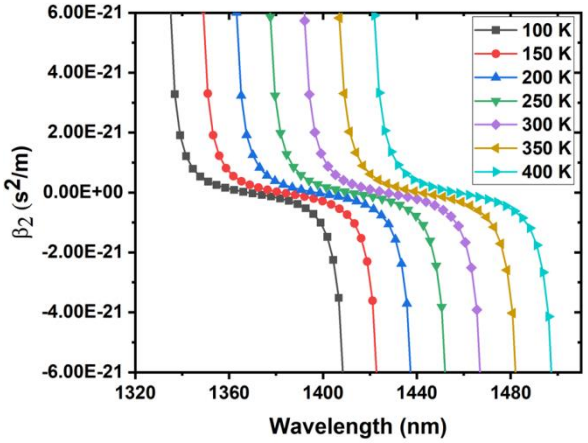

(a)

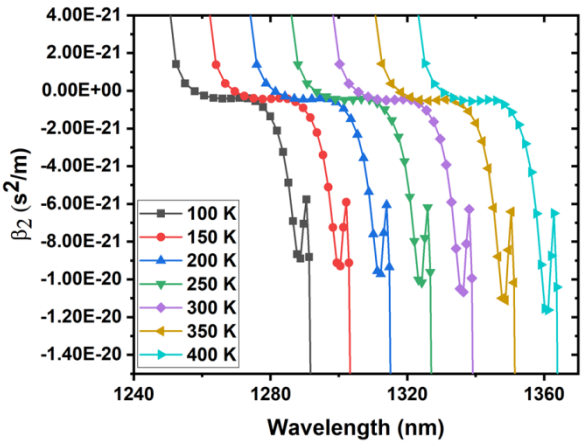

(f)

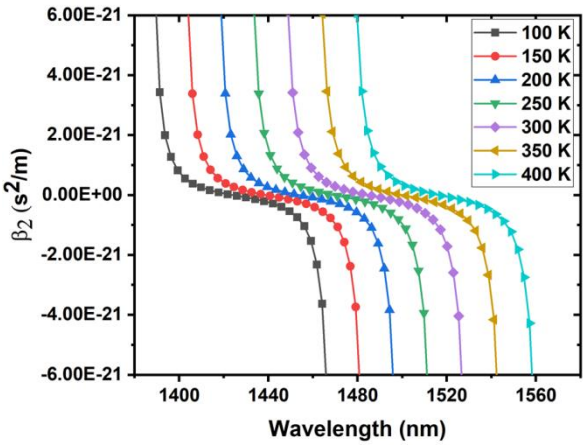

(b)

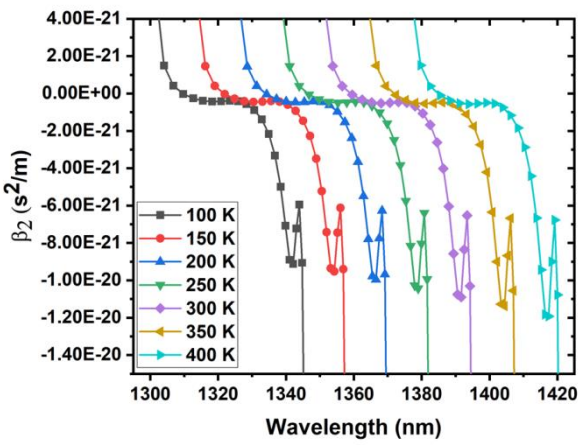

(g)

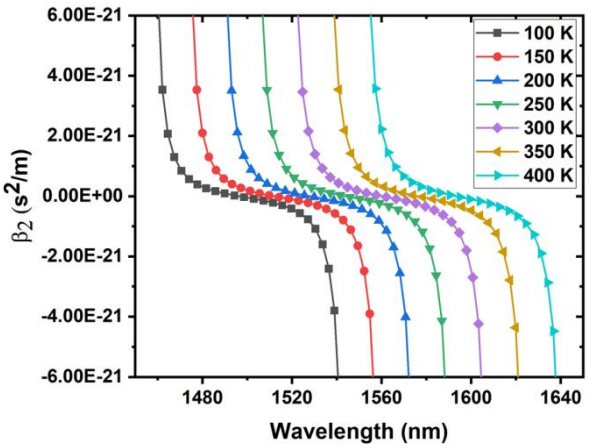

(c)

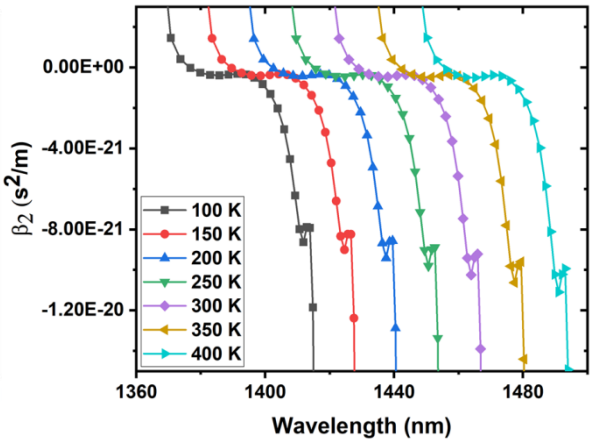

(h)

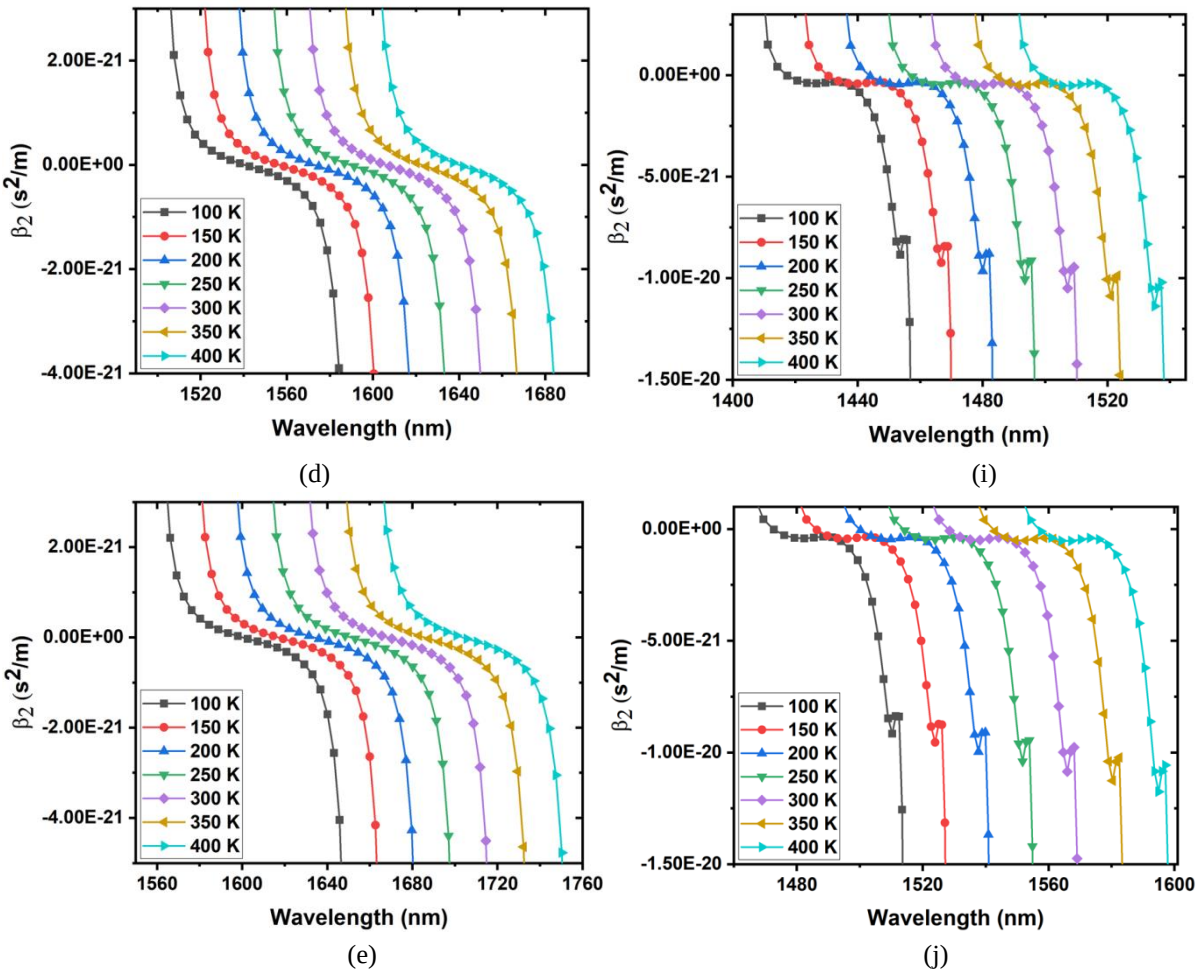

Figure 4.18: Second order dispersion (β_2) as a function of wavelength, calculated at band 16 in (a) O – band, (b) E – band (c) S – band (d) C – band (e) L – band and calculated at band 17 in (f) O – band (g) E – band (h) S – band (i) C – band and (j) L – band.

From figure 4.18, it can be observed that the magnitude of β_2 is of the order of 10^{-20} s^2/m or of the order of ps^2/mm, which is an acceptable range for the applications based on PCW. In our observation, at all the communication bands and at all the temperatures, the β_2 is in the permissible range. This confirms the possible applications of the PCW with low dispersion at the designated communication bands.

4.4 Conclusions

To conclude, we have shown that the PBG of a 2-dimensional PCW can be tunable using the electro-optic effect and thermo-optic effect. This results in tunable PBG ranging from 24 nm to 58 nm with a shift of about 34 nm. Tunability is achieved by introducing an external electric field in the range of 0 - 500 kV/cm and temperature in the range of 100 K to 400 K. The tunable structures are simulated in all communication bands.

The quadratic electro-optic effect is used to evaluate the refractive indices of the slab material with the applied electric field. The results reveal that there is a change in the

bandgap with the applied field. The shift in bandgap is calculated, and it is of the order of 10^{-4} *c/a*. In the PCW, a lattice shift is introduced to enhance the effect. With a shift in the range of 0.00*a* – 0.15*a*, the PCW resulted in tunable PBG. Lattice constants of the PC and PCW are calculated and found to be 447 nm and 355 nm, respectively, to observe the eigen wavelengths in the telecommunication bands.

Even though the electro-optic effect produces a smaller shift in the PBG, higher shifts can be attained by introducing defects in the structure or electrically active materials such as liquid crystals and electro-active polymers. Moreover, the method can be easily adaptable in optical networks.

To realize the effect of temperature on the tunability of the PBG, the variation in PBG is plotted against the temperature of the PCW. The lattice constants are calculated for all communication bands to realize the structure.

The dispersion in the waveguide is also studied, and the corresponding group index values are calculated as a function of wavelength. The effect of temperature is also studied on the slow light dispersion, and it is observed that the slow light dispersion region is shifting with the temperature rise. The dispersion analysis confirms the lower dispersion at the selected wavelengths. These tunable PBG structures can be used in optical filters, wavelength routers, optical shutters, dynamic detectors and interconnectors. This may also help in the development of on-chip integrated circuits due to their small size and material compatibility. However, more investigations are needed on the dispersion of light in such structures and fabrication methods. Moreover, the quick heating and cooling of the device need to be studied for real-time applications.

References

[1] J. D. Joannopoulos, P. R. Villeneuve, and S. Fan, "Photonic crystals: Putting a new twist on light," *Nature*, vol. 386, no. 6621, pp. 143–149, Mar. 1997, https://doi.org/10.1038/386143a0

[2] D. M. Pustai, A. Sharkawy, S. Shi, and D. W. Prather, "Tunable photonic crystal microcavities," *Appl. Opt.*, vol. 41, no. 26, pp. 5574-5579, Sep. 2002, https://doi.org/10.1364/AO.41.005574

[3] B. K. Singh, P. Kumar, and P. C. Pandey, "Tunable photonic band-gaps in one-dimensional photonic crystals containing linear graded index material," *Appl. Phys. B Lasers Opt.*, vol. 117, no. 3, pp. 947–956, Aug. 2014, https://doi.org/10.1007/s00340-014-5913-z

[4] M. Notomi, A. Shinya, K. Yamada, J. Takahashi, C. Takahashi and I. Yokohama, "Structural tuning of guiding modes of line-defect waveguides of silicon-on-insulator photonic crystal slabs," *IEEE J. Quantum Electron.*, vol. 38, no. 7, pp. 736-742, Jul. 2002, https://doi.org/10.1109/JQE.2002.1017583

[5] H. Nemec, L. Duvillaret, F. Garet, P. Kuzel, P. Xavier, J. Richard, and D. Rauly, "Thermally tunable filter for terahertz range based on a one-dimensional photonic crystal with a defect," *J. Appl. Phys.*, vol. 96, no. 8, pp. 4072-4075, Oct. 2004, https://doi.org/10.1063/1.1787623

[6] J. Hwang et al., "Electro-tunable optical diode based on photonic bandgap liquid-crystal heterojunctions," *Nat. Mater.*, vol. 4, no. 5, pp. 383–387, Apr. 2005, https://doi.org/10.1038/nmat1377

[7] J. Cos, J. Ferré-Borrull, J. Pallarès, and L. F. Marsal, "Analysis of tunable bandgaps in liquid crystal-infiltrated 2D silicon photonic crystals," *Appl. Phys. B Lasers Opt.*, vol. 100, no. 4, pp. 833–839, Aug. 2010, https://doi.org/10.1007/s00340-010-4172-x

[8] M. Ebnali-Heidari, C. Monat, C. Grillet, and M. K. Moravvej-Farshi, "A proposal for enhancing four-wave mixing in slow light engineered photonic crystal waveguides and its application to optical regeneration," *Opt. Express*, vol. 17, no. 20, pp. 18340-18353, Sep. 2009, https://doi.org/10.1364/oe.17.018340

[9] B. K. Singh and P. C. Pandey, "Tunable temperature-dependent THz photonic bandgaps and localization mode engineering in 1D periodic and quasi-periodic structures with graded-index materials and InSb," *Appl. Opt.*, vol. 57, no. 28, pp. 8171-8181, Oct. 2018, https://doi.org/10.1364/AO.57.008171

[10] O. Painter et al., "Lithographic tuning of a two-dimensional photonic crystal laser array," *IEEE Photonics Technol. Lett.*, vol. 12, no. 9, pp. 1126–1128, Sep. 2000, https://doi.org/10.1109/68.874210

[11] M. Roussey, M. P. Bernal, N. Courjal, D. Van Labeke, F. I. Baida, and R. Salut, "Electro-optic effect exaltation on lithium niobate photonic crystals due to slow photons," *Appl. Phys. Lett.*, vol. 89, no. 24, pp. 87–90, Dec. 2006, https://doi.org/10.1063/1.2402946

[12] T. Goto, H. Sato, H. Takagi, A. V. Baryshev, and M. Inoue, "Novel magnetophotonic crystals controlled by the electro-optic effect for non-reciprocal high-speed modulators," *J. Appl. Phys.*, vol. 109, no. 7, pp. 7–10, Apr. 2011, https://doi.org/10.1063/1.3562882

[13] Y. Fu, J. Zhang, X. Hu, and Q. Gong, "Electro-optic tunable multi-channel filter in two-dimensional ferroelectric photonic crystals," *J. Opt.*, vol. 12, no. 075202, pp. 1-7, Jul. 2010, https://doi.org/10.1088/2040-8978/12/7/075202

[14] P. T. Lin, Z. Liu, and B. W. Wessels, "Ferroelectric thin film photonic crystal waveguide and its electro-optic properties," *J. Opt. A Pure Appl. Opt.*, vol. 11, no. 075005, pp. 1-7, May 2009, https://doi.org/10.1088/1464-4258/11/7/075005

[15] F. Ghasemi, S. R. Entezar, and S. Razi, "Terahertz tunable photonic crystal optical filter containing graphene and nonlinear electro-optic polymer," *Laser Phys.*, vol. 29, no. 056201, pp. 1-8, Mar. 2019, https://doi.org/10.1088/1555-6611/ab05c2

[16] S. M. Weiss, M. Haurylau, and P. M. Fauchet, "Tunable photonic bandgap structures for optical interconnects," *Opt. Mater.*, vol. 27, no. 5, pp. 740–744, Feb. 2005, https://doi.org/10.1016/j.optmat.2004.08.007

[17] F. Du, Y. Q. Lu, and S. T. Wu, "Electrically tunable liquid-crystal photonic crystal fiber," *Appl. Phys. Lett.*, vol. 85, no. 12, pp. 2181–2183, Sep. 2004, https://doi.org/10.1063/1.1796533

[18] X. Dai, Y. Xiang, S. Wen, and H. He, "Thermally tunable and omnidirectional terahertz photonic bandgap in the one-dimensional photonic crystals containing semiconductor InSb," *J. Appl. Phys.*, vol. 109, no. 053104, pp. 1-6, Mar. 2011, https://doi.org/10.1063/1.3549834

[19] P. Halevi and F. Ramos-Mendieta, "Tunable photonic crystals with semiconducting constituents," *Phys. Rev. Lett.*, vol. 85, no. 9, pp. 1875–1878, Aug. 2000, https://doi.org/10.1103/PhysRevLett.85.1875

[20] R. Ozaki, T. Matsui, M. Ozaki, and K. Yoshino, "Electrically color-tunable defect mode lasing in one-dimensional photonic-band-gap system containing liquid crystal," *Appl. Phys. Lett.*, vol. 82, no. 3593, pp. 3593–3595, May 2003, https://doi.org/10.1063/1.1577829

[21] M. Haurylau, S. P. Anderson, K. L. Marshall, and P. M. Fauchet, "Electrical modulation of silicon-based two-dimensional photonic bandgap structures," *Appl. Phys. Lett.*, vol. 88, no. 061103, pp. 22–25, Feb. 2006, https://doi.org/10.1063/1.2172070

[22] V. Skoromets, H. Němec, C. Kadlec, D. Fattakhova-Rohlfing, and P. Kužel, "Electric-field-tunable defect mode in one-dimensional photonic crystal operating in the terahertz range," *Appl. Phys. Lett.*, vol. 102, no. 241106, pp. 1–5, Jun. 2013, https://doi.org/10.1063/1.4809821

[23] G. Wang, J. P. Huang, and K. W. Yu, "Electrically tunable photonic crystals with nonlinear composite materials," *Appl. Phys. Lett.*, vol. 91, no. 191117, pp. 1–4, Nov. 2007, https://doi.org/10.1063/1.2809389

[24] B.E.A. Saleh, and M.C. Teich, "*Fundamentals of Photonics*," 3rd edn., Wiley, Mar. 2007.

[25] J. A. McCaulley, V. M. Donnelly, M. Vernon, and I. Taha, "Temperature dependence of the near-infrared refractive index of silicon, gallium arsenide, and indium phosphide," *Phys. Rev. B*, vol. 49, no. 11, pp. 7408–7417, Mar. 1994, https://doi.org/10.1103/PhysRevB.49.7408

[26] Y. Lianghong, L. Qiang, and G. P. Agrawal, "Dispersion tailoring and soliton propagation in silicon waveguides," *Opt. Lett.*, vol. 31, no. 9, pp. 1295-1297, May 2006, https://doi.org/10.1364/OL.31.001295

[27] P. Colman, S. Combrié, G. Lehoucq, and A. De Rossi, "Control of dispersion in photonic crystal waveguides using group symmetry theory," *Opt. Express*, vol. 20, no. 12, pp. 13108-13114, Jun. 2012, https://doi.org/10.1364/oe.20.013108

[28] J. Li, T. P. White, L. O'Faolain, A. Gomez-Iglesias, and T. F. Krauss, "Systematic design of flat band slow light in photonic crystal waveguides," *Opt. Express*, vol. 16, no. 9, pp. 6227-6232, Apr. 2008, https://doi.org/10.1364/OE.16.006227

[29] T. Baba, "Slow light in photonic crystals," *Nat. Photonics*, vol. 2, no. 8, pp. 465-473, Aug. 2008, https://doi.org/10.1038/nphoton.2008.146

[30] J. Hou, D. Gao, H. Wu, R. Hao, and Z. Zhou, "Flat band slow light in symmetric line defect photonic crystal waveguides," *IEEE Photonics Technol. Lett.*, vol. 21, no. 20, pp. 1571–1573, Oct. 2009, https://doi.org/10.1109/LPT.2009.2030160

Chapter – 5
Tunable Photonic Bandgap based Temperature Sensor

In this chapter, a temperature sensor is modelled to perform the measurements over a broad temperature range. The active tuning of the photonic bandgap is used for this purpose. Simulations are performed in MIT Photonic-Bands software to calculate the eigen frequencies of the structure. The bands are linearly shifting with a temperature change. The structure is designed to get the eigen wavelengths in the near-infrared region. In these studies, the sensitivity of the sensor is found to be in the range of $375.16 \pm 0.791 \times 10^{-3}$ *to* $378.55 \pm 0.794 \times 10^{-3}$ *pm/K. The proposed structure may be used as a temperature sensor at high and low-temperature regions with higher sensitivity.*

5.1 Temperature sensing by photonic crystal waveguide:

Owing to their advantages, optical sensors have increased the interest of the scientific community for temperature measurement [1-5]. Fibre Bragg grating (FBG) sensors and long-period grating (LPG) sensors are more popular in fibre optic sensors (FOSs) for temperature measurement [6-10]. Both point and distributed sensing are feasible with these sensing techniques [11-12].

PC and PC fibre (PCF) based temperature sensors have been developed in recent years with various working ranges and sensitivities. Different methods are adopted along with PC and PCF for temperature measurement. Larrion et al. [13] used quantum dot nano-coatings on the innermost holes of a PCF and developed a temperature sensor working in the range of – 40 ^{o}C to + 70 ^{o}C. By measuring the position of the transmission peak, a theoretical temperature sensor with a sensitivity of 6.6 pm/ ^{o}C is proposed by using the FDTD method by Fu et al. [14]. This method was based on the thermo-optic effect in silicon material. Qian et al. [15] proposed a highly sensitive temperature sensor using alcohol-filled PCF. This sensor was experimentally demonstrated with a sensitivity of 6.6 nm/ ^{o}C. A temperature sensor using the concept of surface plasmon resonance in PCF was proposed by Lu et al. [16].

PCF filled with silver nanowires are used to demonstrate this sensor with a sensitivity of 2.7 nm/ ^{o}C. Using liquid crystals filled in the PC lattice, a highly sensitive temperature sensor was proposed by Hameed et al. [17]. A sensitivity of 10 nm/ ^{o}C in the temperature range of 30 ^{o}C – 50 ^{o}C was reported. A high range (25 ^{o}C – 60 ^{o}C) temperature sensor using PCF was presented by Yang et al. [18]. A sensitivity of – 2.08 nm/ ^{o}C was experimentally achieved in this work. All these sensors were developed with different working principles to measure the temperature with various working ranges and sensitivities.

Here, we modelled a PCW that can develop a broad range temperature sensor. For the proposed structure, GaAs is used as the base material. Air cylinders in a hexagonal lattice are considered to form the waveguide. The studies are performed in the temperature range of 10 K to 400 K. Thermo-optic effect is used to calculate the RI and dielectric constant of the slab [19]. These calculated RI and dielectric constants are used during the simulations in MPB [20]. The outputs of these programs provide the eigen frequencies of the structures, which are further analysed to find the band edges and operating wavelengths of the structure. We focused on obtaining the eigen frequencies in the near-infrared regions for various applications of the structure. This PCW can be used with a broadband source (BBS) and optical spectrum analyser (OSA) to measure the temperatures with higher sensitivity which we discussed in subsequent sections.

5.2 Design of the sensor:

The proposed PCW based temperature sensor setup is shown in figure 5.1 (a). It consists of a PCW connected with BBS using multimode fibre (MMF). The PCW is placed inside a temperature-controlled chamber. The output of the PCW is measured by an OSA. The PCW is formed by considering air cylinders of radius 0.18a in a hexagonal lattice of lattice constant (a) 304 nm to form the periodic structure in GaAs slab of thickness 240 nm. Three rows of air cylinders are considered on both sides of the waveguide. The geometrical parameters are calculated to make the PBG as small as possible for the sensing applications. Figure 5.1 (b) shows the three-dimensional view of the PCW.

We have used equation (4.2) to calculate the RI and the corresponding dielectric constants of the slab with applied temperatures. For the present work, T_{ref} is chosen as 300 K, and β is taken as 2.25 x 10^{-4} K^{-1}.

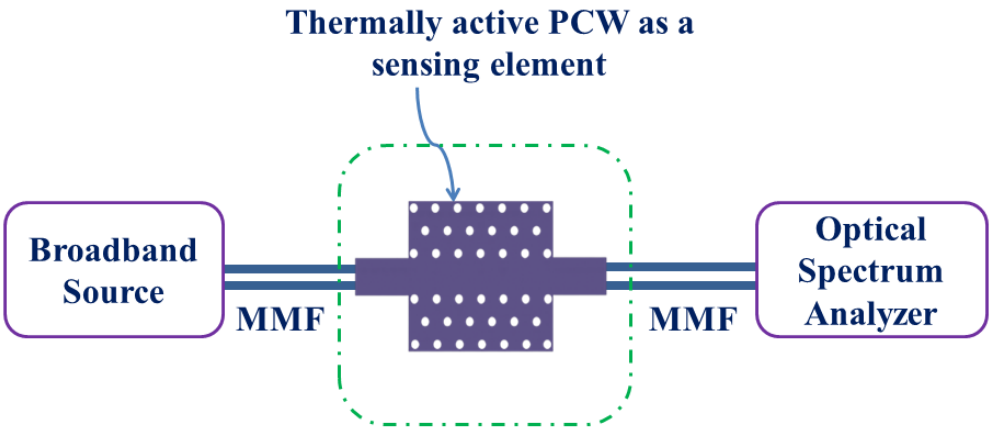

(a)

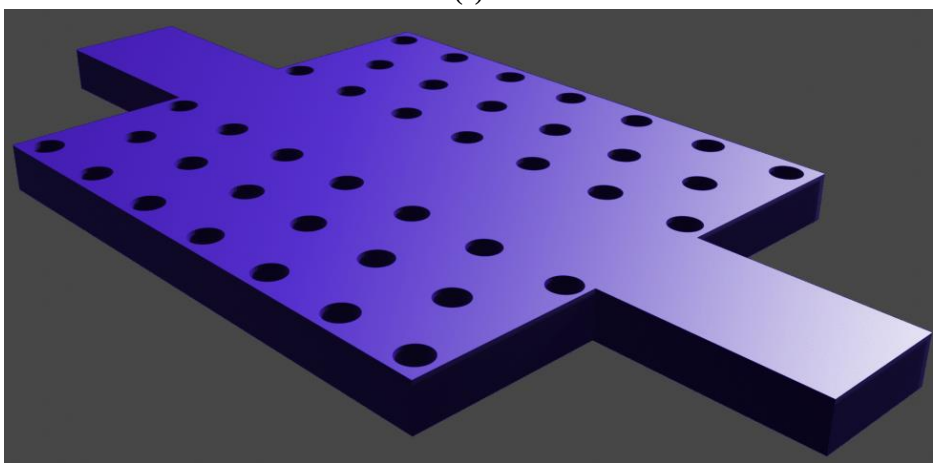

(b)

Figure 5.1: Schematic of the proposed PCW (a) the sensor set-up and (b) 3-dimensional view of the PCW

5.3 Temperature sensing by photonic bandgap:

Figure 5.2 (a) and (b) shows the 2-dimensional view of the TE and TM bands of the PCW, respectively. Figure 5.2 (c) and (d) shows the corresponding 3-dimensional view of the modes. The preliminary observations confirm the presence of PBG between bands 7 and 8 for this structure. The calculated PBG is 0.4087% for the TM modes and 4.994% for TE modes at 300 K temperature. The TM modes are distributed over a narrow band and thus are useful for sensing applications. The obtained output from the simulations is normalized data and needs to employ the lattice constant to calculate the eigen frequencies and eigen wavelengths. To observe the bands in the near-infrared wavelengths, the lattice constant is calculated and is found to be 304 nm for the present structure. As the PBG exists between bands 7 and 8, the frequencies and wavelengths corresponding to these bands are analyzed further.

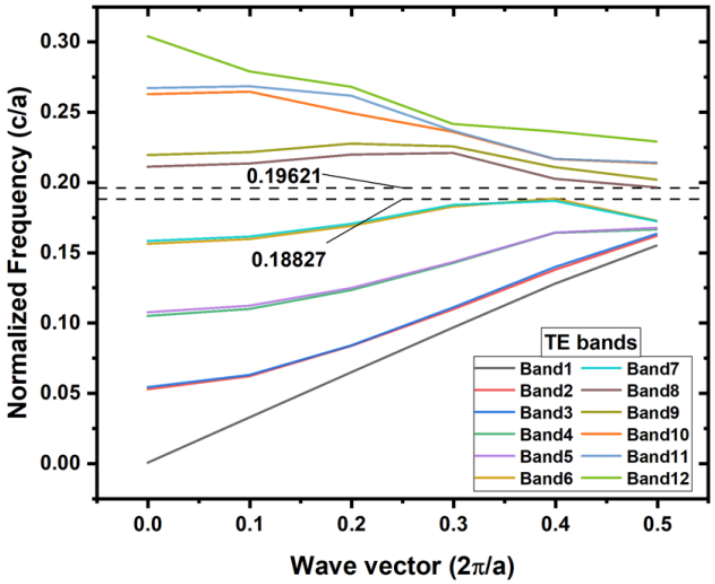
Normalized Frequency (c/a)
Wave vector (2π/a)
0.19621
0.18827
TE bands
Band1
Band2
Band3
Band4
Band5
Band6
Band7
Band8
Band9
Band10
Band11
Band12

(a)

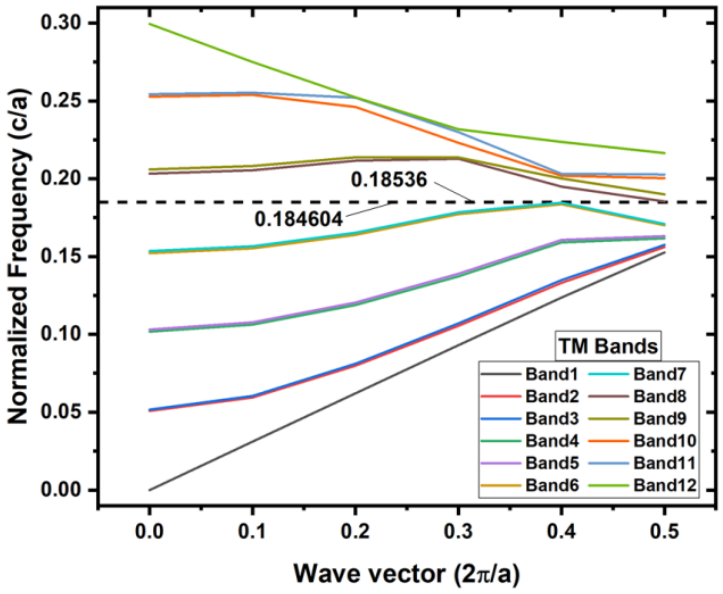
Normalized Frequency (c/a)
Wave vector (2π/a)
0.18536
0.184604
TM Bands
Band1
Band2
Band3
Band4
Band5
Band6
Band7
Band8
Band9
Band10
Band11
Band12

(b)

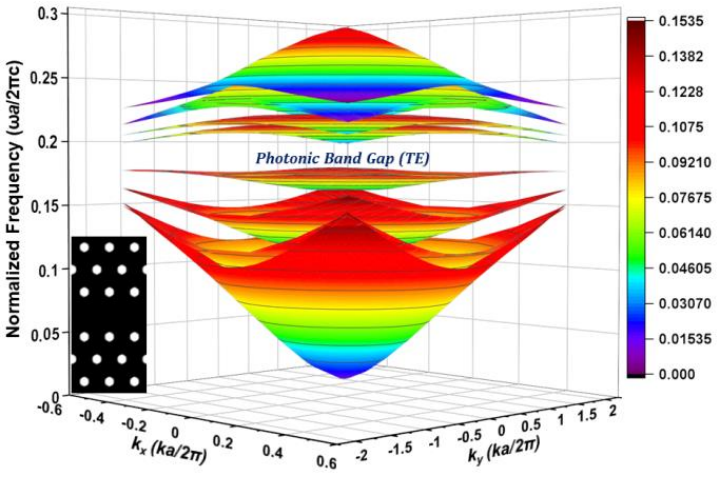
Normalized Frequency (ωa/2πc)
Photonic Band Gap (TE)
k_x (ka/2π)
k_y (ka/2π)

(c)

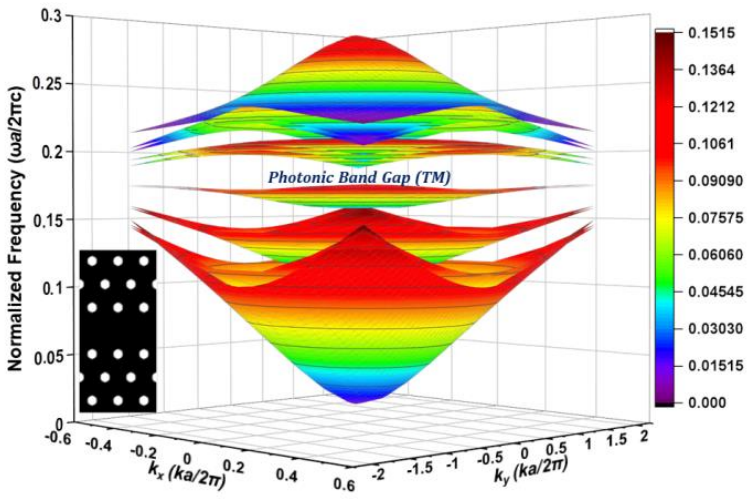

(d)

Figure 5.2: 2-dimensional view of the band diagrams of the PCW (a) TE bands and (b) TM bands 3-dimensional view of the (c) TE bands (d) TM bands.

Figure 5.3 shows the PBG in TM modes between bands 7 and 8. With the TM modes, a bandgap of 0.00076 *c/a* is observed here, which is useful for sensor applications. Using the lattice constant value, this PBG is about 6.341 nm at 300 K temperature. Moreover, for this PCW, wavelengths in the range of 1440 nm to 1600 nm are used as source wavelengths.

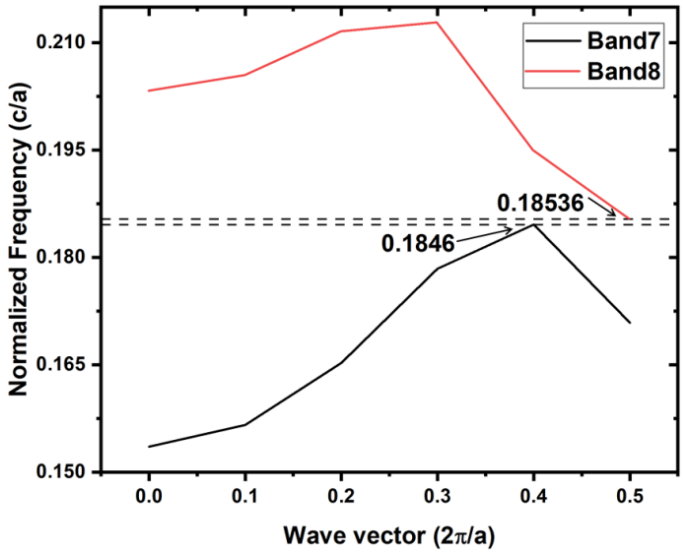

Figure 5.3: Bands 7 and 8 of the PCW with TM mode. A bandgap of 0.00076 *c/a* is observed here

Figure 5.4 (a) and (b) shows the variation in the edge/position of band 7 and band 8 with temperature. The plots are linear, which recommends the possible application of the proposed structure as a temperature sensor for both lower and higher temperature regions.

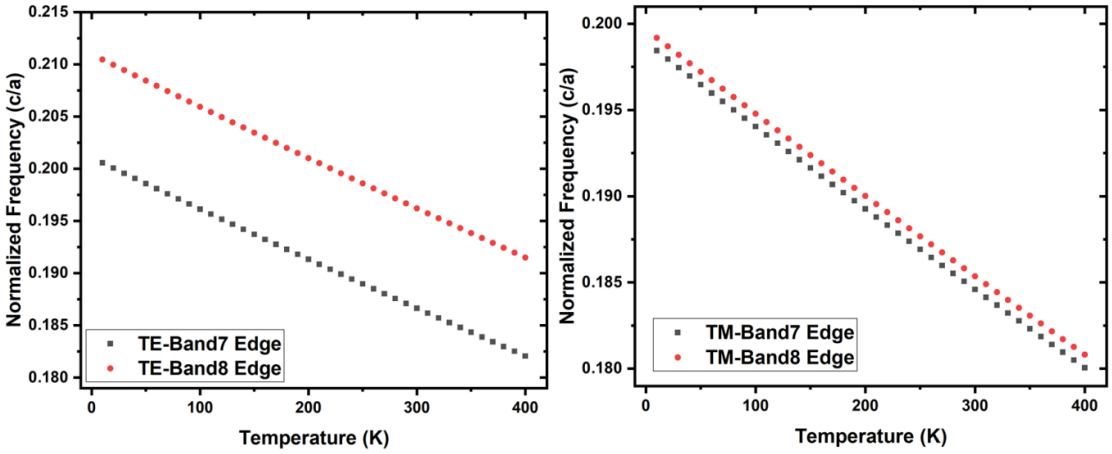

(a) (b)

Figure 5.4: Normalized frequencies of the PCW at band 7 and band 8 with temperature (a) TE mode and (b) TM mode.

In the simulations, it is observed that the PBG of the PCW is increasing linearly with the applied temperature. Hence, by measuring the PBG, the temperature can be estimated. Figure 5.5 (a) shows the distribution of the PBG of the PCW at various wavelengths. Figure 5.5 (b) shows the variations of the PBG of the PCW with the temperature. These PBG and band edges can be detected by the OSA to measure the temperature.

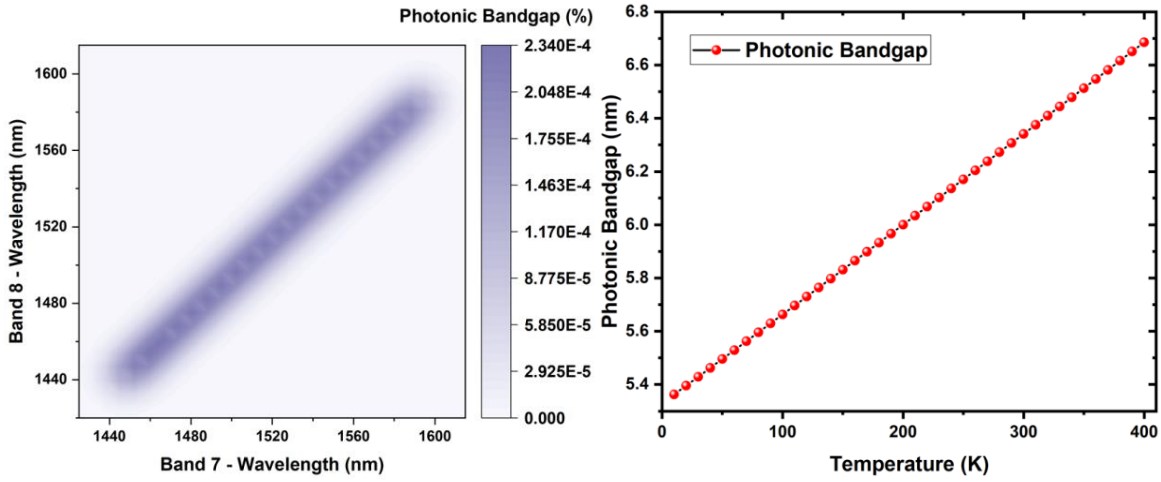

(a) (b)

Figure 5.5: (a) Distribution of the PBG at various eigen wavelengths (b) variation in PBG with temperature

Figure 5.6 (a) shows the applied temperatures and the corresponding eigen wavelengths. The changes are linear, with a sensitivity in the range of $375.16 \pm 0.791 \times 10^{-3}$ to $378.55 \pm 0.794 \times 10^{-3}$ pm/K. This sensitivity is higher than the sensitivity achieved by other optical sensors [13-14,16,18]. Figure 5.6 (b) shows a calibrated plot for the temperature sensing by the proposed PCW. By measuring the eigen wavelengths either at band 7 or at band 8, one can sense the temperature.

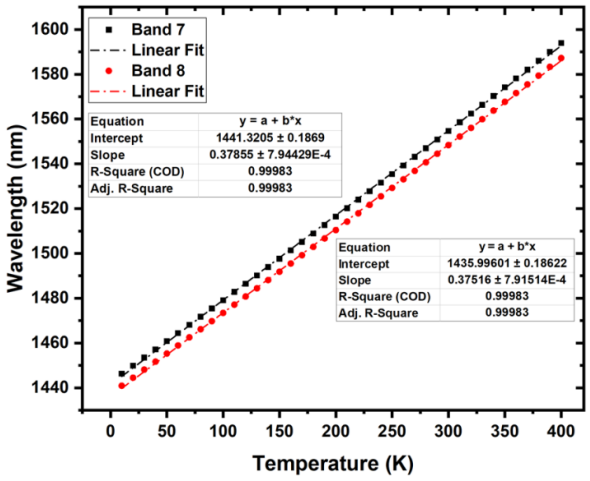

(a)

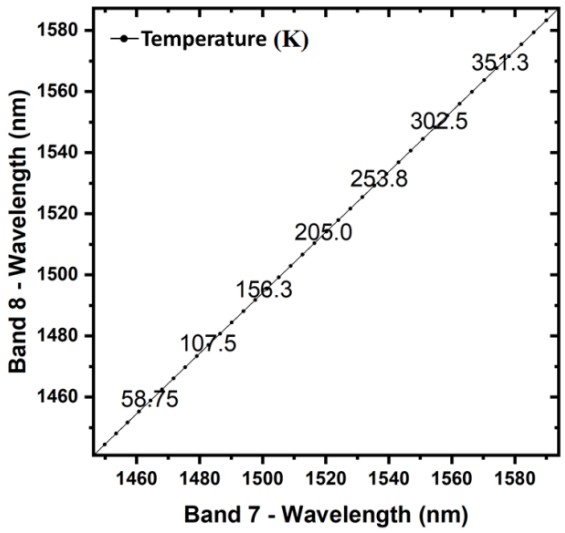

(b)

Figure 5.6: (a) Eigen wavelengths at band 7 and band 8 of the PCW with TM mode and (b) Calibration of the PCW with temperature.

5.4 Discussion on temperature sensing:

This PCW can be used for temperature sensing using a BBS and an OSA. In order to measure the temperature, the PCW can be placed inside a temperature-controlled furnace or a heat source or a heat sink. At room temperature, all the wavelengths from the BBS will be coupled to the PCW, and the eigen wavelengths will be detected at the OSA. As the temperature of the PCW changes, the RI of the slab material changes and this leads to the change in the eigen wavelength, as represented by figure 5.6 (a). These changes in the eigen wavelengths can be measured by the OSA. A re-calibration of the sensor system gives the advantage of the design for various temperature sensing applications involving the measurement of high and low temperatures.

Thermal expansion of GaAs is also included in the simulation process to find the effect of temperature on the geometry. For this purpose, the thermal expansion coefficient of

GaAs is considered and included in the simulation. It is found that the thermal expansion of GaAs does not affect the PBG as it is negligible in magnitude. However, for the other materials, thermal expansion may also affect the PBG with temperature. Therefore, a shift in the bandgap in the present case is purely due to the changes in the RI, which is emerging from the thermo-optic effect. Further, the cost of the sensor can be reduced, and a compact design is feasible by replacing the OSA using an LPG (as an edge filter) and a photo-detector as discussed by Mamidi et al. [6]. The schematic is shown in figure 5.7.

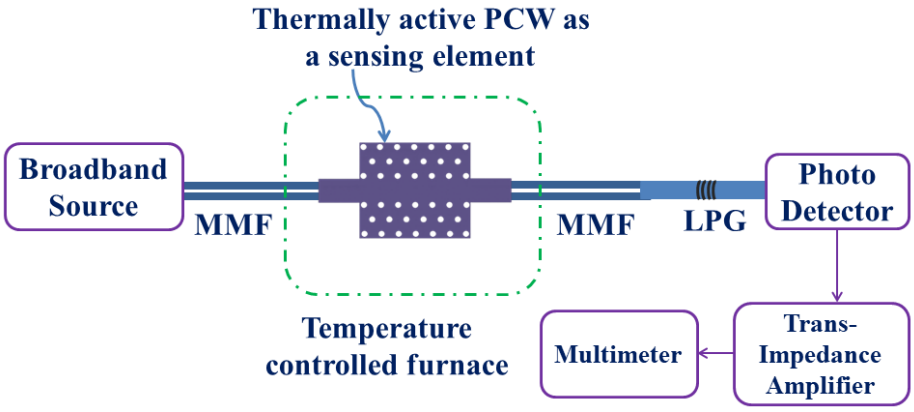

Figure 5.7: Schematic of the temperature sensor using LPG as an edge filter.

The present proposal is interesting because of the enhanced range with sufficient sensitivity. The sensor has better sensitivity compared to that of FBG based and other optical technique-based temperature sensors. Also, within the PC and PCW temperature sensors, the present sensor has a better working range. Table 5.1 compares between previously reported sensing methods and the present study.

Table 5.1: Comparison of various temperature sensors using PC and PCW with the present study

S. No.	Author	Method	Working range	Sensitivity
1	Larrion B., et. al. [13]	Quantum dot nanocoatings on PCF	233 K – 343 K	163.6 pm/K
2	Hai-wei F., et. al. [14]	Straight PC with thermo-optic effect	273 K – 373 K	6.6 pm/K
3	Lu Y., et. al. [16]	PCF filled with analyte and silver nanowires	283 K – 313 K	2,700 pm/K
4	Yang X. C., et. al. [18]	PCF filled with analyte and silver nanowires	298 K – 333 K	− 2,080 pm/K
5	**Present study**	**PCW with thermo-optic effect**	**10 K – 400 K**	**$375.16 \pm 0.791 \times 10^{-3}$ to $378.55 \pm 0.794 \times 10^{-3}$ pm/K**

5.5 Conclusions

To conclude, we proposed a temperature sensor based on an active PCW covering a broad range of temperatures. For this purpose, a waveguide is designed with hexagonal lattice in GaAs. The geometrical parameters are chosen to achieve the narrow PBG for sensing application. Using the thermo-optic effect, the RI of the slab material is calculated, and these calculated values are used in the simulations are performed in MPB. The eigen frequencies and the corresponding eigen wavelengths are calculated in the temperature range 10 K to 400 K. A complete and narrow PBG is observed between bands 7 and 8 TM modes. This narrow PBG can be used for sensing applications. The change in band edges with temperature is recorded, and sensitivity of $375.16 \pm 0.791 \times 10^{-3}$ to $378.55 \pm 0.794 \times 10^{-3}$ pm/K is observed. For the static temperature measurements, this sensor is a better alternative to the existing temperature sensors due to its operating range. However, the slow heating and cooling rates of the PCW material may restrict the usage of this structure for real-time and high-speed applications. By conquering this, the proposed structure may find application as a real-time temperature sensor with high accuracy.

References:

[1] E. Li, X. Wang, and C. Zhang, "Fiber-optic temperature sensor based on interference of selective higher-order modes," *Appl. Phys. Lett.*, vol. 89, no. 9, pp. 9–12, Aug. 2006, https://doi.org/10.1063/1.2344835

[2] L. Duan, H. Zhang, W. Shi, X. Yang, Y. Lu, and J. Yao, "High-resolution temperature sensor based on single-frequency ring fiber laser via optical heterodyne spectroscopy technology," *Sensors*, vol. 18, no. 10, pp. 1-9, Sep. 2018, https://doi.org/10.3390/s18103245

[3] B. Lee, "Review of the present status of optical fiber sensors," *Opt. Fiber Technol.*, vol. 9, no. 2, pp. 57–79, Apr. 2003, https://doi.org/10.1016/S1068-5200(02)00527-8

[4] L. Bilro, N. Alberto, J. L. Pinto, and R. Nogueira, "Optical sensors based on plastic fibers," *Sensors*, vol. 12, no. 9, pp. 12184–12207, Sep. 2012, https://doi.org/10.3390/s120912184

[5] B. Degamber, J. Tetlow, and G. F. Fernando, "Design and development of low-cost optical-fiber sensors for temperature metrology: Process monitoring of an epoxy resin system," *J. Appl. Polym. Sci.*, vol. 94, no. 1, pp. 83–95, Jul. 2004, https://doi.org/10.1002/app.20745

[6] V. R. Mamidi, S. Kamineni, L. N. S. P. Ravinuthala, M. Martha, S. S. Madhuvarasu, and V. R. Thumu, "High-temperature measurement using fiber Bragg grating sensor accompanied by a low-cost detection system," *J. Appl. Remote Sens.*, vol. 9, no. 1, Art. ID: 094098, pp. 1-10, May 2015, https://doi.org/10.1117/1.jrs.9.094098

[7] B. Hopf, B. Fischer, T. Bosselmann, A. W. Koch, and J. Roths, "Strain-independent temperature measurements with surface-glued polarization-maintaining fiber bragg grating sensor elements," *Sensors*, vol. 19, no. 144, pp. 1-14, Jan. 2019, https://doi.org/10.3390/s19010144

[8] G. Palumbo, D. Tosi, A. Iadicicco, and S. Campopiano, "Analysis and Design of Chirped Fiber Bragg Grating for Temperature Sensing for Possible Biomedical Applications," *IEEE Photonics J.*, vol. 10, no. 3, pp. 1-15, Jun. 2018, https://doi.org/10.1109/JPHOT.2018.2829623

[9] S. W. James and R. P. Tatam, "Optical fibre long-period grating sensors: Characteristics and application," *Meas. Sci. Technol.*, vol. 14, no. 5, pp. R49-R61, Mar. 2003, https://doi.org/10.1088/0957-0233/14/5/201

[10] M. G. Pulido-Navarro, P. J. Escamilla-Ambrosio, S. Marrujo-García, J. A. Álvarez-Chávez, and F. Martínez-Piñón, "Temperature sensing through long period fiber gratings mechanically induced on tapered optical fibers," *Appl. Opt.*, vol. 56, no. 19, pp. 5526-5531, Jul. 2017, https://doi.org/10.1364/ao.56.005526

[11] P. Lu et al., "Distributed optical fiber sensing: Review and perspective," *Appl. Phys. Rev.*, vol. 6, no. 4, Article No. 041302, pp. 1-35, Oct. 2019, https://doi.org/10.1063/1.5113955

[12] M. Amanzadeh, S. M. Aminossadati, M. S. Kizil, and A. D. Rakić, "Recent developments in fibre optic shape sensing," *Meas. J. Int. Meas. Confed.*, vol. 128, pp. 119–137, Nov. 2018, https://doi.org/10.1016/j.measurement.2018.06.034

[13] B. Larrió.n, M. Hernáez, F. J. Arregui, J. Goicoechea, J. Bravo, and I. R. Matías, "Photonic Crystal Fiber Temperature Sensor Based on Quantum Dot Nanocoatings," *J. Sensors*, vol. 2009, Article ID 932471, pp. 1-6, Jun. 2009, https://doi.org/10.1155/2009/932471

[14] H. wei Fu, H. Zhao, X. guang Qiao, Y. Li, D. zhuang Zhao, and Z. Yong, "Study on a novel photonic crystal temperature sensor," *Optoelectron. Lett.*, vol. 7, no. 6, pp. 419–422, Dec. 2011, https://doi.org/10.1007/s11801-011-0065-4

[15] W. Qian et al., "High-sensitivity temperature sensor based on an alcohol-filled photonic crystal fiber loop mirror," *Opt. Lett.*, vol. 36, no. 9, pp. 1548-1550, May 2011, https://doi.org/10.1364/ol.36.001548

[16] Y. Lu, M. T. Wang, C. J. Hao, Z. Q. Zhao, and J. Q. Yao, "Temperature Sensing Using Photonic Crystal Fiber Filled With Silver Nanowires and Liquid," *IEEE Photonics J.*, vol. 6, no. 3, Article No. 6801307, pp. 1-7, Jun. 2014, https://doi.org/10.1109/JPHOT.2014.2319086

[17] M. F. O. Hameed, M. Y. Azab, A. M. Heikal, S. M. El-Hefnawy, and S. S. A. Obayya, "Highly sensitive plasmonic photonic crystal temperature sensor filled with liquid crystal," *IEEE Photonics Technol. Lett.*, vol. 28, no. 1, pp. 59–62, Jan. 2016, https://doi.org/10.1109/LPT.2015.2480339

[18] X. C. Yang, Y. Lu, B. L. Liu, and J. Q. Yao, "Temperature Sensor Based on Photonic Crystal Fiber Filled with Liquid and Silver Nanowires," *IEEE Photonics J.*, vol. 8, no. 3, pp. 1-9, Jun. 2016, https://doi.org/10.1109/JPHOT.2016.2568101

[19] J. A. McCaulley, V. M. Donnelly, M. Vernon, and I. Taha, "Temperature dependence of the near-infrared refractive index of silicon, gallium arsenide, and indium phosphide," *Phys. Rev. B*, vol. 49, no. 11, pp. 7408–7417, Mar. 1994, https://doi.org/10.1103/PhysRevB.49.7408

[20] S. G. Johnson, and J. D. Joannopoulos, "Block-iterative frequency-domain methods for Maxwell's equations in a planewave basis," *Opt. Express*, vol. 8, no. 3, pp. 173 – 190, Jan. 2001, https://doi.org/10.1364/OE.8.000173

Chapter – 6
Reconfigurable Photonic Crystal Waveguides using Liquid Infiltration

In this chapter, we present readily reconfigurable photonic crystal waveguides using liquid infiltration. Group index and dispersive properties of the PCW can be varied by microfluidic infiltration. In a lattice shifted PCW, the air cylinders are filled with liquid of refractive index 1.3. Due to the shift in the innermost row and the microfluidic infiltration, the dispersive properties are altered, and the group index is maintained constant over a wider band. The structures are immediately reconfigurable by using liquids of different refractive indices. Electrically active liquids can also be introduced inside the lattice, and methods such as the electro-optic effect can be accompanied to enhance the features of the PCW. Reconfigurable optical devices can be realized from these studies.

6.1 Reconfigurable Photonic Crystal Waveguides:

Dispersion engineering is mainly performed by tailoring the geometry of the PC or PCW [1-3]. The tailoring of the PC or PCW is limited due to the fabrication restrictions. Also, once the waveguide is fabricated, it is difficult to change the dispersive features. In recent years, the research community has been looking forward to develop the reconfigurable and active PCW for various light controlling applications [4-5].

The reconfigurable PCW or active PCW are achieved by altering the dispersive features of the waveguide after the fabrication [5]. Methods such as electro-optic effect, thermo-optic effect and magneto-optic effect are used to modify the dispersion features of a PCW post-fabrication [6-8]. These methods produce a change in the refractive index of the material of the waveguide and transform the dispersion characteristics [9]. In some cases, mechanical pressure is also used to slightly vary the geometry and alter the features of the PCW [10]. Microfluidic infiltration and liquid crystals in the lattice of the waveguide are relatively new methods to achieve finer group indices and dispersion features [5, 11-12]. Also, it increases the degrees of freedom to design the reconfigurable PCW and modify the waveguide's characteristics.

Optofluidics is relatively a new branch of photonics, integrating microfluidics with photonics [9]. With air holes present in the PCW, the waveguide can be filled with liquids, and the effective engineering of the waveguide can be executed. This method actively tunes the waveguide and provides flexibility to approach various linear and nonlinear optical properties. By changing the refractive index of the liquid, the properties of the waveguide can be readily modified. Ebnali-Heidari et al. [13] demonstrated an optofluidic-based method that successfully achieved small dispersion slow light PCW. Using a standard waveguide and selective micro-fluids slow light was demonstrated in this method. Lu et al. [14] showed that by filling the air holes on one side of the waveguide, the dispersion features alter and result in a more significant delay bandwidth product (DBP). A W1 waveguide with liquids of refractive index in the range of 1.3 to 1.9 is used in this method.

The air holes in the first two rows adjacent to the waveguide are infiltrated with liquids of refractive index higher than air, and significant group indices were achieved by Casas-Bedoya et al. [12]. Group velocity in the range of $c/80$ was achieved in this method over a bandwidth of 3 nm. Similar work was performed by Khodamohammadi et al. [15], and the group index of the waveguide was controlled by the refractive index of the infiltrated liquid. The NDBP of the waveguide was maintained constant while the group index of the waveguide was increased and decreased.

Though various methods discuss the microfluidic infiltration in PCW, most of them are focused on either the filling ratio or the refractive index of the liquid. In our study, we used the microfluidic infiltration in a geometrically perturbed waveguide for enhancing the dispersion features and slow light characteristics. We present the lattice shifted GaAs based PCW in which the air holes are filled with liquid of refractive index 1.3. The dispersive curves, group index and the GVD of the waveguide are calculated to characterize the features of the lattice shifted PCW. The features of the liquid infiltrated PCW are compared with that of waveguide with air cylinders. The structures are reconfigurable and can be used for devices that require active tuning.

6.2 Geometrical design:

The proposed PCW is shown in figure 6.1 (a). Initially, hexagonal lattice-based PCW with air cylinders is studied. Air holes in GaAs substrate are used for this purpose. The waveguide with a width of $1.72a$ is formed by eliminating one row of air cylinders, where 'a' is the lattice constant. The air cylinders are taken with a radius of $0.25a$. Before studying the microfluidic infiltration in the waveguide, a shift in the range of $0.12a$ to $0.16a$ with step size

0.01*a* is introduced in the first innermost row (figure 6.1 (b)), and the dispersion features are studied. In these lattice shifted waveguides, a liquid of refractive index 1.3 is introduced (figure 6.1 (c)), and the characterizing parameters are calculated. The method can be extended by varying the refractive indices of the liquid or by introducing other geometrical perturbations to enhance the dispersive features.

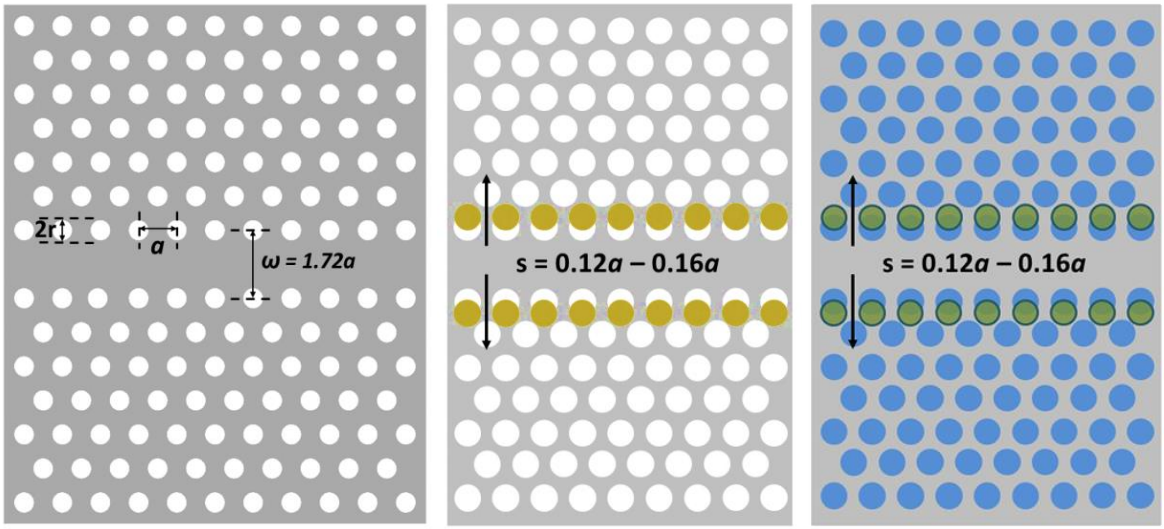

(a) (b) (c)

Figure 6.1: (a) Schematic of the initial waveguide. (b) lattice shifted waveguide with air cylinders (c) lattice shifted waveguide with liquid infiltration in the air cylinders.

6.3 Simulations and results:

The initial unperturbed PCW has a substrate band between band 14 and band 15. The first bandgap exists between bands 15 and 16. Figure 6.2 shows the band diagram of the unperturbed PCW at 1550 nm wavelength. The calculated PBG is 0.0062 *c/a* for this structure. To enhance the slow light features and dispersive properties of this PCW, a shift is introduced in the first innermost row of the waveguide. From our previous studies, we used a lattice shift of 0.12*a* – 0.16*a* for the effective enhancement of the dispersive features. For each perturbed structure, the group index and the GVD are calculated without and with microfluid in the lattice. At every step, it is observed that the filling of the lattice resulted in a shift in the flat band of the slow light and expanded the bandwidth. For the present structures, the lattice constant is taken as 465 nm for observing the eigen wavelengths in C and L bands with reconfiguration. For observing the eigen wavelengths in the other bands of the telecommunication spectrum, one can choose a different lattice constant.

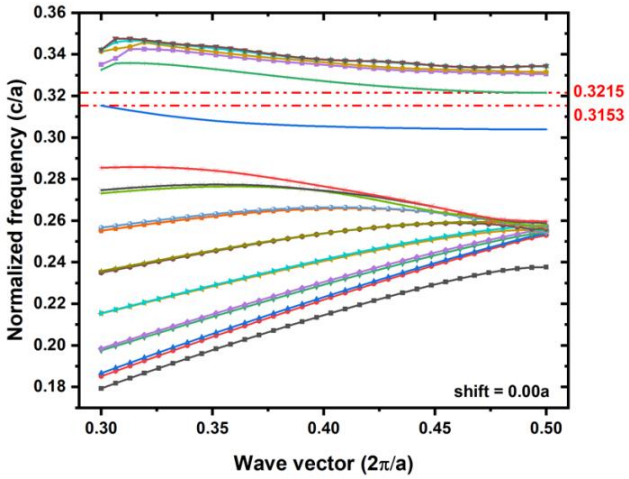

Figure 6.2: Band diagram of the unperturbed waveguide. The observed band gap is 0.0062 *c/a*.

As the PBG exists between band 15 and band 16, in our further studies, we focused on the position of these bands for evaluating the PCW's performance. The group index and the GVD are calculated at these bands to study the dispersive features and slow light properties of the waveguide. From the wavelength and group index plot, the DBP of the PCW is calculated.

Figure 6.3 (a-e) shows the dispersive curves of the PCW structure with different lattice shifts. In each graph, we have shown band 15 from the band diagram of the PCW infiltrated with air and liquid of refractive index 1.3. In each case, it is observed that the PCW infiltrated with liquid has improved the slope of the dispersive curve, which is evident in the presence of slow light. Differentiation of these dispersive curves is used to find the group index of the structure.

These graphs also confirm that the dispersive features of the waveguide can be controlled by infiltration of the lattice of a PCW with a liquid. Further, the active tuning and reconfiguration are achievable with these structures by changing the refractive index of the liquid used.

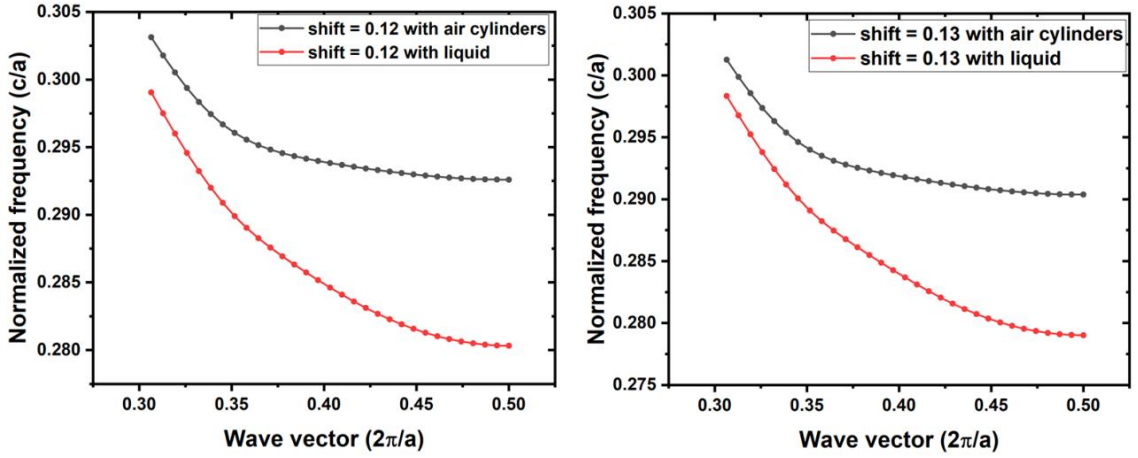

(a) (b)

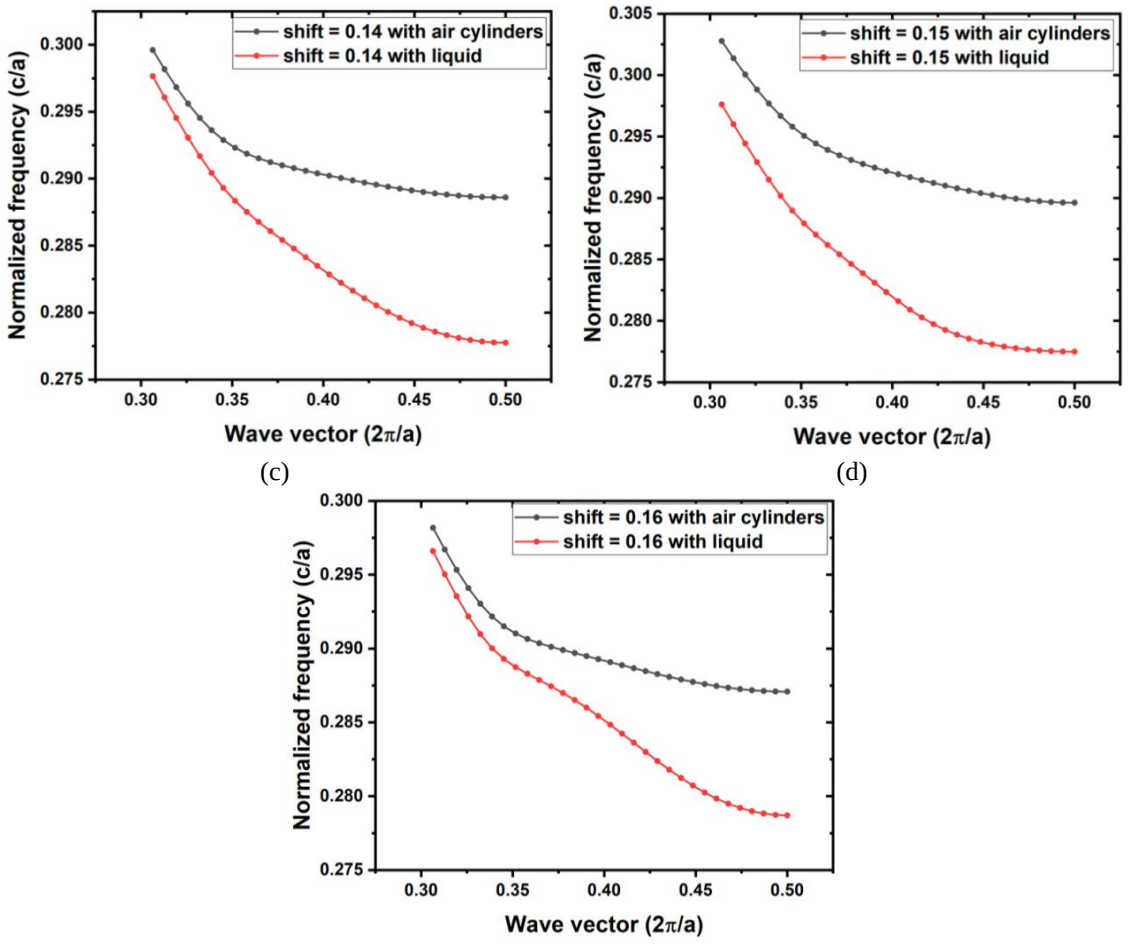

Figure 6.3: Dispersion curves (band 15) of the lattice shifted PCW with shift (a) 0.12*a* (b) 0.13*a* (c) 0.14*a* (d) 0.15*a* (e) 0.16*a*

Figure 6.4 (a-e) shows the calculated group index against the normalized frequency. All the lattice shifts except 0.12*a* and 0.13*a* resulted in a constant group index. The band over which the group index is maintained constant is referred to as flat band, or bandwidth and this flat band is increasing with an increase in lattice shift. However, the flat band further broadened by introducing the microfluid in the PCW lattice.

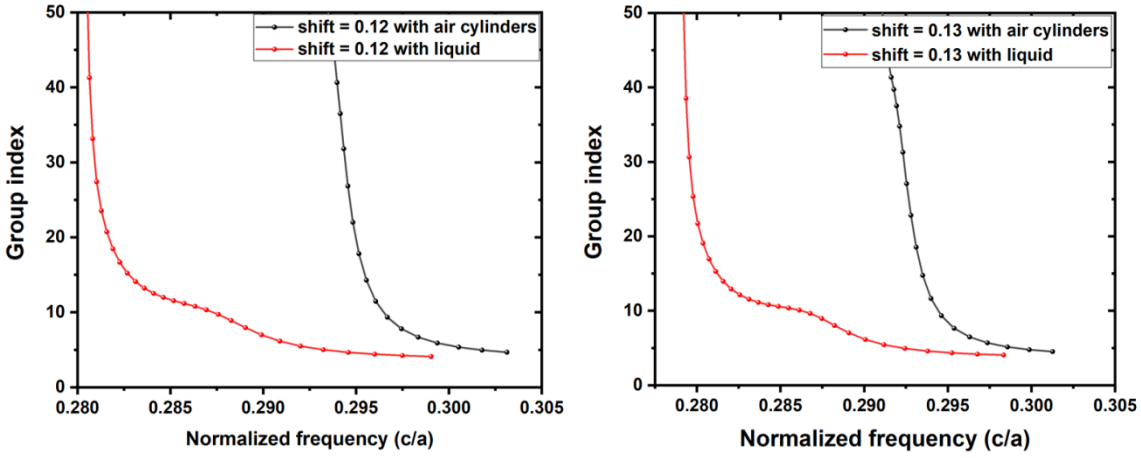

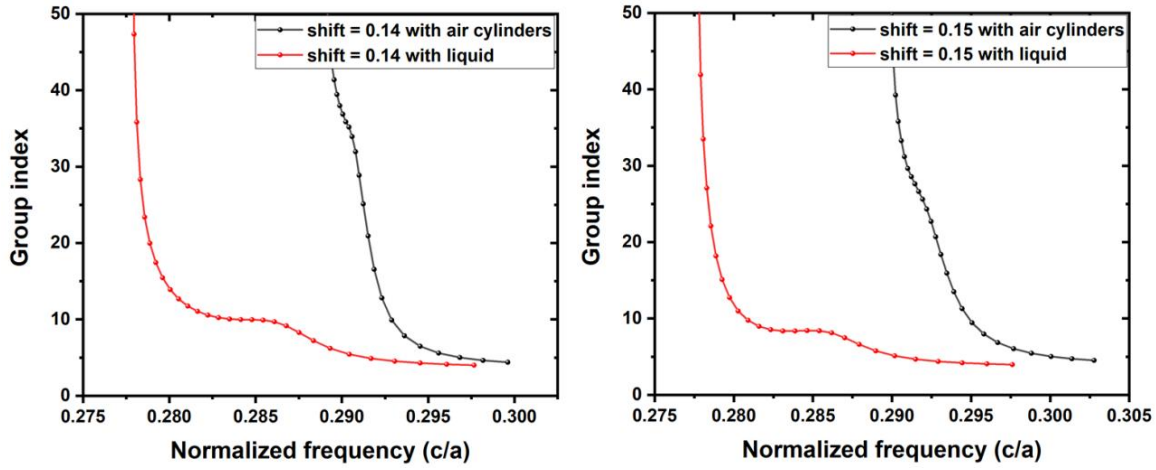

(c) (d)

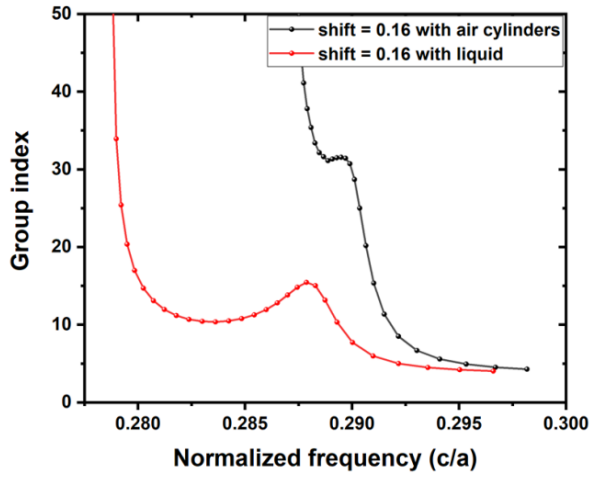

(e)

Figure 6.4: Calculated group index of the lattice shifted PCW against the normalized frequency with a shift of (a) 0.12*a* (b) 0.13*a* (c) 0.14*a* (d) 0.15*a* (e) 0.16*a*

Here both the flat band and the group index are directly controlled by the refractive index of the liquid used for infiltration. In the PCW with a lattice shift of 0.12*a* and 0.13*a*, liquid infiltration resulted in a flat band. For practical applications of the PCW, the lattice constant of the waveguide is taken as 465 nm.

Figure 6.5 (a-e) shows the calculated group index against the calculated wavelength. Table 6.1 shows the comparisons between designed PCWs. The calculated group indices and the observed bandwidths in each case are tabulated. DBP of the waveguides is calculated.

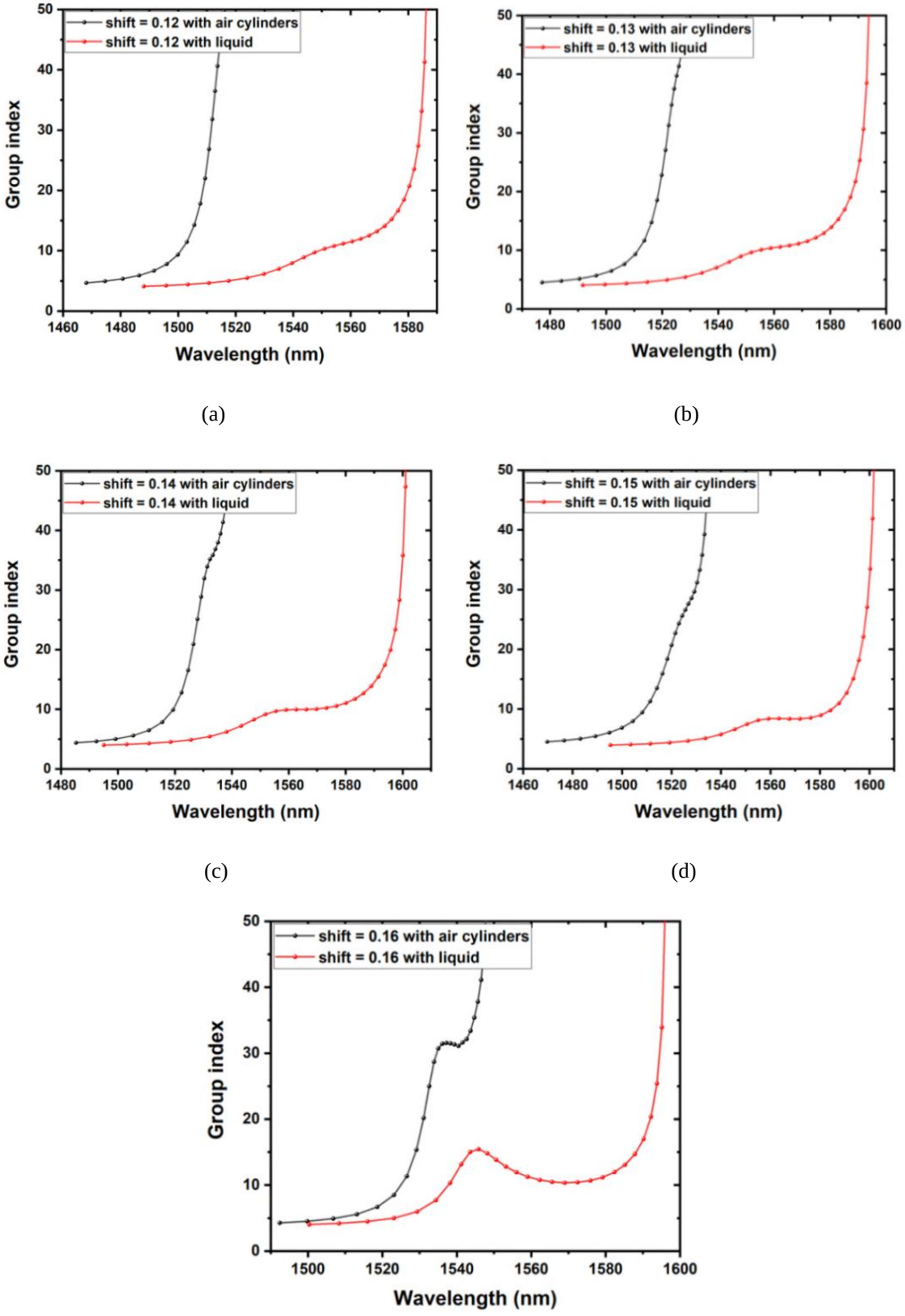

Figure 6.5: Calculated group index of the lattice shifted PCW with a shift of (a) 0.12*a* (b) 0.13*a* (c) 0.14*a* (d) 0.15*a* (e) 0.16*a*

Table 6.1: Group index, bandwidth and DBP of the designed PCWs

Shift (units of *a*)	**Filling**	**Group index (n_g)**	**Bandwidth (ω)** (nm)	**DBP** (n_g x ω)
0.12	Air	-	-	No flat band
0.12	Liquid	11.56	6.1	70.516
0.13	Air	-	-	No flat band
0.13	Liquid	10.46	10.11	105.75
0.14	Air	35.51	0.96	34.08
0.14	Liquid	9.73	14.41	140.20
0.15	Air	26.11	1.28	33.42
0.15	Liquid	8.44	25.36	214.04
0.16	Air	31.31	6.55	205.08
0.16	Liquid	11.01	26.34	290.01

Table 6.1 confirms the presence of the flat band with constant group index in the lattice shifted PCW and its improvement with the liquid infiltration in the lattice. The introduced lattice shift generated the flat bands, and liquid infiltration widened these flat bands. The constant group index is taken with $\pm 5\%$ variation. At the shift values 0.12*a* and 0.13*a*, the flat band is not observed. However, with the liquid infiltration in the waveguide with 0.12*a* and 0.13*a* lattice shift, the group index becomes constant over a bandwidth of 6.1 nm and 10.11 nm, respectively. The lattice shifted PCWs may have ameliorated performance with liquids of different refractive indices. This also results in slow light in different regimes with reasonable bandwidth.

The observed results also show a commutation within the group index and the bandwidth. This trade-off is most common in all the dispersion engineering approaches. Hence, depending on the requirement, the PCW must be selected. In addition to this, external electric and magnetic fields, variation in temperature and mechanical pressure may provide additional parameters for designing the reconfigurable PCWs.

To study the dispersive features of the designed PCW, the GVD of the waveguides is calculated. Figure 6.6 (a-e) shows the calculated GVD against the wavelength in each case. Compared to the air-filled lattice, liquid infiltrated lattice improved the GVD, and the curve became relatively flat. Also, the GVD curve of the liquid infiltrated lattice is closer to the zero-dispersion line. The presence of both positive and negative peaks in the curve may direct the possible applications on dispersion compensation.

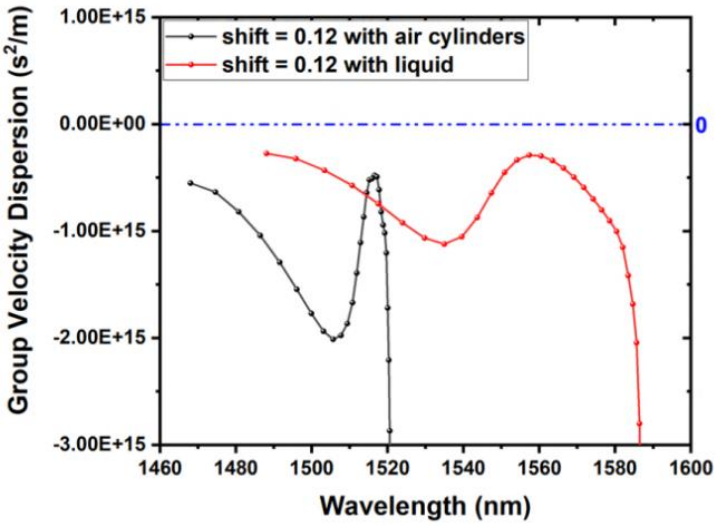
shift = 0.12 with air cylinders
shift = 0.12 with liquid
Group Velocity Dispersion (s²/m)
Wavelength (nm)
1.00E+15
0.00E+00
-1.00E+15
-2.00E+15
-3.00E+15
0
1460
1480
1500
1520
1540
1560
1580
1600

(a)

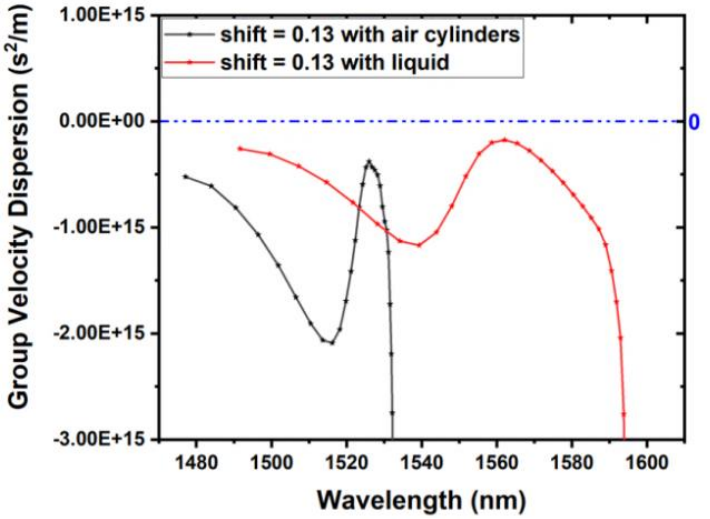
shift = 0.13 with air cylinders
shift = 0.13 with liquid
Group Velocity Dispersion (s²/m)
Wavelength (nm)
1.00E+15
0.00E+00
-1.00E+15
-2.00E+15
-3.00E+15
0
1480
1500
1520
1540
1560
1580
1600

(b)

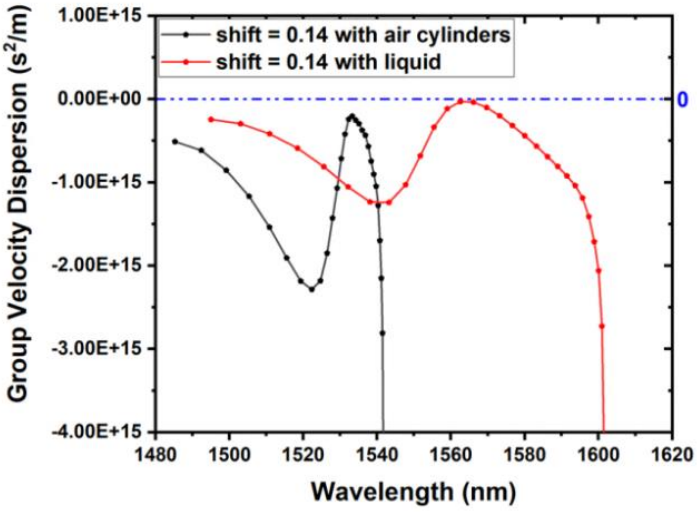
shift = 0.14 with air cylinders
shift = 0.14 with liquid
Group Velocity Dispersion (s²/m)
Wavelength (nm)
1.00E+15
0.00E+00
-1.00E+15
-2.00E+15
-3.00E+15
-4.00E+15
0
1480
1500
1520
1540
1560
1580
1600
1620

(c)

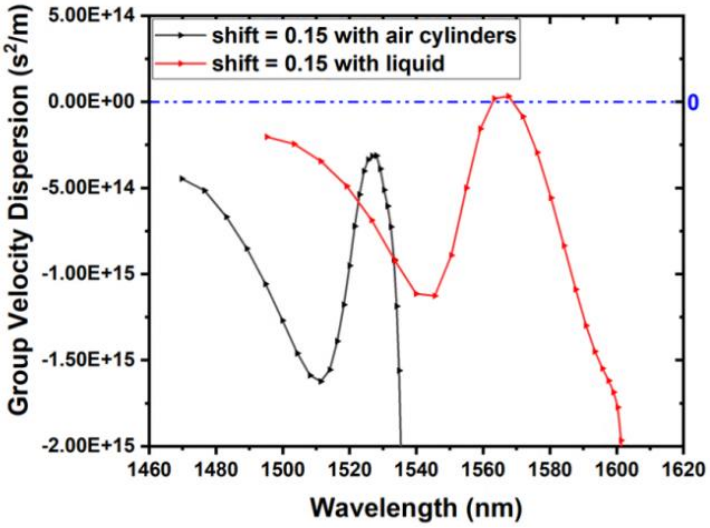

(d)

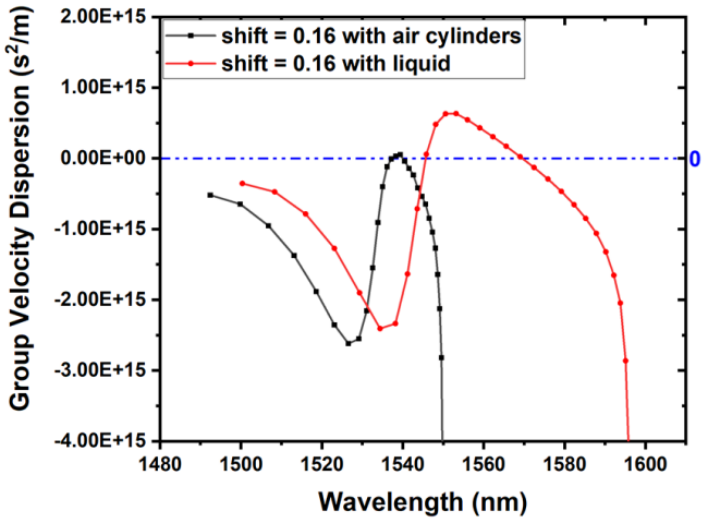

(e)

Figure 6.6: Group velocity dispersion of the PCW against the wavelength at lattice shift of (a) 0.12*a* (b) 0.13*a* (c) 0.14*a* (d) 0.15*a* (e) 0.16*a*

6.4 Discussion on reconfiguration using liquid infiltration:

The reconfigurable or active PCWs are relatively new in the dispersion engineering of the waveguides. Most of the previous designs are subjected to precise fabrication. Moreover, the fabrications at the nanometre level are challenging. Once the PCW is fabricated, its dispersive features are fixed. Any error in the fabrication results in no use of the PCW. Infiltration methods are easy to use and can achieve a wide range of applications. Also, various selective infiltration techniques are experimentally demonstrated [12-13], where the planar PCW properties are modified using liquid infiltration. Integrated microfluidic circuits, actuated micro-tip and micro-pipette, are used to realize this method. Water-based solutions

(refractive index around 1.35), silicone oil (refractive index 1.4) and Cargille fluids (refractive index 1.8) can be used for effective infiltration.

6.5 Comparisons:

The liquid infiltration method is easy to implement and provides a solution to achieve various dispersion characteristics after the fabrication. By selecting proper liquids, the infiltration technique can alter the slow light features. For instance, in our study, the PCW with a lattice shift of 0.15*a* with air cylinders has a DBP of 33.42, while the same PCW with liquid infiltration resulted in a DBP of 214.04 (table 6.1). Similarly, the liquid infiltration also generates slow light regimes and widens them with liquids of different refractive indices. In our observation, PCW with a lattice shift of 0.12*a* and 0.13*a* have no flat band regions. With liquid infiltration, a constant group index with the flat band is observed. In the designed structures, the GVD is also improved with liquid infiltration (figure 6.6).

Most of the previous dispersion engineering methods are realized by geometrical tailoring. This engineering results in the tuning of the PBG, which affects the slow light features. Electro-optic methods, thermo-optic methods, and liquid crystal infiltration provide active tuning of the PBG. Like these active tuning methods, liquid infiltration also provides practical solutions in dispersion engineering.

6.6 Conclusions

To conclude, liquid infiltration in the lattice shifted PCWs improves its characteristics. Initially, a GaAs based PCW is designed with air cylinders. The first innermost row of the waveguide is shifted to generate the slow light features. The shift is introduced in the range of 0.12*a* to 0.16*a*, and the slow light features are studied. In these lattice shifted PCWs, liquid of refractive index 1.3 is introduced, and the characterizing features are studied.

The lattice shift that we introduced in the liquid infiltration technique resulted in improved characteristics of the PCW. It is observed that the DBP of the infiltrated waveguides is larger than that of waveguides with air cylinders. On average, the DBP is improved by 4-6 times that of the base structure. The dispersion in the liquid infiltrated waveguides is under control. In addition to this, one can design the reconfigurable waveguides and can modify the dispersion features using liquids of different refractive indices. This method also reduces the constraints in designing the application-specific waveguides. The other geometrical perturbations, such as the radius of the hole, and lattice twist, may also affect the reconfiguration of the PCW.

References:

[1] Y. Hamachi, S. Kubo, and T. Baba, "Slow light with low dispersion and nonlinear enhancement in a lattice-shifted photonic crystal waveguide," *Opt. Lett.*, vol. 34, no. 7, pp. 1072 – 1074, Apr. 2009, https://doi.org/10.1364/OL.34.001072

[2] L. H. Frandsen, A. V. Lavrinenko, J. Fage-Pedersen, and P. I. Borel, "Photonic crystal waveguides with semi-slow light and tailored dispersion properties," *Opt. Express.*, vol. 14, no. 20, pp. 9444 – 9450, Oct. 2006, https://doi.org/10.1364/OE.14.009444

[3] J. Hou, D. Gao, H. Wu, R. Hao, and Z. Zhou, "Flat band slow light in symmetric line defect photonic crystal waveguides," *IEEE Photonics Technol. Lett.*, vol. 21, no. 20, pp. 1571–1573, Oct. 2009, https://doi.org/10.1109/LPT.2009.2030160

[4] M. Vieweg et al., "Ultrafast nonlinear optofluidics in selectively liquid-filled photonic crystal fibers," *Opt. Express*, vol. 18, no. 24, pp. 25232-25240, Nov. 2010, https://doi.org/10.1364/oe.18.025232.

[5] Y. Zhao, Y. N. Zhang, and Q. Wang, "Optimization of slow light in slotted photonic crystal waveguide with liquid infiltration," *J. Light. Technol.*, vol. 31, no. 14, pp. 2448–2454, Jun. 2013, https://doi.org/10.1109/JLT.2013.2267272.

[6] Y. Fu, J. Zhang, X. Hu, and Q. Gong, "Electro-optic tunable multi-channel filter in two-dimensional ferroelectric photonic crystals," *J. Opt.*, vol. 12, no. 7, pp. 1-7, Jul. 2010, https://doi.org/10.1088/2040-8978/12/7/075202

[7] X. Dai, Y. Xiang, S. Wen, and H. He, "Thermally tunable and omnidirectional terahertz photonic bandgap in the one-dimensional photonic crystals containing semiconductor InSb," *J. Appl. Phys.*, vol. 109, no. 053104, pp. 1-6, Mar. 2011, https://doi.org/10.1063/1.3549834

[8] P. Zu, C. Chiu Chan, T. Gong, Y. Jin, W. Chang Wong, and X. Dong, "Magneto-optical fiber sensor based on bandgap effect of photonic crystal fiber infiltrated with magnetic fluid," *Appl. Phys. Lett.*, vol. 101, no. 241118, pp. 1-4 Dec. 2012, https://doi.org/10.1063/1.4772017

[9] K. D. Xuan et al., "Influence of temperature on dispersion properties of photonic crystal fibers infiltrated with water," *Opt. Quantum Electron.*, vol. 49, no. 2, pp. 1–12, Feb. 2017, https://doi.org/10.1007/s11082-017-0929-3

[10] S. Kim and V. Gopalan, "Strain-tunable photonic band gap crystals," *Appl. Phys. Lett.*, vol. 78, no. 20, pp. 3015–3017, May 2001, https://doi.org/10.1063/1.1371786

[11] S. Kubo, Z. Z. Gu, K. Takahashi, A. Fujishima, H. Segawa, and O. Sato, "Tunable photonic band gap crystals based on a liquid crystal-infiltrated inverse opal structure," *J. Am. Chem. Soc.*, vol. 126, no. 26, pp. 8314–8319, Jun. 2004, https://doi.org/10.1021/ja0495056

[12] A. Casas-Bedoya, C. Husko, C. Monat, C. Grillet, N. Gutman, P. Domachuk, and B. J. Eggleton, "Slow-light dispersion engineering of photonic crystal waveguides using selective microfluidic infiltration," *Opt. Lett.*, vol. 37, no. 20 pp. 4215 – 4217, Oct. 2012, https://doi.org/10.1364/OL.37.004215

[13] M. Ebnali-Heidari, C. Grillet, C. Monat, and B. J. Eggleton, "Dispersion engineering of slow light photonic crystal waveguides using microfluidic infiltration," *Opt. Express.*, vol. 17, no. 3, pp. 1628 – 1635, Feb. 2009, https://doi.org/10.1364/OE.17.001628

[14] S. Lü, J. Zhao, and D. Zhang, "Flat band slow light in asymmetric photonic crystal waveguide based on microfluidic infiltration," *Appl. Opt.*, vol. 49, no. 20, pp. 3930–3934, Jul. 2010, https://doi.org/10.1364/AO.49.003930

[15] A. Khodamohammadi, H. Khoshsima, V. Fallahi, and M. Sahrai, "Wideband slab photonic crystal waveguides for slow light using differential optofluidic infiltration," *Appl. Opt.*, vol. 54, no. 5, pp. 1002-1009, Feb. 2015, https://doi.org/10.1364/ao.54.001002

Chapter – 7
Broadband Generation in Dispersion Engineered Photonic Crystal Waveguide

To generate spectral broadening, one needs a larger PBG in PCW. By tailoring the geometry, the PBG of a PCW is tailored. The zero-dispersion points are identified to launch the pump beam. With a PCW of 3 mm long and a pump at 1515 nm, we noticed a spectral broadening of 89 nm in the near infra-red region. The broadening of the spectrum is useful to generate multiple carrier waves in optical fibre communication and in fluorescence microscopy.

7.1 Broadband generation in PCW:

The arrangement of air holes and their geometrical tailoring in PC structures can generate various linear and nonlinear applications. The adjustable zero-dispersion wavelengths, tunability and effective refractive index, are additional features that are reliable in PC tuning for dispersion studies and nonlinear applications. Broadband generation (BBG), narrowband generation (NBG) and supercontinuum generation (SCG) are such phenomena in which a collection of nonlinear processes acts together on a pump beam and generate spectral broadening or narrow down.

PC and PCF structures have been explored by many researchers in the past two decades for observing spectral broadening. Ebnali-Heidari et al. [1] proposed a technique based on opto-fluidic infiltration to design a PCF to control chromatic dispersion for SCG. Based on this technique, a PCF of length more than 250 mm with selective infiltration can generate supercontinua. Low confinement loss and ultra-flattened near-zero dispersion were achieved in these studies. Willinger et al. [2] reported the first demonstration of narrowband parametric amplification in a PC structure. A dispersion engineered $Ga_{0.5}In_{0.5}P$ PCW was used to demonstrate the phenomenon. The PCW with two zero crossings was used with a pulsed pump. The conversion efficiency of – 10 dB was observed with a peak pump power of 650 mW.

The first optical memory in a hollow-core PCF was demonstrated by Sprague et al. [3]. Using far-detuned Raman interactions, a gigahertz bandwidth light was stored in the hyperfine coherence of caesium atoms at room temperature. A memory efficiency of 27+/-1% was demonstrated in this work. In another study, a PCF with a circular lattice and engineered diameter of air holes was used to observe SCG [4]. With zero dispersion, operational wavelengths in the visible and near-infrared regions were obtained in this study.

Coherent SCG was observed in a toluene filled PCF by Van et al. [5]. The hollow core of a PCW was filled with toluene, and the dispersion characteristics were studied. Two structures with lattice constant 2 µm each with filling fractions 0.3 and 0.35 and toluene core of diameters of 3.34 and 3.23 µm have flat dispersion in the near-infrared region. Coherent SCG in the range of 1.0 – 1.7 µm with the pulse energy conversion of 16% was observed in 4 cm long PCF with standard femtosecond lasers.

Saini et al. [6] proposed a new design with a triangular core PCF in As_2Se_3-based chalcogenide glasses. The structure has nearly zero dispersion. The numerical results show that ultra-broadband supercontinuum spanning 1.9 – 10 µm can be obtained using 6 mm long PCF pumped with 50 femtosecond laser pulses at 4.5 µm wavelength. Compared to previously described works, ultra-broadband supercontinuum spectra were achieved using a relatively lower peak power.

In these reported works, most of the SCG and BBG studies involved PCF with tailored features and liquid infiltration. However, we propose a dispersion engineered PCW that can be used for BBG in the near infra-red region. We noticed a spectral broadening of the order of 75 nm and above with pumps placed at 1492, 1515, and 1534 nm wavelengths. For achieving BBG in PCW, initially, we tailored a PCW with hexagonal lattice. Three rows of air cylinders adjacent to the line defect are shifted to maximize the PBG. The group index and the GVD are calculated to identify the flat band region and zero-dispersion points, respectively. The pump is fixed near the zero-dispersion regions, and the spectral broadening is measured. MATLAB code by J. M. Dudley [7] with appropriate changes is used to analyse spectral broadening and power quantities. Also, we changed the length of the PCW and studied the variation in spectral broadening. With a waveguide of length 3 mm, and pump at wavelength 1515 nm, we noticed a BBG of about 89 nm, which is the highest broadening in our studies.

7.2 Tailoring the geometry:

To study the BBG in PCW, initially, the PBG is maximized. A line defect is created in a hexagonal lattice-based PC structure by eliminating one row of air cylinders, and this made a waveguide with a width of 1.72*a*. The geometry is tailored by introducing a lattice shift. Three rows of air cylinders adjacent to the line defect are moved away to increase the PBG. In the initial study, the shift is introduced in the range of 0.19*a* to 0.21*a* in the first, second and third innermost rows with a step size of 0.01*a*. The radius of air cylinders is taken as 0.25*a*. To realize the PCW in the near infra-red region, the lattice constant is taken as 465 nm. With a shift of value 0.21*a*, introduced in the three innermost rows, a PBG of 98.83 nm is estimated. Figure 7.1 shows the schematic of the PCW structure with a shift in three rows.

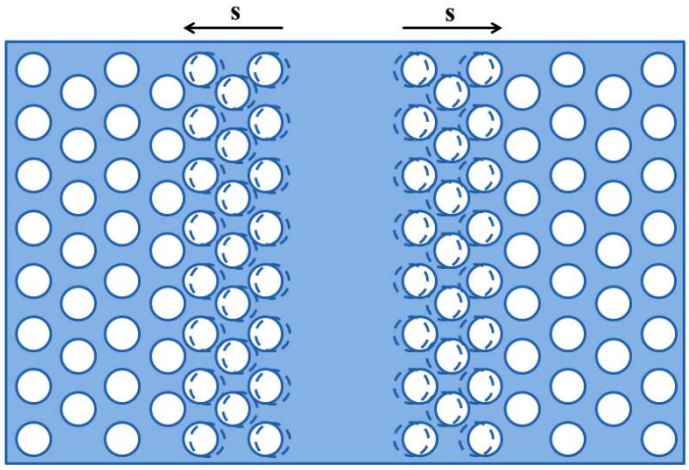

Figure 7.1: 2-dimensional view of the line-defect PCW with shift in three innermost rows

7.3 Spectral broadening in PCW:

To maximize the PBG, the shift is introduced in the three innermost rows of the line-defect PCW. Initially, at lower shift values and shifts in the first and second rows, the PBG is relatively small. However, with a shift of magnitude 0.21*a* in three innermost rows, considerable PBG is observed to study BBG. The shift can be increased further at the cost of a constant group index. Hence, as a trade-off between PBG and group index, the shift value is selected as 0.21*a*. Figure 7.2 shows bands 16 and 17 of geometry tailored PCW with a PBG of 0.02182 *c/a*. Using the lattice parameter, the PBG is found to be 98.83 nm. This tailored PCW is used further to study BBG.

The group index of the waveguide is calculated to find the flat band region, which is helpful to explore nonlinear applications. With a variation of 5% in the group index, the flat band is measured to be 36 nm. Figure 7.3 shows the variation of group index with wavelength. This flat band region is essential to study nonlinear applications such as slow light.

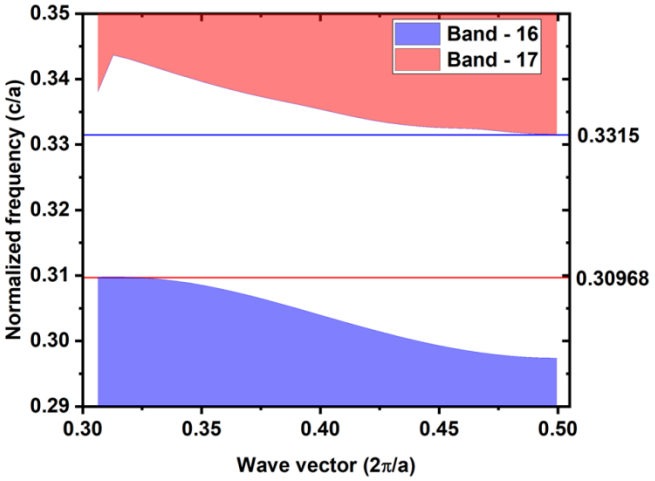

Figure 7.2: Band 16, 17 and PBG of tailored PCW. The shift is introduced in three innermost rows to maximize the PBG.

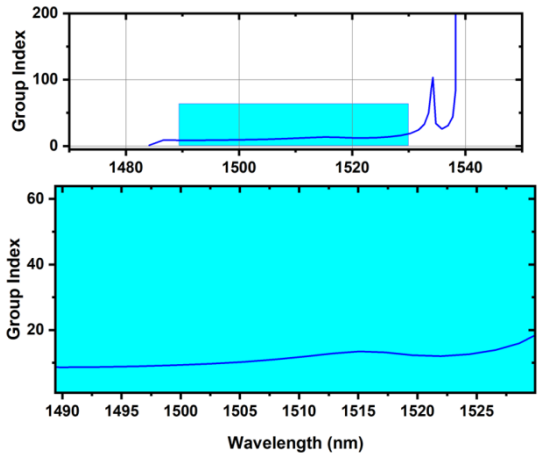

Figure 7.3: Calculated group index of the structure with wavelength

To study BBG in the present structure, the GVD is calculated at the flat band region. Figure 7.4 shows the variation in GVD with wavelength. Three zero-dispersion points are identified in the GVD plot, at which the pump beam is used to study the spectral broadening.

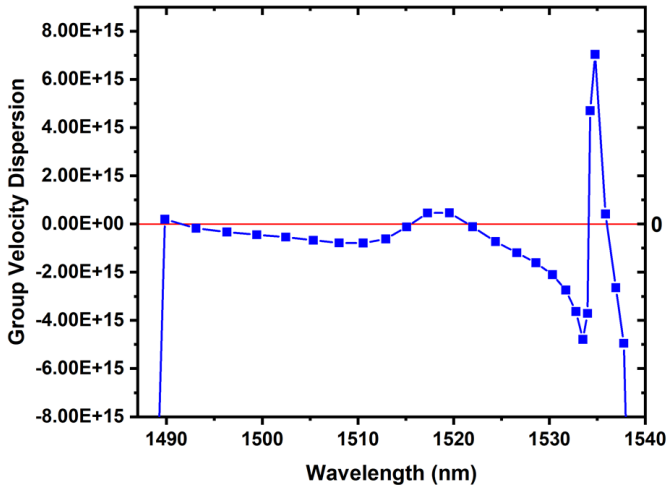

Figure 7.4: Calculated GVD of the structure with wavelength

To confirm the low dispersion in the structure, second and fourth-order dispersion values (β_2 and β_4) are calculated. Figure 7.5 shows the calculated β_2 and β_4 plots against the wavelength. By these plots, it is again confirmed that at zero-dispersion points identified by the GVD plot (figure 7.4), the β_2 and β_4 curves also cross each other and produce zero-dispersion. Apart from the zero-dispersion points, at the other wavelengths also, the β_2 and β_4 are within the acceptable range to observe low dispersion in the PCW. Hence, in this PCW, we can study the BBG by launching a pump beam near the zero-crossing points.

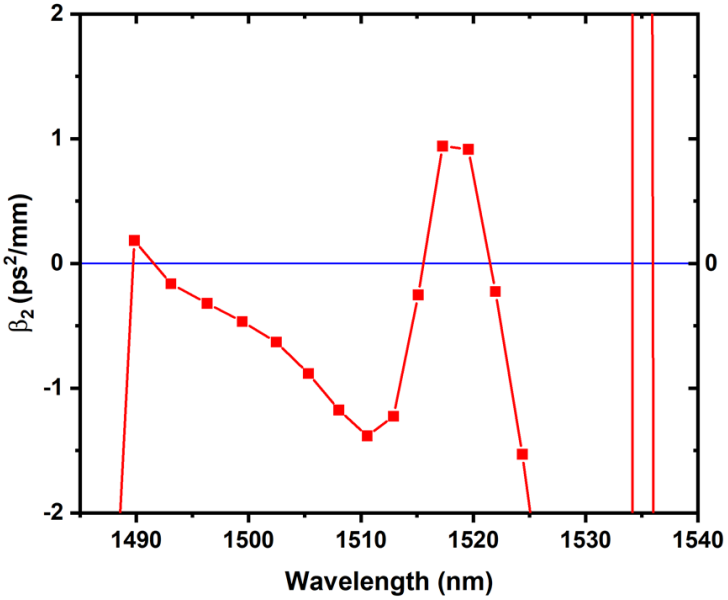

(a)

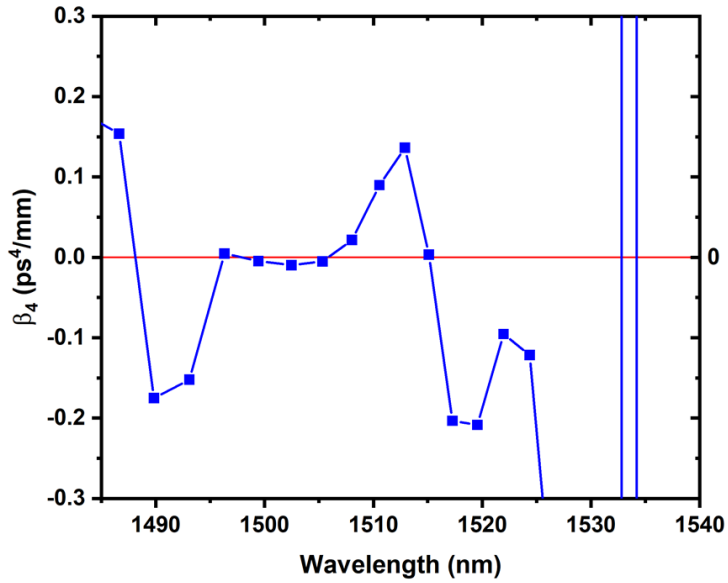

(b)

Figure 7.5: (a) Second order dispersion (b) fourth order dispersion against the wavelength in the tailored PCW

For studying the BBG in the geometry tailored PCW, MATLAB code by J. M. Dudley [7-8] is used. Since it is developed for studying spectral broadening in optical fibres,

we made appropriate changes to the code to study PCW. The pump beam is launched near the zero-dispersion points, which are 1492 nm, 1515 nm and 1534 nm. Figure 7.6 (a-c) shows the spectral broadening of the output power in the tailored PCW. A relatively smaller spectral broadening is observed when the pump is used at 1492 nm and 1534 nm. By launching the pump at 1515 nm, we noticed a broadening of 81.85 nm with considerable output power.

To study the effect of the length of the waveguide on BBG, the study is carried out by varying the waveguide's length. The BBG is studied in 1 mm, 2 mm and 3 mm long waveguides. Figure 7.7 shows the spectral broadening in tailored PCW with a pump beam located at 1515 nm and different lengths. In our observation, we noticed the spectral broadening of 89.08 nm in 3 mm long PCW with an optical pump located at 1515 nm. This is the maximum broadening with considerable output power we achieved by tailoring the PCW.

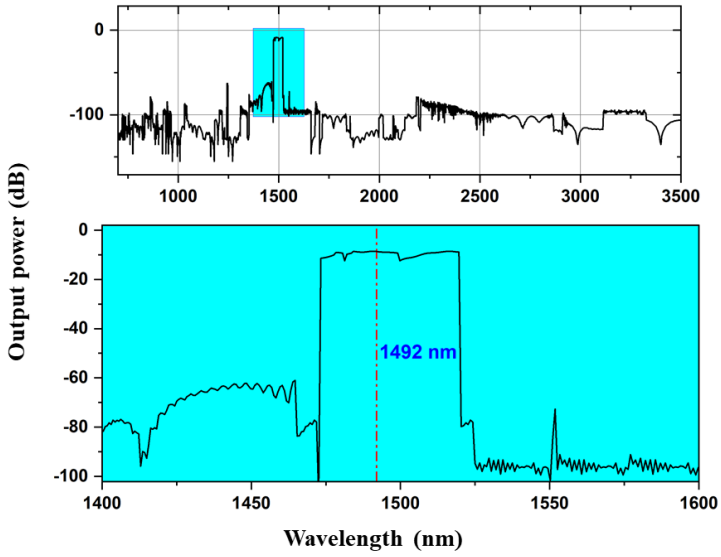

(a)

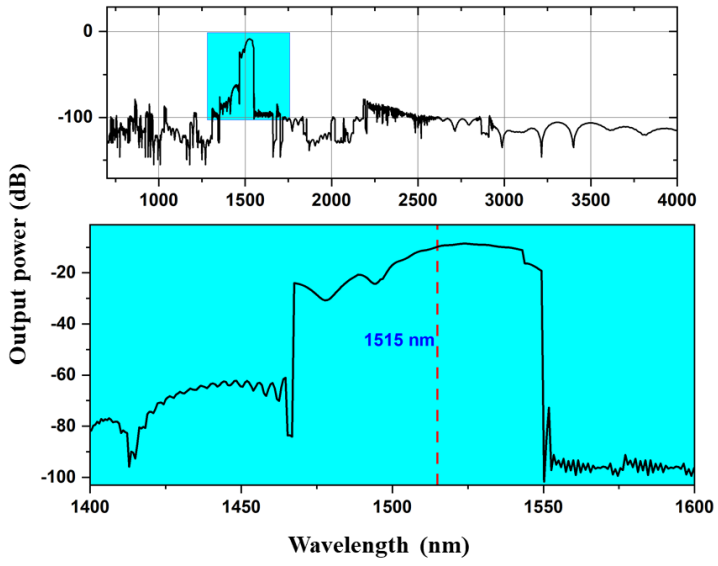

(b)

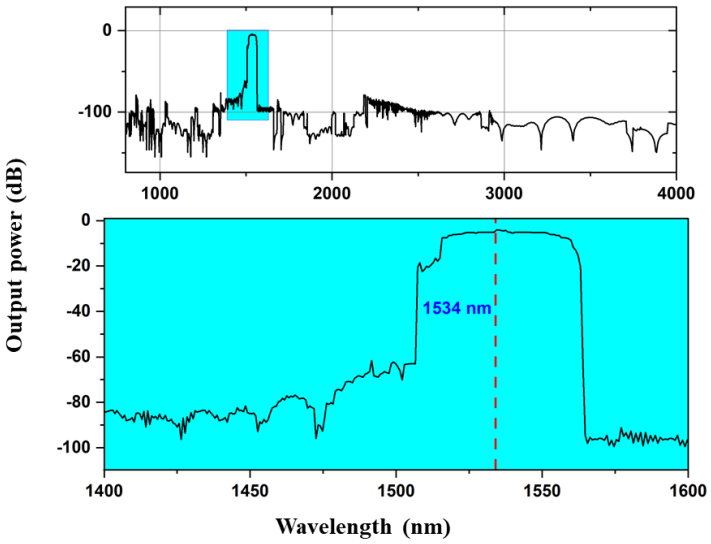

(c)

Figure 7.6: Spectral broadening in tailored PCW with pump beam located at (a) 1492 nm (b) 1515 nm and (c) 1534 nm.

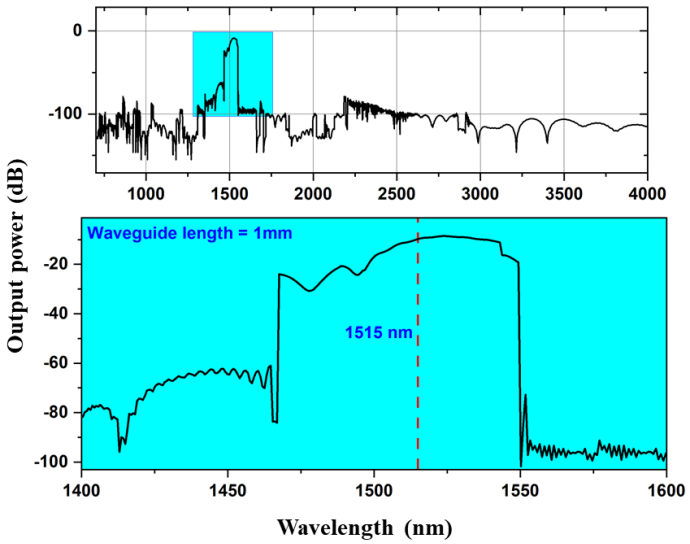

(a)

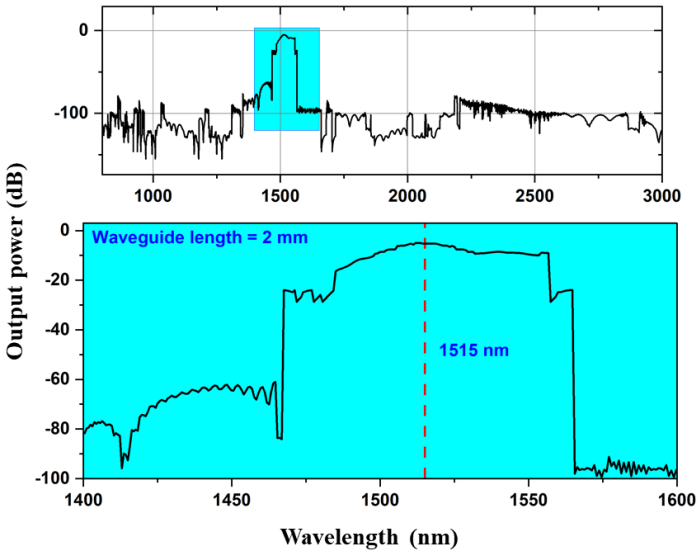

(b)

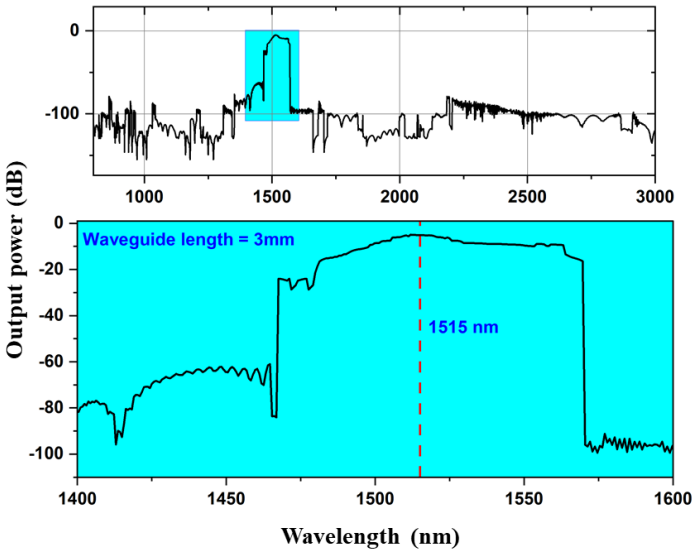

(c)

Figure 7.7: Spectral broadening in PCW with pump of wavelength 1515 nm and waveguide of length (a) 1 mm (b) 2 mm and (c) 3 mm.

7.4 Discussion on broadband generation in photonic crystal waveguide:

The spectral broadening in optical fibres and engineered PCF is most common. Many researchers reported such broadening, including SCG, in different regions of the electromagnetic spectrum. The PCW structures are popular due to their adaptability in tuning the features. In the conventional processes, one can use long fibres to observe SCG. In waveguides, such long structures are not feasible. Hence, one needs to produce high nonlinearity in limited dimensions. By tailoring the geometry, we attempted to study the spectral broadening in PCW. Using the geometrical tuning in PCW, initially, the PBG is maximized to accommodate the broadened spectra. The zero-dispersion points are identified to launch the pump beam. The length of the waveguide is varied to enhance the effect of spectral broadening. With tailored geometry and pump beam at 1515 nm, we noticed nearly 89 nm long spectral broadening in PCW, which is the first of its kind.

7.5 Conclusions

To study the spectral broadening in PCW, a hexagonal lattice-based waveguide is geometrically tailored. The innermost rows are shifted to maximize the PBG. At the zero-dispersion points, the pump is used, and a spectral broadening is observed in the PCW. With a waveguide of length 3 mm and pump at 1515 nm, 89.03 nm long spectral broadening is observed with considerable output power. The study can be further extended by tailoring the geometry in various possible directions. The study can find applications in generating multiple carrier waves in optical fibre communication systems, fluorescence microscopy and imaging techniques.

References:

[1] M. Ebnali-Heidari, H. Saghaei, F. Koohi-Kamali, M. Naser Moghadasi and M. K. Moravvej-Farshi, "Proposal for Supercontinuum Generation by Optofluidic Infiltrated Photonic Crystal Fibers," *IEEE J. Sel. Top. Quantum Electron.*, vol. 20, no. 5, pp. 582-589, Sept.-Oct. 2014, https://doi.org/10.1109/JSTQE.2014.2307313

[2] A. Willinger, S. Roy, M. Santagiustina, S. Combrié, A. De Rossi, and G. Eisenstein, "Narrowband optical parametric amplification measurements in $Ga_{0.5}In_{0.5}P$ photonic crystal waveguides," *Opt. Express*, vol. 23, no. 14, pp. 17751-17757, Jun. 2015, https://doi.org/10.1364/oe.23.017751

[3] M. R. Sprague et al., "Broadband single-photon-level memory in a hollow-core photonic crystal fibre," *Nat. Photonics*, vol. 8, no. 4, pp. 287–291, Mar. 2014, https://doi.org/10.1038/nphoton.2014.45

[4] H. Saghaei and A. Ghanbari, "White light generation using photonic crystal fiber with sub-micron circular lattice," *J. Electr. Eng.*, vol. 68, no. 4, pp. 282–289, Aug. 2017, https://doi.org/10.1515/jee-2017-0040

[5] L. C. Van, A. Anuszkiewicz, and A. Ramaniuk, "Supercontinuum generation in photonic crystal fibres with core filled with toluene." *J. Opt.*, vol. 19, no. 125604, pp. 1-9, Nov. 2017, https://doi.org/10.1088/2040-8986/aa96bc.

[6] T. S. Saini, A. Kumar, and R. Kumar Sinha, "Broadband mid-IR supercontinuum generation in As2Se3 based chalcogenide photonic crystal fiber: A new design and analysis," *Opt. Commun.*, vol. 347, pp. 13–19, Jul. 2015, https://doi.org/10.1016/j.optcom.2015.02.049

[7] J. M. Dudley, G. Genty, and S. Coen, "Supercontinuum generation in photonic crystal fiber," *Rev. Mod. Phys.*, vol. 78, no. 4, pp. 1135–1184, Oct. 2006, https://doi.org/10.1103/RevModPhys.78.1135

[8] Supercontinuum Generation in Optical Fibers, MATLAB source code: https://github.com/jtravs/SCGBookCode

Chapter – 8
Simulating Photonic Crystal Waveguides using Machine Learning

Artificial neural networks in machine learning are popular in solving complex data problems. This chapter proposes a neural network for predicting the dispersion and group indices of dispersion engineered photonic crystal waveguide designed for slow light applications. The model is trained by the data sets generated from MPB programming. A supervised feed-forward multilayer perceptron neural network is used for predicting the data. Three hidden layers are used with 500 nodes in each layer. One hundred epochs are used to achieve the lowest mean squared error. For generating the training data sets, waveguide structures with lattice shifts in the range of 0.00a to 0.25a are used. After the training, the model can predict the dispersion and group indices values within the trained data range. The model is effective in reducing the computational time.

8.1 Introduction:

Designing the dispersion engineered PCs and PCWs involve simultaneous optimization of various geometrical parameters [1-5]. Such modelling requires larger computational efficiency and time. For instance, to design dispersion engineered slow light PC structures, one requires optimizing different geometrical parameters such as dimensions of the slab, radius of the air holes, lattice constant, and waveguide width at the same time [6-11]. This process also generates large data which needs to be analyzed for characterizing the PC structures.

Conventional approaches of numerical and analytical methods are time-consuming. ML and DL are the advanced methods to study a large amount of data and is envisioned to play a decisive role in addressing many applications, ranging from light modulation to high power fibre amplifiers to nonlinear optical signal processing to sensing applications [12-14]. By training a machine with the data patterns, the machine can predict the physical parameters of a PCW with less computational time. The designing process can be accelerated, and better dispersion engineered structures can be framed within a short period of time.

ANN is an algorithm used in ML for analyzing and solving complex processes [15]. The ANN is like a biological neural network connecting artificial neurons. Each neuron in the

network is interconnected with the nodes from the preceding layer and connected with the neurons in the next layer, like the synapses in the biological brain. The neurons are aggregated or clustered as layers and each layer can perform a different operation on the data.

Dispersion relations of a PC can be computed using ANN modelling. Ferreira et al. [16] optimized 2-dimensional and 3-dimensional structures using an MLP and predicted the dispersion relations and PBG. These ANN models could provide accurate dispersion relation curves in a very short time. Asano and Noda [17] presented an approach to optimize the Q factors of a two-dimensional PC nano-cavity based on DL. For training the model, a data set generated from 1000 nano-cavities was used. A four-layer ANN consisting of a convolutional layer was trained to identify the relationship between the displacement of the air holes and the Q-factors. After the training, the ANN model could estimate the Q-factor of the PC cavity with an error of 13% in standard deviation.

Mescia et al. [18] have proposed another method based on ANNs to perform refinement and design of erbium-doped PCF amplifiers. Using ANN, the nonlinear functional link among the physical and geometrical characteristics of the fibre amplifier was captured by a neural network and is exploited. Malheiros-Silveira and Hernández-Figueroa [19] presented the prediction of dispersion relations and PBG in a 2-dimensional PC using MLP. The design and spectral response of an optical filter can also be predicted using ML based mathematical model [20]. This method considerably reduced the simulation time and efforts. Recently, ML techniques were used to calculate numerous optical properties of the PCF [21]. These ML algorithms based on ANNs made accurate predictions of the optical properties in a silica solid-core PCF.

ANNs based on ML can interpolate well within the trained dataset. However, their ability to extrapolate is highly limited by several fundamental issues. Wu et al. [22] introduced an operator parameter space to improve the network's capability outside the trained data range. Physical entities encoded with Maxwell's equations are used for this process. PCs were studied using this model, which was trained with operator parameter. Improved results were observed both within and beyond the trained space. ML assisted PC design and analysis offers a great potential for transforming the field of quantum optics [23]. While the initial design and analysis results are encouraging, the fundamental limits of ML in artificial intelligence and the analysis techniques in general are yet to be explored.

We propose an ANN model composed of three hidden layers, each with 500 nodes and the input and output layers, to simulate the parameters of PCWs. The data sets are generated from conventional MPB programming and are used to train the proposed model.

The trained model predicts the dispersion relations and group index of a lattice shifted PCW. The predicted data is compared with the standard data generated from the MPB program and found to be close enough.

8.2 Modelling the Artificial Neural Network:

The ANN chosen here is the most popular and commonly used supervised feed-forward MLP architecture. Generally, the model consists of an input layer, a set of hidden layers, and an output layer. Figure 8.1 illustrates the schematic of the proposed ANN model to study the lattice shifted PCW structures.

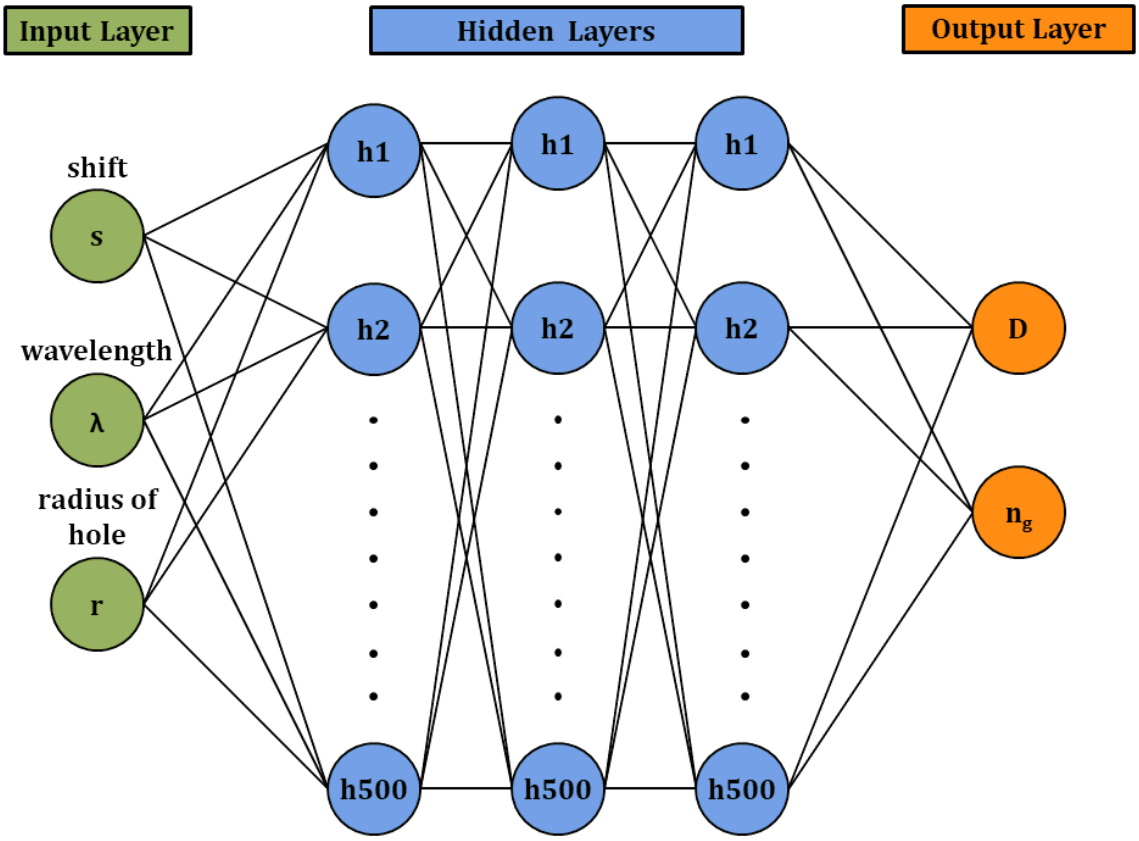

Figure 8.1: Schematic of the artificial neural network

In the present ANN model, 26,000 data sets are used, out of which 90% of the data points are used for training the model, and 10% are used for testing. The data points consist of three input parameters: shift, wavelength, and radius of hole and two output parameters: dispersion and group index. The proposed model consists of three hidden layers, with 500 nodes in each layer. Nodes generally hold one or more weighted input connections and are organized into layers to form a neural network. In the initial study, it is observed that a fair and stable mean squared error (MSE) can be achieved using 500 nodes in each hidden layer.

Further, it is also observed that the increase in the number of layers or the number of nodes creates an additional computational load which must be avoided to reduce the computational time.

The number of epochs (iterations) plays an important role in achieving a well-trained ANN model. The cardinal number of epochs that generates the lowest MSE is advantageous for this reason. One hundred epochs have been considered for our proposed model, which has been optimized to achieve the lowest MSE. The MSE loss in the proposed model with the number of epochs is shown in figure 8.2.

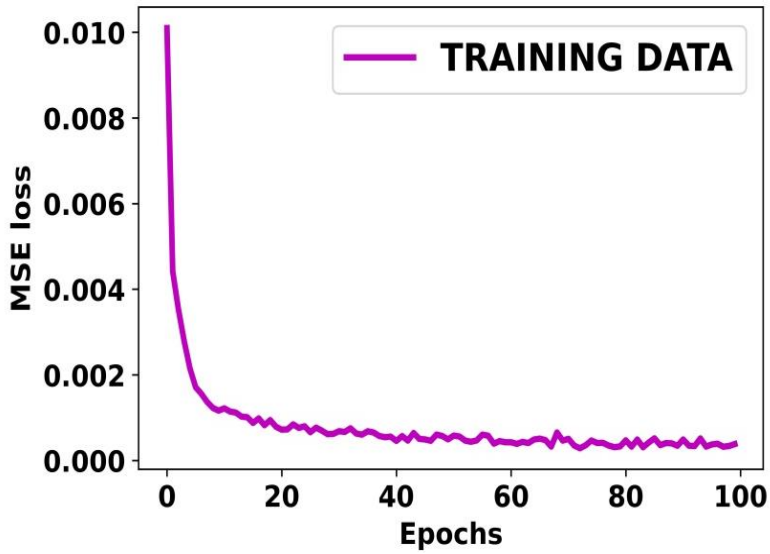

Figure 8.2: MSE loss against the number of epochs for training

8.3 Geometrical Design of the Waveguide:

Figure 8.3 illustrates the schematic design of the proposed waveguide is used for the ANN-based study. A hexagonal air cylinder pattern in a 180 nm thick GaAs slab forms the waveguide. The lattice constant (a) of the waveguide is taken as 465 nm with air cylinders of radius 0.25a. One row of air cylinders is eliminated to form the line-defect waveguide. The air cylinders in the first innermost row are shifted in the range of 0.00a to 0.25a to enhance the waveguide features.

To investigate the properties of the PCW, in the commencement of the work, the dispersion relations and group indices are calculated. The simulations are performed in MPB software. Shift with a step size of 0.01a is introduced in the innermost row and then the lattice shifted structures are simulated. The data sets generated in this process are used for training the ANN model.

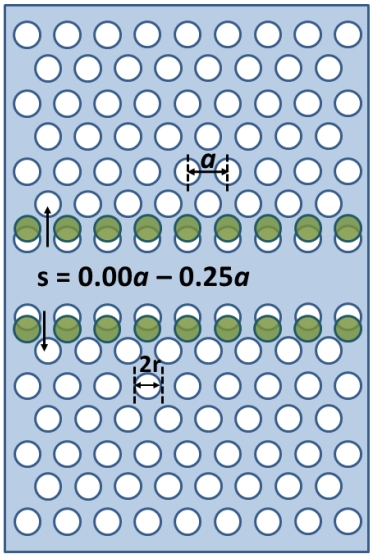

Figure 8.3: Schematic of the 2-dimensional PCW structure and illustration of shift in the lattice

8.4 Results and Discussion:

The initial simulations show that the first PBG exists between bands 15 and 16. For an unperturbed structure, it is found to be 28.5062 nm. As the data generated in this step is used for training the ANN model, the dispersion and group indices values are calculated at 1,000 wave vector points resulting 1,000 normalized frequency values. A shift in the range of 0.00*a* to 0.25*a* with a step size of 0.01*a* is used to develop lattice shifted waveguide structures.

8.4.1 Numerical results based on MPB:

By introducing the geometrical perturbations in the waveguide structure, a relatively constant group index can be achieved over a substantial bandwidth [9, 24]. The introduced shift in the waveguide directly controls the dispersive curves and generates constant flat bands. These flat band structures have potential linear and nonlinear applications [25-26]. However, the computational time is contingent to the geometrical parameters of the structure and the computational efficiency. Using the conventional computational methods, the computational time ranges from 20-26 hours or even more as the structure becomes more complex. With a step size of 0.01*a*, the shift (s) in the range of 0.00*a* to 0.25*a* is introduced in the lattice and simulated for the eigen frequencies. We used the MPB software on Ubuntu 20.04 LTS platform in an i7 (9^{th} generation) processor with 12 GB RAM. In the present case, the program with 35 wave vector points is executed in 6-8 hours range, while the same program with 1,000 wave vector points was executed in 27-28 hours. In figure 8.4 (a) the variations in the position of band 15 with applied shift is shown and in the figure 8.4 (b) the group indices are plotted against the calculated normalized frequency.

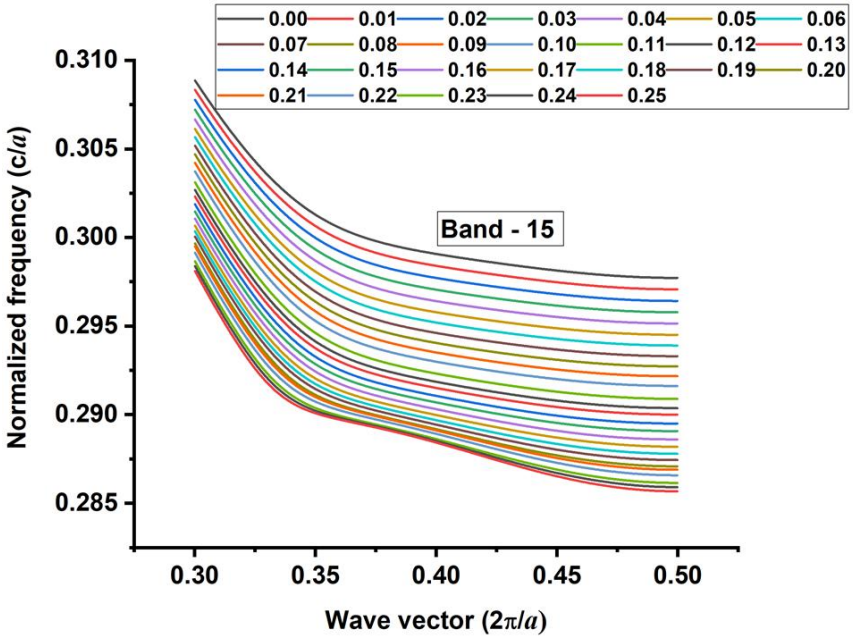

(a)

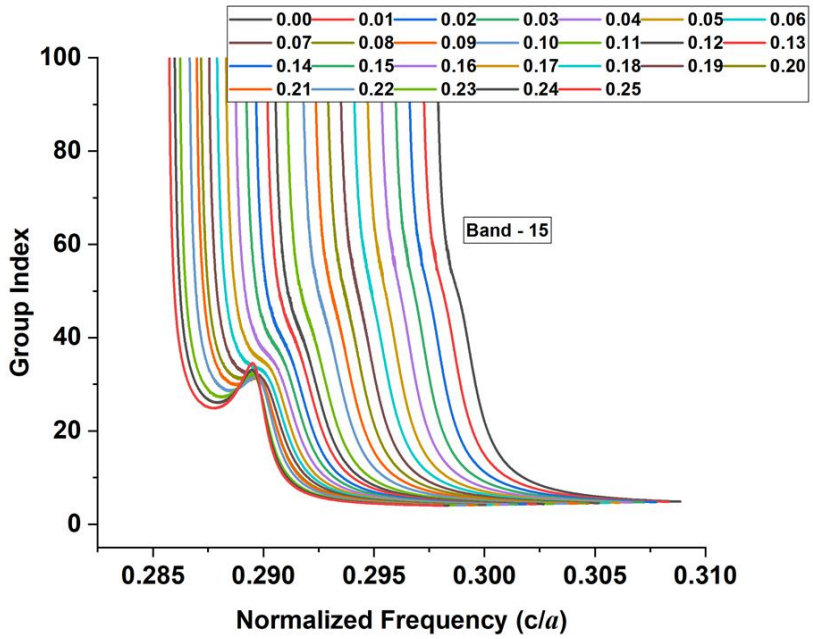

(b)

Figure 8.4: (a) Position of band 15 from the band diagram with applied shift (b) group index corresponding to (a)

The generated data is employed to train the proposed ANN model for predicting the dispersion and group indices values of the PCW within the trained range. For this purpose, the data sets (1,000 points each) with three input parameters, shift, hole radius and wavelength are used. The eigen wavelengths are calculated from the normalized frequency and the lattice constant of the structure. The predicted dispersion and group index values are noted at the output layer. After training, the model is tested for random shift values within the trained data range.

8.4.2 Numerical results based on ANN modelling:

In this sub-section, we present the predictions of the proposed ANN model at untrained data sets. The predicted data is compared with conventional data and the performance of the ANN model is evaluated. Dispersion and group indices values at different shifts within the trained data range are predicted by the model followed by the training. The model can predict the dispersion and group indices values in 70 – 90 seconds. Again this predicted data is evaluated using the simulation data from the conventional MPB method. Figures 8.5 (a) and (b) show the machine predicted and conventionally simulated data of dispersion and group indices at different untrained shift values.

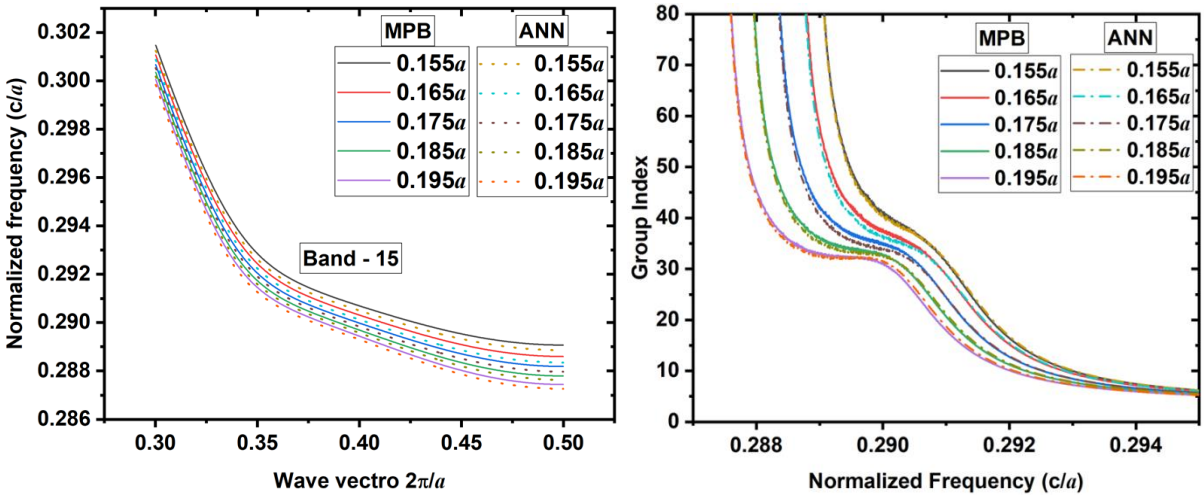

(a) (b)

Figure 8.5: (a) Position of band 15 as predicted by the ANN model and standard data simulated by MPB (b) group indices corresponding to (a)

Within the trained data range, the model was evaluated. The error was reduced by increasing the number of data sets used for training. For this purpose, we increased the resolution in the shift. The shift is introduced in the innermost row with a step size of 0.01a, and the eigen frequencies are calculated using MPB. Since we are interested only in the eigen frequencies and group index at band 15, the model was trained using data sets containing only band 15 information. The error in prediction is quantified in the following sub-section.

8.4.3 Error analysis:

In the initial studies, we noticed that 500 nodes in each hidden layer could generate stable and least MSE. Using 100 epochs, the model resulted in the lowest MSE (figure 8.2). Identifying the appropriate number of nodes and epochs reduces the error and controls the computational time. The final predictions of a model depend on the training and tuning abilities with relevant data. Cross-validation [27] is one of the methods in machine learning

that is used to test the model by resampling the data from different portions of the data sets. The training and test data are supplied from the master data set.

For performing the error analysis on our model, out of the 26 data sets generated from the MPB program, the data set at shift (s) = 0 is unused during the cross-validation. The 25 data sets are sub-divided as training data (80%) and test data (20%). Here since the data is non-uniform, we adopted repeated random subsampling cross-validation. In five iterations, the model is trained using 80% of the data and the validation is done by the rest of the 20% data. The data split is done randomly during the training and testing. Figure 8.6 illustrates the repeated random subsampling cross-validation and data selection for training and testing. Here the data selection can be random, and the number of iterations is not fixed.

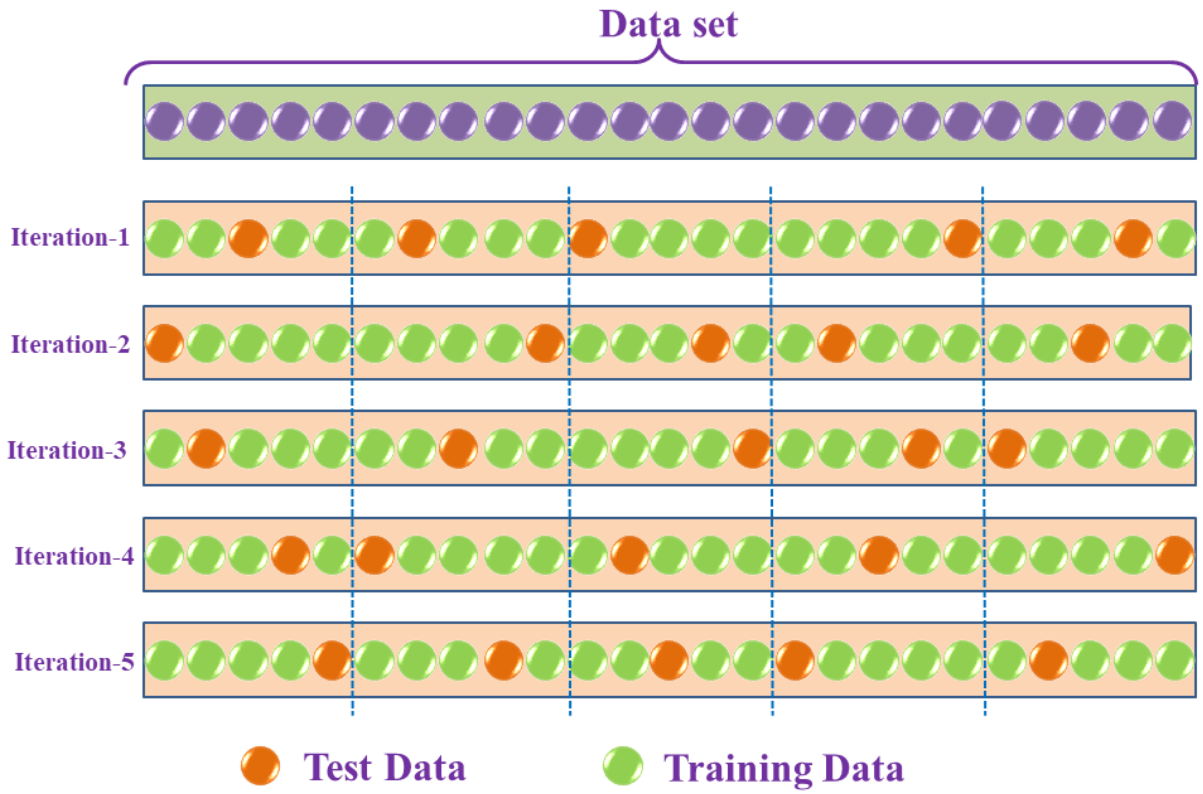

Figure 8.6: Repeated random subsampling cross validation method for analyzing the error

Figure 8.7 (a – e) shows the test data, and the machine predicted data at different random data points. The random data points (20% of the complete data set) are selected at 0.04*a*, 0.08*a*, 0.12*a*, 0.16*a* and 0.20*a* in one of the iterations and the rest of the data (80% of the complete data set) is used for training the model. Though the error is small, this can be further reduced by training the model with many data points or by reducing the step size of the shift.

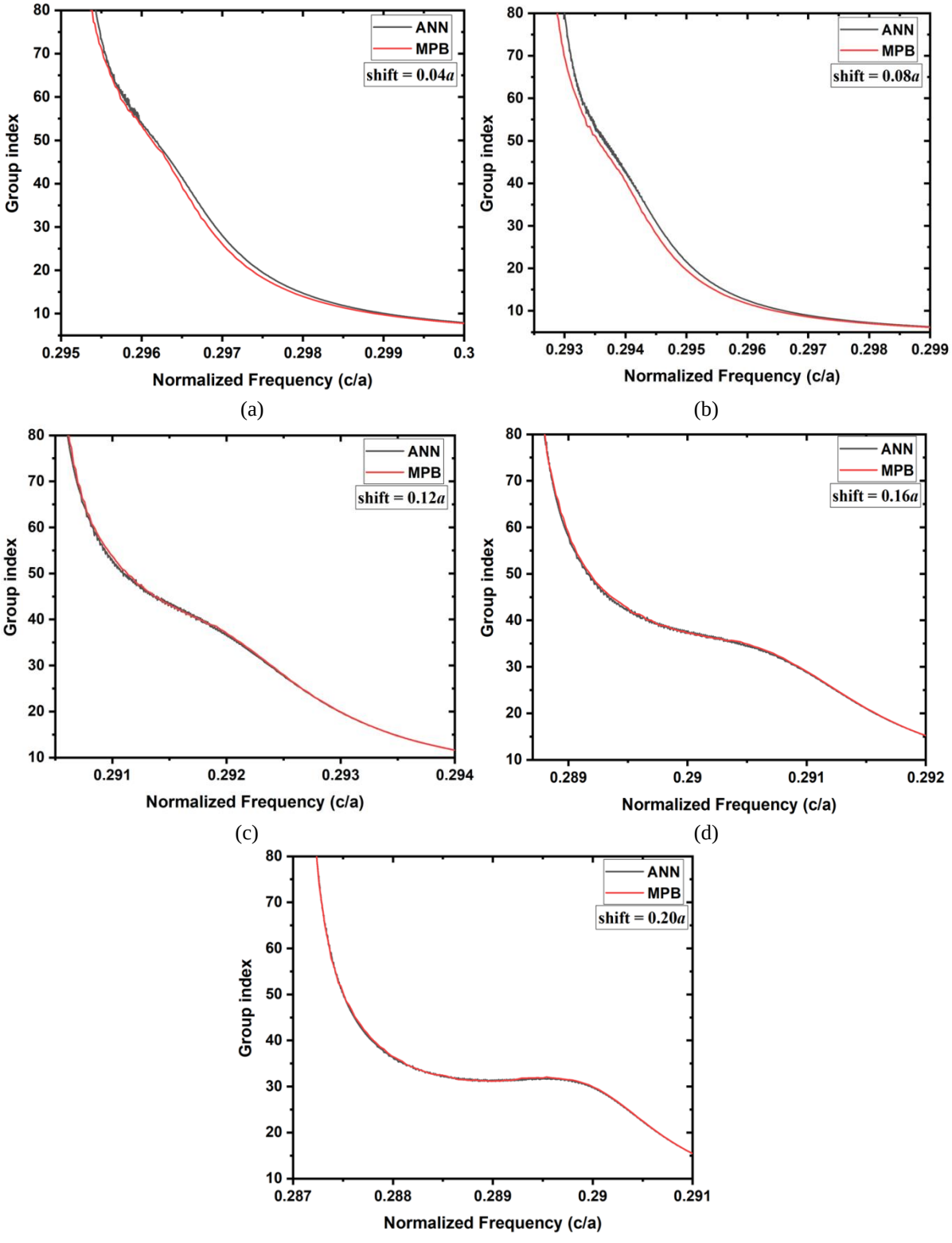

Figure 8.7: Group index as predicted by the ANN model under the repeated random subsampling cross validation method and corresponding error at (a) 0.04*a* (b) 0.08*a* (c) 0.12*a* (d) 0.16*a* and (e) 0.20*a*

From our observation, in the lower shift values, the magnitude of the error is larger, and the deviation from the actual value is high. The model can predict the parameters with the least error at the higher shift values. In figure 8.8, the error in the group index predictions

at untrained data points is shown. The predictions are made within the trained data range, and the model can predict the dispersion relations and group index with permissible error.

The model proposed here is based on MLP since the data cannot be linearly separable. Since the back-propagation is used for training the model, the error in the predictions depends on the trained data set. Rectified linear activation unit (ReLU) is used as an activation function in the model. Adam optimizer is used for performing gradient descent back-propagation optimization since it accelerates the weights and biases the ANN model over each epoch. Moreover, this also offers a balance between learning rate and training time.

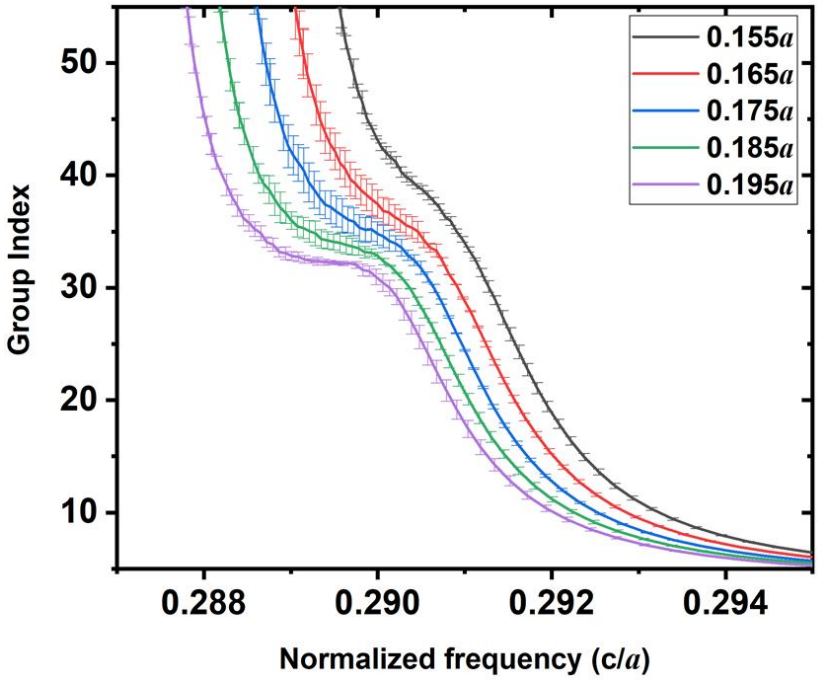

Figure 8.8: Error in the group index prediction at untrained data points

Another significant achievement of this study is computational time. Usually, the conventional methods require 6-8 hours of computational time to find the dispersion values with decent error. This computational time increases further when the geometry becomes more complex, or the number of wave vector points is increased. The present model can predict the dispersion and group indices values within the trained data range in 70-90 seconds. However, the model needs the data from conventional methods for training and evaluation purposes. Further, in the input layers, one can introduce other geometrical parameters, effective refractive index, and lattice perturbations to enhance the model's accuracy.

8.5 Conclusions:

To conclude, in this chapter, we present an ANN model based on MLP for predicting the dispersion values and group indices values of a lattice shifted PCW. The model is trained by data sets generated from conventional MPB programming. For this purpose, a 2-dimensional PCW with hexagonal lattice is used. For slow light applications, the PCW is engineered by introducing a lattice shift in the range of 0.00*a* to 0.25*a* with a step of 0.01*a*. The dispersion and group indices values are generated for every structure, and this data is used to train the model. The trained model can predict the parameters of the waveguide with acceptable error. The error can be further reduced by increasing the input nodes and number of data points for training the model.

References:

1. O. Sigmund and K. Hougaard, "Geometric properties of optimal photonic crystals," *Phys. Rev. Lett.*, vol. 100, no. 15, pp. 1-4, Apr. 2008. https://doi.org/10.1103/PhysRevLett.100.153904
2. L. Shen, Z. Ye, S. He, and S. He, "Design of two-dimensional photonic crystals with large absolute band gaps using a genetic algorithm," *Phys. Rev. B - Condens. Matter Mater. Phys.*, vol. 68, no. 11, pp. 1–5, Jul. 2003. https://doi.org/10.1103/PhysRevB.68.035109
3. S. Li, H. Lin, F. Meng, D. Moss, X. Huang, and B. Jia, "On-Demand Design of Tunable Complete Photonic Band Gaps based on Bloch Mode Analysis," *Sci. Rep.*, vol. 8, no. 1, pp. 1–8, Sep. 2018. https://doi.org/10.1038/s41598-018-32422-1
4. S. Roy, M. Santagiustina, P. Colman, S. Combrie and A. De Rossi, "Modeling the Dispersion of the Nonlinearity in Slow Mode Photonic Crystal Waveguides," *IEEE Photonics J.*, vol. 4, no. 1, pp. 224-233, Feb. 2012. https://doi.org/10.1109/JPHOT.2011.2181942
5. S. Roy and P. Roy Chaudhuri, "Analysis of Nonlinear Multilayered Waveguides and MQW Structures: A Field Evolution Approach Using Finite-Difference Formulation," *IEEE J. Quantum Electron.*, vol. 45, no. 4, pp. 345-350, Apr. 2009. https://doi.org/10.1109/JQE.2009.2013084
6. T. F. Krauss, "Slow light in photonic crystal waveguides," *J. Phys. D. Appl. Phys.*, vol. 40, no. 9, pp. 2666–2670, May 2007. https://doi.org/10.1088/0022-3727/40/9/S07
7. T. Baba, "Slow light in photonic crystals," *Nat. Photonics*, vol. 2, no. 8, pp. 465–473, Aug. 2008. https://doi.org/10.1038/nphoton.2008.146

8. S. A. Schulz, L. O'Faolain, D. M. Beggs, T. P. White, A. Melloni, and T. F. Krauss, "Dispersion engineered slow light in photonic crystals: A comparison," *J.Opt.*, vol. 12, no. 10, pp. 1-10, Sep. 2010. https://doi.org/10.1088/2040-8978/12/10/104004
9. J. Li, T. P. White, L. O'Faolain, A. Gomez-Iglesias, and T. F. Krauss, "Systematic design of flat band slow light in photonic crystal waveguides," *Opt. Express*, vol. 16, no. 9, pp. 6227-6232, Apr. 2008. https://doi.org/10.1364/OE.16.006227
10. B. K. Singh, and P. C. Pandey, "Tunable temperature-dependent THz photonic bandgaps and localization mode engineering in 1D periodic and quasi-periodic structures with graded-index materials and InSb," *Appl. Opt.*, vol. 57, no. 28, pp. 8171-8181, Oct. 2018. https://doi.org/10.1364/AO.57.008171
11. S. Roy, A. Willinger, S. Combrié, A. De Rossi, G. Eisenstein, and M. Santagiustina, "Narrowband optical parametric gain in slow mode engineered GaInP photonic crystal waveguides," *Opt. Lett.*, vol. 37, no. 14, pp. 2919-2921, Jul. 2012. https://doi.org/10.1364/OL.37.002919
12. Z. A. Kudyshev, A. V. Kildishev, V. M. Shalaev, and A. Boltasseva, "Machine learning-assisted global optimization of photonic devices," *Nanophotonics*, vol. 10, no. 1, pp. 371–383, Oct. 2020. https://doi.org/10.1515/nanoph-2020-0376
13. W. Ma, Z. Liu, Z. A. Kudyshev, A. Boltasseva, W. Cai, and Y. Liu, "Deep learning for the design of photonic structures," *Nat. Photonics*, vol. 15, no. 2, pp. 77–90, Oct. 2020. https://doi.org/10.1038/s41566-020-0685-y
14. Z. Liu, D. Zhu, L. Raju, and W. Cai, "Tackling Photonic Inverse Design with Machine Learning," *Adv. Sci.*, vol. 8, no. 5, pp. 1–15, Jan 2021. https://doi.org/10.1002/advs.202002923
15. J. J. Hopfield, "Artificial neural networks," IEEE Circuits Syst. Mag., vol. 4, no. 5, pp. 3-10, Sep. 1988. https://doi.org/10.1109/101.8118
16. A. Da Silva Ferreira, G. N. Malheiros-Silveira, and H. E. Hernandez-Figueroa, "Computing Optical Properties of Photonic Crystals by Using Multilayer Perceptron and Extreme Learning Machine," *J. Light. Technol.*, vol. 36, no. 18, pp. 4066–4073, Sep. 2018. https://doi.org/10.1109/JLT.2018.2856364
17. T. Asano and S. Noda, "Optimization of photonic crystal nanocavities based on deep learning," *Opt. Express*, vol. 26, no. 25, pp. 32704-32717, Dec. 2018. https://doi.org/10.1364/oe.26.032704
18. L. Mescia, G. Fornarelli, D. Magarielli, F. Prudenzano, M. De Sario, and F. Vacca, "Refinement and design of rare earth doped photonic crystal fibre amplifier using an

ANN approach," *Opt. Laser Technol.*, vol. 43, no. 7, pp. 1096–1103, Oct. 2011. https://doi.org/10.1016/j.optlastec.2011.02.005

19. G. N. Malheiros-Silveira and H. E. Hernandez-Figueroa, "Prediction of dispersion relation and PBGs in 2-D PCs by using artificial neural networks," *IEEE Photonics Technol. Lett.*, vol. 24, no. 20, pp. 1799–1801,Oct. 2012. https://doi.org/10.1109/LPT.2012.2215846
20. Y. Khan et al., "Mathematical Modeling of Photonic Crystal based Optical Filters using Machine Learning," *2018 International Conference on Computing, Electronic and Electrical Engineering (ICE Cube)*, 2018, pp. 1-5. https://doi.org/10.1109/ICECUBE.2018.8610986
21. S. Chugh, A. Gulistan, S. Ghosh, and B. M. A. Rahman, "Machine learning approach for computing optical properties of a photonic crystal fiber," *Opt. Express*, vol. 27, no. 25, pp. 36414-36425, Nov. 2019. https://doi.org/10.1364/oe.27.036414
22. B. Wu, K. Ding, C. T. Chan, and Y. Chen, "Machine Prediction of Topological Transitions in Photonic Crystals," *Phys. Rev. Appl.*, vol. 14, no. 4, pp.1-7 Sep. 2020. doi.org/10.1103/PhysRevApplied.14.044032
23. Z. A. Kudyshev, V. M. Shalaev, and A. Boltasseva, "Machine Learning for Integrated Quantum Photonics," *ACS Photonics*, vol. 8, no. 1, pp. 34–46, Dec. 2020. https://doi.org/10.1021/acsphotonics.0c00960
24. P. Colman, S. Combrié, G. Lehoucq, and A. De Rossi, "Control of dispersion in photonic crystal waveguides using group symmetry theory," *Opt. Express*, vol. 20, no. 12, pp. 13108-13114, Jun. 2012. https://doi.org/10.1364/OE.20.013108
25. Y. Hamachi, S. Kubo, and T. Baba, "Slow light with low dispersion and nonlinear enhancement in a lattice-shifted photonic crystal waveguide," *Opt. Lett.*, vol. 34, no. 7, pp. 1072-1074, Apr. 2009. https://doi.org/10.1364/OL.34.001072
26. R. Hao et al., "Improvement of delay-bandwidth product in photonic crystal slow-light waveguides," *Opt. Express*, vol. 18, no. 16, pp. 16309-16319, Aug. 2010. https://doi.org/10.1364/oe.18.016309
27. S. Arlot, and A. Celisse, "A survey of cross-validation procedures for model selection," Statist. Surv., vol. 4, no. 2010, pp. 40 - 79, Mar. 2010. https://doi.org/10.1214/09-SS054

Chapter – 9
Conclusions and Future Work

9.1 Conclusions:

In this dissertation, we have presented detailed investigations on the dispersion engineering of the waveguides by systematic geometrical tailoring and refractive index tuning. Our study is majorly focused on developing dispersion engineered structures for slow light applications. The studies are performed using MPB software. To reduce the computational time, ML is adopted. Dispersion and group indices are predicted using a trained model.

With geometrical perturbation, the dispersion features are improved, and the control over the slow light region is enhanced. For this purpose, we revisited the waveguide's dispersion engineering by tailoring the geometry. The radius of the air cylinders, the lattice positions of the air cylinders are varied systematically, and the dispersion features are improved. Ring-like structures (rings) are introduced in the innermost rows to improve the dispersion features further. Later, we have combined all the geometrical perturbations and studied the collective effect. The group index, delay-bandwidth product, and second-order dispersions are analysed to characterise the waveguide.

Further, the waveguide features are studied by modulating the refractive index of the slab. We have introduced an external electric field and heat to the waveguide and incorporated the variations in the material's refractive index. The variations in the refractive index are calculated using electro-optic and thermo-optic effect equations in the near-infrared region. Improved results are observed with the application of external heat and electric fields. Based on the enhanced features of the designed waveguides, a temperature sensor and reconfigurable waveguide are modelled. Further, broadband generation in the waveguide with wider PBG is studied.

Computational time is a challenging factor while simulating the PCW structures. The time and memory requirement increase as the structure becomes complex. ML is adopted to reduce the computational time. Conventionally generated data from MPB programs is used to train the neural network. Within the trained data range, predictions are observed to be accurate and close enough to the actual data. The computational time is primarily reduced by adopting the ML.

9.2 Key Observations and Achievements:

i. Systematic shift, twist, variation in the radius of the air cylinder and introducing ring-like structures in the lattice of PCW controlled the dispersion features over a broad bandwidth with desired group index. The method has also increased the degrees of freedom to control the dispersive curve. This dispersion engineering has also enhanced the group index – bandwidth product. Based on this study, one can design a waveguide with a nearly constant and low n_g over a broad wavelength range or a waveguide with a nearly constant and high n_g with a narrow band.

ii. Introducing the twist and shift in the second row of the PCW further elevated the studying parameters. With applied shift and twist in the lattice, a constant group index of 31.42 over a bandwidth of 7.97 nm and 7.64 over 30.41 nm with very low dispersion is achieved. β_2 and β_4 values are in the range of 10^{-20} s^2/m and 10^{-45} s^4/m, respectively, indicating the controlled dispersion. Even these results apply to PCW made from other materials. However, the magnitude of change in a physical parameter may depend on the material properties.

iii. Group index, bandwidth, DBP, second and fourth-order dispersions are calculated in a PCW with ring-like structures to characterise the SL. With rings in the first row, a flat band of 17.71 nm is observed with a group index value of 12.72. The NDBP is observed as 0.1378. With rings in the second row, the group index is decreased to 7.77, increasing the flat band over 40.15 nm.

iv. The NDBP is observed as 0.18740. This value is nearly 4.3 times higher in comparison with the NDBP value of the base structure (0.0436) and approximately two times higher than the engineered structure (0.0927). This study can help in designing application-specific devices like optical buffer memories, optical switches, to generate efficient nonlinear effects such as supercontinuum generation, and devices with desired slow light features.

v. We have shown the active tuning of PBG in a 2-dimensional PCW, using electro-optic effect and thermo-optic effect. This results in tunable PBG ranging from 24 nm to 58 nm with a shift of about 34 nm. Tunability is achieved by introducing an external electric field in the range of 0 - 500 kV/cm and temperature in the range of 100 K to 400 K. The tunable structures are simulated in all communication bands.

vi. Even though the electro-optic effect produces a smaller shift in the PBG, higher shifts can be attained by introducing defects in the structure or electrically active materials

such as liquid crystals and electro-active polymers. Moreover, the method can be easily adaptable in optical networks.

vii. These tunable PBG structures can be used in optical filters, wavelength routers, optical shutters, dynamic detectors and interconnectors. This may also help to develop on-chip integrated circuits due to their small size and material compatibility. However, more investigations are needed on the dispersion of light in such structures and fabrication methods. Moreover, the quick heating and cooling of the device need to be studied for real-time applications.

viii. A temperature sensor is modelled using an active PCW covering a broad range of temperatures. In the temperature range, 10 K to 400 K, a complete and narrow PBG is observed between band 7 and 8 TM modes. The change in band edges with temperature is recorded, and sensitivity of $375.16 \pm 0.791 \times 10^{-3}$ to $378.55 \pm 0.794 \times 10^{-3}$ pm/K is observed. This sensor is a better alternative to the existing temperature sensors for static temperature measurements due to its operating range. However, the slow heating and cooling rates of the PCW material may restrict the usage of this structure for real-time and high-speed applications.

ix. Liquid infiltration in the lattice shifted PCWs improves its characteristics. Initially, a GaAs based PCW is designed with air cylinders. The first innermost row of the waveguide is shifted to generate the slow light features. The shift is introduced in the range of $0.12a$ to $0.16a$, and the slow light features are studied. In these lattice shifted PCWs, liquid of refractive index 1.3 is introduced, and the characteristics are analysed.

x. The lattice shift we introduced in the liquid infiltration technique improved PCW characteristics. It is observed that the DBP of the infiltrated waveguides is more significant than that of waveguides with air cylinders. On average, the DBP is improved by 4-6 times that of the base structure. The dispersion in the liquid infiltrated waveguides is under control. In addition, one can design the reconfigurable waveguides and modify the dispersion features using liquids of different refractive indices.

xi. Broadband generation is studied in the wideband PCW structures. The wideband PCW with a pump at 1515 nm is used in this study. The study reveals that PCWs with tailored geometry can offer wideband PBG, which can be used for observing broadband generation.

xii. An ANN model is proposed based on MLP for predicting the dispersion and group indices values of a lattice-shifted PCW. The model is trained by data sets generated from conventional MPB programming. The model is trained using geometrical parameters, eigen wavelengths as input parameters, dispersion and group indices as output parameters. The trained model can predict the parameters of the waveguide with acceptable error within the trained data range. Repeated random subsampling cross-validation is adopted for the error analysis. The error can be further reduced by increasing the input nodes and number of data points for training the model.

9.3 Scope of Future Work:

Considering the light modulating capacities of the PCW structures, we are interested in designing the waveguides for nonlinear applications. In addition to this, we would like to explore machine learning for more parameter prediction and extrapolation. In specific,

- Studying wideband engineered structures for nonlinear applications such as parametric amplification, mode mixing phenomena, and supercontinuum generation.
- ML based study of reconfigurable structures using liquids of various refractive indices.
- Studying nonlinear behaviour of PCW structures using ML.
- Fabrication of PC structures by colloidal method for device applications.

List of publications

Journal Publications:

1. **Vadapalli Durga Rama Pavan**, and Sourabh Roy, "Tuning of photonic bandgap in lithium niobate photonic crystal slab structures for wavelength filtering," *Indian Journal of Pure & Applied Physics*, vol. 57, no. 12, pp. 923-927, Dec. 2019.
2. **Vadapalli Durga Rama Pavan**, and Sourabh Roy, "Analyzing two-dimensional tunable photonic crystal waveguides for communication band optical filter applications," *Journal of Optics*, vol. 50, pp. 346–353, Sep. 2021, https://doi.org/10.1007/s12596-021-00721-y
3. **Vadapalli Durga Rama Pavan**, and Sourabh Roy, "Analyzing dispersion properties of photonic crystal waveguides with hole and ring like lattice by introducing systematic shift and twist," *Optical and Quantum Electronics*, vol. 53, Article ID: 711, pp. 1-27, Nov. 2021, https://doi.org/10.1007/s11082-021-03333-9
4. **Vadapalli Durga Rama Pavan**, and Sourabh Roy, "Exploring the Slow Light Features of Lattice Shifted Twist Induced Photonic Crystal Waveguides with Ring Like Holes," *IETE Journal of Research*, vol. 2022, pp. 1-8, Jan. 2022, https://doi.org/10.1080/03772063.2021.2016503
5. **Vadapalli Durga Rama Pavan**, K. Dey, N. Vangety, Umamaheswara Sharma, and Sourabh Roy, "Interpolation of Dispersion Relations and Group Index in Photonic Crystal Waveguides using Artificial Neural Network" – *Optical and Quantum Electronics* – In review as on 31-05-2022.

Conference Publications:

1. **Vadapalli Durga Rama Pavan**, Sourabh Roy, and M. Sai Shankar, "Electrically Tuned Bandgap Structures for Optical Switching Applications," *JSAP-OSA Joint Symposia 2018*, paper ID: 18p_221B_15, Sep. 2018. https://opg.optica.org/abstract.cfm?URI=JSAP-2018-18p_221B_15
2. **V. D. R. Pavan** and S. Roy, "Temperature Effects on Dispersion Tailoring of Slow Light Engineered Photonic Crystal Waveguide," *24th Microoptics Conference (MOC) 2019*, pp. 268-269, Nov. 2019, https://doi.org/10.23919/MOC46630.2019.8982894

Journal Publications outside thesis work:

1. **Vadapalli Durga Rama Pavan**, K. Dey, and Sourabh Roy "Optical Fiber-Based Intensity-Modulated Cost-Effective Small Lean Angle Measurement Sensor," *MAPAN*, vol. 36, pp. 925–930, Apr. 2021, https://doi.org/10.1007/s12647-021-00451-3
2. Sravanthi Alamandala, R. L. N. Sai Prasad, Rathish Kumar Pancharathi, **V. D. R. Pavan**, and P. Kishore "Study on bridge weigh in motion (BWIM) system for measuring the vehicle parameters based on strain measurement using FBG sensors" *Optical Fiber Technology*, vol. 61, Article ID: 102440, pp 1-9, Jan. 2021, https://doi.org/10.1016/j.yofte.2020.102440
3. Koustav Dey, **V. D. R. Pavan**, Ramesh Buddu, and Sourabh Roy "Axial force analysis using half-etched FBG sensor," *Optical Fiber Technology*, vol. 64, Article ID: 102548, pp. 1-6, Jul. 2021, https://doi.org/10.1016/j.yofte.2021.102548